Lasers in the Preservation of Cultural Heritage

Guest Editors: Costas Fotakis, Wolfgang Kautek, and Marta Castillejo

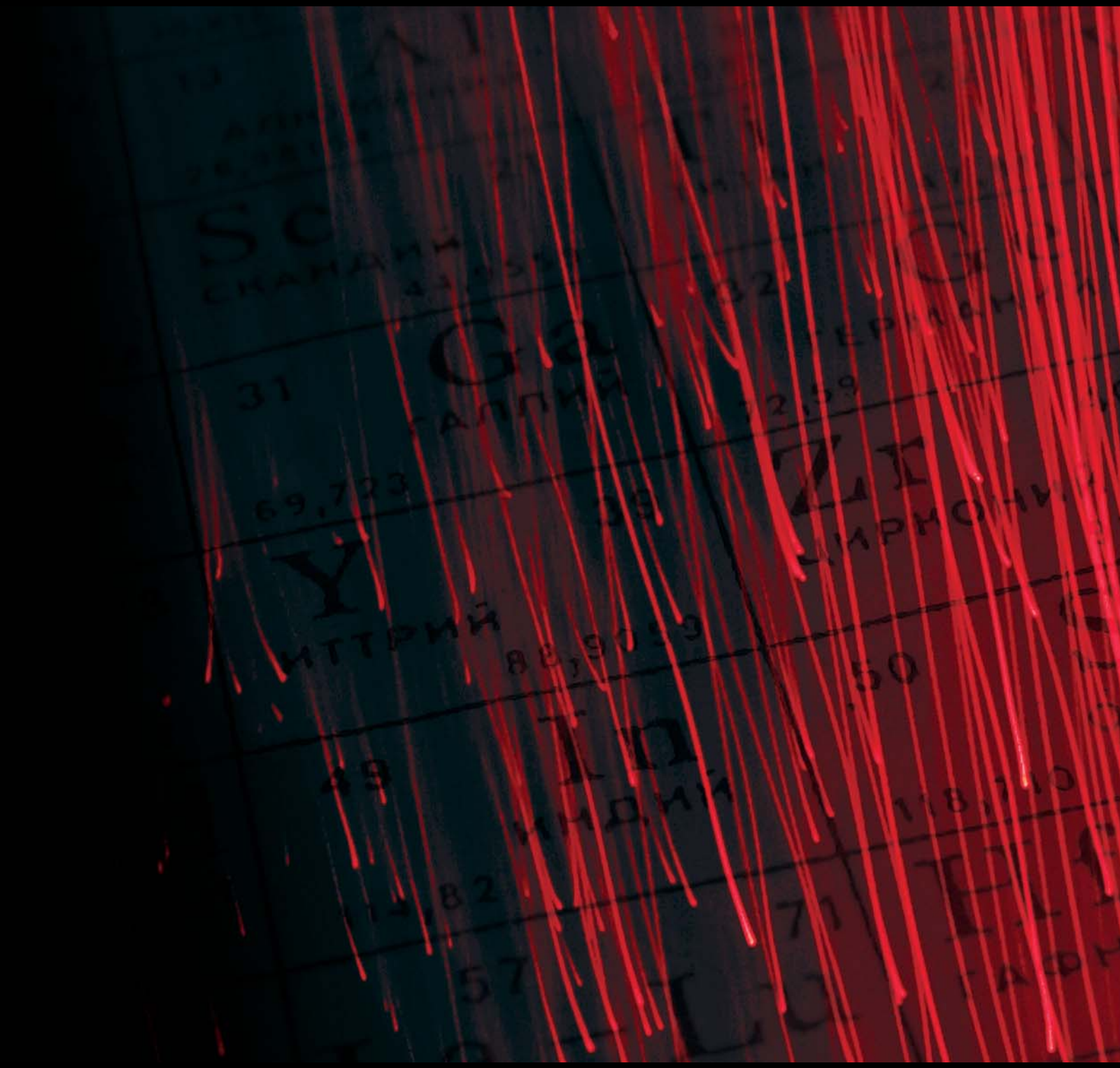

Lasers in the Preservation of Cultural Heritage

Laser Chemistry

Lasers in the Preservation of Cultural Heritage

Guest Editors: Costas Fotakis, Wolfgang Kautek, and Marta Castillejo

Contents

Hindawi Publishing Corporation
Laser Chemistry
Volume 2006, Article ID 74791, 1 page
doi:10.1155/2006/74791

Editorial
Lasers in the Preservation of Cultural Heritage

Costas Fotakis,[1] Wolfgang Kautek,[2] and Marta Castillejo[3]

[1] *Foundation for Research and Technology-Hellas, Institute of Electronic Structure and Laser, 71110 Heraklion, Greece*
[2] *Department of Physical Chemistry, University of Vienna, 1090 Vienna, Austria*
[3] *Spanish National Research Council (CSIC), Serrano 117, 28006 Madrid, Spain*

Received 31 December 2006; Accepted 31 December 2006

To date, it has been proven that modern laser technology may well serve the future of our past, the preservation and revelation of cultural heritage. This field is now coming to an era of maturity both in terms of the level of understanding of the fundamental aspects involved and the practical diagnostics and restoration applications, which have been demonstrated. The workshop on "Lasers in the Preservation of Cultural Heritage," held in June 27-28, 2006 in St. Petersburg, Russia, was organized in the framework of the Laser Optics Conference, attracting contributions which reflect the state of the art and the potential for future developments. The workshop took place in the premises of the State Heritage Museum and included presentations of fundamentals and test case studies, some of which are described in this special issue of laser chemistry.

In particular, laser-based spectroscopic techniques of noninvasive character, such as laser-induced fluorescence (LIF) and raman spectroscopy are now capable of providing in situ and remote analytical information of organic materials. Novel aspects of laser-induced breakdown spectroscopy (LIBS) for the elemental analysis of the original materials or pollutants of artifacts by using ultra-fast lasers (fs-LIBS) were also presented, together with a range of test case applications.

Besides the established use of lasers emitting pulses of nanosecond duration for cleaning applications, femtosecond lasers also present interesting new possibilities for demanding conservation cases (e.g., for cleaning of polychromes and sensitive materials like those used in modern paintings). It is the extremely high spatial resolution of the ablation processes and the minimal thermal and photochemical effects which may be achieved by using femtosecond lasers that leads to the success of these applications.

Finally, interferometric techniques for the detection and evaluation of defects and the structural status of artifacts appear to come to age. Along these lines, optical coherence tomography (OCT) was reported to be a promising technique for exciting new applications.

Costas Fotakis
Wolfgang Kautek
Marta Castillejo

Hindawi Publishing Corporation
Laser Chemistry
Volume 2006, Article ID 57934, 6 pages
doi:10.1155/2006/57934

Research Article

Remote Multicolor Excitation Laser-Induced Fluorescence Imaging

Rasmus Grönlund,[1] Jenny Hällström,[2] Ann Johansson,[1] Kerstin Barup,[2] and Sune Svanberg[1]

[1] *Atomic Physics Division, Lund University, P.O. Box 118, SE-221 00 Lund, Sweden*
[2] *Architectural Conservation and Restoration, Lund University, P.O. Box 118, SE-221 00 Lund, Sweden*

Received 15 September 2006; Revised 31 October 2006; Accepted 3 November 2006

Recommended by Costas Fotakis

Remote laser-induced fluorescence of stone materials was performed with application towards cultural heritage. Fluorescence was induced in targets ~60 m from a mobile lidar laboratory by ultraviolet laser light, either from a frequency-tripled Nd:YAG laser or from an optical parametric oscillator system. Analysis was performed on combined spectra from the different excitation wavelengths and it was noted that important additional information can be gained when using several excitation wavelengths.

1. INTRODUCTION

Laser-induced fluorescence (LIF) can be used to distinguish different areas on surfaces in numerous applications, for example, tissue diagnostics [1]. Laser light illuminating a surface excites the material which reemits fluorescence light when relaxing. Different molecules have different fluorescence features, and thus areas containing different materials give different signals. From stone materials, typically the fluorescence spectra have little features and only small variations occur. The fluorescence usually peaks in the blue/green wavelength region and falls off towards red wavelengths. Variations between materials may be displayed as differences in the slopes and wavelength for the maximum fluorescence. Certain molecules may give more specific fluorescence signals, such as chlorophyll, which shows two sharp peaks in the near infrared [2]. Due to the limited penetration depth of ultraviolet light, only the superficial layer of the target can be investigated.

By studying details in the fluorescence spectra from different parts of a building, it may, for example, be possible to assess surface damage and detect traces of chemicals previously used for restoration purposes, which are often unnoticed in visual inspections. These signals can aid in understanding the effects of earlier restoration techniques and could ultimately form a basis for future maintenance and intervention.

Remote laser-induced fluorescence, also known as fluorescence lidar [3], has earlier been applied by our group to aquatic monitoring [4], studies of vegetation status [5] and surfaces of historical buildings [6, 7]. In these measurements, performed with single wavelength excitation, we have illustrated that chlorophyll-rich areas, regions previously exposed to chemical treatment, as well as different stone types can be demarcated.

Remote fluorescence spectra can be gathered by transmitting a powerful laser pulse onto the target and collecting the induced fluorescence with a telescope and a spectrometer system. To perform measurements at daytime, gating of the detector is usually required to suppress background light. By scanning the laser beam over a target area and recording the fluorescence spectrum in each spot, imaging can be achieved.

In this paper, we present remote fluorescence imaging measurement results from measurement campaigns in both laboratory and field settings. Although much information can be extracted from a single excitation wavelength, the use of two or more excitation wavelengths is demonstrated to add significant information to the analysis, improving the possibilities to discriminate between areas with different fluorescent/physical characteristics. Furthermore, we discuss different analysis methods for extracting useful information from huge fluorescence data sets.

2. EXPERIMENT

Laser-induced fluorescence was used to remotely study stone surfaces. Some measurements were performed in a laboratory environment, while others were performed as field campaigns at cultural heritage sites. By excitation of the material using ultraviolet laser pulses, fluorescence was induced from a distance of about 60 m. The signal was remotely gathered by a telescope and the spectral shape was analyzed. By scanning the laser beam over the building and detecting the fluorescence from each spot, imaging could be performed. When performing measurements on buildings with historical value, it is important to note that the surfaces of buildings are not at all affected by the measurement, which is not the case for many other building investigation methods.

The measurements presented in this paper are from a campaign with brick samples measured in Lund, Sweden, a field campaign at Övedskloster castle in southern Sweden and a field campaign at Coliseum in Rome, Italy. More information on the Övedskloster campaign is presented in [8] and on the Coliseum campaign in [9, 10].

3. MATERIAL AND METHODS

A mobile lidar laboratory [11], which is primarily adapted for atmospheric monitoring by the differential absorption lidar technique, was employed for the experiments. The system has a flexible design and is well suited for monitoring remote fluorescence as has been previously reported [4–7]. The fluorescence lidar transmitter was a frequency-tripled Nd:YAG laser generating radiation at 355 nm in 5-nanosecond-long pulses at a repetition rate of 20 Hz. Typically the transmitted pulse energy was limited to 25 mJ in these experiments. Also, an optical parametric oscillator (OPO) could be used as the excitation source, where the laser wavelength could be selected in a wide range from ultraviolet to infrared. Only ultraviolet wavelengths were used, as fluorescence induction is particularly efficient using these wavelengths, and also due to eye-safety reasons. From the OPO, the transmitted pulse energy was typically 5 mJ. Over a scan, the output integrated over a particular measurement spot was stable to $\sim$20%.

The vertically looking receiving optics was a Newtonian telescope with 40 cm diameter. A 40 cm $\times$ 80 cm folding mirror placed over the telescope in a dome above the vehicle roof can be steered to direct the laser beam onto the desired spot. As the laser beam is coaxial to the field of view of the telescope, the detected radiation is gathered from the correct area. A gated and intensified optical multichannel analyzer, more closely described in [12], detected the fluorescence radiation from 280 to 810 nm with a spectral resolution of $\sim$3 nm. The laser beam expander, which was coaxial with the receiving telescope, was normally adjusted to give a 5-cm-diameter laser spot on the target. For a typical distance of 60 m between the lidar and the target, the diameter of the image spot in the telescope focal plane was $\sim$1.3 mm. The radiation was transmitted through a high-pass filter to suppress the specular reflection and collected using a 600 μm diameter optical fibre connected to the optical multichannel analyzer system. With the computer-controlled folding mirror the lidar was pointed at selected locations for spectral data collection, or scanned row by row over the façades for image generation. A signal integration of 100 laser shots was normally used. To suppress background interference, time-gated detection was used, with a 100 nanosecond gate set to open at the arrival time of the fluorescence pulse.

From each spot investigated a fluorescence spectrum is collected, and as the laser is scanned over an area, a three-dimensional data set is obtained. To extract useful information from this huge amount of data, efficient data processing is necessary. Different aspects of the fluorescence features can be focused on by forming ratios of intensities in different wavelength bands, by performing correlation between spectra or by principal component analysis. In this study, mainly the correlation technique has been used, where a linear correlation between one reference spectrum and all other spectra within the scan is performed. The result is then a single number for each point, between -1 and $+1$, corresponding to the similarity to the reference spectrum, where $+1$ corresponds to identical spectra and -1 corresponds to negatively correlated spectra. A zero value would indicate totally uncorrelated spectra, as would be expected when correlating two sets of white noise. In this way, areas with similar fluorescence features can quickly be found and delineated. Different analysis methods for these types of data are further discussed in [13].

The measurement campaign on brick samples was performed in a laboratory setting. The lidar system was docked to the Physics Department building at Lund University, and the bricks were set up on the roof of a building 60 m away. The measurement was performed using five different excitation wavelengths: 250 nm, 290 nm, 337 nm, 355 nm, and 375 nm. Spectra from the same point, with different excitation wavelengths, can be combined to make it possible to analyze the results, taking all the excitation wavelengths into account simultaneously. This is done by creating an artificial spectrum for each measured spot, by simply assigning one excitation wavelength to the first 1024 data points, another to the next 1024 data points, and so on. If not all 1024 recorded data points contain significant information, some parts can be excluded [11]. Although some features may be appearing only with a certain excitation wavelength, the main advantage is gained when spectra are combined. In this way, all features appear simultaneously and can easily be presented.

In the measurement campaign at Övedskloster, areas on the façade of the building and on the courtyard portal were scanned using 355 nm excitation from the Nd:YAG laser. Different fluorescence features could be observed and much information could be extracted, even though only this one excitation wavelength was used.

During the Coliseum campaign, different areas on the Coliseum façade were scanned. In particular, one area was scanned using two different excitation wavelengths, 355 nm from the Nd:YAG laser and 250 nm from the OPO.

4. RESULTS

As mentioned, the measurements on the brick samples were performed using five different excitation wavelengths. In the analysis, the spectra for the 355 nm excitation have been divided by 5 to compensate for its greater output energy. After combining the spectra, each resulting spectrum has been normalized with respect to its greatest value. The spectra have not been normalized within each excitation wavelength, as the relative intensities hold information that would otherwise be lost. Spectra from six arbitrary spots, each on a different brick sample, have been plotted in Figure 1. By correlating all spectra with an arbitrarily chosen reference spot, different stones could be isolated, as indicated in Figure 2. This was not possible using data from only one excitation wavelength. We note that none of the neighboring pixels is white, the reason for this being that the noise in the different spectra would have to be identical.

One of the areas studied at Övedskloster castle was an ornamental urn on the roof of the main building. This part of the building is very difficult to reach for close-up examination, and thus remote fluorescence imaging is a good method to study such parts. Despite the use of a single excitation wavelength, several aspects of the fluorescence features could be studied, and other examples are given in [7]. It was noted that the spectra from the base of the urn were quite different from the rest of it. In Figure 3(a), a correlation between the spot marked with a red circle and all other spectra in the scan has been performed. The blue pixels correspond to the degree of similarity, and it can clearly be seen that the parts on the base of the urn are similar to each other and different from the rest. A few points on the upper part of the urn appear as similar, but with low correlation values. Figure 3(b) shows the spectra from two points in the scan, marked by the red and cyan circles in Figure 3(a). It is evident that the red spectrum shows a stronger fluorescence towards longer wavelengths.

One area on the Coliseum was scanned using both 250 nm and 355 nm excitation light. In the analysis, the two spectra from each point were combined to yield a combined spectrum containing information from both scans. Figure 4(a) shows the two spectra from a certain point in the scan. The red spectrum indicates the 250 nm excitation and the blue one the 355 nm excitation. In Figure 4(b), the combined spectrum is shown, where data from both excitation wavelengths have been used.

Figure 5(a) shows the area on the Coliseum which has been scanned. In Figures 5(b)–5(d), correlation has been performed with one of the spectra in the scan (marked by an oval) as the reference point. However, in Figure 5(b), only the 250 nm excitation data and in Figure 5(c), only the 355 nm excitation data have been used. In contrast, the result when using the combined spectra is shown in Figure 5(d). The correlation values in the range 0.96–1.0 have been mapped out. Values below 0.96 are not indicated in the figures. All correlation values are relatively high, which is expected, as all spectra are similar and display only subtle differences. Comparing Figures 5(b)–5(d), it is clear that spectra on the block

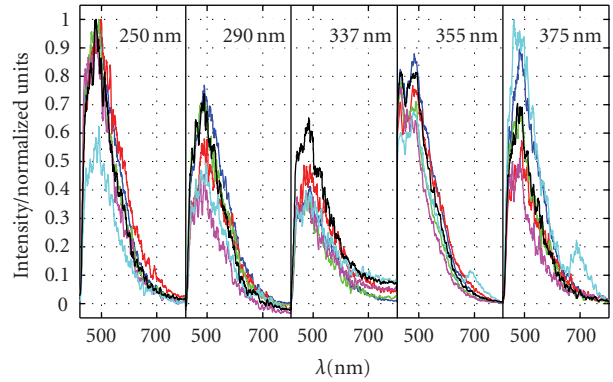

Figure 1: Spectra from six different brick samples, measured using five different excitation wavelengths. The spectra have been combined to make analysis of all data possible simultaneously. The different excitation wavelengths are indicated in the figure. Studying the spectra, it is difficult to distinguish them by using only one excitation wavelength, but with the combined spectra differences can be seen. One spectrum contains the characteristic chlorophyll peak at ∼690 nm, but this fluorescence feature can only be seen with the 355 nm and 375 nm excitation.

Figure 2: The brick samples measured, with an analysis superimposed. It was possible to delineate one of the brick samples by correlating all spectra in the scan with one spectrum on this particular brick. The white spot corresponds to the chosen reference spectrum and the blue points display the correlation coefficient value. Values below a certain threshold value have not been displayed. The scan was performed over all the bricks and contained 26×22 points, as indicated by the red frame. As can be seen, the points on the particular brick have high correlation values and only a few points in the rest of the scan have values above the threshold.

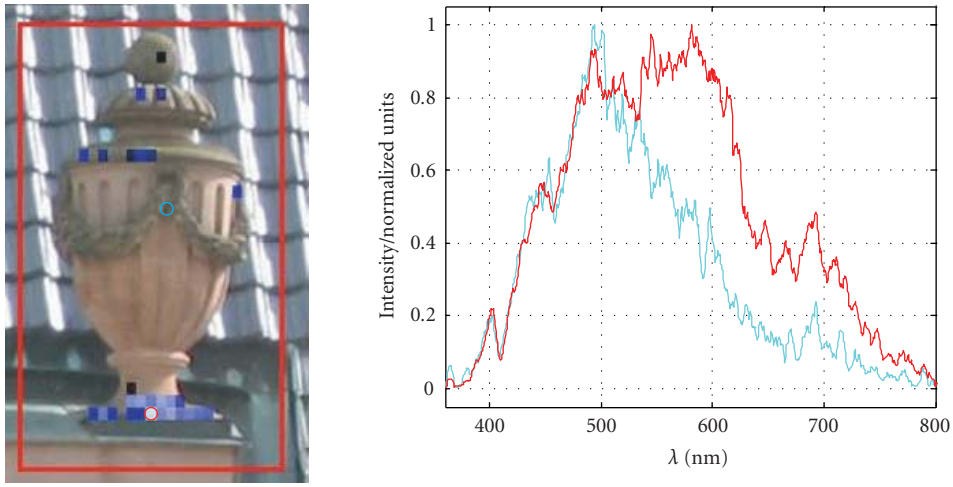

Figure 3: An ornamental urn on the roof of Övedskloster castle. Part (a) shows the correlation between a point on the base of the urn (marked by a red circle) and all other spectra. The frame indicates the measured area. In part (b), the spectra from the selected point and a further point (marked by a cyan circle) are shown, and there is an obvious difference between them. The red spectrum corresponds to the red circle in part (a), and the cyan spectrum to the cyan circle.

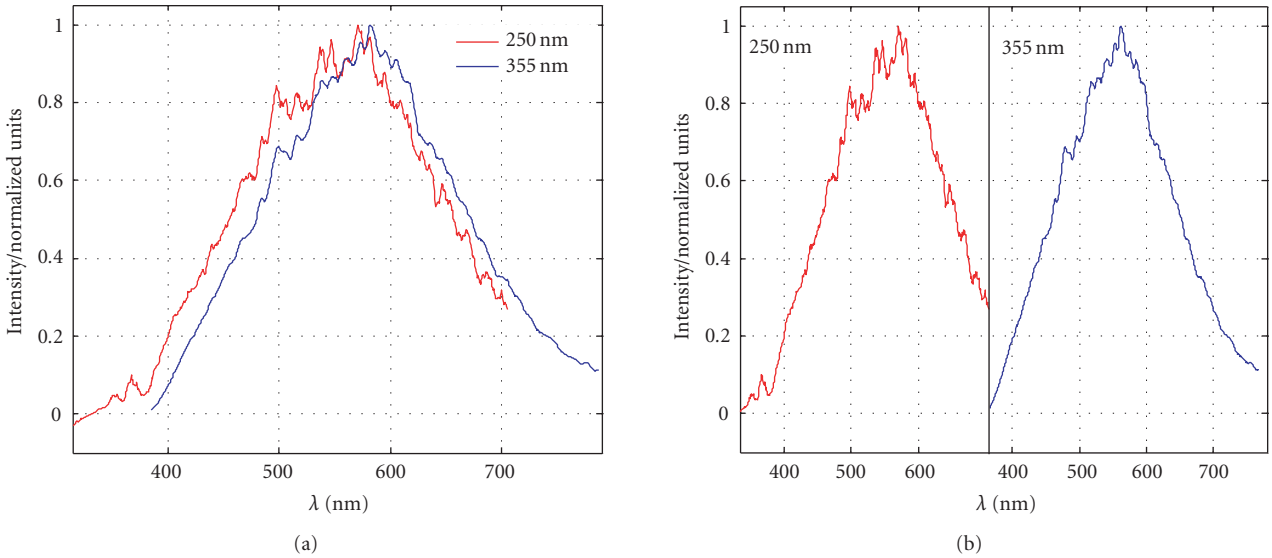

Figure 4: Spectra from a point in a scan on the Coliseum. (a) Shows the two different spectra and (b) shows the combined spectrum. The latter can be used in the analysis to simultaneously use information from both excitation wavelengths.

in the upper part of the pillar and in the bottom line of the scan (corresponding to the edge of a stone further down) are similar. Also, it is seen that these have different fluorescence features than the block between them. It is noted that the correlation using combined spectra discriminates more effectively than the same analysis using only the spectra from one excitation wavelength. In Figure 5(d), only a few points outside the area of interest are above the threshold, and all of them have values within the lower part of the allowed range.

5. DISCUSSION

Our studies show that laser-induced fluorescence is a useful method for studying stone surfaces with application towards cultural heritage. The method is particularly useful when applied remotely, which makes it possible to scan large areas and to reach parts of a building that are not easily accessible to methods that require close-up examination. Further, we would like to emphasize that multicolor excitation

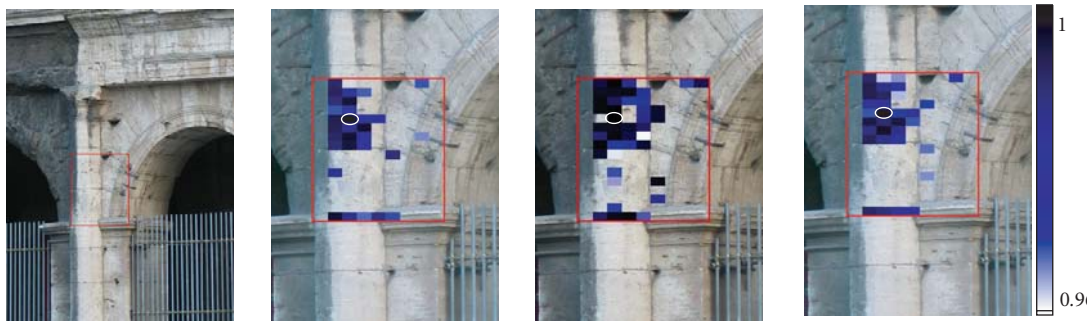

Figure 5: An area on the Coliseum façade, marked in part (a). The close-ups in parts (b)–(d) show correlation between one spectrum (marked by an oval) and all other spectra. In part (b), data from the 250 nm excitation measurement have been used, in part (c), data from the 355 nm excitation have been used, and in part (d), the data from both measurements have been combined. The color scale indicates the correlation value. Note that, since the background stone in light, high correlation values are here demarcated with dark colors, in contrast with Figures 2 and 3. Values lower than 0.96 are not indicated in the figure.

provides more information to the analysis. As different excitation wavelengths are used, different molecules are interrogated or excited to different degrees, thereby causing the observed differences in the radiated fluorescence. As was illustrated in Figures 2 and 5, utilizing the combined data resulting from inducing fluorescence at multiple wavelengths, different regions could be better discriminated and distinguished. The use of correlation analysis was demonstrated to be an efficient tool in extracting relevant information from a large amount of data and by this method it was easy to distinguish areas with similar fluorescence characteristics.

To implement analysis of the fluorescence spectra as a useful tool within the field of cultural heritage, collaborations with building restoration scientists are of utmost importance in the data extraction from fluorescence imaging experiments.

ACKNOWLEDGMENTS

The authors would like to acknowledge important contributions from Dr. Petter Weibring and Dr. Magnus Bengtsson in the brick-measurement campaign. Also, we would like to thank the CNR-IFAC Flidar group of Dr. Giovanna Cecchi for nice collaboration on the Coliseum campaign and Dottoressa Cinzia Conti for great help in practical arrangements and background information on the Coliseum campaign. This work was supported by FORMAS—The Swedish Research Council for Environment, Agricultural Sciences, and Spatial Planning, the Swedish Research Council, and the Knut and Alice Wallenberg Foundation.

REFERENCES

[1] S. Svanberg, "Tissue diagnostics using lasers," in *Lasers in Medicine*, R. Waynant, Ed., pp. 135–169, CRC Press, Boca Raton, Fla, USA, 2002.

[2] H. K. Lichtenthaler and U. Rinderle, "The role of chlorophyll fluorescence in the detection of stress conditions in plants," *CRC Critical Reviews in Analytical Chemistry*, vol. 19, supplement 1, p. S29, 1988.

[3] S. Svanberg, "Fluorescence spectroscopy and imaging of lidar targets," in *Laser Remote Sensing*, T. Fujii and T. Fukuchi, Eds., CRC Press, Boca Raton, Fla, USA, 2005.

[4] H. Edner, J. Johansson, S. Svanberg, E. Wallinder, G. Cecchi, and L. Pantani, "Fluorescence lidar monitoring of the Arno River," *EARSeL Advances in Remote Sensing*, vol. 1, no. 2, pp. 42–45, 1992.

[5] H. Edner, J. Johansson, S. Svanberg, and E. Wallinder, "Fluorescence lidar multicolor imaging of vegetation," *Applied Optics*, vol. 33, no. 13, pp. 2471–2479, 1994.

[6] P. Weibring, T. Johansson, H. Edner, et al., "Fluorescence lidar imaging of historical monuments," *Applied Optics*, vol. 40, no. 33, pp. 6111–6120, 2001.

[7] D. Lognoli, G. Cecchi, I. Mochi, et al., "Fluorescence lidar imaging of the cathedral and baptistery of Parma," *Applied Physics B: Lasers and Optics*, vol. 76, no. 4, pp. 457–465, 2003.

[8] R. Grönlund, J. Hällström, S. Svanberg, and K. Barup, "Fluorescence lidar imaging of historical monuments - Övedskloster, a Swedish case study," in *Proceedings of The 6th International Congress on Lasers in the Conservation of Artworks (LACONA '05)*, J. Nimmricher, W. Kautek, and M. Schreiner, Eds., Vienna, Austria, September 2005, Springer, Berlin, Germany, 2006 (in press).

[9] CNR-IFAC-SAR Collaboration, "Remote monitoring of conservation status of the Coliseum by laser-induced fluorescence imaging. Part I," manuscript in preparation for *Journal of Cultural Heritage*.

[10] CNR-IFAC-SAR Collaboration, "Remote monitoring of conservation status of the Coliseum by laser-induced fluorescence imaging. Part II," manuscript in preparation for *Journal of Cultural Heritage*.

[11] P. Weibring, H. Edner, and S. Svanberg, "Versatile mobile lidar system for environmental monitoring," *Applied Optics*, vol. 42, no. 18, pp. 3583–3594, 2003.

[12] C. Af Klinteberg, M. Andreasson, O. Sandström, S. Andersson-Engels, and S. Svanberg, "Compact medical fluorosensor for minimally invasive tissue characterization," *Review of Scientific Instruments*, vol. 76, no. 3, Article ID 034303, 6 pages, 2005.

[13] R. Grönlund, M. Lundqvist, and S. Svanberg, "Remote imaging laser-induced breakdown spectroscopy and laser-induced fluorescence spectroscopy using nanosecond pulses from a mobile lidar system," *Applied Spectroscopy*, vol. 60, no. 8, pp. 853–859, 2006.

Hindawi Publishing Corporation
Laser Chemistry
Volume 2006, Article ID 61607, 7 pages
doi:10.1155/2006/61607

Research Article

Spectroscopic Techniques Applied to the Study of Italian Painted Neolithic Potteries

Lucia Angeli,[1] Claudio Arias,[1] Gabriele Cristoforetti,[2] Cristina Fabbri,[1] Stefano Legnaioli,[2] Vincenzo Palleschi,[2] Giovanna Radi,[1] Azenio Salvetti,[2] and Elisabetta Tognoni[2]

[1] *Department of Archaelogical Science, University of Pisa, 56126 Pisa, Italy*
[2] *Institute for Chemical and Physical Processes, National Research Council, 56124 Pisa, Italy*

Received 15 September 2006; Revised 6 November 2006; Accepted 6 November 2006

Recommended by Marta Castillejo

In the field of cultural heritage, the study of the materials used by the artist is useful both for the knowledge of the artwork and for conservation and restoring interventions. In this communication, we present results of some decorations analysis obtained by the use of two complementary laser techniques: micro-LIBS and micro-Raman spectroscopy. With both techniques it is possible to operate in a practically nondestructive way on the artwork itself, without sampling or pretreatment. Micro-Raman spectroscopy gives information on the molecular structure of the pigments used, while micro-LIBS can give quantitative information about the elemental composition of the same materials. In this paper, qualitative results are reported obtained on the study of some Neolithic potteries coming from the archaeological site of Trasano (Matera); the fragments show decorations in different colors, red, black, and white. The aim of the study was detecting whether the colored decorations were made by using added pigments or came from the manufacturing process.

1. INTRODUCTION

The determination of the composition of the pigments used in paintings, frescoes, ceramics, and other painted artworks is useful both for the knowledge of the artwork and for planning for the proper conservation and restoring interventions. In many situations, the information on the materials under study must be obtained in situ, in short times and without compromising the integrity of the artwork; these constraints have made interesting the use of laser techniques for the analysis of painted artworks in cultural heritage [1, 2]. The complexity of the problems involved in this kind of applications, linked in particular to the large variety of the materials used and their possible degradation processes does not permit to determine a specific technique or a standard analytical procedure. In this communication, we present some results obtained by the use of two complementary laser techniques: micro-LIBS and micro-Raman spectroscopy; in particular, the micro-Raman analysis can give mainly qualitative information about the material's molecular structure, whilst the LIBS technique permits also quantitative albeit elemental measurements [3–6]. Moreover, the Raman microscopy is very selective, even if the Raman signal is not too high and in competition with the fluorescence phenomenon, particularly in the case of pigments or organic binding media [7, 8]. In recent years, several groups have proposed the use of laser induced breakdown spectroscopy (LIBS) as a technique capable of giving information on the pigment compositions with minimal damage of the artwork [9–11]. However, until the development of quantitative methods for accurate elemental analysis [9], the LIBS technique was hardly competitive with other methods for quantitative analysis of the samples; a new approach to LIBS spectroscopy, developed by the Applied Laser Spectroscopy Team at IPCF-CNR (Pisa), has reproposed this technique as a viable technique for the self-calibrated, precise quantitative analysis of pigments used in cultural heritage. Moreover, we have also demonstrated the possibility of obtaining micrometric resolutions (μ-LIBS) in LIBS analysis of paintings, reducing the surface damages at minimal levels [12, 13].

2. EXPERIMENTAL

The experimental set-up used for the micro-LIBS measurements on the ceramic samples is sketched in Figure 1.

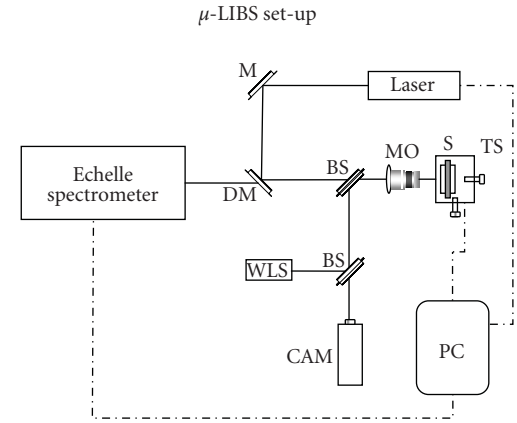

Figure 1: μ-LIBS experimental setup.

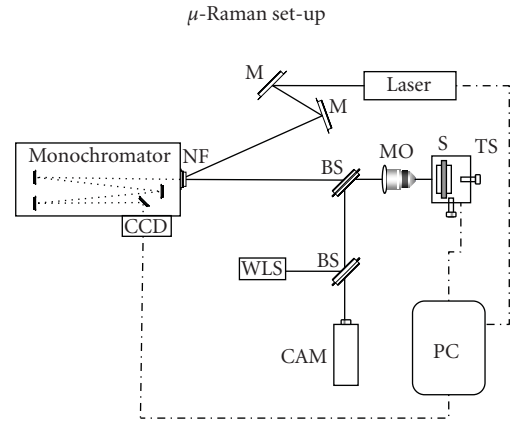

Figure 3: μ-Raman experimental setup.

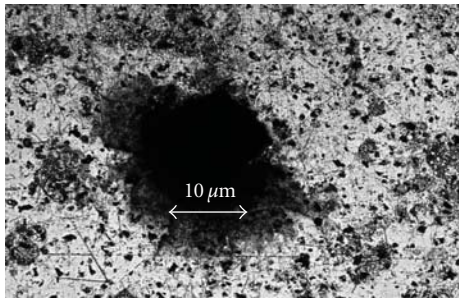

Figure 2: Computer-enhanced enlargement of the crater produced by the laser on the surface.

The laser beam is focussed on the sample surface using a microscope objective, and the signal is taken on axis through the same objective. An optical digital microscope allows for the visual inspection during the measurement; the sample is mounted on a three-axis motorized stage, controlled by a personal computer, for adjustment of the focusing position. The laser source is an Nd : YAG pulsed laser, operating at 1064 nm, which delivers about 10 mJ on the sample surface, in 8 nanoseconds. The spatial lateral resolution of the LIBS measurements corresponds to the dimensions of the micro-crater left by the laser on the sample surface. The same dimensions are also a measurement of the damage induced on the pigment. A computer-enhanced enlargement of a typical laser crater is shown in Figure 2; its diameter does not exceed 10 microns, which makes it practically invisible at naked eye. The reduced size of the crater also allows for a high spatial resolution of the LIBS analysis.

The LIBS spectral signal is detected using an Echelle spectrometer + iCCD camera, which provides the whole time-resolved NUV-NIR spectrum in a single laser shot. A computer controls the whole measurement process; dedicated software allows to perform surface scanning, spectral averages, and acquisition of the spectra. In typical experimental conditions, the micro-LIBS spectra are taken in a single laser shot, from 300 nanoseconds to 2 microseconds after the laser pulse and using a measuring gate ranging from a few ns to 1or 2 microseconds, depending on the laser characteristics (e.g., a faster signal decrease using a UV instead of a near IR exciting laser) [14]. The LIBS spectra are analyzed with proprietary software, developed at IPCF, which implements the Calibration-free LIBS procedure (CF-LIBS) and allows the precise quantitative determination of the elemental composition of the material without any reference sample or calibration curve. The software also automatically implements the corrections for plasma self-absorption recently developed by the IPCF group; a more detailed discussion on the CF-LIBS technique and self-absorption correction has been given in [4]. In typical experimental conditions, the complete characterization of the material is performed in less than five minutes, with practically no damage of the decorated surface.

The experimental set-up used for micro-Raman measurements shown in Figure 3 is essentially identical to the one used for the micro-LIBS analysis. In this case, the laser beam (generated by either a multimode Ar+ laser working at the 514.5 nm wavelength or an He-Ne laser operating at 632.8 nm) is reflected by a notch filter, which, in a first phase, behaves exactly as a mirror, then is focused on the sample by a 50X microscope objective. The diffused light goes back to the notch filter, which does not transmit the laser wavelength. The light is collected onto the entrance slit of a spectrometer (Jobin Yvon THR1000) with a 600 lines/mm grating, flat field, and long focal length (1000 mm), allowing a spectral resolution of about 1 cm^{-1}. The spectral signal is detected by a cooled CCD (KAF-1001E, produced by DTA scientific instrument) and then analyzed with appropriate software.

Figure 4: Some of the pottery fragments analyzed (clockwise TR06-TR13-TR03-TR05-TR15-TR09).

The sample is mounted on a three-axis motorized stage, controlled by a personal computer, for adjustment of the focusing position. Moreover, a camera allows the visualization of the examining zone, assuring a perfect focusing of the position.

3. RESULTS AND DISCUSSION

Fifteen samples of decorated pottery coming from the Trasano site have been analyzed. The Trasano site is located near Masseria Trasano (Matera, Italy) and it has been systematically excavated from 1984 to 1991 [15]. The area involved in the study is particularly wide with a very rich stratigraphic series that covers a long chronologic period: from the early Neolithic age (V Century BC), characterized by stamped pottery (phases I, II, III), to the middle Neolithic age (IV Century BC) with bicolored painted pottery (phase IV) and finally to the late Neolithic age (phase V) [16]. In particular, the samples analyzed belong only to the III, IV, and V phases and have the following typological characterizations:

(1) colored pottery with a purified dough and graffiti, (TR03-TR04-TR06-TR11-TR12-TR13-TR14);

(2) "figulina" type pottery painted with red stripes, (TR01-TR02-TR05-TR07-TR08-TR10);

(3) "figulina" type pottery referring to "Serra d'Alto Culture," (TR09-TR15).

Some of the samples analyzed are shown in Figure 4. They present external glossy surfaces with dark or red color, often decorated with graffiti or stripes.

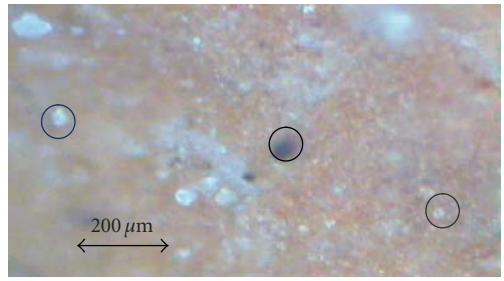

Figure 5: Microscope image of sample TR01.

3.1. Raman analysis

The 15 samples were analyzed by the Raman technique, using an Argon ion laser source operating in CW mode and selecting the 514.5 nm component. The power of the beam on the surface was a few mW. The laser beam was focused onto the sample's surface with a 50X microscope objective, so that the laser spot was a few micrometers in diameter. Figure 5 shows the microscope image of sample TR01. The surface is red, but it reveals also the presence of some impurities like quartz, rutile (silver spot-blue circle), amorphous carbon (dark spot-dark circle) and calcium (white spot-grey circle). The same minerals were present also in the other samples analyzed.

All the Raman spectra were taken with an acquisition time of 150 s. In Figure 6, a spectrum obtained from the red region is shown. All the spectra have been compared with the database of known minerals edited by the Chemistry Department of University College of London (UCL) [17].

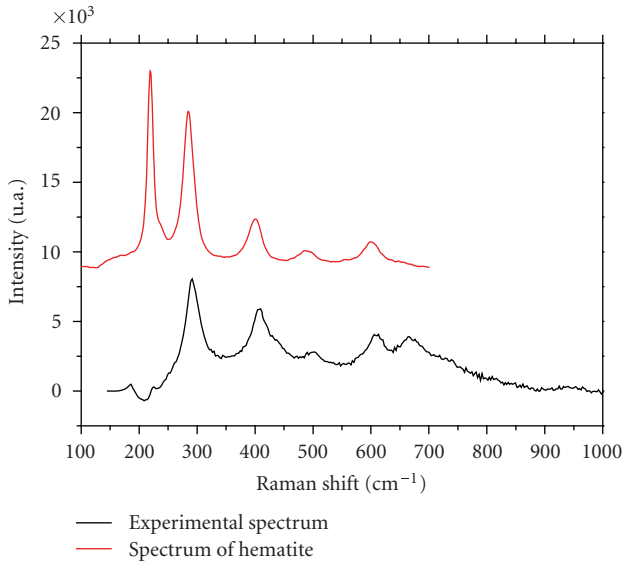

Figure 6: Raman spectrum of the red region (sample TR01).

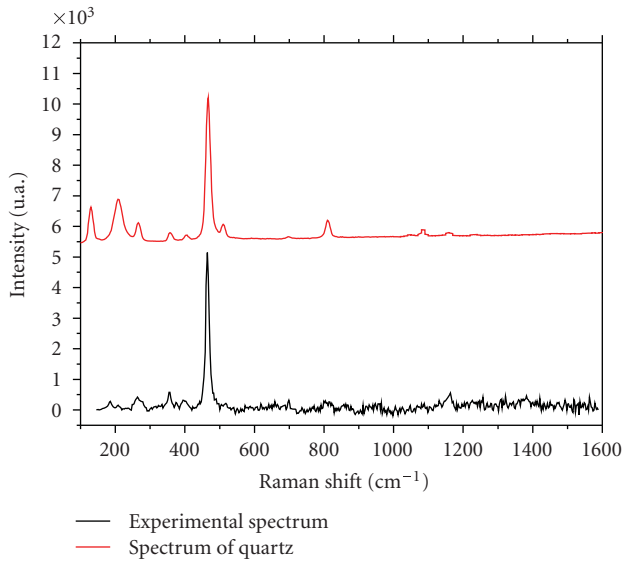

Figure 7: Raman spectrum of quartz (sample TR01).

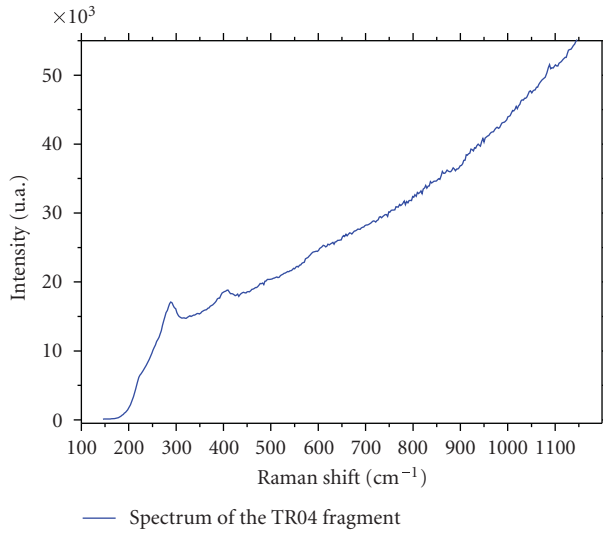

Figure 8: Raman spectrum of the red region (sample TR04).

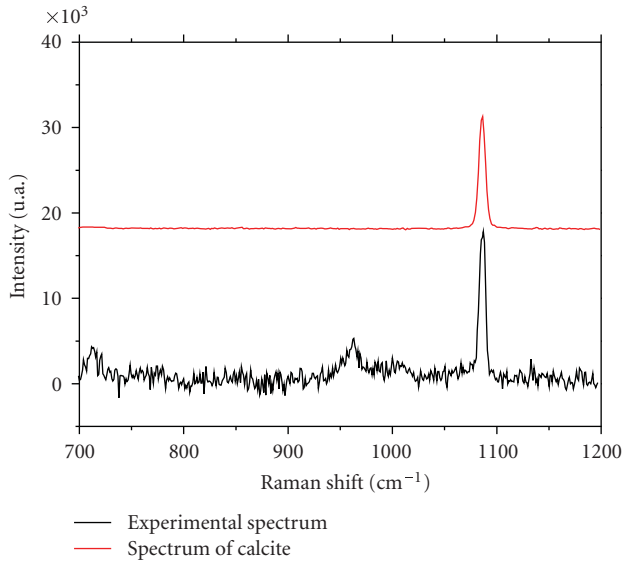

Figure 9: Raman spectrum of calcite (sample TR06).

It can be noted that there is a good correspondence between the experimental spectrum and the one from the UCL database corresponding to hematite: the lines at 291 cm^{-1}, 407 cm^{-1}, 610 cm^{-1} correspond quite well, whereas the first peak at 224 cm^{-1} is not visible, because the notch filter tends to cut off this wavelength region. In Figure 7, instead, the spectrum obtained for one of the silver spots (blue circle) present on the surface is shown: the line at 465 cm^{-1}, typical of the quartz Raman signal, is evident. The presence of this mineral, together with others like titanium oxide is characteristic of the red ochre. This is an inorganic pigment of mineral origin, composed by a clay-based body rich in hydrated iron oxides (hematite) and precipitated aluminium ($Fe_2O_3 * nH_2O + Al_2O_3$).

The Raman analysis has been repeated for the other fragments showing a red coloring (TR02-TR04-TR07-TR08-TR10-TR13-TR14); also in these cases the presence of red ochre has been detected. In particular, for the TR04 sample the main Raman peaks look wider and less intense with respect to the ones found in the others spectra; moreover, the fluorescence background is dominating (see Figure 8). A possible interpretation of this effect can be related to the different kind of clay used as body for the pottery.

The TR03 and TR06 samples present white strips in the decoration; the measurement on the TR06 surface produced

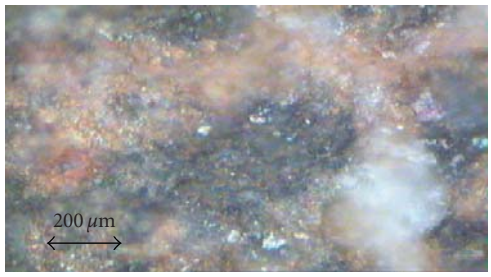

Figure 10: Microscope image of the sample TR03.

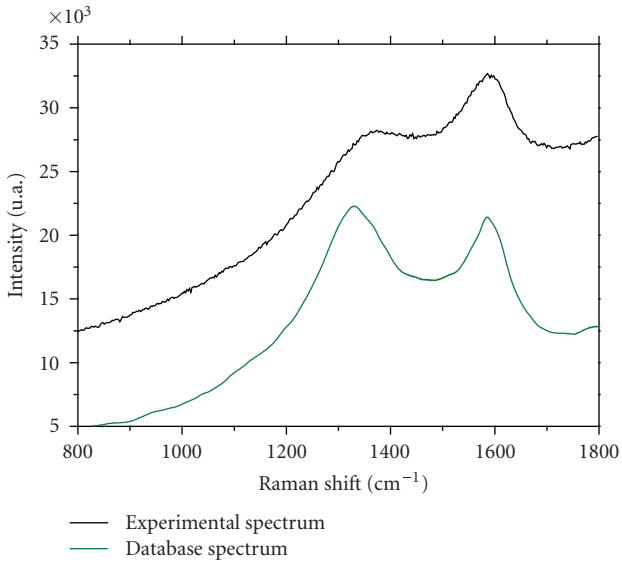

Figure 11: Raman spectrum of the dark region (sample TR03).

the spectrum shown in Figure 9, where a good agreement with the spectrum of calcite is obtained: in fact, the characteristic line around 1088 cm^{-1}, corresponding to the symmetric stretching of the carbonate, is well visible.

The Raman analyses have been also performed on the samples with a dark surface (TR03-TR05-TR06-TR09-TR11-TR12-TR15). In Figure 10, a microscope image of one of the studied surfaces is shown. Some of the spectra obtained are reported in Figures 11 and 12.

In the first spectrum, the typical bands of carbon black at 1325 cm^{-1} and 1580 cm^{-1} are present; while in the spectrum of the TR05 sample, the characteristic magnetite Raman line at 652 cm^{-1}, together with a large band at higher values of the Raman shift, is evident. Actually, according to the literature [18], also the Raman spectrum of lepidocrocite (γ-FeOOH) exhibits a broad band about 1322 cm^{-1}, therefore the presence of some iron oxyhydroxides on the surface of the sample cannot be excluded. While the carbon black is essentially composed by amorphous carbon and is obtained for partial combustion of wood, magnetite (Fe_3O_4) is an inorganic pigment with natural origin.

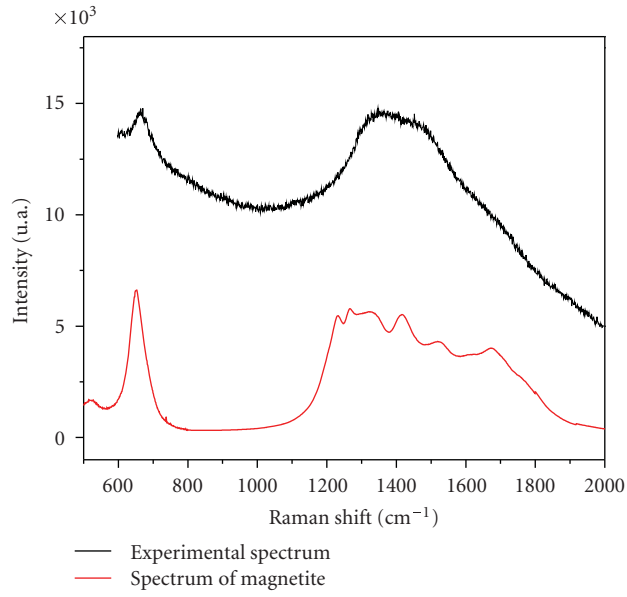

Figure 12: Raman spectrum of the dark region (sample TR05).

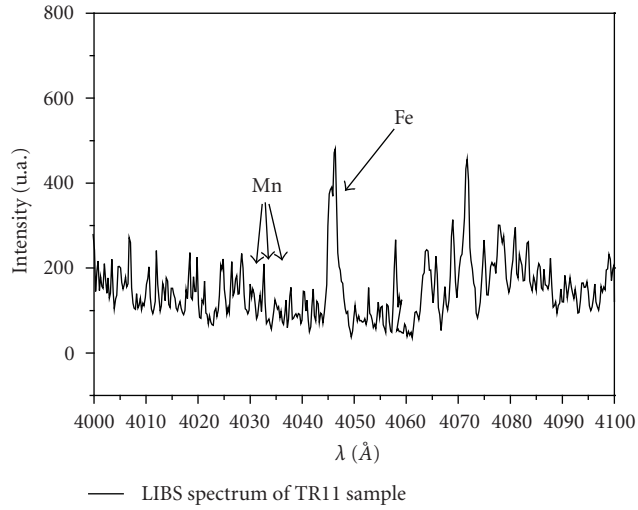

Figure 13: LIBS spectrum of the dark region (TR11 sample).

3.2. LIBS analysis

All the fragments studied with the Raman technique were also analyzed using the LIBS technique. The LIBS spectra have been acquired by averaging 20 laser shots on the sample surface. Every sample was moved after two shots in order to have a uniform measurement not affected by the development of the laser crater. The time delay and the gate of the acquisition were fixed at 1 and 2 microseconds, respectively. For what concerns the dark surfaces, the presence of manganese has not been revealed from the LIBS spectra for all the fragments belonging to the third typological characterization (Serra d'Alto type potteries). Therefore, one can exclude the use of a dark pigment based on manganese oxide for the first

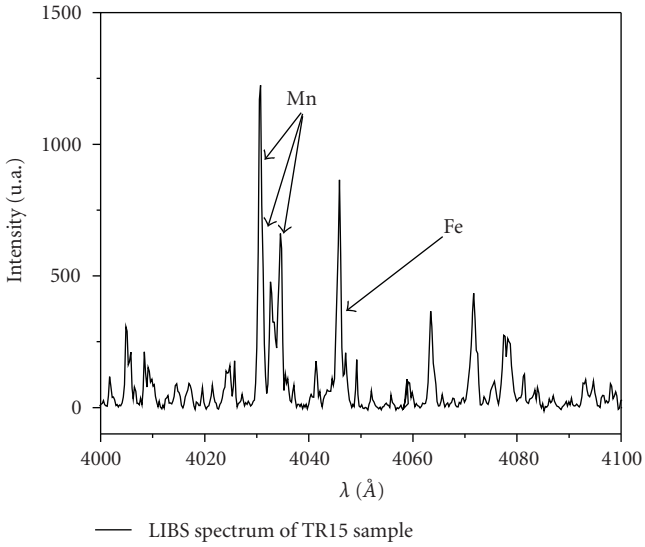

Figure 14: LIBS spectrum of the dark region (TR15 sample).

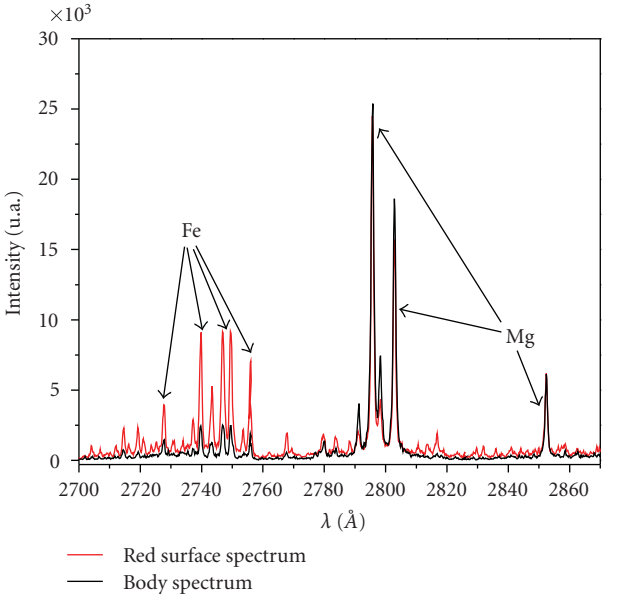

Figure 15: LIBS spectrum of the red region (TR13 sample).

two groups. In Figures 13 and 14, the LIBS spectra of TR11 and TR15 samples respectively are shown. The wavelength interval considered (4000–4100 Å) corresponds to the region where the more intense lines of manganese (4030 Å, 4033 Å and 4034.5 Å) should be visible, in the first case it is evident that they are not present, while in the second one they are well detectable.

On the other hand, the LIBS analyses performed on the red colored fragments showed a higher intensity of iron lines with respect to the clay body. Observing Figures 15 and 16, in fact, the increased intensity of the iron lines in the spectrum

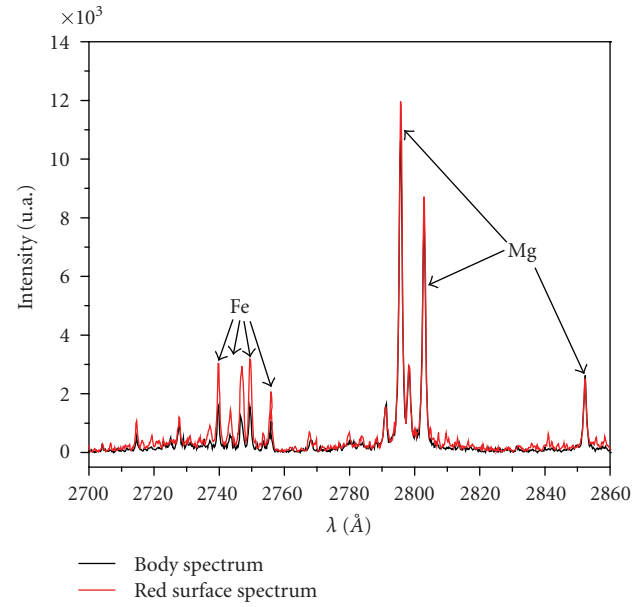

Figure 16: LIBS spectrum of the red region (TR04 sample).

relative to the surface is well visible; the two spectra have been normalized to the magnesium lines, which are characteristic of the clay and practically do not change from the surface to the bulk. This phenomenon appears more evident in the TR13 sample and this is in agreement with the hypothesis of the use of a red added pigment for coloring the sample surface.

3.3. Discussion of the results

Thanks to the joint use of Raman and LIBS techniques and in agreement with the results obtained with more traditional approaches, a good characterization both of the ceramic dough composition and of the pigments has been possible; at the same time, also useful information about the production of the Trasano site can be carried out. In phase III, very pure clay is used, whereas on the decorations amorphous carbon, calcite, and iron oxide have been recognized. Amorphous carbon has been used both for internal and external surface decoration of the pottery fragments in the painted strip. Calcite is the main component of the white traces inside the graffiti (TR03-TR06). In some cases (TR04-TR08-TR10), it has been very difficult to distinguish between the surface and the body due to the very fine granulometry, the partial vitrification, and the extreme thinness of the surface. In other cases (TR13-TR14), the LIBS analyses revealed the presence of a red pigments; while in samples TR03-TR06-TR11-TR12, the measurements suggest the possible coloring due to the making process together with a repetitive rubbing of the surface (according to a chemical phenomenon called peptidation) [19]. In phase IV, the figulina-type pottery starts to be produced, so the supplying of a different type of clay can be hypothesized. For what concerns the decoration styles, which is also changed with respect to Phase

III pottery, hematite, magnetite, and calcite are present. In particular, hematite is present together with calcite in the painted red stripes of TR01, TR02, and TR07 samples, even if the last fragment appears to be darker than the others; magnetite has been detected only in the TR05 sample. In phase V, the figulina-type pottery production belongs to the Serra d'Alto Culture [20], presenting probably the same mineral composition of the clay, but with the introduction of the use of a dark pigment based on manganese oxide (TR09-TR15).

4. CONCLUSIONS

The results reported show that the joint use of micro-LIBS and micro-Raman spectroscopy allows the complete characterization, both structural and elemental, of the pigments under study. The measurements performed with the two techniques are fast, reliable, and virtually nondestructive. The results obtained are, therefore, encouraging for the realization of an integrated micro-LIBS/micro-Raman prototype for *in situ* analysis of cultural heritage.

REFERENCES

[1] V. Tornari, V. Zafiropulos, A. Bonarou, N. A. Vainos, and C. Fotakis, "Modern technology in artwork conservation: a laser-based approach for process control and evaluation," *Optics and Lasers in Engineering*, vol. 34, no. 4–6, pp. 309–326, 2000.

[2] D. Anglos, C. Balas, and C. Fotakis, "Laser spectroscopic and optical imaging techniques in chemical and structural diagnostics of painted artwork," *American Laboratory*, vol. 31, no. 20, pp. 60–67, 1999.

[3] L. Burgio, K. Melessanaki, M. Doulgeridis, R. J. H. Clark, and D. Anglos, "Pigment identification in paintings employing laser induced breakdown spectroscopy and Raman microscopy," *Spectrochimica Acta Part B: Atomic Spectroscopy*, vol. 56, no. 6, pp. 905–913, 2001.

[4] M. Bicchieri, M. Nardone, P. A. Russo, et al., "Characterization of azurite and lazurite based pigments by laser induced breakdown spectroscopy and micro-Raman spectroscopy," *Spectrochimica Acta Part B: Atomic Spectroscopy*, vol. 56, no. 6, pp. 915–922, 2001.

[5] M. Castillejo, M. Martín, D. Silva, et al., "Laser-induced breakdown spectroscopy and Raman microscopy for analysis of pigments in polychromes," *Journal of Cultural Heritage*, vol. 1, supplement 1, pp. S297–S302, 2000.

[6] L. Bussotti, E. Castellucci, and M. Matteini, "The micro-Raman technique in the studies for the conservation of art works: identification of lakes in paints," *Science and Technology for Cultural Heritage*, vol. 5, no. 1, pp. 13–19, 1996.

[7] L. Burgio and R. J. H. Clark, "Library of FT-Raman spectra of pigments, minerals, pigment media and varnishes, and supplement to existing library of Raman spectra of pigments with visible excitation," *Spectrochimica Acta Part A: Molecular and Biomolecular Spectroscopy*, vol. 57, no. 7, pp. 1491–1521, 2001.

[8] C. Lofrumento, A. Zoppi, and E. M. Castellucci, "Micro-Raman spectroscopy of ancient ceramics: a study of French *sigillata* wares," *Journal of Raman Spectroscopy*, vol. 35, no. 8-9, pp. 650–655, 2004.

[9] A. W. Miziolek, V. Palleschi, and I. Schecter, *Laser-Induced Breakdown Spectroscopy (LIBS) Fundamentals and Applications*, Cambridge University Press, Cambridge, UK, 2006.

[10] D. Anglos, S. Couris, and C. Fotakis, "Laser diagnostics of painted artworks: laser-induced breakdown spectroscopy in pigment identification," *Applied Spectroscopy*, vol. 51, no. 7, pp. 1025–1030, 1997.

[11] V. Palleschi, G. Arca, S. Rastelli, A. Ciucci, and E. Tognoni, "Verso il laser intelligente: applicazione alla pulitura di monumenti," Internal Report B01LS/96, IFAM, Pisa, Italy, 1996.

[12] A. Ciucci, M. Corsi, V. Palleschi, S. Rastelli, A. Salvetti, and E. Tognoni, "New procedure for quantitative elemental analysis by laser-induced plasma spectroscopy," *Applied Spectroscopy*, vol. 53, no. 8, pp. 960–964, 1999.

[13] D. Bulajic, M. Corsi, G. Cristoforetti, et al., "A procedure for correcting self-absorption in calibration free-laser induced breakdown spectroscopy," *Spectrochimica Acta Part B: Atomic Spectroscopy*, vol. 57, no. 2, pp. 339–353, 2002.

[14] A. Ciucci, V. Palleschi, S. Rastelli, et al., "Trace pollutants analysis in soil by a time-resolved laser-induced breakdown spectroscopy technique," *Applied Physics B: Lasers and Optics*, vol. 63, no. 2, pp. 185–190, 1996.

[15] C. Corrado and E. Ingravallo, "L'insediamento di Masseria Le Fiatte (Manduria) nel popolamento neolitico del nord-ovest del Salento," *Stdi di Antichità*, vol. 5, pp. 5–78, 1988.

[16] J. Guilaine, G. Cremonesi, G. Radi, and J. Coularou, "Trasano e la céramique gravée materane," in *Autour de Jean Arnal*, pp. 123–137, Université des Sciences et Techniques du Languedoc, Montpellier, France, 1990.

[17] http://www.chem.ucl.ac.uk/resources/raman/pigfiles/.

[18] D. L. A. De Faria, S. Venâncio Silva, and M. T. De Oliveira, "Raman microspectroscopy of some iron oxides and oxyhydroxides," *Journal of Raman Spectroscopy*, vol. 28, no. 11, pp. 873–878, 1997.

[19] G. Radi, "Trasano Basilicata," in *Le ceramiche impresse nel Neolitico antico in Italia e Mediterraneo*, pp. 695–705, Istituto Poligrafico e Zecca dello Stato, Roma, Italy, 2003.

[20] T. DiFraia, "Resti di un villaggio della cultura di Serra D'Alto a Saldone presso Metaponto (Lucania)," *Atti della Società Toscana di Scienze Naturali, Memorie, Serie A*, vol. 77, pp. 54–77, 1970.

Hindawi Publishing Corporation
Laser Chemistry
Volume 2006, Article ID 18792, 8 pages
doi:10.1155/2006/18792

Research Article

Automatic Identification of Artistic Pigments by Raman Spectroscopy Using Fuzzy Logic and Principal Component Analysis

M. Castanys, M. J. Soneira, and R. Perez-Pueyo

Departament de Teoria del Senyal i Comunicacions (TSC), Universitat Politècnica de Catalunya (UPC), C/ Sor Eulàlia de Anzizu s/n, Campus Nord D5, 08034 Barcelona, Spain

Received 15 September 2006; Revised 26 October 2006; Accepted 27 October 2006

Recommended by Marta Castillejo

This work offers an automatic identification system of Raman spectra of artistic pigments. The proposed methodology is based on a fuzzy logic system, and uses principal component analysis to reduce redundancies in data and the correlation operator as an index of similarity between two Raman spectra. Moreover, as sometimes pigments are used in mixtures by artist, the designed system is able to recognize binary mixtures of pigments on the basis of their Raman fingerprints.

1. INTRODUCTION

The identification of materials used in artworks is of great importance for conservation, restoration, and comprehensive study of our historical and cultural heritage. Raman spectroscopy is a well-established tool in the investigation of a wide range of archaeological and art historical artefacts. It has proved particularly useful for identifying pigments [1–6]. Its great popularity stems from its ability to provide definitive identification due to its high specificity; its applicability "in situ" allowing the analysis directly on unprepared sample and its nondestructive behavior. This analytical technique is based on the Raman effect that provides chemical and structural information of almost any material allowing its identification. When monochromatic light encounters matter, most of the scattered light has the same wavelength as the incident light. However, a small fraction of the scattered light is shifted in a different wavelength by the molecular vibrations and rotations in the sample. The representation of this shifted light is named Raman spectrum, and contains many sharp bands characteristics of the sample, allowing its identification without ambiguity. This identification is usually made by a user by visual inspection of the Raman spectrum. There are two strategies to make a visual analysis, one consists of comparing the whole unknown spectrum with the known patterns spectra and the other is based on comparing the wavenumber positions of the Raman bands of the unknown spectrum with those of the reference spectra. In any case, thus are a time consuming process and an imprecise process. Moreover, some problems like noise and fluorescence interference inherent to the own acquisition of the spectra, or the possibility to detect pigment mixtures make this comparison difficult and dependent on user's experience. On effect, artists often paint with pigment mixtures and apply transparent coatings, which complicate spectroscopic signatures and confound protocols for on-painting identification. So, it is useful and desirable to develop methods to identify spectra in an automated way, that is, that do not depend on the subjective assessment of user.

The above commented identification strategies in a conventional visual process are equally valid but there are some differences between them. While the first method involves only one step, which is the comparison of the whole spectrum of the analyzed sample with those of the patterns, the second involves two steps. First, it is necessary to locate the wavenumber position of the Raman bands, this can be made automatically [7] or not. And second, once the Raman bands are detected, the identification of the unknown spectrum is possible by searching the coincidence with the Raman bands of the reference spectra in an automated way [8, 9]. Both approaches to the problem of the automatic identification have been dealt with fuzzy logic which has demonstrated being a

powerful tool with a large number of applications in particular to signal processing [10, 11]. Although both points of view are possible and useful for identifying, the comparison of the whole spectra could be more suitable when the spectra have many bands and/or common bands to each other. Furthermore, when pigments to identify have many common Raman bands, it could be difficult to assess if the analyzed spectrum is representative of one pigment or it corresponds to a mixture of pigments. The comparison of the whole spectrum can overcome this situation. So, the work described in this paper offers an automatic system to identify the pigment or pigments in binary mixtures, to which the measured spectrum can correspond based on fuzzy logic. This signal processing tool has demonstrated to be useful to deal with the uncertainty present in the measured spectrum. The methodology proposed follows the guidelines of visual comparison but automates the decision-making process so that, subjective errors will be avoided. The system checks which spectrum or spectra of the pattern's library of Raman spectra are the most similar to the unknown spectrum. This method of comparison can be more or less laborious based, among other things, on the spectral database and also on the quality of the measured spectrum. Hence, it is desirable and even necessary to define a suitable database of reference pigments taking into account the available data about the analyzed artefact. For instance, the type of painted work of art such as easel paintings, wall paintings, and so forth, supposed date or author of the artwork, can define the Raman spectral library of patterns, well suited for enhancing the efficiency of the identifier system. Furthermore, in order to reduce redundancies in data which may be important as the library database increases, principal component analysis (PCA) is used [12].

This paper is organized as follows: in the second section a brief description of the used mathematical tools is explained; in the third section the proposed fuzzy rule-based identification system is described; in the fourth section the results obtained when apply the proposed system to different Raman spectra are shown and discussed; and in the fifth section the conclusions are summarized.

2. THEORY

It is well known that a Raman spectrum can provide a large amount of information about a sample, and as the majority of signals, it can be divided into two parts: the information signal and the noise. The signal is the part which contains the desired information and which allows a sample characterization, whereas the noise is the unwanted information which does not report any specific trait of the analyzed material. It must be stood out that the consideration of what is signal and what is noise depends on the analysis which will be made, then in the case of pigment identification the useful information is extracted from the Raman bands position. Noise in Raman spectroscopy can be mainly classified into three categories: shot noise, which is the result of the statistical nature of light, fluorescence, and cosmic rays. These three types of noise are inherent on each Raman measure, but taking some precautions and some software and hardware procedures, they can be reduced. Hence, one assumes that the Raman spectra which will be processed will be collected in the optimal conditions to reduce noise as much as possible. As well as, some signal treatment must be done to ensure the success of the analysis which is in our case the identification of the analyzed pigment.

As it has been mentioned, the identification methodology is based on the comparison between spectra, so it is necessary that the spectra were stored in a compatible way. Note that a Raman spectrum could be read as a vector of N points where each of its coordinates, $e(i)$, corresponds to the Raman intensity for the wavenumber v_i. Then, the interpolation step ensures that the same coordinate for each spectrum corresponds to the Raman intensity at the same wavelength, and that each of them has the same number of points. Another arrangement that results useful is to normalize the spectra in order to reduce the impact of measurement conditions. Some characteristics of the Raman bands depend on instrumental conditions as the spot of the laser, its wavelength, or the time of exposure, which can change for different measurements and which are then not specific of the analyzed sample. The normalized spectra maintain the relative relation between their Raman bands and their Raman intensity values ranging from 0 to 1. Finally, the fluorescence is a radiated phenomenon, generated by many materials, which underlies the measured spectra. Several techniques involving hardware and software have been devised to minimize its presence in order to resolve and analyze the Raman spectra. In this work, the most popular polynomial fitting method, available in the software LabSpec of our laboratory, has been used.

Due to the fact that each spectrum is a vector of N points, with N being of the order of 1000, we decide to reduce its dimension by means of a data reduction tool called the principal component analysis (PCA). The most important use of this chemometric technique is to represent the N-dimensional data in a smaller number of dimensions, usually two or three, without loss of information [13–15]. With this data reduction, the searching identification algorithm will be more efficient and less tedious. The PCA is one of the most used multivariate procedures because it is easy to interpret and permit an explanation for the maximum variability of initial distribution. In fact, PCA is a mathematical method of reorganizing information in a data set of samples. What PCA does is to discover new variables called principal components (PCs) which account for the majority of the variability of the data. Then the scores associated with significant PC can be used to represent the spectra. This permits to represent the data in 2-dimensional plots in which one can observe for example groupings of objects or outliers, and define the structure of a data. In some, PCA is a way of identifying patterns and expressing the data in such way so as to highlight their similarities and differences.

The aim of this research is to find out to which pigment corresponds the measured Raman spectrum. As it has been mentioned, the most frequently methodology to identify unknown Raman spectra is based on the comparison of the analyzed spectrum with some well-known spectra, called patterns, searching which of them is the most similar to it. In

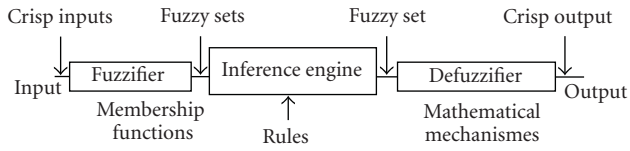

Figure 1: Basic scheme of a fuzzy logic system.

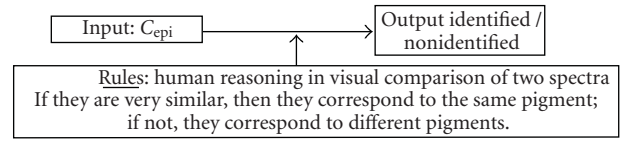

Figure 2: Chart of the fuzzy logic system for the pigment identification.

order to make this process systematic and not depending on the subjectivity of any user, in this work the comparison is made by a mathematic operator which quantifies the similarity between spectra in an automatic and objective way. One standard mathematic operator to estimate the degree of similarity between two spectra is the correlation coefficient [16]. Once the Raman spectrum of the analyzed pigment has been collected, $e(i)$, it is compared with each spectra of the library, $p(i)$. The correlation coefficient between the two spectra is computed as follows:

$$C_{ep} = \frac{\sum_k \left[(e(i) - m_e) \cdot (p(i) - m_p)\right]}{\left(\sqrt{\sum_k (e(i) - m_e)^2} \cdot \sqrt{\sum_k (p(i) - m_p)^2}\right)}, \quad (1)$$

where m_e and m_p are the mean values of e and p, respectively. Note that the higher the coefficients are, with the maximum equal to one, the more similar the spectra are. Nevertheless, even though spectra have been treated as in the preceding paragraph we have described, they inevitably contain some noise which alters the information and makes the correlation analysis nondefinitive. That is, even if we compute the correlation between two spectra coming from the same material, the result could not be the maximum value. So, the results obtained by the correlation coefficient must be interpreted, that is, evaluate if the value is high enough to consider that the two spectra correspond to the same material. This interpretation is made by means of fuzzy logic.

Fuzzy logic aims at exploiting the tolerance of imprecision and uncertainty in order to have a close resemblance to human decision making. Fuzzy logic appeared in the sixties by Lofti Zadeh and as the result of searching a mathematical option to overcome the inflexibility of the classic logic which only contemplates the possibility that one can belong or not to a set. Fuzzy logic is subtended by the theory of fuzzy sets which assigns to each element a degree of membership to it in a range of 0 to 1. Then, in fuzzy logic, the truth of any statement becomes a matter of degree [17]. So, a fuzzy set is a set without a crisp, clearly defined boundary, and it can contain elements with only a partial degree of membership. Fuzzy logic is concerned with the formal principles of approximate reasoning, with precise reasoning viewed as a limiting case. In this sense, fuzzy logic incorporates an alternative way of thinking, which allows modeling complex systems using a higher level of abstraction originating from human knowledge and experience. A fuzzy logic system, Figure 1, maps nonlinearly crisp inputs into crisp outputs. It is unique in that it is able to simultaneously handle numerical data and linguistic knowledge by means of a group of rules which models the proposed problem [18]. These rules are expressed as a collection of if-then statements which may be provided by experts or can be extracted from numerical data. The fuzzifier assigns to every numerical input value a degree of membership to each input Fuzzy sets through the membership functions associated to them. This first step is needed in order to active rules which are in terms of linguistic variables, with Fuzzy sets associated to them. The inference engine provides the way in which rules are combined and by means of different logical operators modifies the defined output fuzzy sets. Finally, the defuzzifier maps output fuzzy sets into crisp numbers applying mathematical mechanisms in order to obtain the final result.

Hence, in our frame, Fuzzy logic appears as the best tool for modeling in a mathematical language and by means of a Fuzzy system the human perception of similarity.

3. FUZZY RULE-BASED IDENTIFICATION SYSTEM

As we had seen in a previous section, in order to identify a pigment, we will apply the correlation coefficient to compare the unknown spectrum to each of the selected patterns. The problem of the noise in the measures will make the value of correlation difficult to interpret. Moreover, it is known that a correlation equal to 1 corresponds to two signals which are identical, and a value of 0 corresponds to two completely different signals (uncorrelated signals), but what happens with the others values? What do we have to interpret with a correlation of 0.23? The interpretation of all the possible values will be made by means of a fuzzy logic system. The crisp input value will be the correlation coefficient computed between the unknown spectrum (e) and one of the patterns (p_i), the if-then rules model the human reasoning employed in a visual comparison, and finally the output of the system will be the identification or not of the analyzed pigment (see Figure 2).

On the other hand, in a practical situation, the complexity of pictorial layer is a problem to be solved and mixtures of pigments are the first step for a comprehensive view of artworks. So, the Raman trace of two or more pigments could appear in a measured Raman spectrum. The mixtures could then confound searching protocols for on-painting identification. Then, we propose a system to identify artistic pigments including cases where various pigments are mixed.

The proposed design is then based on two fuzzy logic systems (see Figure 3). The first step is to compare the unknown spectrum with each of the patterns; the result of this system is a list of patterns which are candidates to be the unknown

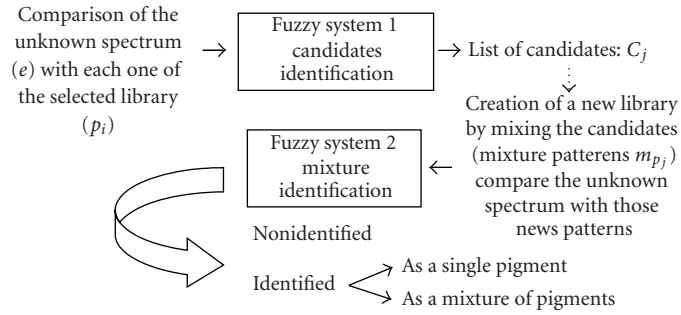

Figure 3: Chart of the global fuzzy logic system for the pigment identification.

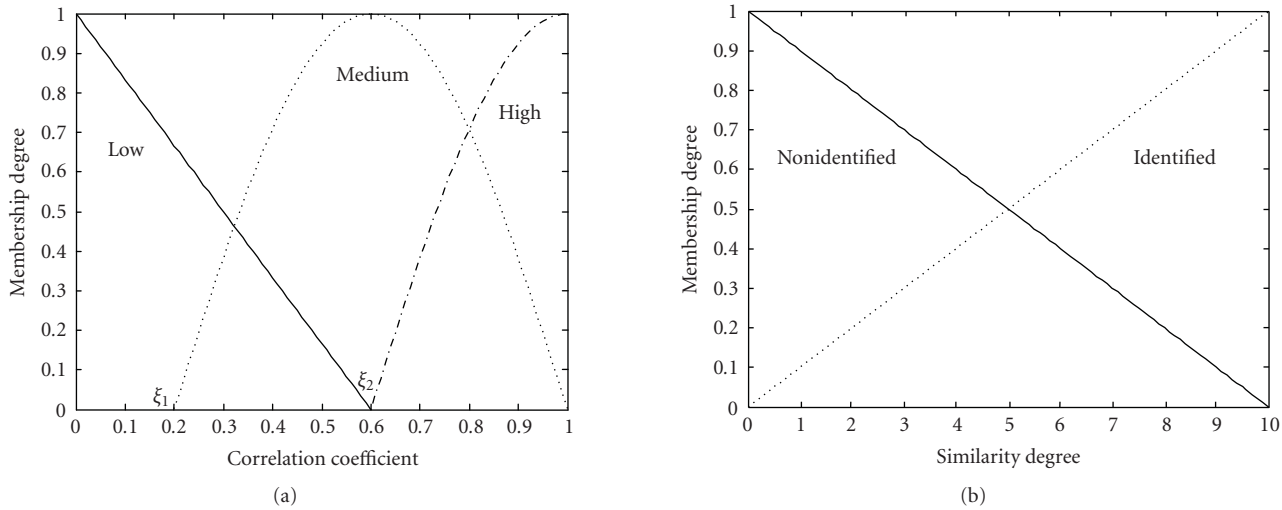

Figure 4: (a) Input fuzzy sets, (b) the output fuzzy sets.

pigment. Then, if there is only one candidate, the unknown spectrum can be identified or not. But, if there is more than one candidate, a new library is made by mixing them. The second step is to compare the analyzed Raman spectrum with each of these new patterns. The final result would be that the analyzed spectrum was identified as a mixture, as a single pigment, or simply nonidentified.

The first system design follows the guideline proposed in [7]. The crisp inputs are the correlation coefficients, C_{epi}, computed between the unknown spectrum (e) and each of the reference Raman spectra (p_i) stored in the selected library. For this input linguistic concept, three fuzzy sets "low," "medium," and "high" have been chosen. Each of them is defined by a particular membership function that is to say, the fuzzy set "low" has a trapezoidal membership function while the membership functions associated with the fuzzy sets "high" and "medium" are cosine functions (see Figure 4(a)).

The two threshold values called ξ_1 and ξ_2, in Figure 4(a) divide the universe of discourse (input space range) into three different zones. As we have mentioned, the reference library will be constructed depending on the pigments that we want to analyze and/or taking into account the available information about the sample. The identification process depends on this selection, with the more similar patterns are, the more difficult the identification is. In order to overcome this dependence, the bounds of each fuzzy set are computed from the maximum correlation coefficient between patterns as follows: $\xi_1 = 2 * C_{\max} - 1$ and $\xi_2 = C_{\max}$, where $C_{\max}$ is the maximum correlation coefficient between the reference Raman spectra (it determines which are the more similar patterns). So, they determine the degree of membership of the input correlation coefficient to the fuzzy sets; high, medium or low.

As we have said before, two output fuzzy sets labeled with the linguistic concepts "identified" and "nonidentified" (see Figure 4(b)) have been defined. The output crisp variable is a single number obtained by the defuzzifier process by means of the centroide computation of the final output fuzzy set. This output value is called "degree of similarity" (g_{nepi}) and quantifies the likeness of the two compared spectra.

The fuzzy rules define the way to obtain the final crisp values from the input data, in our identification problem, there are only four rules to be considered.

Rule 1. If C_{epi} is *low*, then the spectrum **e** is *nonidentified* with p_i.

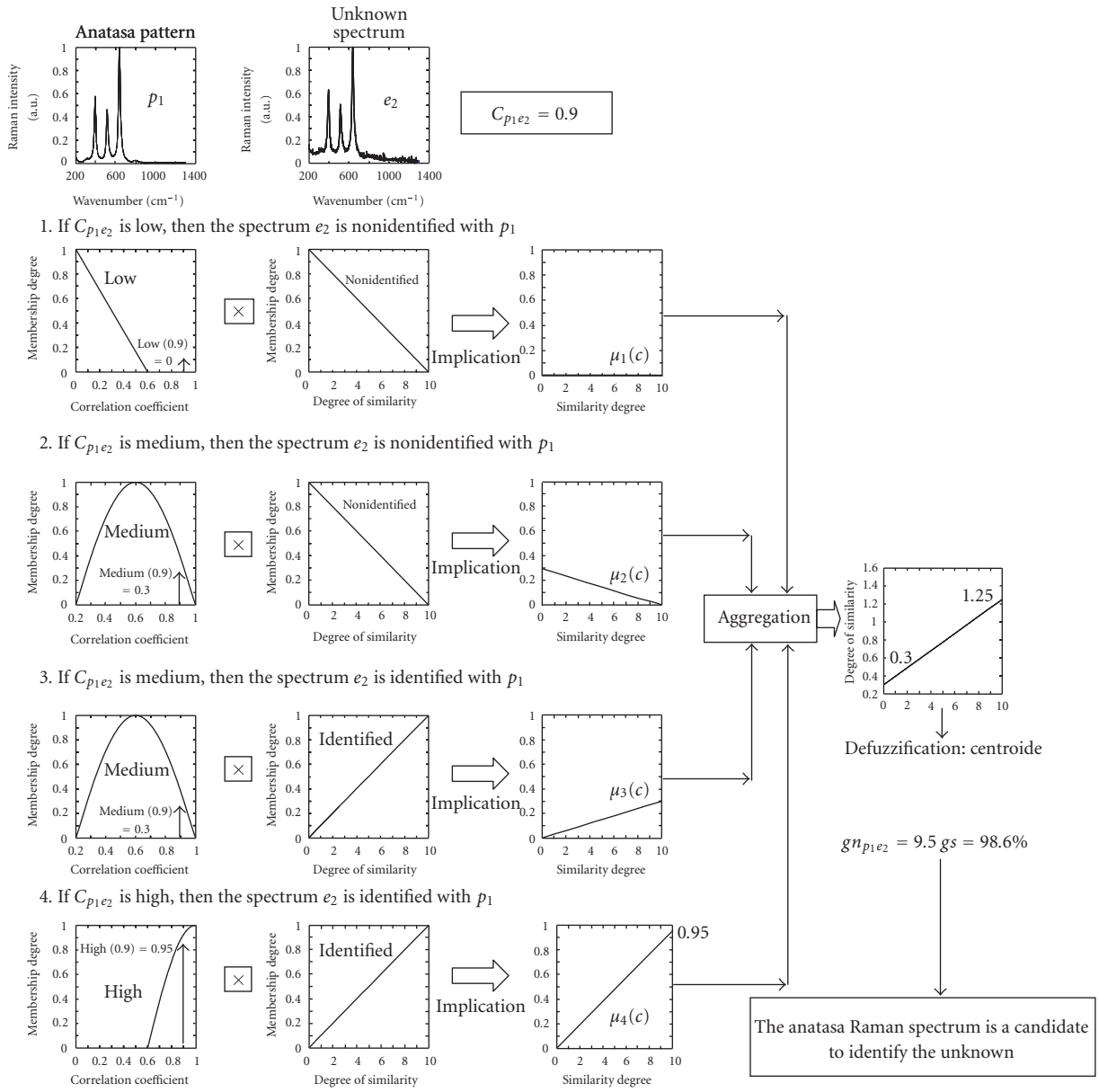

Figure 5: Application example of the identification of an unknown spectrum.

Rule 2. If C_{epi} is *medium*, then the spectrum **e** is *nonidentified* with p_i.

Rule 3. If C_{epi} is *medium*, then the spectrum **e** is *identified* with p_i.

Rule 4. If C_{epi} is *high*, then the spectrum e is *identified* with p_i.

The rules 2 and 3 which have the same antecedent but a different consequent are used to solve the cases where the values of correlation are ambiguous. For example, when two spectra have some Raman bands in common, they are similar but not identical, so the output of the system must be *nonidentified* even if a medium value for its correlation coefficient is obtained. Another example could be when the analyzed spectrum is compared with its corresponding pattern, but the measure is strongly affected by noise, and then the correlation coefficient is not as high as it is supposed to be. In such case, although the correlation is medium too, the unknown pigment must be *identified* with its corresponding pattern.

The implication of rules is made using the product operator and a fuzzy set is obtained for each one. Every output fuzzy set is aggregated, by means of the sum, into a single output fuzzy set. Finally, using the centroide method, the degree of similarity between e and $p_i(g_{\text{nepi}})$, is calculated. The system

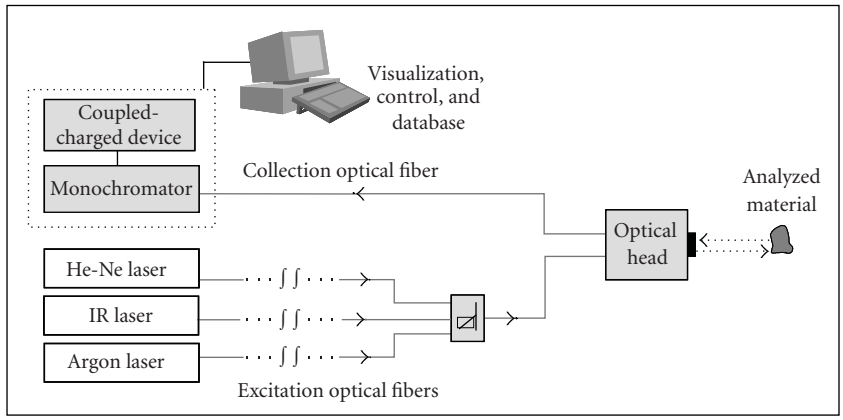

Figure 6: Schematic diagram of the Raman laboratory at the UPC.

has been scheduled for considering each pattern a candidate with which the degree of similarity is higher than 5/10. With the purpose to evaluate the reliability when a reference spectrum is considered by the system as a candidate to identify the unknown spectrum, we define a new variable named degree of security or certainty (g_S). The definition of this degree has been obtained empirically and it is calculated as $g_s(g_{\text{nepi}}) = 100(g_{\text{nepi}}/8 - 1/4)$. Next, in order to clarify how this first system works, an application example is shown. An unknown Raman spectrum is compared with the pattern spectrum of the anatase pigment. The spectra and the evaluation of the four rules are shown in Figure 5.

The design of the second fuzzy logic system is based on the first one. Nevertheless, in this system, the library is not initially defined, but it changes depending on which candidates have been found by the first system. As we have mentioned, the reference spectra of the new library are obtained mixing the candidates two by two. So, in this first approach, the global system can only identify binary mixtures that are the most common mixtures made by artists. The extension of the system in order to be able to identify mixtures of more than two pigments will be a future work. The system runs like the first one, that is, it has the same variables and fuzzy sets, as well as the same rules but it uses the new spectral library. Then, if the first system considers C candidates for the identification, in the second system the used library will be formed by $C(C-1)/2$ patterns.

4. EXPERIMENTAL RESULTS

Let we see some experimental results of the proposed system. The Raman spectra analyzed had been measured in the Raman laboratory of the UPC. This laboratory incorporates optical fibre which allows Raman measurements to be made far from the Raman analyzer without extraction of any sample. Its main instrumentation is a laser (monochromatic source), a monochromator, a CCD (charge-coupled device) detector, and a computer (see Figure 6). The output of the laser (which can be a He-Ne, Argon, or IR laser) is guided by the excitation optical fibre through the optical head to the analyzed material. The radiation scattered by the material, which contains the Raman signal, is guided through the collection fiber to the monochromator where it is spectrally split and then detected to the CCD. The spectrum is stored and visualized in the PC which, furthermore, controls the Raman equipment.

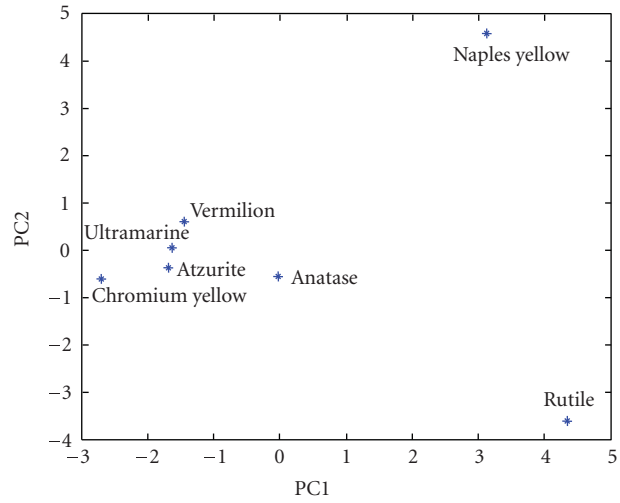

Figure 7: The library projection in the space of PC.

On the other hand, the chosen library for testing the system has been made selecting some of the more usual pigments found in paintings, which are the anatase, the ultramarine blue, the atzurite, the vermillion, the Naples yellow, the rutile, and the chromium yellow. In Figure 7 it is shown the representation of each of there projection in the space of PCA (PC1 versus PC2). Note that the closer they are, the more similar they are.

The first example represents the identification of the unknown Raman spectrum represented in Figure 8(a). The first fuzzy system returns as candidates, the anatase and rutile pigments. By means of the application of the second system, the analyzed pigment is identified as a mixture of anatase and rutile with a similarity degree equal to 8, 5/10 and a security

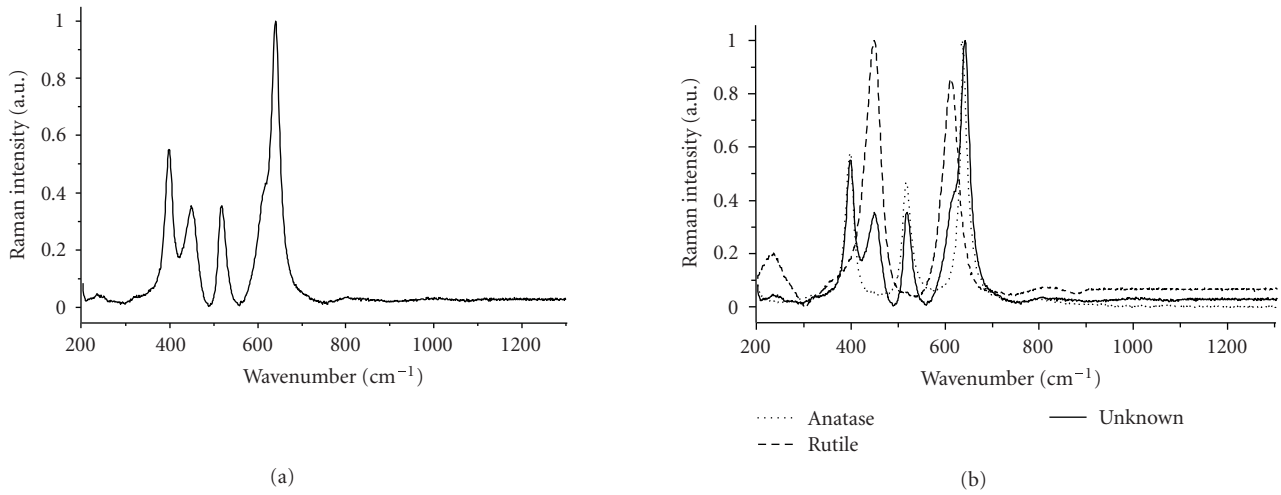

Figure 8: (a) Unknown Raman spectrum, (b) the recognized two patterns in the unknown spectrum.

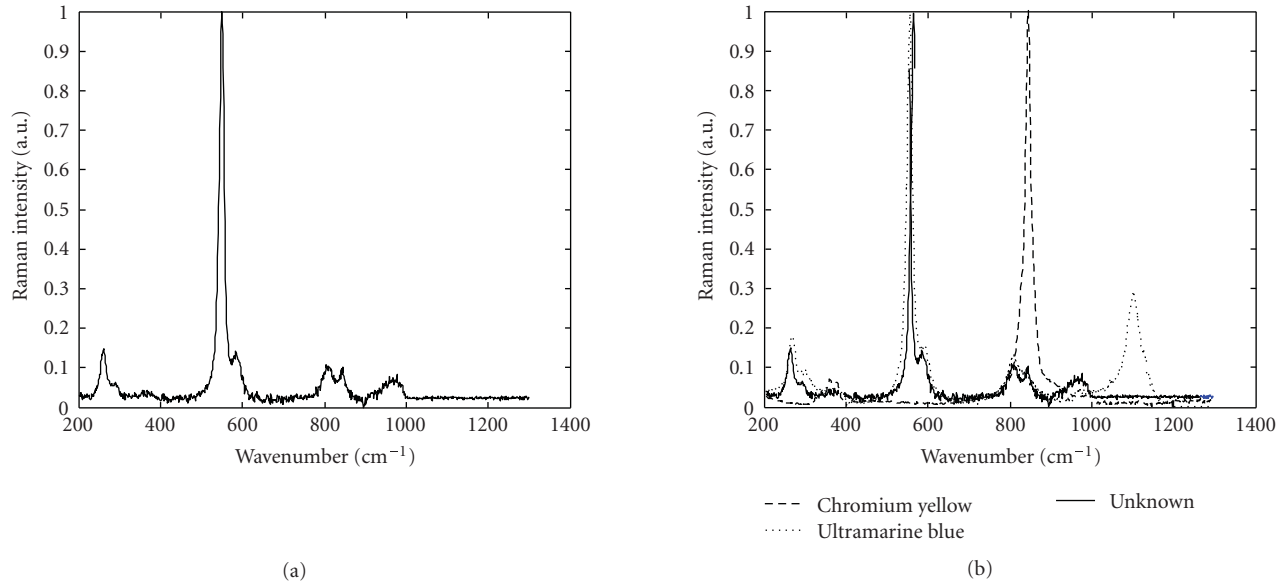

Figure 9: (a) Unknown Raman spectrum, (b) the recognized two patterns in the unknown spectrum.

degree of 81%. This mixture could appear in artwork analysis if, for example, a white point painted originally with anatase has been later repainted with the most modern white pigment as the rutile.

In the second example, three candidates have been determined by the first fuzzy logic system: ultramarine blue, chromium yellow, and Naples yellow. The second system which uses a library formed by the binary mixtures of these three candidates identifies the analyzed pigment as a mixture of ultramarine blue and chromium yellow. In this case the similarity degree with the mixture is 6.3/10, and the security degree is equal to 53.7%. It can be noted that the degree of similarity is lower than the first example. It is because, as it can be seen in Figure 9, the intensity of the Raman band of the analyzed spectrum which corresponds to the fundamental Raman band of the chromium yellow is lower than the one of the pattern. This difference in the intensities is not decisive because its position is the same, and this is what contains the Raman information for identifying.

It must be pointed out that if in a measured spectrum there is no Raman band of a pigment which is in a mixture, it is not possible to identify it neither in a visual way and nor in automatic way. Obviously, if there is no Raman fingerprint, the identification is impossible.

5. CONCLUSIONS

This work presents a fuzzy logic system like a useful and valid system to recognize automatically experimental Raman spectra following the guidelines of the visual identification. The

obtained results show that fuzzy logic offers a versatile and flexible technique, easily adapted to the requirements of the problem to solve. With the proposed system, a nonexpert on Raman spectroscopy is able to identify the Raman fingerprint of any pigment, overcoming ambiguous situations which could be produced by noise or pigments mixtures. Note that, even if the system is robust, it is required that the experimental conditions of measurement should be as suitable as possible. Finally, it must be pointed out that the system has been designed in MATLAB and has a very short time of processing.

ACKNOWLEDGMENT

This work was supported by the CICYT project reference TEC 2005-07239 of the Spanish government.

REFERENCES

[1] A. P. Middleton, H. G. M. Edwards, P. S. Middleton, and J. Ambers, "Identification of anatase in archaeological materials by Raman spectroscopy: implications and interpretation," *Journal of Raman Spectroscopy*, vol. 36, no. 10, pp. 984–987, 2005.

[2] T. D. Chaplin, A. Jurado-López, R. J. H. Clark, and D. R. Beech, "Identification by Raman microscopy of pigments on early postage stamps: distinction between original 1847 and 1858–1862, forged and reproduction postage stamps of Mauritius," *Journal of Raman Spectroscopy*, vol. 35, no. 7, pp. 600–604, 2004.

[3] Ph. Colomban and V. Milande, "On-site Raman analysis of the earliest known Meissen porcelain and stoneware," *Journal of Raman Spectroscopy*, vol. 37, no. 5, pp. 606–613, 2006.

[4] R. J. H. Clark and S. Mirabaud, "Identification of the pigments on a sixteenth century Persian book of poetry by Raman microscopy," *Journal of Raman Spectroscopy*, vol. 37, no. 1–3, pp. 235–239, 2006.

[5] T. L. Weis, Y. Jiang, and E. R. Grant, "Toward the comprehensive spectrochemical imaging of painted works of art: a new instrumental approach," *Journal of Raman Spectroscopy*, vol. 35, no. 8-9, pp. 813–818, 2004.

[6] D. Anglos, "Laser-induced breakdown spectroscopy in art and archaeology," *Applied Spectroscopy*, vol. 55, no. 6, pp. 186A–205A, 2001.

[7] R. Perez-Pueyo, M. J. Soneira, and S. Ruiz-Moreno, "A fuzzy logic system for band detection in Raman spectroscopy," *Journal of Raman Spectroscopy*, vol. 35, no. 8-9, pp. 808–812, 2004.

[8] P. M. Ramos, J. Ferré, I. Ruisánchez, and K. S. Andrikopoulos, "Fuzzy logic for identifying pigments studied by Raman spectroscopy," *Applied Spectroscopy*, vol. 58, no. 7, pp. 848–854, 2004.

[9] M. Castanys Tutzò, R. Perez-Pueyo, M. J. Soneira, and S. Ruiz Moreno, "Fuzzy logic: a technique to Raman spectra recognition," *Journal of Raman Spectroscopy*, vol. 37, no. 10, pp. 1003–1011, 2006.

[10] J. Hsieh, "Image enhancement with a fuzzy logic approach," *Electronics Letters*, vol. 31, no. 9, pp. 708–710, 1995.

[11] F. Russo, "Fuzzy systems in instrumentation: fuzzy signal processing," *IEEE Transactions on Instrumentation and Measurement*, vol. 45, no. 2, pp. 683–689, 1996.

[12] D. L. Massart, B. G. M. Vandeginste, S. N. Deming, Y. Michotte, and L. Kaufman, *Data Handling in Science and Technology*, Chemometrics: A Textbook, Elsevier, Amsterdam, The Netherlands, 1998.

[13] P. Vandenabeele, A. Hardy, H. G. M. Edwards, and L. Moens, "Evaluation of a principal components-based searching algorithm for Raman spectroscopic identification of organic pigments in 20th century artwork," *Applied Spectroscopy*, vol. 55, no. 5, pp. 525–533, 2001.

[14] D. Uy and A. E. O'Neill, "Principal component analysis of Raman spectra from phosphorus-poisoned automotive exhaust-gas catalysts," *Journal of Raman Spectroscopy*, vol. 36, no. 10, pp. 988–995, 2005.

[15] H. G. M. Edwards, N. F. Nik Hassan, and N. Arya, "Evaluation of Raman spectroscopy and application of chemometric methods for the differentiation of contemporary ivory specimens I: elephant and mammalian species," *Journal of Raman Spectroscopy*, vol. 37, no. 1–3, pp. 353–360, 2006.

[16] F. M. Howari, "Comparison of spectral matching algorithms for identifying natural salt crusts," *Journal of Applied Spectroscopy*, vol. 70, no. 5, pp. 782–787, 2003.

[17] J. Yen and R. Langari, *Fuzzy Logic Intelligence, Control and Information*, Prentice-Hall, Upper Saddle River, NJ, USA, 1999.

[18] J. M. Mendel, "Fuzzy logic systems for engineering: a tutorial," *Proceedings of the IEEE*, vol. 83, no. 3, pp. 345–377, 1995.

Hindawi Publishing Corporation
Laser Chemistry
Volume 2006, Article ID 82823, 5 pages
doi:10.1155/2006/82823

Research Article

Assisted Interpretation of Laser-Induced Fluorescence Spectra of Egg-Based Binding Media Using Total Emission Fluorescence Spectroscopy

Austin Nevin[1,2] and Demetrios Anglos[1]

[1] *Institute of Electronic Structure and Laser, Foundation for Research and Technology-Hellas (IESL-FORTH), P.O. Box 1527, 71110 Heraklion, Greece*
[2] *Courtauld Institute of Art, Somerset House, Strand, London WC2R 0RN, UK*

Received 13 September 2006; Revised 20 October 2006; Accepted 27 October 2006

Recommended by Marta Castillejo

Laser-induced fluorescence (LIF) spectroscopy can provide nondestructive, qualitative analysis of protein-based binding media found in artworks. Fluorescence emissions from proteins in egg yolk and egg white are due to autofluorescent aromatic amino acids as well as other native and age-related fluorophores, but the potential of fluorescence spectroscopy for the differentiation between binding media is dependent on the choice of a suitable excitation wavelength and limited by problems in interpretation. However, a better understanding of emission spectra associated with LIF can be achieved following comparisons with total emission fluorescence spectra where a series of consecutive emission spectra are recorded over a specific range. Results using nanosecond UV laser sources for LIF of egg-based binding media are presented which are rationalised following comparisons with total emission spectra. Specifically, fluorescence is assigned to tryptophan and oxidation products of amino acids; in the case of egg yolk, fatty-acid polymerisation and age-related degradation products account for the formation of fluorophores.

1. INTRODUCTION

The analysis and understanding of painting materials is central to conservation, and often requires determination of the binding medium. Paintings often consist of multiple layers of pigments, colourants, and dyes which are typically dispersed in a matrix (binding medium) applied over a substrate and are often coated (varnished). Protein-based materials including egg white and egg yolk have traditionally been used as binding media and in conservation treatments; their identification can be critical for conservation, is of art historical interest, and is a challenge to the conservation scientist. However, analysis of proteins and other binding media typically involves taking samples so that characterisation using noninvasive methods is clearly advantageous due to the limitations associated with sampling of paintings. Recent advances in laser-induced fluorescence (LIF) spectroscopy have demonstrated a potential alternative nondestructive, qualitative means of investigating and analysing materials found in works of art; the interpretation of LIF spectra aided by information from total emission spectra is the focus of this article.

Fluorescence spectroscopy is widely applied for protein analysis in many fields, due to intrinsic fluorescence from aromatic amino acids tryptophan, tyrosine, and phenylalanine [1, 2]. Especially sensitive to changes in the structure and environment, fluorescence emissions of amino acids are often used to follow dynamic reactions of known molecules in solution rather than for the identification of specific materials or proteins. In addition to amino acid fluorescence, a large range of fluorescent degradation products from aged proteins have been identified [3]. These include both photooxidation products from the combination and modifications of amino acids and cross-linkage reactions between amino acids and other compounds (e.g., sugars). For instance, the formation of dityrosine, which can occur both at the ortho- and para- positions, has been documented both with free amino acids [4] and in solid protein films [5].

However, fluorescence spectroscopy, including LIF, has not had widespread applications in the analysis of paintings,

and specifically binding media. Initial research using spectrofluorimetry on artists' materials focused on the fluorescence of films of oil-based media [6] as well as on pigments bound in various media [7, 8]. Investigations of LIF for the analysis of protein-based binding media have been limited to few instances; for example, LIF has been used as a monitoring tool for the laser cleaning of egg tempera [9].

One problematic aspect of fluorescence analysis of proteins, especially in mixtures, is the interpretation of fluorescence spectra. This is due to characteristically broad signals found with macromolecular fluorescence, and to the lack of investigations of the fluorescence properties of complex mixtures of the proteins found in works of art. Fluorescence databases or standards of binding media are not available, and single excitation spectra alone do not always provide sufficient diagnostic information for the determination of the origin of protein-based films. However, studies on analogous samples of proteins from food have demonstrated the potential of total emission spectroscopy for discrimination between complex multiple protein [10] and multiple oil-based systems [11]. Total emission spectroscopy, although more time-consuming to record than a single emission spectrum, can provide more complete information, especially regarding the presence of fluorophores, their wavelength dependence, their emission and excitation maxima, and the relationship between multiple fluorophores.

The aim of this work is to investigate the potential of total emission spectroscopy combined with LIF for the assessment of the fluorophores present in egg white and egg yolk films.

2. EXPERIMENTAL

Following investigations of LIF to identify and discriminate among protein samples of binding media found in works of art using various excitation sources [2], further analysis of films of egg-based binding media was carried using total emission spectroscopy. Although the major proteinaceous components of both egg yolk and egg white are the same (ovalbumin and lysozyme), egg yolk also contains significant fatty acids (including palmitic and oleic acid).

3. METHODOLOGY AND METHODS

Egg white and egg yolk used as binding media were prepared as indicated in artists' accounts and historical recipes [12]. Egg white was beaten to form stiff peaks and left for 24 hours; foam was skimmed and removed and a solution of 50% w/w clear egg white in nanopure water was prepared. Egg yolk was extracted from egg by piercing the yolk and allowing the liquid to drip from the encasing film; the yolk was diluted in nanopure water to give a 50% w/w emulsion. Films of proteins were cast on polished fused silica disks to give film thickness of approximately 15 μm (perthometer S5P profilometer) and were examined 1 year after their preparation.

Laser-induced fluorescence of films of proteins was recorded using 248 nm excitation from a KrF excimer laser (TUI Laser AG BraggStar 200), 10 ns pulse duration. A maximum of 500 pulses at a fluence 5 mJcm^{-2} per pulse with a spot size 1 × 1 mm was used when recording spectra. Spectra were also recorded using the 3rd harmonic (355 nm) of a Q-switched Nd : YAG (Spectron Laser Systems), 10 ns pulse duration, a maximum of 300 pulses, and fluence 5 mJcm^{-2} per pulse. LIF emission was collected using a fibre-optic placed at approximately 60° to the sample axis coupled to an Ocean Optics HD4000 spectrophotometer with approximately 0.13 nm resolution. In addition, films were analysed using a scanning spectrofluorimeter with excitation provided by a Xenon arc lamp (Jobin-Yvon/Horiba Fluoromax-P). Typical scanning parameters were integration time of 0.2 s per point, intervals of 1 nm, and excitation/emission slits between 1–5 nm. Films of proteins were analysed at 30° from the sample-axis. Total emission spectra were constructed by recording a series of excitation spectra with an interval of 5 nm between successive excitation scans and using a resolution of 1 nm emission spectra; scans were recorded with excitation from 220 nm to 400 nm, and first- and second-order Rayleigh scattering was eliminated.

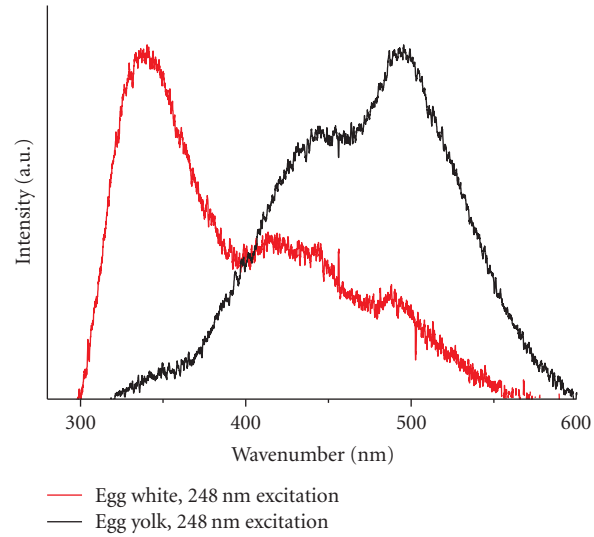

Figure 1: LIF spectra of egg white and egg yolk at the excitation wavelength of 248 nm (KrF excimer laser, 10 ns excitation).

4. RESULTS AND DISCUSSION

For clarity, results of LIF spectral analysis on model films are presented first, and these are followed by detailed spectrofluorimetric analysis using total emission spectroscopy undertaken to characterise the emission pattern of each mixture.

4.1. *Laser-induced fluorescence of films*

Autofluorescence of proteins seen in LIF spectra of egg white (Figure 1) is due to the presence of aromatic amino acids tryptophan, tyrosine, and phenylalanine, which account for fluorescence emissions between approximately 280 nm–380 nm [1, 2].

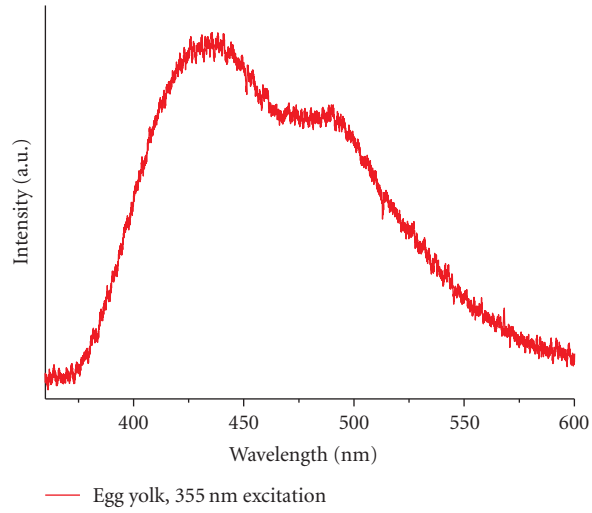

FIGURE 2: LIF spectra of film of egg yolk at the excitation wavelength of 355 nm (3rd harmonic of Nd : YAG 3rd laser, 10 ns).

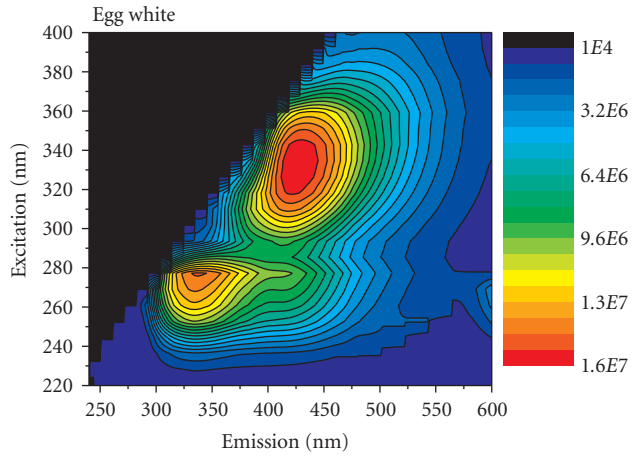

FIGURE 3: Total emission spectrum of a film of egg white, right scale counts, with intervals of 3×10^6 counts between each line/colour.

Further emissions at wavelengths greater than 380 nm are especially apparent in egg yolk (Figure 1). In addition, a strong emission from egg yolk following excitation at 355 nm is observed (Figure 2). However, fluorescence at wavelengths greater than 380 nm cannot be ascribed to amino acid side chains.

4.2. Total emission spectroscopy

Spectrofluorimetric analysis of samples of egg white films to produce total emission spectra yields significantly different results for egg white and egg yolk, as seen in Figures 3 and 4.

Examination of total emission spectra immediately allows the location of emission maxima and indicates the presence of multiple fluorophores and the dependence of the emission on excitation. Clear differences in the spectral patterns of egg white and egg yolk are visible; the former is associated with multiple and relatively sharp emissions, and the latter with a single-broad emission. Both media exhibit a maximum emission at approximately 425 nm (excitation maximum at 355 nm), which can be ascribed to the accumulation of photodegration products of egg proteins and other compounds present in the complex mixtures found within eggs.

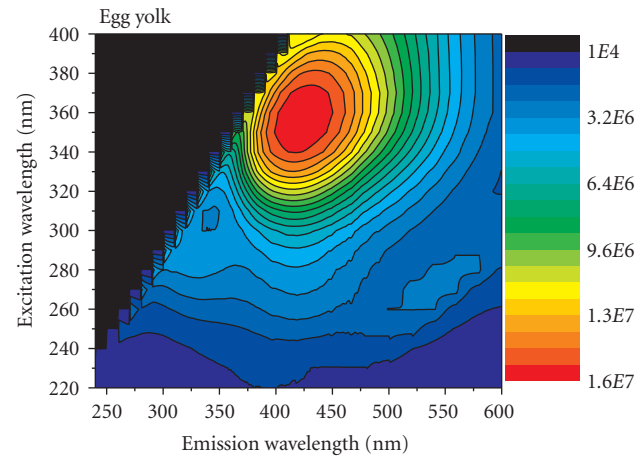

FIGURE 4: Total emission spectrum of a film of egg yolk, right scale counts, with intervals of 3×10^6 counts between each line/colour.

Degradation can result from photooxidation of amino acids and of other compounds found within eggs (including flavins, free glucose and, lipids (in egg yolk)), or from cross-linkage reactions between amino acids and sugars [13]. While collagen-based materials used in binding media are characterised by fluorophores which develop following the Maillard reaction [14], uncooked and untreated egg proteins used as binding media, which have been reported to form Maillard reaction products [15], do not exhibit characteristic fluorescence profiles at 380 nm [2]. Rather, the formation of dityrosine [16], suggested in the case of photooxidised collagen-based binding media [17], and tryptophan oxidation products N-formylkynurenine (NFK) and kynurenine (associated with emissions at approximately 435 nm) [18] may further account for observed emissions.

4.3. Interpretation of total emission spectra

In the total emission spectra, differences in the shape of the excitation-emission maxima and the contour lines surrounding the maximum suggest the presence of more than one fluorophore, especially in the case of films of egg white, which likely contains oxidised tyrosine (emission maximum at approximately 410 nm). In egg white, other fluorescence emissions observed at 335 nm (excitation maximum at 290 nm) are likely due to native tryptophan; contributions from tyrosine can also be inferred from the emission at approximately 300–320 nm. Importantly, no similar emissions are found in egg yolk films. The assignment of fluorescence to photooxidation products of tyrosine degradation is based on

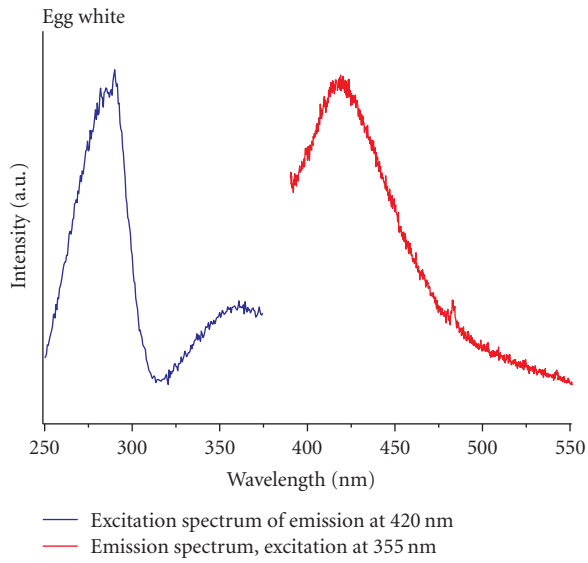

Figure 5: Excitation spectrum (blue) (maxima at 285 and 355 nm) and emission spectrum (red) (excitation at 355 nm) of a film of egg white.

the characteristic excitation spectrum of dityrosine (emission maximum of 410 nm, excitation maxima at 285 and 355 nm) [19] seen in Figure 5.

Importantly, the assignment of emissions observed in egg proteins to dityrosine and oxidised tryptophan based on florescence data alone can be misleading, due to additional fluorophores which have been documented to fluoresce in the same range [20]. Nonetheless, total emission spectra allow a greater understanding of the fluorphores found in single-wavelength excitation, as in LIF.

4.4. Interpretation of LIF spectra

Therefore, a possible interpretation of the LIF spectra of egg yolk (Figure 3) is that fluorescence observed at 425 nm is a combination of emission from dityrosine (emission 410 nm), NFK (emission 435 nm), and DOPA (emission at 480 nm), as well as potential contributions from riboflavin (emission between 500–550 nm) [21] and flavin photooxidation products (lumichrome and lumiflavin); fatty-acid polimerisation could result in the production of new flourophores. Additionally, the generation of photooxidation products may be induced by sensitisation of riboflavin by visible radiation, present in both egg white and egg yolk [22].

5. CONCLUSIONS

Results demonstrate that LIF can be used to distinguish between proteins in art works, and that emissions have a strong wavelength dependency; the fluorescence "fingerprint" or total emission spectrum can greatly assist the choice of laser wavelength for LIF spectroscopy as well as provide more information regarding the fluorophores present in complex mixtures. In this case, examination of the total emission spectra of egg yolk and egg white immediately allows their separation and provides a useful tool for the interpretation of LIF spectra.

Within the context of organic analysis in conservation, LIF is advantageous as it is a noninvasive, nondestructive, simple, and rapid technique which can be used to distinguish between different proteins, provided a difference in fluorescence is apparent. Due to the identification of multiple fluorophores in the complex protein mixtures found in binding media and seen in total emission spectra, techniques capable of better separating fluorescence contributions would be useful. In addition, changes in the fluorescence emission spectra as a result of ageing should be investigated. Finally, future work should focus on the ageing of protein media, pigment-media interactions, and investigations of fluorescence lifetime.

ACKNOWLEDGMENT

The first author's research was supported by the European Union 6th Framework Programme Marie Curie Early Stage Training Fellowship as part of the ATHENA Project (MEST-CT-2004-504067).

REFERENCES

[1] A. S. Ladokhin, "Fluorescence spectroscopy in peptide and protein analysis," in *Encyclopedia of Analytical Chemistry*, R. Meyers, Ed., pp. 5762–5779, John Wiley & Sons, New York, NY, USA, 2000.

[2] A. Nevin, S. Cather, D. Anglos, and C. Fotakis, "Analysis of protein-based binding media found in paintings using laser induced fluorescence spectroscopy," *Analytica Chimica Acta*, vol. 573-574, pp. 341–346, 2006.

[3] Z. Deyl, I. Mikšík, and J. Zicha, "Multicomponent analysis by off-line combination of synchronous fluorescence spectroscopy and capillary electrophoresis of collagen glycation adducts," *Journal of Chromatography A*, vol. 836, no. 1, pp. 161–171, 1999.

[4] W. G. Liu, K. D. Yao, G. C. Wang, and H. Li, "Intrinsic fluorescence investigation on the change in conformation of cross-linked gelatin gel during volume phase transition," *Polymer*, vol. 41, no. 20, pp. 7589–7592, 2000.

[5] M. Lacroix, T. C. Le, B. Ouattara, et al., "Use of γ-irradiation to produce films from whey, casein and soya proteins: structure and functionals characteristics," *Radiation Physics and Chemistry*, vol. 63, no. 3–6, pp. 827–832, 2002.

[6] E. R. de la Rie, "Fluorescence of paint and varnish layers (part I)," *Studies in Conservation*, vol. 27, no. 1, pp. 1–7, 1982.

[7] T. Miyoshi, "Fluorescence from pigments in fresh and stored oil colours under N_2 laser excitation," *Japanese Journal of Applied Physics*, vol. 24, no. 8, pp. 1113–1114, 1985.

[8] T. Miyoshi, "Fluorescence from Resins for oil painting under N_2 laser excitation," *Japanese Journal of Applied Physics*, vol. 29, pp. 1727–1728, 1990.

[9] M. Castillejo, M. Martín, M. Oujja, et al., "Evaluation of the chemical and physical changes induced by KrF laser irradiation of tempera paints," *Journal of Cultural Heritage*, vol. 4, suppl. 1, pp. 257s–263s, 2003.

[10] C. M. Andersen and R. Bro, "Practical aspects of parafac modeling of fluorescence excitation-emission data," *Journal of Chemometrics*, vol. 17, no. 4, pp. 200–215, 2003.

[11] E. Sikorska, T. Górecki, I. V. Khmelinskii, M. Sikorski, and J. Kozioł, "Classification of edible oils using synchronous scanning fluorescence spectroscopy," *Food Chemistry*, vol. 89, no. 2, pp. 217–225, 2005.
[12] C. Cennino D'Andrea, *Il libro dell'Arte*, Dover, New York, NY, USA, 1960.
[13] M. J. Davies, S. Fu, H. Wang, and R. T. Dean, "Stable markers of oxidant damage to proteins and their application in the study of human disease," *Free Radical Biology and Medicine*, vol. 27, no. 11-12, pp. 1151–1163, 1999.
[14] D. G. Dyer, J. A. Blackledge, S. R. Thorpe, and J. W. Baynes, "Formation of pentosidine during nonenzymatic browning of proteins by glucose: identification of glucose and other carbohydrates as possible precursors of pentosidine in vivo," *Journal of Biological Chemistry*, vol. 266, no. 18, pp. 11654–11660, 1991.
[15] L. Campbell, V. Raikos, and S. R. Euston, "Modification of functional properties of egg-white proteins," *Nahrung - Food*, vol. 47, no. 6, pp. 369–376, 2003.
[16] C. Giulivi, N. J. Traaseth, and K. J. A. Davies, "Tyrosine oxidation products: analysis and biological relevance," *Amino Acids*, vol. 25, no. 3-4, pp. 227–232, 2003.
[17] M. Oujja, E. Rebollar, C. Abrusci, A. Del Amo, F. Catalina, and M. Castillejo, "UV, visible and IR laser interaction with gelatine," to appear in *Journal of Applied Physics: Conference Series*.
[18] J. L. E. Reubsaet, J. H. Beijnen, A. Bult, R. J. van Maanen, J. A. D. Marchal, and W. J. M. Underberg, "Analytical techniques used to study the degradation of proteins and peptides: chemical instability," *Journal of Pharmaceutical and Biomedical Analysis*, vol. 17, no. 6-7, pp. 955–978, 1998.
[19] A. J. Kungl, M. Breitenbach, and H. F. Kauffmann, "Molecular dynamics simulation of the rare amino acid LL-dityrosine and a dityrosine-containing peptide: comparison with time-resolved fluorescence," *Biochimica et Biophysica Acta-General Subjects*, vol. 1201, no. 3, pp. 345–352, 1994.
[20] P. Guptasarma and D. Balasubramanian, "Dityrosine formation in the proteins of the eye lens," *Current Eye Research*, vol. 11, no. 11, pp. 1121–1125, 1992.
[21] S. Hustad, P. M. Ueland, and J. Schneede, "Quantification of riboflavin, flavin mononucleotide, and flavin adenine dinucleotide in human plasma by capillary electrophoresis and laser-induced fluorescence detection," *Clinical Chemistry*, vol. 45, no. 6 pt 1, pp. 862–868, 1999.
[22] A. M. Edwards and E. Silva, "Effect of visible light on selected enzymes, vitamins and amino acids," *Journal of Photochemistry and Photobiology B: Biology*, vol. 63, no. 1–3, pp. 126–131, 2001.

Hindawi Publishing Corporation
Laser Chemistry
Volume 2006, Article ID 31862, 5 pages
doi:10.1155/2006/31862

Research Article

Characterization of Laser-Generated Microparticles by Means of a Dust Monitor and SEM Imaging

Roland Wurster,[1] Simone Pentzien,[2] Andrea Conradi,[2] and Jörg Krüger[2]

[1] *Institute for Physics and Meteorology, Hohenheim University, Garbenstraße 30, 70599 Stuttgart, Germany*
[2] *Division VI.4 Surface Technologies, Federal Institute for Materials Research and Testing (BAM), Unter den Eichen 87, 12205 Berlin, Germany*

Received 13 September 2006; Revised 9 November 2006; Accepted 16 November 2006

Recommended by Costas Fotakis

Nanosecond laser (1064 nm wavelength) cleaning of artificially soiled paper as a model sample simulating a real-world artwork was performed. During the cleaning process, the ejection of particles was monitored in situ by means of a dust monitor (8 size classes, ranging from 0.3 μm to $> 2\,\mu$m) and ex situ using a mini-cascade impactor (MKI, 5 stages). The cleaning result was analyzed by scanning electron microscopy (SEM) considering possible laser-induced damages to the substrate. Size distributions of emitted particles were measured depending on the processing parameters: laser fluence, F, and pulse number per spot, N. High numbers of large ($>2\,\mu$m) particles were collected by the mini-cascade impactor indicating a gas dynamical liftoff process. Obviously, these particles were not affected by the laser-matter interaction. The different methods (SEM, MKI, and dust monitor) are compared with respect to their usefulness for a proper interpretation of the cleaning results.

1. INTRODUCTION

Laser cleaning of soiled paper is a challenging task due to the fact that a contamination (e.g., a layer, dispersed foreign material or even particulates) has to be removed and a fragile organic material has to be preserved. Laser radiation offers the potential of a spatial and temporal concentration of energy. In an ideal case, the laser energy can be deposited in a sharply defined volume of the soil to remove it and leave the paper intact. In reality, laser cleaning of paper is a complex process depending on the (optical, thermal, chemical, and mechanical) properties of the pollutant and of the matrix and also on the laser parameters like wavelength, pulse duration, spatial intensity distribution, and repetition rate. In recent years, a few papers were published concerning the topic [1–8]. To avoid an undesirable destruction of the paper, a working range for the laser has to be found. The laser parameters have to be chosen that the damage threshold of the matrix material is not reached. Generally, the term "damage" includes immediate as well as long-term effects which might cause an irreversible change of the paper material (e.g., thermal destabilization of the substrate [2, 8], color changes [4, 5], and any influence on the ageing behavior [8]).

An in situ monitoring process of the laser cleaning procedure is desirable. Laser-induced breakdown spectroscopy of the plasma plume (LIBS [9]) and acoustic techniques [8] were established. The ejection of particles forms a major channel for the removal of unwanted surface layers. The micro-analytical characterization of particles ejected from the contamination film can be a source of complementary information [10]. However, this paper aims at a multimethod approach by in situ (dust monitor) and ex situ investigations (SEM and mini-cascade impactor) of 1064 nm nanosecond laser processing of sensitive samples to determine a laser working range (F, N) and to understand the mechanism of the cleaning process.

2. EXPERIMENTAL

Charcoal was mechanically rubbed and distributed with a brush on a Whatman filter paper no. 1506. The pulverized soiling was sucked in with a hoover for 2 minutes to achieve a stable contact between pollution and paper. The model samples should simulate a real-world artwork. Homogeneity of the soiling was controlled down to a lateral scale of < 0.5 mm. Differences of lightness measurements of $\pm 10\%$

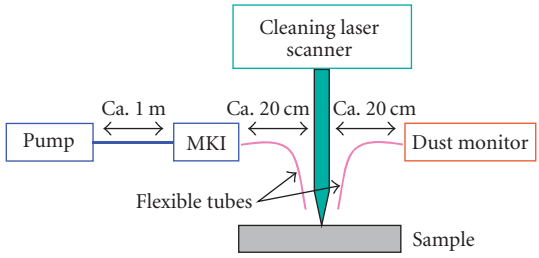

Figure 1: Scheme of the experimental setup.

were detected employing a multispectral imaging system (MUSIS 2007, Model D-HFA-12). Energy dispersive X-ray spectra of the model system clearly showed major (C, O) and minor (K, Ca, Cu, Zn) elemental components of the powder.

The experimental setup is depicted in Figure 1 showing the laser cleaning system combined with two particle collection devices (dust monitor and MKI). A computer-controlled cleaning station [11] was applied for the laser treatment. The Nd : YAG-laser was operated in its fundamental mode at 1064 nm wavelength at a pulse duration of 8 ns and a repetition rate of 500 Hz. The laser fluence F was varied between 0.45 and 12.8 J/cm^{-2}. Depending on the number of laser pulses per spot, a 3 mm square was scanned in 9 seconds (for $N = 1$) or 7 minutes ($N = 36$), respectively. For safety reasons, the whole laser-processing compartment fulfils Laser Class I conditions.

During the cleaning procedure, a commercial dust monitor (Portable Dust Monitor Mod. 1.108, GRIMM-Aerosol Technik) was used for the measurement of particle size distributions in airborne state. The aerosol inlet of the dust monitor is positioned next to the laser impact area (1 mm distance). Particle size distributions (eight size classes) were recorded at a time resolution of one second. The single particle detection bases on light scattering (using a laser diode) with a minimal detectable particle size of 0.3 μm. Aerosol flow control was adjusted and stabilized to 1.2 l/min.

Additionally, particles released from the treated area were collected actively with an aerosol flow of 0.7 l/min by means of a five stage mini-cascade impactor (MKI) both on ultrathin substrate films (pioloform) covering standard made copper grids and Al foils for off-line microscopic inspection. Scanning electron microscopy (high resolution SEM ABT DS 150F, Topcon, Tokyo) was applied to collected particles (MKI) and irradiated sample areas as well.

3. RESULTS AND DISCUSSION

Figure 2 displays the result of the preparation of the model samples. The SEM pictures show the original surface morphology of a Whatman filter paper (Figure 2(a)) and the appearance after the mechanical soiling of the paper (Figure 2(b)). It can be clearly seen that the structure of the paper was not modified due to the mechanical conditioning.

The results of single-pulse ($N = 1$) laser processing tests utilizing different laser fluences (energy densities) are depicted in Figure 3. For these illumination conditions, the

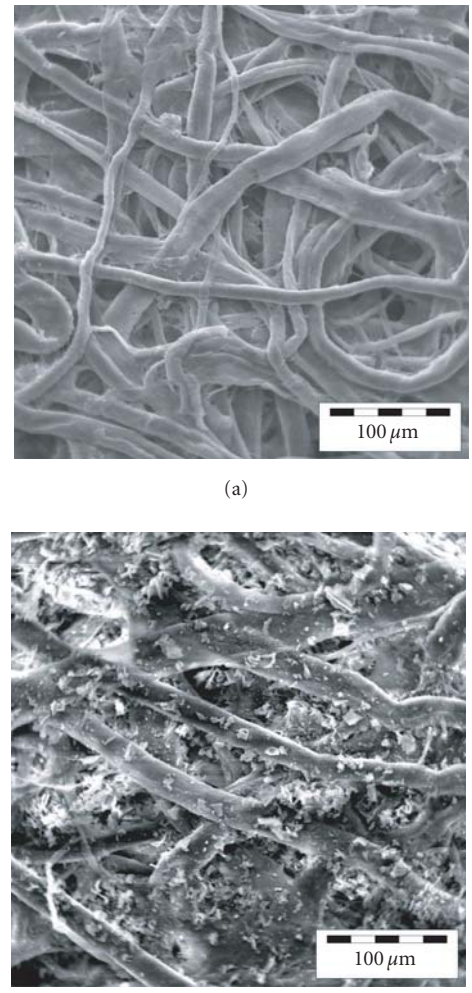

Figure 2: Scanning electron microscope (SEM) pictures of Whatman filter no. 1506: (a) as received, (b) mechanically soiled with charcoal dust.

cleaning effect increases with rising laser fluence up to the maximum value of 12.8 J/cm^{-2} which was the highest achievable energy density for the focusing conditions described here.

After laser illumination with energy densities up to about 2 J/cm^{-2} (areas "A"–"D", Figure 3), a discoloration (yellowing) of the treated samples was not observed with the multi spectral imaging system MUSIS 2007. A closer inspection of a part of area "E" (Figure 3) is illustrated in Figure 4. Obviously, a satisfying cleaning effect could be reached (compare Figure 2(b)). The paper structure remained unchanged (compare the original paper surface without any soiling in Figure 2(a)) and no evidence of laser-induced damage can be observed. It should be pointed out that this result was obtained for the application of one single laser pulse per spot and cannot be transferred to multipulse conditions.

During the removal of the soil, ejected particles were deposited onto five stages of a mini-cascade impactor (MKI [12]). The impact of particles occurred according to the

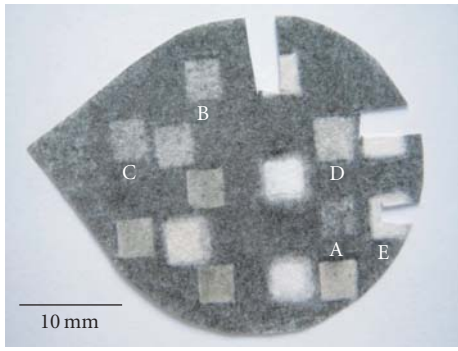

A 0.45 J/cm^2
B 0.83 J/cm^2
C 1.22 J/cm^2
D 2.4 J/cm^2
E 12.8 J/cm^2

Figure 3: Results of different cleaning procedures with varying laser fluence and $N = 1$.

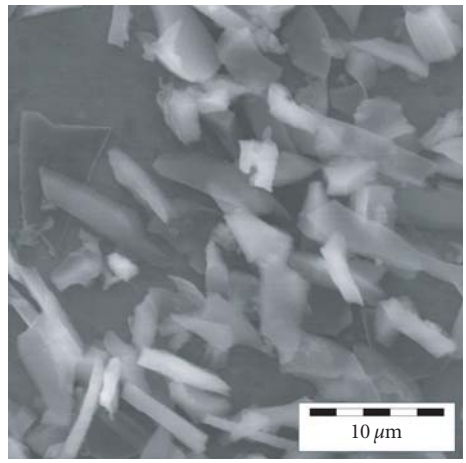

(a)

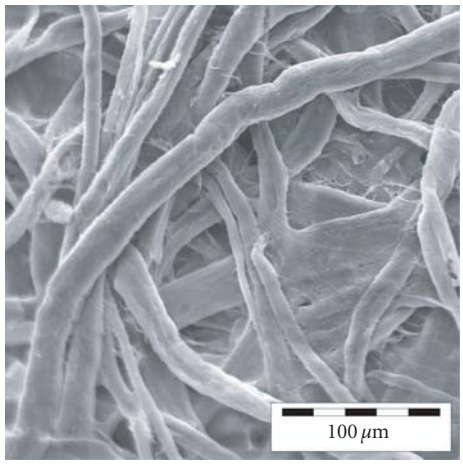

Figure 4: SEM picture of a cleaning result after a laser treatment with $N = 1$ and $F = 12.8\,\text{J/cm}^{-2}$.

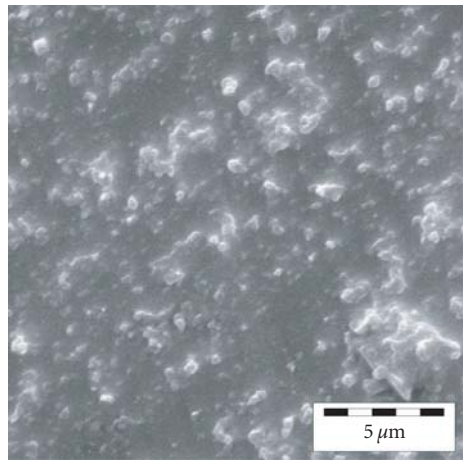

(b)

Figure 5: SEM pictures of particles deposited on different stages ((a) stage 2, (b) stage 5) of the mini-cascade impactor (MKI) during laser cleaning with $N = 1$ and $F = 12.8\,\text{J/cm}^{-2}$.

aerodynamic size decreasing from stage 1 to stage 5. SEM pictures of particles deposited on stages 2 and 5 of the MKI are depicted in Figure 5.

The coarse particles (Figure 5(a)) do not show any modification of shape and morphology induced by the laser illumination while the fine particles (Figure 5(b)) tend to have a convex and well-rounded shape. The latter is attributed to a laser-induced melting process. The investigation of aerodynamically separated particle size fractions leads to the conclusion that especially an efficient mechanical liftoff behavior contributes to the laser cleaning process.

During the laser processing of the model samples, size distributions of ejected particles were recorded. Particle concentrations right next to the laser-treated surface exceeded the background aerosol concentration of the laboratory air by 2 to 4 orders of magnitude. Figure 6 displays the dependence of the particle concentration on the size class employing five different laser fluences. For comparison, laser pulses with the maximum fluence of 12.8 J/cm^{-2} were impinged on the filter paper without soil. The difference of the signal (particles/litre) for the samples with and without contamination was evident. For all fluences applied, a peak-valley structure of the signal versus size class curve was found. This behavior may reflect different particle production and emission paths but is not yet understood. An artefact of the measuring system can be ruled out. Contrary to Figure 6 for a real-world soiled paper, a deviating curve was found (Figure 7). For the model sample (Figure 6), the number concentration of particles for all size classes was not a monotone function of the laser fluence. Only for the two lowest fluences, the particle number concentrations did increase with increasing energy density in all 8 size categories. For the highest fluence of 12.8 J/cm^{-2} and the application to the soiled paper, a significant enhancement of the recorded number concen-

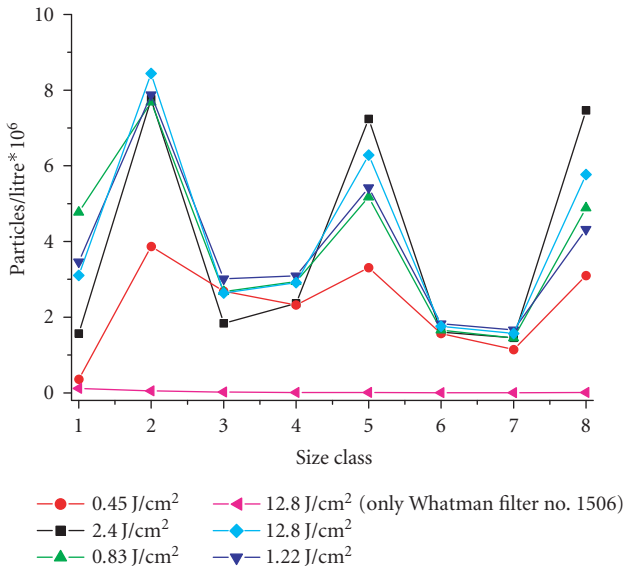

Figure 6: Size distribution of laser-ablated particles for different fluences applied and single-pulse illumination conditions. Each data point represents the average over an integration time of 5 seconds. Size class 1 = 0.3–0.4 μm, size class 2 = 0.4–0.5 μm, size class 3 = 0.5–0.65 μm, size class 4 = 0.65–0.8 μm, size class 5 = 0.8–1.0 μm, size class 6 = 1.0–1.6 μm, size class 7 = 1.6–2.0 μm, size class 8 > 2.0 μm.

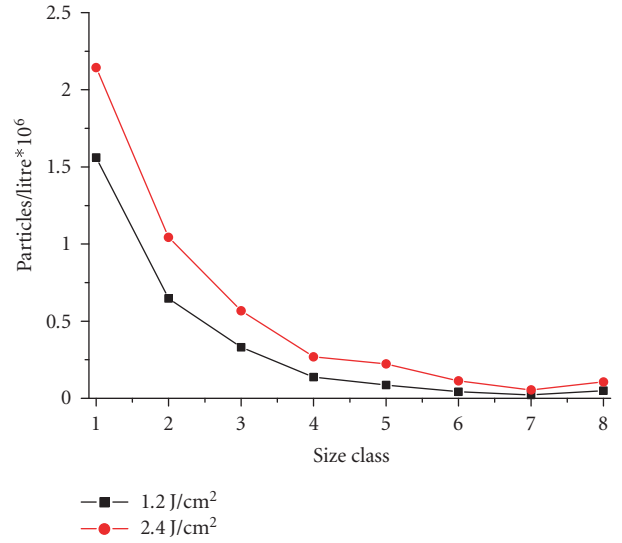

Figure 7: Size distribution of laser-ablated particles for two different laser fluences and single-pulse illumination conditions for a real-world sample (drawing board soiled with soot).

trations was not observed. Therefore, most probably the paper stayed intact and the signal can mainly be attributed to the carbon particles (and no additional cellulose particles). This observation corresponds to the SEM picture (Figure 4) that shows the cleaning result after a laser treatment with the same parameters.

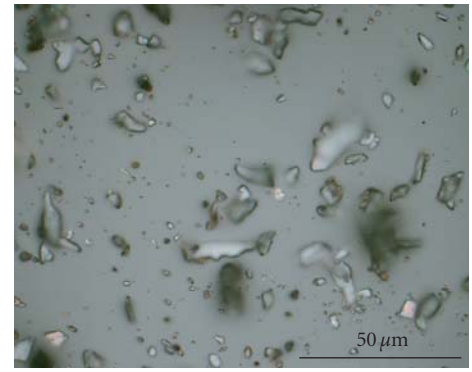

Figure 8: Optical microscope picture of a part of the soiling particles.

To get an information about the sizes of the soiling particles before laser illumination, a model sample was beat and the particles were collected on a microscopic slide. An optical microscopic picture was taken (Figure 8), and the number of large (> 2.0 μm) and small particles (∼ 0.3 μm) was counted visually. A ratio of about 1 : 1 was found between these "extreme" size classes.

Comparing this rough estimation of the fine to coarse particle number ratio to the measured size distributions of laser-ablated particles (Figure 6), it may cautiously be stated that no preferential particle removal does occur for these experimental conditions.

4. CONCLUSIONS

Nanosecond laser cleaning of artificially soiled paper was carried out. For single-pulse treatment, an improved cleaning effect could be observed for an increasing laser fluence up to an energy density of 12.8 J/cm^{-2}. SEM revealed that the paper structure remained unchanged. During the cleaning process, laser-generated particle concentrations exceeded the background laboratory air level by 2 to 4 orders of magnitude. The measurements with the dust monitor confirmed the SEM investigations with respect to the damage threshold of the paper. Mini-cascade impactor investigations of aerodynamically separated particle size fractions suggest an efficient mechanical liftoff process contributing to the laser cleaning. A significant preferential ejection of a particular size class could not be observed for the model sample.

REFERENCES

[1] W. Kautek, S. Pentzien, P. Rudolph, J. Krüger, and E. König, "Laser interaction with coated collagen and cellulose fibre composites: fundamentals of laser cleaning of ancient parchment manuscripts and paper," *Applied Surface Science*, vol. 127–129, pp. 746–754, 1998.

[2] J. Kolar, M. Strlič, S. Pentzien, and W. Kautek, "Near-UV, visible and IR pulsed laser light interaction with cellulose," *Applied Physics A*, vol. 71, no. 1, pp. 87–90, 2000.

[3] J. Kolar, M. Strlič, D. Müller-Hess, et al., "Near-UV and visible pulsed laser interaction with paper," *Journal of Cultural Heritage*, vol. 1, supplement 1, pp. 221–224, 2000.

[4] M. Strlič, J. Kolar, V.-S. Šelih, and M. Marinček, "Surface modification during Nd:YAG (1064 nm) pulsed laser cleaning of organic fibrous materials," *Applied Surface Science*, vol. 207, no. 1–4, pp. 236–245, 2003.

[5] P. Rudolph, F. J. Ligterink, J. L. Pedersoli Jr., et al., "Characterization of laser-treated paper," *Applied Physics A*, vol. 79, no. 2, pp. 181–186, 2004.

[6] P. Rudolph, F. J. Ligterink, J. L. Pedersoli Jr., et al., "Laser-induced alteration of contaminated papers," *Applied Physics A*, vol. 79, no. 4–6, pp. 941–944, 2004.

[7] A. Kamińska, M. Sawczak, M. Ciepliński, G. Śliwiński, and B. Kosmowski, "Colorimetric study of the post-processing effect due to pulsed laser cleaning of paper," *Optica Applicata*, vol. 34, no. 1, pp. 121–132, 2004.

[8] M. Strlič, V.-S. Šelih, J. Kolar, et al., "Optimisation and on-line acoustic monitoring of laser cleaning of soiled paper," *Applied Physics A*, vol. 81, no. 5, pp. 943–951, 2005.

[9] K. Melessanaki, A. Mastrogiannidou, S. Chlouveraki, S. C. Ferrence, P. P. Betancourt, and D. Anglos, "Analysis of archaeological objects with LMNTI, a new transportable LIBS instrument," in *Lasers in the Conservation of Artworks*, K. Dickmann, C. Fotakis, and J. F. Asmus, Eds., pp. 443–451, Springer, New York, NY, USA, 2005.

[10] R. Wurster, S. Pentzien, and W. Kautek, "Imaging and mass spectrometry of microparticles generated during surface decontamination of an ancient parchment sample by laser radiation," in *Lasers in the Conservation of Artworks, LACONA VI Proceedings*, Springer, New York, NY, USA, 2006.

[11] W. Kautek and S. Pentzien, "Laser cleaning system for automated paper and parchment cleaning," in *Lasers in the Conservation of Artworks*, K. Dickmann, C. Fotakis, and J. F. Asmus, Eds., p. 403, Springer, New York, NY, USA, 2005.

[12] P. Wieser and R. Wurster, "Application of laser-microprobe mass analysis to particle collections," in *Physical and Chemical Characterization of Individual Airborne Particles*, K. R. Spurny, Ed., pp. 251–270, Ellis Horwood, Chichester, UK, 1986.

Hindawi Publishing Corporation
Laser Chemistry
Volume 2006, Article ID 35373, 11 pages
doi:10.1155/2006/35373

Review Article

Optical Coherence Tomography for Artwork Diagnostics

Piotr Targowski, Michalina Góra, and Maciej Wojtkowski

Institute of Physics, Nicolaus Copernicus University, ul. Grudziądzka 5, 87 100 Toruń, Poland

Received 15 September 2006; Revised 8 December 2006; Accepted 15 December 2006

Recommended by Costas Fotakis

An overview of the optical coherence tomography (OCT) technique is given. Time domain, spectral and sweep source modalities are briefly described, and important physical parameters of the OCT instrument are discussed. Examples of the application of OCT to diagnosis of various art objects such as oil paintings on canvas (imaging of glaze and varnish layers), porcelain, faience, and parchment are presented. Applications to surface profilometry of painting on canvas are also discussed.

1. INTRODUCTION

For more than a century, since a year after their discovery by W. Roentgen in 1895, X-rays have been used for investigation of art objects [1]. Since then, this and other noninvasive methods for diagnosis of artwork structure and properties have been developing rapidly. Such methods generally fall into two categories: (a) those directly revealing structure, and (b) profilometric ones which provide a 3D surface profile of the object. This second approach may also lead to structural information such as location of cracks or detachments [2]. Analytical methods requiring the extraction of a sample of the material, and therefore in principle destructive, and limited as to choice of position and number of samples, are not considered further. Some other methods, such as laser induced breakdown spectroscopy (LIBS) [3, 4], Raman spectroscopy [4, 5] or, among more classical approaches, UV [6–8] and laser induced fluorescence (LIF) [9], and IR reflectography [10], are either limited to the object surface, or the information provided is integrated over the whole thickness of the object. In the latter case, structural information has to be obtained indirectly. X-ray radiography and neutron activation autoradiography [11] of paintings serve as examples in which such an indirect approach is taken. In both cases, the location of certain pigments in the picture may be revealed, and sometimes lead to the discovery of different, underlying images. However, assignment of the pigment to a certain paint layer has to be made by comparison with the visible image. Whilst routine tomographic methods like ultrasonography, X-radiography, electron paramagnetic resonance, and nuclear magnetic resonance have been successfully used for artwork diagnosis, the resolution of even highly developed modern instruments, usually designed for medical diagnosis, is not sufficient for detailed examination of certain objects of art, for example, paintings. A more detailed discussion of noninvasive testing is beyond the scope of this short review. However, despite the tremendous proliferation of many, very advanced diagnostic techniques, there is still a need for a fast, portable, easy-to-use, and simple-to-interpret, method of high resolution, noninvasive structural imaging. These requirements may, to some extent, be fulfilled by optical coherence tomography (OCT), since this method needs neither pretreatment of the object, nor special mounting conditions, such as an optical table. Modern medical OCT devices are suitably mobile, and achieve micrometre resolution.

OCT is a novel optical technique enabling cross-sectional imaging of the internal structure of semitransparent objects. This technique is based on interferometry of partially coherent light [12]. OCT has the great advantage of yielding high resolution cross-sectional images in a noncontact and noninvasive way, with very high sensitivity [13]. Because of these advantages, OCT is particularly suitable for medical applications, especially for investigating structures in the human eye, which is naturally transparent to visible and near-infrared light, and almost inaccessible by any other diagnostic instrumentation [14]. OCT has been under development over the last fifteen years, and has successfully been commercialized for ophthalmological use.

In all OCT devices, the interference phenomenon is used to reveal the axial structure of the object analyzed, that is,

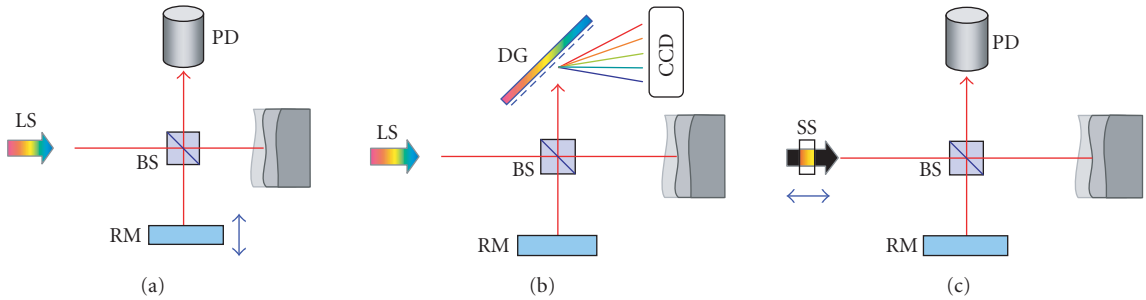

Figure 1: Consecutive generations of OCT devices: (a) time domain OCT, (b) spectral OCT, (c) sweep source OCT. Legend: LS—broadband light source, BS—beam splitter, PD—photodiode, DG—diffraction grating, RM—reference mirror, SS—sweep light source.

the distribution of back-scattering or back-reflecting points along the penetrating light beam. In order to obtain an interference fringe pattern carrying information about the axial structure of the object, the input light beam is split into two beams in the interferometer setup. The object is placed in the direct-beam arm of the interferometer, while the reference beam in the other arm is reflected back by the reference mirror (see Figure 1). The probing light, which is back-scattered or reflected by the internal structures of the object, is brought to interference with the reflected light returning from the reference arm. Since all light sources used for OCT have very short coherence times, this interference enables precise measurement of the optical path difference between the reference mirror position and the locations of the scattering or reflecting centres within the object. The basis of the technique is somewhat similar to that of radar, but the wavelengths utilized are much shorter and provide resolution in the micrometre range. In the next section, a simple basic description of the OCT technique is presented. A more comprehensive review may be found in many papers, for example, the article of Tomlins and Wang [15].

2. THE OCT INSTRUMENT

The majority of OCT instruments at present utilize optical fibres. However, for simplicity of description, the optical arrangements presented in this section are depicted in Figure 1 with bulk optics. They should therefore not be considered as experimental layouts, but rather as illustrating the physical ideas.

2.1. *The first generation: time domain OCT*

Time domain OCT (TdOCT, Figure 1(a)) was introduced [12] in 1991. In its most widespread version, it comprises a light source (LS) emitting light of high spatial and low temporal coherence, and a Michelson interferometer which divides the light beam and directs it into two orthogonal arms. The direct arm (object arm) terminates at the object to be analyzed. It usually contains collimating optics enabling formation of a narrow beam which penetrates the object. In order to reconstruct two-dimensional cross-sectional images of the object, the beam is galvanometrically scanned across its surface. Light backscattered or reflected from the various structures returns to the interferometer and is brought to interference with light propagating in the orthogonal arm (reference arm) which is terminated with a mirror (RM). The reference mirror RM is scanned back and forth through the required depth of imaging. The interfering light is detected by a photodiode (PD) backed up with a bandpass filter tuned to the Doppler frequency, often called the "carrier frequency," which is related to the scanning speed of the reference mirror. This procedure helps to eliminate extraneous signals arising from background light.

When the optical path length of the reference arm and object arm are properly matched, an interference fringe signal appears. When partially coherent light is used, the change of reference mirror position away from the matched one causes a rapid decrease of fringe contrast. Assuming that the measured object contains more than one reflecting interface or scattering structure, the condition of matched optical path lengths of the interferometric arms will be fulfilled many times during the scan of the reference mirror. As a result, a set of interferometric signals will be detected as a function of the reference mirror position. This set corresponds with the axial distribution of scattering and reflecting interfaces within the object, and it is named, by analogy with ultrasound biomicroscopy, the A-scan. For the next scan of the reference mirror, the probing beam is shifted to an adjacent position and so on, to yield a set of consecutive A-scans. These A-scans are then combined into a single picture to form a cross-sectional image of the object, the B-scan.

A major advantage of the time domain OCT instrument is its simple basic design and essentially unlimited depth of imaging, which depends only on the range of movement of the reference mirror. However, this movement is simultaneously a major drawback. Despite very sophisticated construction, this movable part slows down the data acquisition process to no better than 200 A-scans/second, even in the most advanced systems [16].

Instruments based on this principle are available commercially for medical diagnostic purposes. The most popular is the Stratus OCT™ from Zeiss-Meditec (USA), designed for imaging of the human retina. This system is optimized for medical applications, and it cannot directly be used for imaging materials. Instruments dedicated to the anterior chamber

of the eye (Visante OCT™ from Zeiss-Meditec) and other medical purposes are available, though less popular, but are also suitable for this application.

2.2. The second generation: spectral OCT

The theoretical basis for spectral OCT (SOCT, also called spectral domain OCT, Figures 1(b) and 2) [17] was published only two years after that of time domain OCT, but due to technological limitations (in particular the lack of very fast imaging systems) it did not generate much interest for a number of years. However, advances in high-speed and high-sensitivity CCD technology eventually enabled the development of spectral OCT instrumentation suitable for medical studies, and the first *in-vivo* images of the eye [18] were published in 2002. More recently, improvements in this technology have been developing rapidly [19–22].

In SOCT systems (Figure 1(b)), the single light intensity detector (PD in Figure 1(a)) is replaced by a spectrograph comprising a diffraction grating (DG) and fast camera (CCD). The spectrum of the light source registered by this camera is modulated by interference fringes of frequency corresponding to the position of the reflective or scattering layer in the object: the deeper the layer, the higher the modulation frequency. In contrast to time domain OCT, information about the entire axial structure of the object analyzed is collected simultaneously in one "shot" of the CCD camera. This information is encoded in the frequency signal. It is stored and subsequently decoded by numerical (reverse) Fourier transformation (FFT), conveniently performed on a personal computer.

The major advantage of SOCT is the lack of movable parts in the reference arm of the interferometer. Here, change of optical delay in the time domain is replaced by analysis of interference signals in the frequency domain. Due to this modification, the data collection period is significantly decreased, and acquisition speeds of up to 25,000 A-scans/second are currently attainable. The high speed of the SOCT system, which is very important for medical imaging, may also play a significant role in the application of OCT to art objects. For instance, it allows the multislice data collection necessary for 3D imaging of whole varnish layers and the subsequent analysis of varnish thickness. Spectral OCT also exhibits higher sensitivity than time domain OCT.

The main disadvantages of SOCT are directly related to the limitations of the CCD camera: the spectral sensitivity currently available restricts the wavelength range, and the number of pixels limits the range of modulation frequencies that can be recorded. In consequence, the depth of imaging of the system is limited. However, it is still usually not less than 1 mm, which is sufficient for the majority of OCT applications to the imaging of art objects. Another disadvantage is that SOCT systems appear to be somewhat more sensitive than TdOCT to saturation by mirror reflections from the sample. In spite of these drawbacks, the recently developed short acquisition time and high resolution now offered by SOCT instruments are beginning to take over in the market of medical diagnostic tools. At present (December 2006), the most advanced, commercially available SOCT instruments, are the SOCT Copernicus from Optopol S.A. (Poland) and the RTVue from Optovue Corp. (USA).

2.3. The third generation: sweep source OCT

In sweep source OCT (SSOCT, Figure 1(c)), detection is again performed by a single photodiode (PD) but, as in spectral OCT, interference spectra are measured, in this case by changing the wavelengths of the monitoring light with time. This is accomplished by using a sweep source laser (SS) as the light source. This device enables a change of the wavelength generated over a range of up to 100 nm within a couple of microseconds [23–27]. As in SOCT, reverse Fourier transformation is utilized to recover the structure of the object. The major advantage of this emerging OCT technology is the similar high speed of data acquisition to SOCT, but without its drawbacks, that is, spectral limitations of the CCD camera, imaging depth limitations due to the limited number of pixels in CCD devices, and loss of sensitivity with depth, all inherent to SOCT. The price currently to be paid is that the light source is very expensive and so far still not reliable in operation, as well as it presently being available only for a limited range of wavelengths around 1300 nm. However, it is expected that the spectral range available will be expanded in the near future.

2.4. General considerations

The most important parameters of OCT systems for application to the imaging of art objects are axial and lateral resolution, range of axial imaging, central wavelength of probing light, sensitivity, and acquisition speed.

Similarly to confocal microscopy, the lateral resolution is related to the focused spot size Δx of the probing beam. This depends on the magnification and numerical aperture of the optics used in the object arm, and can be expressed in terms of the focal length of the lens f forming the probing beam, and the original beam diameter d. It is estimated from the central wavelength λ_{centre} and the refractive index (n_R) of the medium examined:

$$\Delta x = \frac{1}{n_R}\frac{4\lambda_{\text{centre}}}{\pi}\left(\frac{f}{d}\right). \tag{1}$$

The axial resolution (Δz) depends on the spectral properties of the probing light through its central wavelength λ_{centre} and spectral span $\Delta\lambda_{\text{FWHM}}$:

$$\Delta z = \frac{1}{n_R}\frac{2\ln 2}{\pi}\frac{\lambda^2_{\text{centre}}}{\Delta\lambda_{\text{FWHM}}}. \tag{2}$$

It should be emphasized that (2) is derived with some idealized assumptions such as Gaussian shape for the spectrum. This condition is not fulfilled for real light sources. Also, in real systems, dispersion in the material examined causes additional broadening of the signal. This effect may be compensated both optically and numerically, but only to a certain extent. Numbers obtained from (2) should therefore serve rather as lower estimates for expected values.

Table 1: Examples of light sources used for OCT and available optical properties of the OCT system. In all cases, common values of $n_R = 1.4$ and $f/d = 12$ were used in (1)–(3).

The light source	λ_{centre} [nm]	$\Delta\lambda_{\text{FWHM}}$ [nm]	Δz [μm]	Δx [μm]	DOF [μm]
SLD	830	19	11.5	9	220
SLD (broadband)	830	50	4.4	9	220
SLD	1300	50	10.6	14	340
SLD	1560	100	7.6	17	410
The Broadlighter^{TM}	830	70	3.1	9	220
Integral OCT^{TM}	800	120	1.7	9	210
Femtosecond Ti: sapphire laser	850	144	1.6	9	220

The range of axial imaging is determined by various factors. Firstly, in all SOCT systems and the majority of TdOCT systems, it is limited by the depth of focus (DOF) of the probing beam

$$\text{DOF} = 2\Delta x\left(\frac{f}{d}\right). \tag{3}$$

This limitation may be overcome in TdOCT by using a focusing lens which moves simultaneously with the reference mirror to keep the coherence gate always in focus. In such a system, the imaging range may be extended to even as much as a few centimetres. In SOCT instruments, the imaging range is additionally and predominantly limited by the number of pixels of the CCD camera, which determines the maximum detectable frequency of spectral fringes. In practice, SOCT systems have an imaging range of about 2 mm.

The major factor determining the properties of any OCT system is the light source. To ensure high sensitivity, it has to emit highly spatially coherent light. Simultaneously, according to (2), it should have as broad a spectrum as possible. The most popular light sources fulfilling these conditions are semiconductor superluminescent diodes (SLD). Incandescent white light sources and specially designed lasers are also used for OCT applications [28]. Recent developments in the field of semiconductor lasers have yielded novel and cost effective spectrally broadband light sources built up from systems of SLDs, coupled together with optical fibres into a single source (the Broadlighter^{TM}).

Available light sources are limited to the near infrared range, namely, from 700 nm to 1500 nm. The exact choice of the central wavelength depends on the prospective application, and is mostly determined by the absorption properties of the medium under investigation, though the expected resolution must also be taken into account. In Table 1, common examples of light sources used in OCT, and the resulting system properties, are listed.

As can be seen from (2) and Table 1, the axial resolution deteriorates quickly with increasing central wavelength. This conclusion is important for the application to stratigraphy of paintings, because many pigments become transparent at longer wavelengths.

The sensitivity of the OCT instrument is a particularly important factor in nonprofilometric applications. It is defined as the reflectivity of the sample corresponding to the smallest signal which can be detected by the OCT system. The main source of noise in OCT devices is shot noise [22]. Assuming shot-noise-limited detection, the sensitivity of TdOCT instruments depends on the product of optical power (P_0) and exposure time (T_{ex}):

$$\text{Sensitivity}_{\text{TdOCT}} \propto T_{\text{ex}} \cdot P_0. \tag{4}$$

As compared with time domain OCT, SOCT systems have inherently higher sensitivity. This is due to the fact that SOCT enables simultaneous detection by the multipixel device (the CCD camera), and the integration time is effectively extended compared with that in TdOCT. The noise is therefore averaged out more effectively, the sensitivity being improved by a factor of N/2 (Nyqvist limit)

$$\text{Sensitivity}_{\text{SOCT}} \propto \frac{N}{2}\text{Sensitivity}_{\text{TdOCT}}, \tag{5}$$

where N is the number of pixels of the CCD camera used in the detector train.

The final operational parameter is the acquisition speed. As mentioned previously, SOCT systems are up to 100 times faster than TdOCT ones, which allows real-time monitoring of certain processes and the collection of volume (3D) data.

2.5. Exemplary hardware solutions

By choosing from time domain, spectral, and sweep source OCT systems, and by adopting a suitable light source (Table 1), one may assemble a system best fitting the prospective application. Some examples of such devices are described in detail elsewhere in this volume: the medium-resolution time-domain instrument, built in the Medical University in Vienna, and additionally capable of birefringence measurements, is depicted by Góra et al. [29]. Another bulk optics system of similar resolution, but of the spectral type, is described in the article concerning varnish ablation monitoring with OCT [30]. The latter instrument was utilized also for obtaining the stratigraphic images shown in Figures 3–5 and 8. To provide an example of a fibre optics device of slightly higher resolution, one of the instruments built in our laboratory for medical imaging, but also used for art diagnostics (see [31] and Figures 6 and 7), will be described below. It utilizes a Broadlighter^{TM} (from Superlum, Russia) as a light source, and so may be considered a high-resolution system. This broadband light source LS (Figure 2) comprises two coupled superluminescent diode modules with slightly

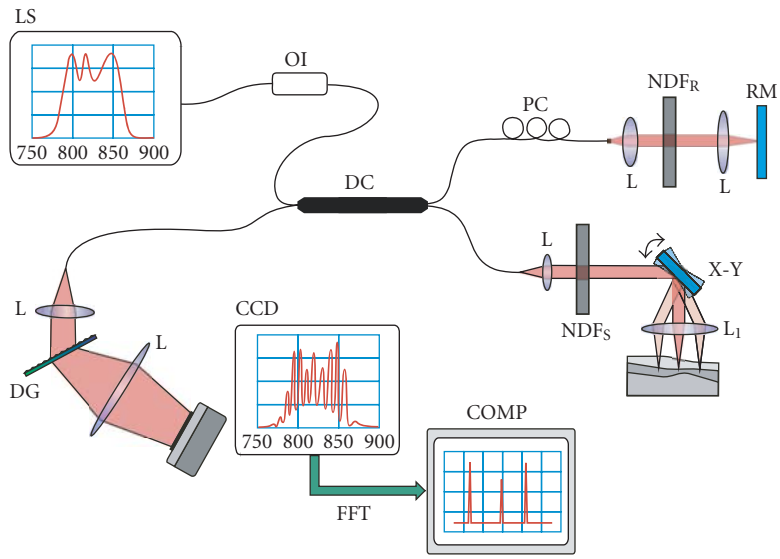

Figure 2: The setup of a spectral OCT instrument. Legend: LS—light source, OI—optical isolator, DC—directional coupler, PC—polarization controller, NDF—neutral density filters, RM—reference mirror, X-Y—scanners, L—lenses, DG—diffraction grating, CCD—linear CCD camera, COMP—personal computer where data processing (primarily fast Fourier transformation) is performed.

shifted central wavelengths. As a result, light of 5 mW output power and high spatial but low temporal coherence, with a spectrum (see insert in Figure 2) at $\lambda_{centre} = 823$ nm and $\Delta\lambda_{FWHM} = 74$ nm, is launched into one of the single mode fibres of the 50 : 50 fibre coupler DC through an optical isolator OI. The optical isolator protects the light source from light back-reflected from the elements of the interferometer, to which it is very sensitive. In the coupler, the incoming light is split into two arms: the reference and object arms. The reference arm consists of a polarization controller PC, a collimator, and an open-air delay line with a reflective mirror RM held in a fixed position. The object arm comprises a collimator, transversal scanners X-Y, and lenses L and L_1. The lens L_1 is placed between the scanner and the object in such a manner that the separation between lens and object, and between the pivot point of the scanner and the lens, are equal to the focal length of the lens. This optics produces a narrow beam of light which penetrates the object, and scatters from elements of its structure. Part of the scattered light is collected by the same optics L_1 and L, and directed back to the coupler DC. It then interferes with the light returning from the reference arm, and this signal is directed into a custom-designed spectrometer. The main part of the detector is a volume phase holographic grating DG with 1200 lines/mm. An achromatic lens L ($f = 150$ mm) focuses the spectrum on a 12-bit line scan CCD camera. The spectral fringe patterns registered by this detector are then transferred to a personal computer COMP. The resulting signal, that is, the spectral fringe pattern, is Fourier-transformed into a single line (A-scan) of a cross-sectional image. In order to obtain either a 2D slice (B-scan, Figure 3(a), e.g.) or a 3D volume tomogram, the beam is scanned transversely by galvanometric scanners X-Y.

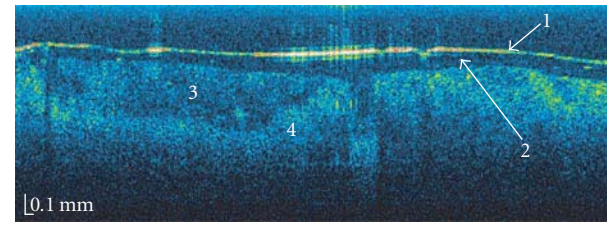

(a)

(b)

(c)

Figure 3: An example of OCT stratigraphy (a) of the oil painting on canvas, (b) the *Portrait of Sir James Wylie*. The tomogram (a) shows the cross-section taken at the place indicated by the vertical bar in the macro-photograph (c). Paintings by courtesy of the Institute for the Study, Restoration, and Conservation of Cultural Heritage, N. Copernicus University, Poland.

The system is shot-noise-limited (the intensity of light in the reference arm of the interferometer is controlled by the neutral density filter NDF) and the overall sensitivity is 90 dB. The exposure time per A-scan is 50 μs, so that a single 2D slice (composed usually of 2000 to 5000 A-scans) is collected in a fraction of a second. In addition to straightforward FFT processing, subtraction of noninterference background, spectral shaping [32], and numerical dispersion correction are carried out [33].

3. OCT DIAGNOSTICS OF MUSEUM OBJECTS

Over the last four years, an increasing number of applications of OCT to various aspects of art diagnostics have been reported. Both time-domain and spectral OCT modalities have been utilized. In this section, an overview of these applications will be given.

3.1. Stratigraphic applications

Since OCT examination is nondestructive, this method of analyzing the internal structure of such delicate objects as paintings on canvas is an obvious application, and has been quite widely explored. The major limitation is the restricted transparency of pigments, even in the infrared. Systematic studies [34] of 47 pigments showed that about a third of them exhibited good transparency at 1500 nm, and about a fifth of them at 820 nm. About another one eighth could be examined in thin layers at either wavelengths. Especially good results are obtained for red pigments (see Figure 3) [35].

The SOCT image (a B-scan) is shown in false colours: white and red colours indicate high scattering of penetrating light, while blue indicates low scattering. The light (λ_{centre} = 830 nm) penetrates the object from the top, and the first structure evident in the image is the surface of the painting (1). The varnish layer (2) does not scatter light, and is visible as a dark strip. Below this, the semitransparent glaze layers (3) and the absorbing paint layer (4) are visible.

Due to its ability to collect a large quantity of data in a short time, spectral OCT is especially well suited for obtaining volume information. In this case, a set of consecutive, adjacent B-scans is collected to cover a desired area of the object's surface. This data may be used to create flow-through films (see supplementary AVI file available at doi 10.1155/2006/35373).

It must be emphasized that, since many pigments are not transparent enough to permit clear structural imaging, this application of OCT is at present restricted to selected areas of paintings. Since the transparency of many pigments increases with the wavelength of penetrating light, significant progress may be expected from the application of longer wavelengths, in the range of 1.5–2.5 μm. However, to maintain reasonable axial resolution, these sources are required to have extremely broad spectra. Together, these conditions point to sweep source OCT as the most promising technique of the future.

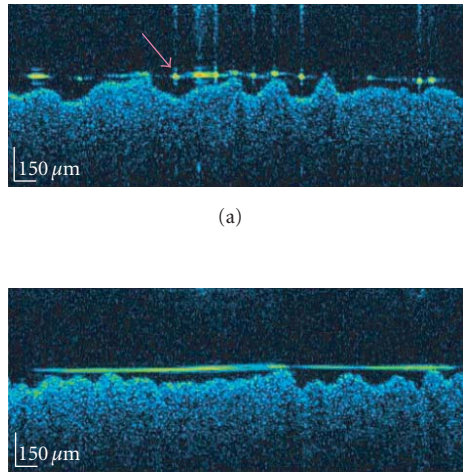

Figure 4: Contemporary layer of varnish: (a) acryl (Talens 114) of high molecular weight—local mirror reflections are seen as bright dots (arrow), (b) ketone (Talens 002) of low molecular weight—in this case the varnish surface is practically mirror flat.

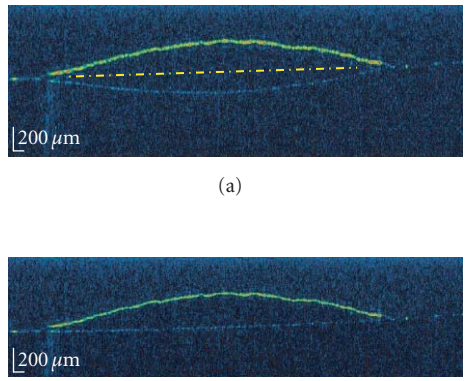

Figure 5: A drop of Rembrandt Varnish Matt from Talens (the Netherlands) on a glass substrate. (a) An uncorrected image. The originally flat glass plate appears concave in the cross-section due to refraction. (b) Image corrected by ray tracing procedure with n_R(varnish) = 1.55.

3.2. Varnish layer analysis

Limitations connected with pigment transparency are not of concern in imaging the varnish layer (Figures 4 and 5(a), see also Figure 3(a), layer 2). Although this layer is particularly easy to image, instruments with high axial resolution are nevertheless highly desirable. Direct comparison with a microscope cross-sectional image corresponding to the area analyzed with OCT shows perfect agreement of the results obtained by means of these two different methods [36]. High resolution OCT also permits the distinguishing of old and new varnish layers [37].

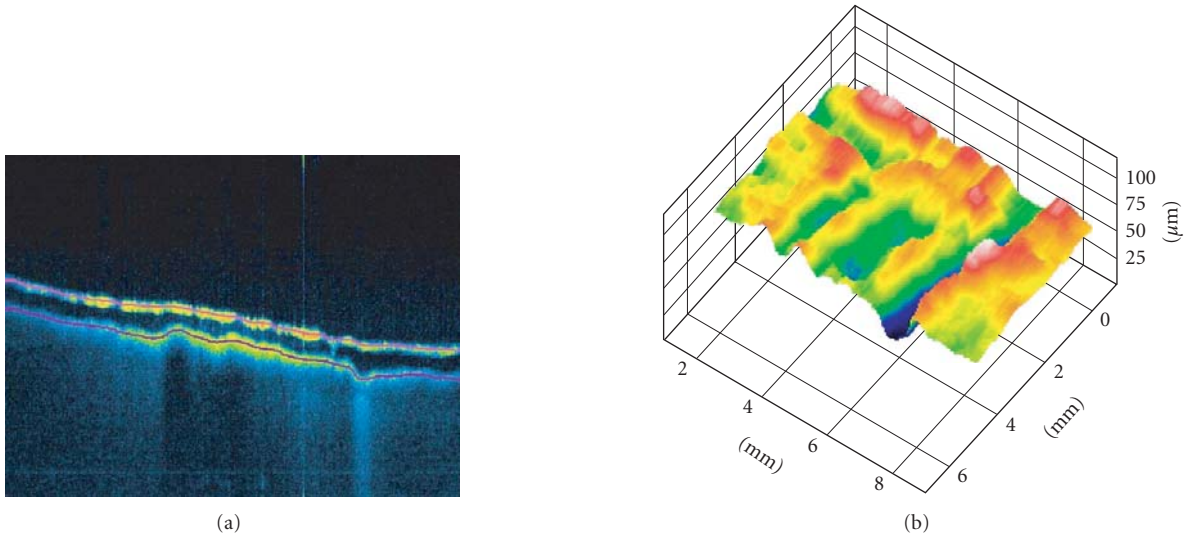

(a) (b)

Figure 6: (a) An OCT tomogram (B-scan) of a varnish layer over a nontransparent paint layer. Red lines denote the recognized interfaces: air-varnish and varnish-paint layer. (b) Varnish thickness map obtained by consecutive collection of 55 parallel OCT B-scans.

When a glossy varnish is imaged, mirror reflections from its surface become a significant difficulty (because of possible saturation of the detector). However, these reflections are a more significant problem in the imaging of fresh, contemporary layers. For historical varnishes, the surface is much less glossy, and tilting the picture slightly is usually enough to overcome the problem. Despite the above difficulty, reflections from the varnish surface also may serve as a measure of its roughness. Preliminary studies of Liang et al. [38] show that the surface of the acrylic varnish Paraloid B72 becomes less smooth and starts to follow the roughness of the substrate as it dries. They consider this as a convenient way of monitoring the wetting and drying process of paint and varnish layers.

In addition to the point raised above, this ability of acrylic varnish to reproduce the surface roughness of the paint layer is linked to the influence of varnish properties on the appearance of paintings. According to de la Rie [39], the varnish determines the final appearance of a picture in two ways: through its refractive index and through the roughness of its dried surface. It was shown that varnishes of high molecular weight (and thus of high viscosity), like modern acrylic media, reproduce the roughness of the surface of the paint layer. This effect, obtained in our laboratory with acrylic Talens 114 varnish (Paraloid B67), is presented in Figure 4(a). On the other hand, a varnish of low molecular weight, ketone Talens 002 (Figure 4(b)), levels the surface of the painting, which is much smoother after the varnish has dried—the mirror reflection is more homogeneous [35]. Historical varnishes composed of natural resins (e.g., dammar and mastic) also have low molecular weight and low viscosity in their liquid form. Consequently, the dried surface is mirror flat, which eliminates scattering of white light and thus increase the colour saturation.

Images of the varnish layer may be also utilized for a convenient measurement of its thickness. However, one must remember that the distances measured are optical and must be corrected to geometrical distances by dividing by the refractive index of the varnish. This effect is visible in Figure 5, as an artificial bending of the glass substrate. There are procedures available to correct images for this effect, if necessary. However, if layers are reasonably flat, simple vertical scale recalculation is sufficient.

If the varnish layer is well defined (compare Figure 3(a) with Figure 4(a)), automatic recognition of both air-varnish and varnish-paint layer interfaces is possible. An example is seen in Figure 6(a) (red lines). If such a procedure is applied to a set of parallel images, the varnish thickness map may be generated (see Figure 6(b)) [31].

An emerging, potentially important, application of imaging varnish layers with OCT is the use of OCT tomography to control the laser-induced varnish ablation process. In this case, OCT may be used to assay the ablation conditions, and to monitor the ablation process *in-situ* [30], the faster SOCT being particularly appropriate to the latter case.

3.3. Other structural analysis

One of the first applications of OCT to investigate the structure of cultural heritage artefacts was the imaging of glaze layers, on a porcelain cup and on a faience plate [40, 41]. OCT tomograms made in the same conditions and with the same instrument clearly show a thicker, less-scattering glaze layer on the porcelain (see Figure 7).

A similar application concerned imaging the structure of archaic jade artefacts from the Qijia and Liangzhu cultures in China [42]. With the aid of TdOCT instrumentation ($\lambda_{\text{centre}} = 800\,\text{nm}$, $\Delta\lambda_{\text{FWHM}} = 50\,\text{nm}$, $\Delta z(\text{in jade}) = 3.5\,\mu\text{m}$,

(a) (b)

Figure 7: Comparison between OCT tomograms of Japanese porcelain (a) and faience (b).

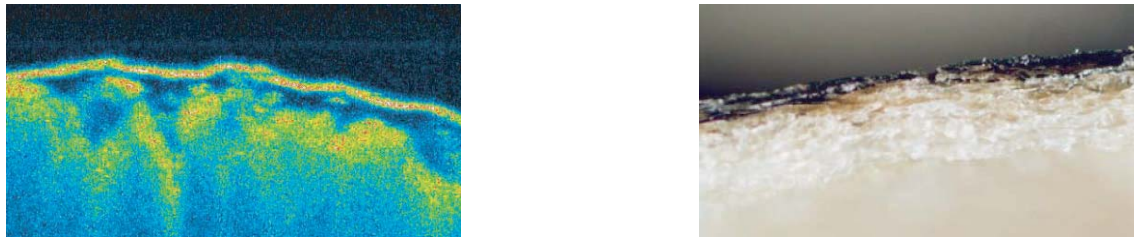

(a) (b)

Figure 8: Comparison between an OCT tomogram (a) and a cut view taken in the same place ((b), photograph by Z. Rozłucka) of an artificially aged sample of parchment covered by iron gall ink.

and $\lambda_{\text{centre}} = 1240\,\text{nm}$, $\Delta\lambda_{\text{FWHM}} = 65\,\text{nm}$, $\Delta z\,(\text{in jade}) = 7.5\,\mu\text{m}$), the authors were able to distinguish between artificially treated (burned) and naturally whitened objects. This provides a valuable reference point for authenticating archaic jades.

A particularly interesting application of TdOCT has recently been proposed by Liang et al. [37]. They used an *en-face* modality of this technique to visualize underdrawings (preparatory drawings under the paint layer). In their system, a one layer (T-scan) perpendicular to the penetrating light is registered by scanning the probing beam over the investigated sample with an appropriate fixed position of the reference mirror. The mirror is then translated to the next position, and the whole procedure is repeated, and so on. Due to the narrow coherence gate (1), information from any given depth may be extracted with high contrast. When the position of the coherence gate is set to the depth at which underdrawings are expected, they are visible with a much better contrast than is available with classical methods, such as infrared imaging with a Vidicon or an InGaAs camera. Moreover, this technique allows, for the first time, the noninvasive determination of the layer in which the underdrawings appear.

Another potentially important application is in the imaging of parchment structure (see Figure 8). Preliminary studies have shown that it should be possible to use the OCT technique to trace structural deterioration caused by iron ink or other similar factors [29].

3.4. Profilometric applications

In these applications, OCT data is used to recover the first interface (i.e., that with air, see Figure 6(a), upper red line, e.g.). When the tracking procedure is applied to each slice in a set of 3D data, an elevation map of the surface may be recovered.

The first profilometric OCT experiment enabling analysis of the structure of a crack in a painting on canvas was performed in our laboratory [41, 43, 44]. The sample was placed in a climate chamber in which the temperature and relative humidity could be controlled. Surface maps were obtained before and after a significant humidity jump to assay the canvas response. The second experiment [45], also involving control in the climate chamber, was aimed at quantitative monitoring of whole canvas deformation. In this experiment, the position of a marker (a submillimetre spot of easy removable contrasting paint), placed at a chosen point on the canvas surface, was monitored simultaneously in 3 dimensions. Every 80 seconds, the area around a marker was scanned with the OCT probing beam. First, the IR reflectometric image of the surface was generated from the OCT data by integration over the whole depth of imaging. Then, the in-plane displacement of the marker was retrieved by numerical correlation with the previous image. Since the new in-plane position of the marker was established, its distance from the OCT head (the out-of-plane position) could be obtained from the OCT data by automatic recognition of the

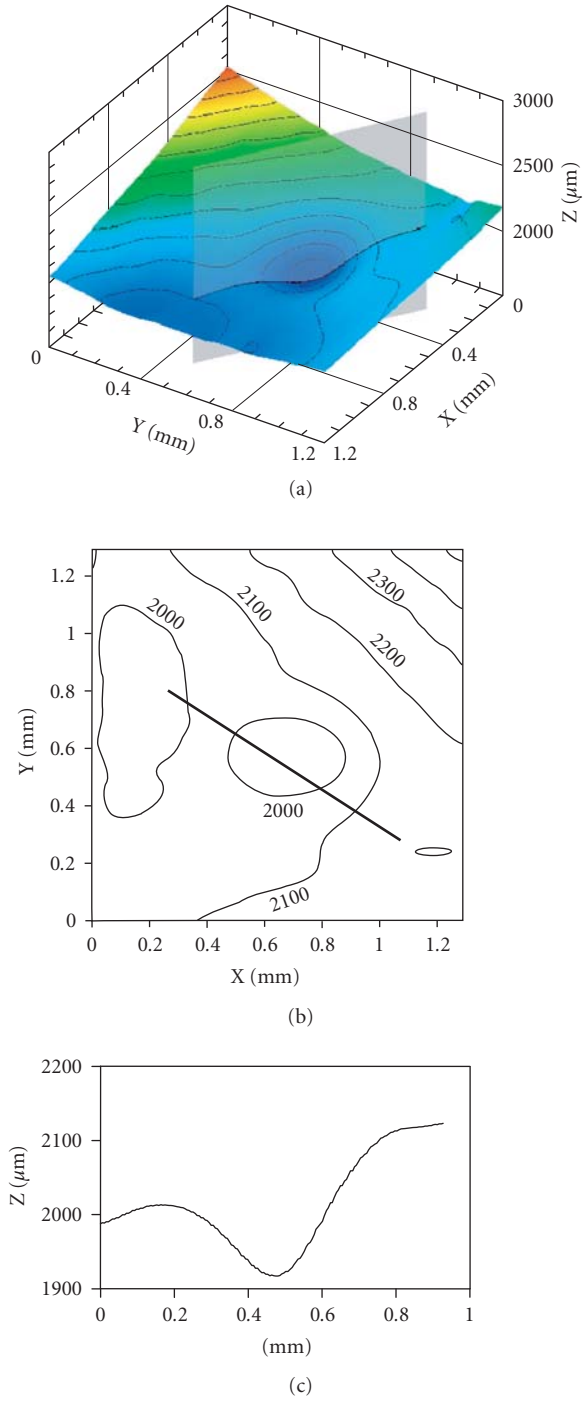

Figure 9: An example of alternative visualisations of the surface profile of an epoxy resin with the ablation crater visible; (a) orthographic surface view, (b) contour map—the heavy line indicates an arbitrary cross-section; (c) cross-sectional profile.

first scattering interface at the position of the marker. Tests show that the precision of marker position recognition is much better than the OCT image resolution of the same instrument (2 versus 8 μm for out-of-plane, and 8 versus 15 μm for in-plane displacements).

Surface profilometry may also prove useful in monitoring varnish removal processes. For example, in the case of laser ablation, the profile and depth of the ablation crater may be recovered. A detailed description and some results are given elsewhere [30]. In Figure 9, an example of our three presently available surface profile analyses is given. All these images were obtained from 3D OCT data comprising 200 parallel A-scans, each made up of 400 B-scans.

4. CONCLUSIONS

In conclusion of this short review of present and potential applications of OCT to diagnostics and documentation of art objects, it should be emphasized that at present it is still seeking for a subject best served by this analytic method. It seems that, for now, the role of the physicist is well defined. Further significant progress will only be possible if this method becomes adopted by art conservationists and analysts. Only experts directly involved in the investigation of the art object are able to ask questions of significant importance for an understanding of the structure and properties of the object examined. The physicist's further role is limited to modification of current instrumentation, and the design and implementation of new modalities, to provide a desirable diagnostic tools in response to this.

ACKNOWLEDGMENTS

This work was supported by Polish Ministry of Science Grant 2 H01E 025 25. Authors wish to thank Dr. Robert Dale for very valuable discussions.

REFERENCES

[1] C. F. Bridgman, "The future of radiography," *Bulletin of the American Institute for Conservation of Historic and Artistic Works*, vol. 14, no. 2, pp. 78–80, 1974.

[2] D. Ambrosini and D. Paoletti, "Holographic and speckle methods for the analysis of panel paintings. Developments since the early 1970s," *Reviews in Conservation*, vol. 5, pp. 38–48, 2004.

[3] D. Anglos, S. Couris, and C. Fotakis, "Laser diagnostics of painted artworks: laser-induced breakdown spectroscopy in pigment identification," *Applied Spectroscopy*, vol. 51, no. 7, pp. 1025–1030, 1997.

[4] M. Castillejo, M. Martín, D. Silva, et al., "Laser-induced breakdown spectroscopy and Raman microscopy for analysis of pigments in polychromes," *Journal of Cultural Heritage*, vol. 1, supplement 1, pp. S297–S302, 2000.

[5] P. Vandenabeele and L. Moens, " The application of Raman spectroscopy for the non-destructive analysis of art objects," in *Proceedings of the 15th World Conference on Nondestructive Testing*, Roma, Italy, October 2000, accessed 2006.

[6] E. R. de la Rie, "Fluorescence of paint and varnish layers—part I," *Studies in Conservation*, vol. 27, no. 1, pp. 1–7, 1982.

[7] E. R. de la Rie, "Fluorescence of paint and varnish layers—part II," *Studies in Conservation*, vol. 27, no. 2, pp. 65–69, 1982.

[8] E. R. de la Rie, "Fluorescence of paint and varnish layers—part III," *Studies in Conservation*, vol. 27, no. 3, pp. 102–108, 1982.

[9] D. Anglos, M. Solomidou, I. Zergioti, V. Zafiropulos, T. G. Papazoglou, and C. Fotakis, "Laser-induced fluorescence in artwork diagnostics: an application in pigment analysis," *Applied Spectroscopy*, vol. 50, no. 10, pp. 1331–1334, 1996.

[10] E. Walmsley, C. Metzger, J. K. Delaney, and C. Fletcher, "Improved visualization of underdrawings with solid-state detectors operating in the infrared," *Studies in Conservation*, vol. 39, no. 4, pp. 217–231, 1994.

[11] K. K. Taylor, M. J. Cotter, and E. V. Sayre, "Neutron activation autoradiography as a technique for conservation examination of paintings," *Bulletin of the American Institute for Conservation of Historic and Artistic Works*, vol. 15, no. 2, pp. 93–102, 1975.

[12] D. Huang, E. A. Swanson, C. P. Lin, et al., "Optical coherence tomography," *Science*, vol. 254, no. 5035, pp. 1178–1181, 1991.

[13] E. A. Swanson, J. A. Izatt, M. R. Hee, et al., "In vivo retinal imaging by optical coherence tomography," *Optics Letters*, vol. 18, no. 21, pp. 1864–1866, 1993.

[14] M. R. Hee, J. A. Izatt, E. A. Swanson, et al., "Optical coherence tomography of the human retina," *Archives of Ophthalmology*, vol. 113, no. 3, pp. 325–332, 1995.

[15] P. H. Tomlins and R. K. Wang, "Theory, developments and applications of optical coherence tomography," *Journal of Physics D: Applied Physics*, vol. 38, no. 15, pp. 2519–2535, 2005.

[16] A. M. Rollins, M. D. Kulkarni, S. Yazdanfar, R. Ung-Arunyawee, and J. A. Izatt, "In vivo video rate optical coherence tomography," *Optics Express*, vol. 3, no. 6, pp. 219–229, 1998.

[17] T. Dresel, G. Hausler, and H. Venzke, "Three-dimensional sensing of rough surfaces by coherence radar," *Applied Optics*, vol. 31, no. 7, pp. 919–925, 1992.

[18] M. Wojtkowski, R. Leitgeb, A. Kowalczyk, T. Bajraszewski, and A. F. Fercher, "In vivo human retinal imaging by Fourier domain optical coherence tomography," *Journal of Biomedical Optics*, vol. 7, no. 3, pp. 457–463, 2002.

[19] M. Wojtkowski, T. Bajraszewski, P. Targowski, and A. Kowalczyk, "Real-time in vivo imaging by high-speed spectral optical coherence tomography," *Optics Letters*, vol. 28, no. 19, pp. 1745–1747, 2003.

[20] M. Wojtkowski, V. J. Srinivasan, T. H. Ko, J. G. Fujimoto, A. Kowalczyk, and J. S. Duker, "Ultrahigh-resolution, high-speed, Fourier domain optical coherence tomography and methods for dispersion compensation," *Optics Express*, vol. 12, no. 11, pp. 2404–2422, 2004.

[21] R. A. Costa, M. Skaf, L. A. S. Melo Jr., et al., "Retinal assessment using optical coherence tomography," *Progress in Retinal and Eye Research*, vol. 25, no. 3, pp. 325–353, 2006.

[22] R. Leitgeb, C. K. Hitzenberger, and A. F. Fercher, "Performance of fourier domain vs. time domain optical coherence tomography," *Optics Express*, vol. 11, no. 8, pp. 889–894, 2003.

[23] S. H. Yun, C. Boudoux, M. C. Pierce, J. F. De Boer, G. J. Tearney, and B. E. Bouma, "Extended-cavity semiconductor wavelength-swept laser for biomedical imaging," *IEEE Photonics Technology Letters*, vol. 16, no. 1, pp. 293–295, 2004.

[24] S. H. Yun, G. J. Tearney, B. E. Bouma, B. H. Park, and J. F. De Boer, "High-speed spectral-domain optical coherence tomography at 1.3 μm wavelength," *Optics Express*, vol. 11, no. 26, pp. 3598–3604, 2003.

[25] R. Huber, M. Wojtkowski, K. Taira, J. G. Fujimoto, and K. Hsu, "Amplified, frequency swept lasers for frequency domain reflectometry and OCT imaging: design and scaling principles," *Optics Express*, vol. 13, no. 9, pp. 3513–3528, 2005.

[26] R. Huber, M. Wojtkowski, and J. G. Fujimoto, "Fourier Domain Mode Locking (FDML): a new laser operating regime and applications for optical coherence tomography," *Optics Express*, vol. 14, no. 8, pp. 3225–3237, 2006.

[27] R. Huber, M. Wojtkowski, J. G. Fujimoto, J. Y. Jiang, and A. E. Cable, "Three-dimensional and C-mode OCT imaging with a compact, frequency swept laser source at 1300 nm," *Optics Express*, vol. 13, no. 26, pp. 10523–10538, 2005.

[28] A. Dubois, L. Vabre, A.-C. Boccara, and E. Beaurepaire, "High-resolution full-field optical coherence tomography with a Linnik microscope," *Applied Optics*, vol. 41, no. 4, pp. 805–812, 2002.

[29] M. Góra, M. Pircher, E. Götzinger, et al., "Optical coherence tomography for examination of parchment degradation," *Laser Chemistry*, vol. 2006, Article ID 68679, 2006, 6 pages.

[30] M. Góra, P. Targowski, A. Rycyk, and J. Marczak, "Varnish ablation control by optical coherence tomography," *Laser Chemistry*, vol. 2006, Article ID 10647, 2006, 7 pages.

[31] I. Gorczyńska, M. Wojtkowski, M. Szkulmowski, et al., "Varnish thickness determination by spectral optical coherence tomography," in *Proceedings of the 6th International Congress on Lasers in the Conservation of Artworks (LACONA VI '05)*, J. Nimmrichter, W. Kautek, and M. Schreiner, Eds., Vienna, Austria, September 2006.

[32] M. Szkulmowski, M. Wojtkowski, P. Targowski, and A. Kowalczyk, "Spectral shaping and least square iterative deconvolution in spectral OCT," in *Coherence Domain Optical Methods and Optical Coherence Tomography in Biomedicine VIII*, vol. 5316 of *Proceedings of SPIE*, pp. 424–431, San Jose, Calif, USA, January 2004.

[33] B. Cense, N. A. Nassif, T. C. Chen, et al., "Ultrahigh-resolution high-speed retinal imaging using spectral-domain optical coherence tomography," *Optics Express*, vol. 12, no. 11, pp. 2435–2447, 2004.

[34] A. Szkulmowska, M. Góra, M. Targowska, et al., "The applicability of optical coherence tomography at 1.55 um to the examination of oil paintings," in *Proceedings of the 6th International Congress on Lasers in the Conservation of Artworks (LACONA VI '05)*, J. Nimmrichter, W. Kautek, and M. Schreiner, Eds., Vienna, Austria, September 2006.

[35] M. Targowska, "Pomiary konserwatorskie z wykorzystaniem metody tomografii optycznej -OCT (Examination of objects of art with optical coherence tomography)," M.S. thesis, Department of Conservation of Paintings and Polychrome Sculpture, Nicolaus Copernicus University, Toruń, Poland, 2006, B. Rouba Advisor.

[36] T. Arecchi, M. Bellini, C. Corsi, et al., "Optical coherence tomography for painting diagnostics," in *Optical Methods for Arts and Archaeology*, vol. 5857 of *Proceedings of SPIE*, pp. 278–282, Munich, Germany, June 2005.

[37] H. Liang, M. G. Cid, R. G. Cucu, et al., "En-face optical coherence tomography—a novel application of non-invasive imaging to art conservation," *Optics Express*, vol. 13, no. 16, pp. 6133–6144, 2005.

[38] H. Liang, M. G. Cid, R. G. Cucu, et al., "Optical coherence tomography: a non-invasive technique applied to conservation of paintings," in *Optical Methods for Arts and Archaeology*, vol. 5857 of *Proceedings of SPIE*, pp. 9 pages, Munich, Germany, June 2005.

[39] E. R. de la Rie, "The influence of varnishes on the appearance of paintings," *Studies in Conservation*, vol. 32, no. 1, pp. 1–13, 1987.

[40] P. Targowski, B. Rouba, M. Wojtkowski, I. Gorczyńska, and A. Kowalczyk, "Zastosowanie optycznej tomografii do nieinwazyjnego badania obiektów zabytkowych," in *Ars longa - vita brevis. Tradycyjne i nowoczesne metody badania dzieł sztuki. Materiały z sesji naukowej poświęconej pamięci profesora Z. Brochwicza*, J. Flik, Ed., pp. 121–129, Wydawnictwo UMK, Toruń, Poland, 2003.

[41] P. Targowski, B. Rouba, M. Wojtkowski, and A. Kowalczyk, "The application of optical coherence tomography to nondestructive examination of museum objects," *Studies in Conservation*, vol. 49, no. 2, pp. 107–114, 2004.

[42] M.-L. Yang, C.-W. Lu, I.-J. Hsu, and C. C. Yang, "The use of optical coherence tomography for monitoring the subsurface morphologies of archaic jades," *Archaeometry*, vol. 46, no. 2, pp. 171–182, 2004.

[43] T. Bajraszewski, I. Gorczyńska, B. Rouba, and P. Targowski, "Spectral domain optical coherence tomography as the profilometric tool for examination of the environmental influence on paintings on canvas," in *Proceedings of the 6th International Congress on Lasers in the Conservation of Artworks (LACONA VI '05)*, J. Nimmrichter, W. Kautek, and M. Schreiner, Eds., Vienna, Austria, September 2006.

[44] P. Targowski, T. Bajraszewski, I. Gorczyńska, et al., "Spectral optical coherence tomography for nondestructive examinations," submitted to *Optica Applicata*.

[45] P. Targowski, M. Góra, T. Bajraszewski, et al., "Optical coherence tomography for tracking canvas deformation," *Laser Chemistry*, vol. 2006, Article ID 93658, 2006, 8 pages.

Hindawi Publishing Corporation
Laser Chemistry
Volume 2006, Article ID 93658, 8 pages
doi:10.1155/2006/93658

Research Article

Optical Coherence Tomography for Tracking Canvas Deformation

Piotr Targowski,[1] Michalina Góra,[1] Tomasz Bajraszewski,[1] Maciej Szkulmowski,[1] Bogumiła Rouba,[2] Teresa Łękawa-Wysłouch,[2] and Ludmiła Tymińska-Widmer[2]

[1] *Institute of Physics, Nicolaus Copernicus University, Ul. Grudziadzka 5, 87-100 Toruń, Poland*
[2] *Institute for the Study, Restoration and Conservation of Cultural Heritage, Nicolaus Copernicus University, Ul. Gagarina 9, 87-100 Toruń, Poland*

Received 16 September 2006; Revised 28 November 2006; Accepted 29 November 2006

Recommended by Costas Fotakis

Preliminary results of the application of optical coherence tomography (OCT), in particular in its spectral mode (SOCT), to tracking of deformations in paintings on canvas caused by periodical humidity changes are presented. The setup is able to monitor the position of a chosen point at the surface of a painting with micrometre precision, simultaneously in three dimensions, every 100 seconds. This allows recording of deformations associated with crack formation. For the particular painting model examined, it was shown that the surface moves in-plane towards the corner, and bulges outwards (Z-direction) in response to a rise in humidity. Subsequent to the first humidification/drying cycle, translation in the Z-direction is decreased, whilst in-plane translations increase somewhat. It was also shown that the response of the painting on canvas begins immediately on changing the relative humidity in the surroundings.

1. INTRODUCTION

Differences between environmentally induced dimensional changes in each of the hygroscopic layers composing the multilayer complex of an oil painting on canvas result in deformations, cracks, and detachments between layers, causing severe damage to the structure of the painting. An ongoing research project aims at the gathering of detailed data for a better understanding of the relationships between the painting technique employed, the subsequent history of the painting (age and storage conditions), and its susceptibility to dimensional deformation influenced by fluctuations of relative humidity and temperature, as well as quantifying the range and direction of the changes. The project demands an accurate and convenient method of tracking three-dimensional deformation of the object subjected to environmental stress. The present study was to assess the applicability of optical coherence tomography (OCT) for nondestructive and noncontact monitoring of such deformations in microregions of the surface examined, namely, to estimate the rapidity, range, and direction of dimensional changes in a typical (model) painting on canvas in response to periodical changes of relative humidity.

OCT is a noninvasive technique, well established in medical diagnostics, especially in ophthalmology, where it is routinely used for imaging precise cross-sections of the eye in vivo. This method has also been used for investigating the internal structure of some objects of art, like varnish and glaze layers of paintings on canvas, and also parchment and porcelain objects (see [1] for a brief review). This new application of OCT broadens the spectrum of nonintrusive techniques for measuring deformations and strains occurring in works of art. Among noncontact methods, generally based on optical phenomena, the most popular are double-exposure holography, electronic pattern interferometry and photogrammetry. A review of this subject recently published by Dulieu-Barton et al. [2] contains not only a comprehensive list of references, but also descriptions of all the methods used mainly for examinations of art works made of rigid materials such as plaster, stone, wall paintings, mosaics, ceramics, and panel paintings. A review article by Ambrosini and Paoletti [3] is devoted specifically to methods used for examination of paintings on wooden supports. The

investigation of deformations in flexible materials, for example, paintings on canvas, which are more sensitive to vibrations and strain fluctuations, is significantly more difficult. To the best of our knowledge, the major work in this area is that of Young (e.g., [4–8]), who utilised electronic speckle pattern interferometry (ESPI) combined with tensometry (biaxial tensile tester). These experiments generate maps of in-plane strain distribution over an approximately 30×30 cm square surface, and are very useful for assessment of conservation methods for local tear mending [6], lining [7], and canvas mounting on stretcher [8]. Varoli-Piazza et al. [9] used image correlation based on stereophotogrammetry to assess the distortions of textile artefacts caused by their display in different orientations. This method—designed for 3D measurement—is less sensitive to vibrations and fluctuations in strain state than ESPI. Among other tools useful for deformation measurements, resistance (ohmic) strain gauges and optical fiber sensors should be mentioned [2]. However, both of these methods require contact (attachment of the sensor to the object), and must be specifically tuned to the properties of the object of interest.

2. EXPERIMENT

To track canvas displacement, spectral optical coherence tomography (SOCT)—a new, rapidly growing brand of OCT—was chosen, due to its very high speed of imaging. The instrument consists of a light source of high spatial but low time coherence and a Michelson interferometer. One arm of the interferometer is terminated by the reference mirror, the other contains the collimating optics, which also provide scanning of the probing beam over the surface of the object under investigation. The scattered light is collected back by the same optics and brought to interference with the light from the reference arm. The resulting light is spectrally analysed, and the signal obtained is Fourier transformed.

In this application, SOCT is used as a profilometric tool. The position of the surface of the object investigated is recovered from the dominating frequency of interference fringes superimposed on the light source spectrum. The frequency of these fringes is proportional to the optical path difference in the two arms of the interferometer. The major advantages of using the OCT method for this application lie in *simultaneous* detection of position in 3 dimensions, and in the absence of problems characteristic of methods relying on measurements of phase differences. Phase detection methods usually suffer from some difficulties, in particular phase ambiguity and phase unwrapping, especially in the case of large displacements (the interference fringes are then close, and hard to resolve). In addition, phase detection methods are sensitive to microdisplacements (less than a wavelength) of the investigated object with respect to the measuring head: such a dislocation produces additional, unwanted fringes. Lack of this last effect in OCT simplifies the experimental setup and permits long-lasting examination (up to several days), as well as in situ testing. The major disadvantage is in surface (or in-depth in some modalities) scanning, intrinsic to OCT, which always takes more time than the recording of fringe images, such as in phase interferometry.

The method described here combines profilometry with marker tracking. A substantial advantage of such an approach is its simple and unequivocal displacement recognition, with the disadvantage only of the restriction that displacements are monitored to just one chosen point (or, in the near future, a few points) of the surface. The probing beam is scanned over a rectangular region (4×4 mm) of canvas surface to monitor the displacement of the chosen point within this area. Two-directional scanning, which requires collection of $500 \times 500 = 250\,000$ data points, takes only about 12 seconds, which is acceptable for the time-resolved experiments described in this paper. However, it must be admitted that, due to the huge amount of data generated during the scanning, these data must be processed online to reduce the size of information permanently stored. Presently, acquisition and processing takes together about 80 seconds (with a 1.8 GHz AMD Athlon^{TM} 64 processor), which sets a lower limit on the interval between which successive canvas positions can be determined.

The aim of the experiment performed was to track the deformations of a painting on canvas subjected to periodical changes of humidity. These conditions are common in an exhibition area or sacral interior during opening hours, and separated by long intervals with lower relative humidity at night.

Displacements of the canvas surface are a complex result of both slow and fast reactions in separate layers in the multilayer structure of the painting, that also stimulate or restrain changes occurring in other layers. The size layer and linen support react the fastest and the most extensively [10–12]. In paintings made with a technique similar to the sample tested (where the size—applied cold—does not saturate the textile, but fills spaces between treads), dimensional changes in these layers in response to relative humidity rises are usually opposing. Contraction of the canvas in the warp and weft directions resulting from an increase in the crimping of the swelling threads is decreased to some extent by wedges of gelatine glue separating threads and expanding due to their hygroscopic nature. Contraction of the size during drying stresses the whole structure of the painting. The comparatively stiff ground layer and oil paint film respond to both increases and decreases in humidity at a smaller rate and with longer delay. They resist displacements of their support until the moment at which the stress exceeds their cohesion, at which point they crack.

The wooden stretcher also influences the behaviour of the whole painting. Its resistance can prevent contraction of the painting in response to a rise in humidity and thus increase the stress in the structure. The later delayed expansion of the wood can even create additional tension.

3. MATERIALS AND METHODS

3.1. Sample

The painting tested in the present study was chosen from a series of 80 samples prepared with the intention of producing

models that would best represent properties of real paintings.

Modern commercial linen canvas of medium thickness and close weave (15 threads of warp and 13 threads of weft per cm^2, and filling factors, defined in [10, 11] as the percentage projected surface area occupied by threads, calculated as the product of the number density of threads and their average width—$Z_{weft} = 68\%$, $Z_{warp} = 70\%$, $Z_{total} = 90\%$) was used. This canvas was prepared by stretching over a keyed pinewood stretcher (height 30 cm, width 40 cm) with weft in the vertical direction. Staples were used to secure the canvas at hand tension. A cold 5% gelatine size was applied with a spatula and followed by two layers of emulsive gesso serving as priming. Three layers of casein tempera and one of alizarin oil glaze were used to imitate an old paint layer. The sample was tested after six months of seasoning in the ambient conditions of a conservation studio.

3.2. Experimental setup

To create periodical changes in the environment of the sample, an airtight compartment was designed (Figure 1(a)). Its front wall was made of 2 mm glass to allow optical scanning. The humidity increment is induced by trickling water down over a piece of cotton fabric which is hung 15 cm behind the back of the canvas support. The consecutive decrease of humidity (to ambient level) is achieved by ventilation of the compartment. During all experiments, the temperature and relative humidity inside the chamber were monitored with a HygroClip *S* sensor from Rotronic (Switzerland). To simulate the effect of variable environmental conditions on a painting, the model was subjected to two cycles of rapid humidification (see Figure 4, upper panel in results section), lasting for 1.5 hours (up to 90% RH) in every 24 hours, over four days. The cycles were separated by a 1.5-hour period of drying to ambient conditions. The temperature remained fairly constant.

To monitor the position of a chosen point on the canvas, a small reference marker dot (~ 0.4 mm in diameter) of good reflective paint is placed on the paint layer. This marker was located in the bottom right corner, 5 cm from both edges of the canvas (Figure 1(b)), just at the boundary of the area of the canvas covered by the wooden stretcher bar. This position was chosen due to the moderate displacement of this area as compared with that of the central area of the canvas noted previously in [13, 14], and confirmed here in preliminary tests. The positive X'-coordinate axis points towards the vertical canvas edge, parallel to the warp direction, the Y'-axis away from the lower horizontal edge, parallel to the weft direction. The Z'-axis points out of the canvas.

The details of the SOCT instrument used in this study are described elsewhere in this volume [15]. However, it is worthwhile to repeat here that the instrument utilises a superluminescent diode emitting light of central wavelength 835 nm and spectral width (FWHM) 50 nm. The axial (in-depth) resolution obtained was $8\,\mu$m (in air). The light, of $\sim 200\,\mu$W intensity, is focused at the object surface to a spot of $\sim 15\,\mu$m in diameter. It should be noted that the resolutions defined above relate to ordinary cross-sectional imaging. However, in the case of this study, information on displacement is drawn from repeated analysis of the same object, that is, the reference marker. As a result, the real resolution of the displacement measurement depends also on details of the procedures used for data collection and analysis, and must in practice be determined experimentally. For present purposes, this was accomplished by consecutive measurements of the position of the test object, held steady in the X, Y plane, and precisely translated in the Z-direction. Repeatability of the X, Y determination may be considered as a measure of the lateral resolution, and similarly the resolution of the Z-coordinate as a measure of axial resolution. It is not surprising that the lateral and Z-coordinate resolutions ($8\,\mu$m and $2\,\mu$m, resp.) obtained from such a procedure are both smaller than the expected (theoretical) ones cited above, since here it is the same object that is being tracked, and relative displacements that are being recovered. In addition to resolution, a second factor decisive for the application of the method described is the range of translation which it is possible to monitor. For in-plane translation, the latter is limited by the dimensions of the scanned area (here, 4×4 mm), and thus may be estimated to be 2 mm in any in-plane direction. For axial translations, the range is equivalent to the depth of cross-sectional imaging, and is limited by optical properties of the OCT instrument [1]. For the system employed here, the axial range is thus about 1 mm in both (inward and outward) directions. These resolutions and ranges determine the available range over which the effects examined may be investigated, and limit the variety of environment conditions which may be studied.

3.3. Data analysis

Data collection and analysis were performed online in the following 4 steps.

Step 1 (data collection). Volume data for analysis were collected by scanning over a square area 4×4 mm, usually composed of 500×500 pixels. By integrating the OCT signal over the whole depth of scanning, a 2D image of the sample surface is prepared (Figure 2(a)) and used for marker recognition (Step 2). Depth data are used for Z-coordinate recovery (Step 3).

Step 2 (marker recognition and tracking). An image of the marker is stored during the first measurement. In consecutive following measurements, the position of the marker is automatically recovered by seeking the maximum of the 2D correlation function between the new image of the canvas ($I(x, y)$) and the stored image of the marker ($P(x, y)$):

$$C(x,y) = I(x,y) \otimes P(x,y) = \iint I(x,y) \otimes P(x+t, y+s)\,dt\,ds,$$
$$(X,Y) : C(x,y) = \text{Max}, \tag{1}$$

where $I(x, y)$ denotes the newly registered image of the canvas, $P(x, y)$ is the stored image of the marker, and C is the

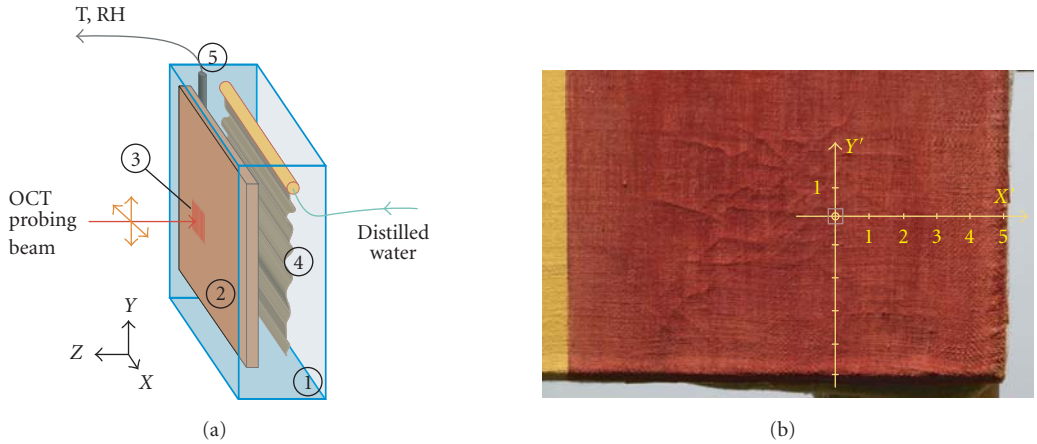

Figure 1: (a) The climate control sample compartment used in the study: (1) airtight chamber with a glass front wall, (2) sample: a painting on canvas on a stretcher, (3) scanned area of the paint layer, (4) cotton fabric used to increase humidity, (5) temperature and relative humidity sensor. (b) Position of the marker (small circle) and the scanned area (square). Axes indicate the orientation of the sample coordinate system.

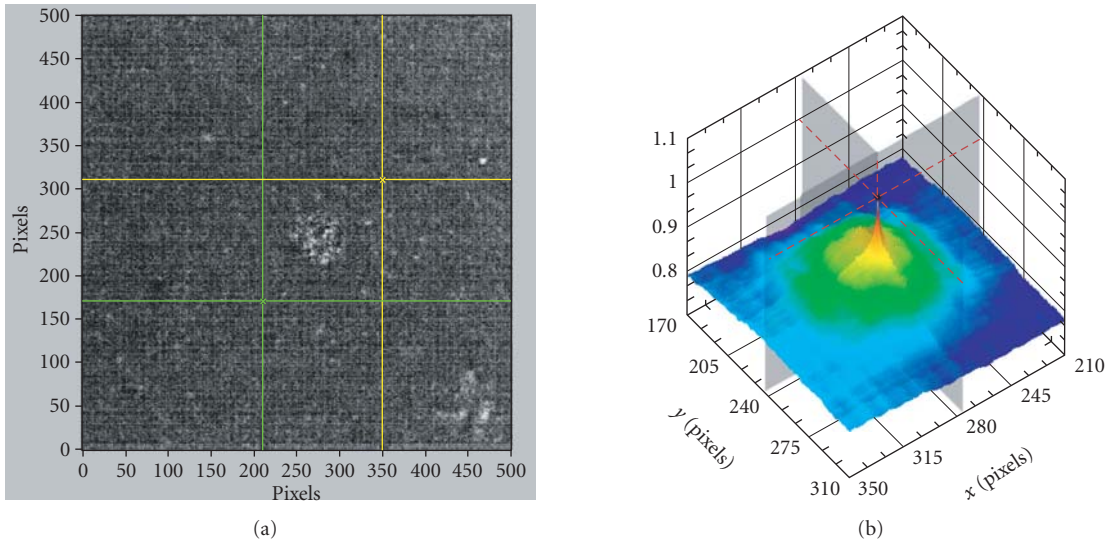

Figure 2: (a) A 2D image of the scanned area (Figure 1(a)-3); the marker is visible as a lighter spot in the centre, within the cursor lines. (b) The correlation function $C(x, y)$: the maximum of this function gives the position of the marker.

correlation function (Figure 2(b)). X, Y are the recovered coordinates of the marker in the laboratory coordinate system.

Step 3 (Z-coordinate determination). The Z-coordinate of the marker is recovered from OCT A-scans. The A-scans from the area centred on the position of the image marker (X, Y) are averaged, and the Z-coordinate is recovered from this averaged signal. A position index of the maximum of this averaged signal is recovered. The relative Z-coordinate is calculated by multiplying the position index by an FFT scale coefficient (4 μm/FFT bin in the system described). This coefficient depends on the design of the spectrometer and can be obtained by calibration.

The resolution of the Z-coordinate determination depends on the algorithm used in the peak detection subroutine. The subroutine uses a least squares quadratic fit to find the peaks; thus the index value is fractional rather than integer.

Step 4 (marker coordinates transformation). The marker coordinates (X, Y, Z) obtained must be transformed to the sample coordinate system (X', Y', Z')—Figure 3(a). To define these new coordinates, it is assumed that the sample Z'-axis is normal to the sample surface and that the sample X'-axis remains in the horizontal X, Z plane.

This new system is attached to a plane obtained by fitting to the surface profile recovered from the OCT data—Figure 3(b). The procedure of determining the coordinate transformation is performed once for the experiment—it is

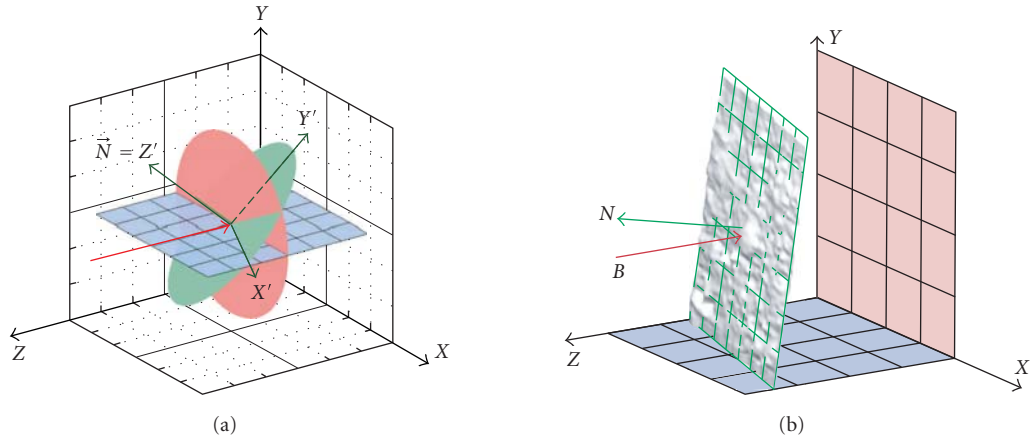

FIGURE 3: (a) mutual orientation of the two coordinate systems. The red plane denotes the (X, Y) surface in the laboratory system, the green one denotes the sample surface. Vector $\vec{N}$ is normal to the sample surface. (b) The sample plane (green mesh) is obtained by fitting to the surface profile. The red arrow (parallel to the Z-axis) denotes the OCT probing beam.

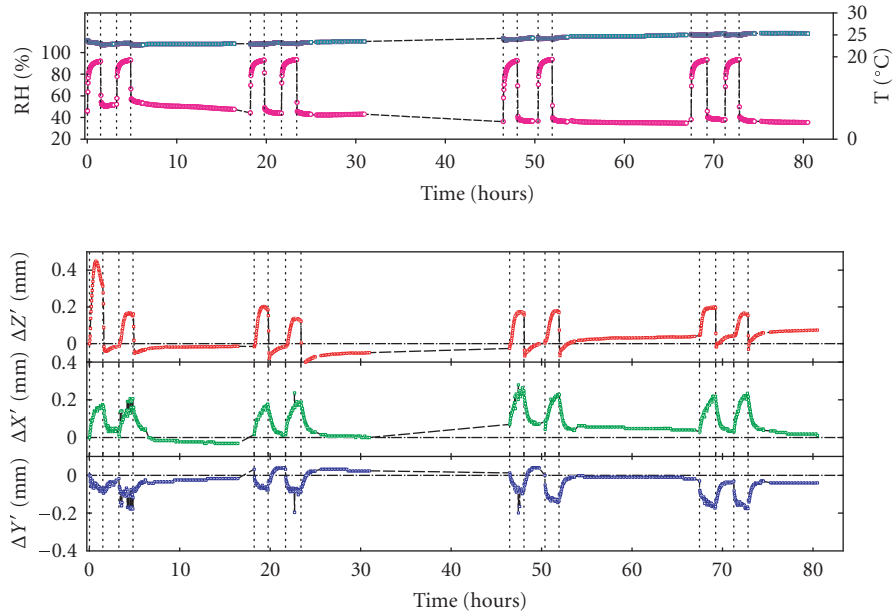

FIGURE 4: Displacements of the position of the marker at the surface of the sample in response to periodical changes in relative humidity (RH, the upper panel).

assumed that the stretcher remains in a constant position thereafter. The details are given in the appendix.

4. RESULTS AND DISCUSSION

The experiment set-up was to monitor the behaviour of painting on canvas subjected to simulated periodical changes of humidity in its surroundings. Within four days, slight but clearly visible cracks had appeared, running across the paint and ground layers (Figure 1(b)). On the microscale, small movements (up to 0.4 mm) of the marker on the surface of the paint layer were observed (Figure 4 and supplementary file). Preliminary tests showed that the choice of the point to be tracked by OCT on the surface of the painting is crucial, as displacements recorded during climatic change are different in the centre of the painting than at the edges, especially those in the Z-direction. For the present tests, a point in a region of the canvas exhibiting moderate deformation was chosen.

Changes in $\Delta X'$, $\Delta Y'$, and $\Delta Z'$ of the marker with respect to its initial position were observed immediately after

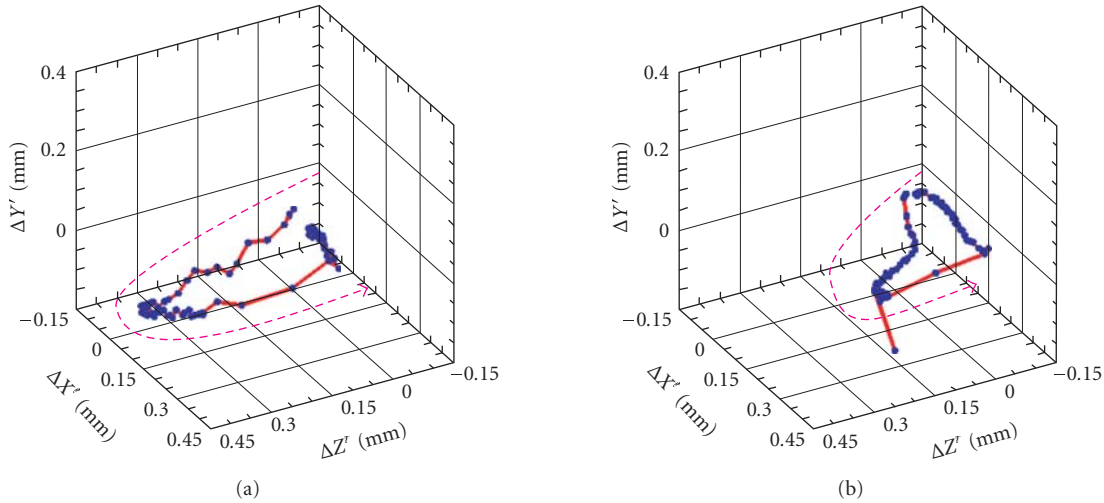

Figure 5: Traces of marker displacements during the first (a) and fourth (b) humidification cycles. Notice the spike evident in panel (b).

every variation in climatic condition. The translation in the X'-Y' plane caused by rise of humidity was directed towards the (near) corner of the painting—see also the AVI movie attached. This displacement was accompanied by simultaneous outward movement (towards the OCT instrument, positive Z'-direction). Around 85% RH, this reaction is reversed: the marker was moving back slightly (negative Z').

Rapid drying out of the test chamber caused an immediate and strong reaction of the painting in the negative Z'-direction: the marker was moving back behind the initial (before humidification) plane, and then relaxing to the initial position during drying in ambient conditions. In contrast with in-plane translations, the movement in the Z'-directions does not simply follow the humidity—the direction alternates during a monotonic change in humidity conditions.

In the X'-Y' plane, the general form and features of the changes ($\Delta X'$ and $\Delta Y'$ curves) are the similar, although larger displacements were registered in the X'-direction parallel to the warp and the long stretcher bar. It is difficult to judge if disproportion in reaction along the X'- and Y'-axes results from the difference in the dimensions of the sample in the two directions, or from the dominance of the overall anisotropic reaction of the canvas itself: for contemporary linen canvases, it is quite common that the warp is less stiff and more susceptible than the weft to dimensional deformation influenced by fluctuations of relative humidity [16–18]. It is important to point out the somewhat irregular character of the $\Delta X'$ and $\Delta Y'$ curves. We believed that the spikes, visible in the $\Delta X'$ and $\Delta Y'$ curves, but not in the $\Delta Z'$ curves, are due to a sudden relaxation of tension in the structure—possibly due to the formation of cracks in the paint layer (such cracks were observed after the experiment), or to rapid movements of the weave or of separate threads in the canvas.

The first day of humidification cycling exhibits somewhat different behaviour, both qualitatively and quantitatively. The effects of the first climate shock are very different to those of the consecutive ones. This first response in the direction perpendicular to the canvas surface (Z') is significantly stronger than that found in the following ones. This is not the case for in-plane displacements, in which the Y' displacement was even somewhat less than in consecutive cycles. The first humidification cycle in the experiment described was also the first major environmental stress applied to the picture, which had previously been stored in ambient conditions. The painting probably settled down on the stretcher during this first cycle of rapid humidification. During the second humidification cycle on the first day, several spikes were observed in the curves representing changes in the X'-Y' plane. Probably, this second climatic shock and rapid rise of tension in the multilayer composite (caused by shrinkage of canvas restrained by the stretcher, and/or expansion of the size and priming layer) resulted in crack formation in the stiffest layers.

In the curves representing further consecutive cycles, spikes only show up around the maximal values of displacement, and they are more prominent in the $\Delta Y'$ curves representing changes in the sample vertical (weft). It is significant that spikes occur during humidification but not during drying.

Comparing the three-dimensional marker displacement traces during the first (Figure 5(a)) and subsequent cycles (the fourth, e.g., Figure 5(b)), it is again evident that, although in all cycles there is hysteresis in the sample deformation (indicating some persistence in deformation), the response to the first climate shock is very different to that of the consecutive ones.

The complicated changes described above reflect the complexity of reactions influencing the behaviour of the whole of the multilayer structure of the painting on canvas. Displacement of the picture in Z'-direction could be caused directly or secondarily: it could result from the movement of

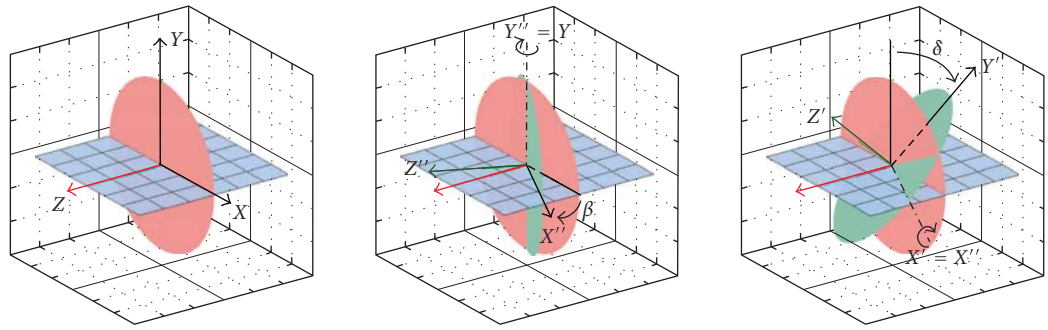

FIGURE 6: (a) The laboratory coordinate system, (b) rotation about Y'' through angle β, (c) rotation about X' through angle δ.

the whole structure due to a change of tension in the painting on the stretcher, bulking of the face caused by uneven shrinkage or expansion of various layers in the composite, and/or change in the thickness of the structure resulting from swelling of hygroscopic layers, as well as out-of-plane distortions in particular sections of the cracked gesso and paint layer.

5. CONCLUSIONS

The present test studies confirmed that OCT is capable of continuously tracking deformation of paintings, with micrometer resolution, simultaneously in three dimensions. Registration of the deformation is automatic, and was made at a high rate (every 100 seconds) over a period of four days. As demonstrated, this permits monitoring of the course of long-term reactions of the painting, including crack formation, to rapid climate changes. The method allows investigation of the relationship between in-and-out-of-plane displacements, and recording of rapidly changing deformations. Although the resolution of the method is somehow lower than that of other available optical techniques, it is combined with a high range of accessible displacements. This allows the tracking of reactions to large changes in environment conditions, but has enough precision for tracking responses to moderate humidity jumps also. Modification of the sample compartment to allow more precise control of humidity conditions is under way.

With regard to the model painting examined, it was shown that, in response to a rise in humidity, the surface moves towards the nearest corner in plane, and bulges outwards. After the first humidification/drying cycle, translations in the Z'-direction are smaller, whilst in-plane translations increase somewhat. It was also shown that the response of the painting on canvas occurs immediately on changing the relative humidity in the surroundings.

To improve our understanding of processes taking place in the structure of the painting in response to rapid climate changes, and to interpret the role of particular components in the behaviour of the overall structure, model paintings prepared using different techniques, and samples at different stages of preparation will be examined in further tests. These experiments will be carried out with pictures mounted on wooden stretchers, as well as on stretchers inert to humidity. Simultaneously, the stress in the painting-stretcher system will be monitored with other methods.

APPENDIX

Before applying any environmental stress to the sample, its initial position must be recovered. To do so, a profile of the canvas surface is first determined from the OCT data, essentially as described elsewhere [19], then the plane is fitted to this profile. If the equation of this plane has the canonical form: $A \cdot x + B \cdot y + C \cdot z + D = 0$, then the coordinates of a vector $\vec{N}$normal to fitted plane are given by

$$N_X = \frac{A}{\sqrt{A^2 + B^2 + C^2}}, \qquad N_Y = \frac{B}{\sqrt{A^2 + B^2 + C^2}}, \qquad N_Z = \frac{C}{\sqrt{A^2 + B^2 + C^2}}. \tag{A.1}$$

The coordinates of this vector contain all available information about the position of the X'-Y' plane with respect to which the sample surface is described. To make the transformation between coordinates unambiguous, an additional assumption is necessary: the X-axis remains in the horizontal plane (marked blue in Figure 6). To transform the laboratory coordinates (X, Y, Z in Figure 6(a)) into the sample coordinates (X', Y', Z' in Figure 6(c)), the following two rotations are necessary.

(i) The (X'', Y'', Z'') axes result from rotation of the (X, Y, Z) axes about Y through an angle β, clockwise relative to the X-Z plane (Figure 6(b)). The X''-axis remains in the horizontal plane and coincides with the sample plane.

(ii) The (X', Y', Z') axes result from rotation of the (X'', Y'', Z'') axes about X'' through an angle δ clockwise relative to the Y''-Z'' plane (Figure 6(c)). The X'' and X' axes coincide.

The matrices describing these rotations may be multiplied to give the overall rotational matrix:

$$\begin{bmatrix} 1 & 0 & 0 \\ 0 & \cos(\delta) & -\sin(\delta) \\ 0 & \sin(\delta) & \cos(\delta) \end{bmatrix} \cdot \begin{bmatrix} \cos(\beta) & 0 & \sin(\beta) \\ 0 & 1 & 0 \\ -\sin(\beta) & 0 & \cos(\beta) \end{bmatrix} = \begin{bmatrix} \cos(\beta) & 0 & \sin(\beta) \\ \sin(\delta)\cdot\sin(\beta) & \cos(\delta) & -\sin(\delta)\cdot\cos(\beta) \\ -\cos(\delta)\cdot\sin(\beta) & \sin(\delta) & \cos(\delta)\cdot\cos(\beta) \end{bmatrix}. \tag{A.2}$$

The vector $\vec{N}$ normal to the sample surface has coordinates (N_X, N_Y, N_Z) in the laboratory system, and coordinates (0, 0, 1) in the sample system. Then angles β and δ may be obtained from

$$\begin{bmatrix} \cos(\beta) & 0 & \sin(\beta) \\ \sin(\delta)\cdot\sin(\beta) & \cos(\delta) & -\sin(\delta)\cdot\cos(\beta) \\ -\cos(\delta)\cdot\sin(\beta) & \sin(\delta) & \cos(\delta)\cdot\cos(\beta) \end{bmatrix} \cdot \begin{bmatrix} N_X \\ N_Y \\ N_Z \end{bmatrix} = \begin{bmatrix} 0 \\ 0 \\ 1 \end{bmatrix} \tag{A.3}$$

giving

$$\tan(\beta) = -\frac{N_X}{N_Z} = -\frac{A}{C}, \qquad \sin(\delta) = N_Y = \frac{B}{\sqrt{A^2 + B^2 + C^2}}. \tag{A.4}$$

Since both angles are small, formulas (A.4) are unambiguous. This procedure is performed once, at the beginning of the experiment, and matrix (A.2) is then used to transform all data retrieved.

ACKNOWLEDGMENTS

This work was supported by Polish Ministry of Science Grant no. 2 H01E 025 25. Authors wish to thank Professor Tadeusz Marszalek and Dr. Robert Dale for their very valuable discussions. The third author gratefully acknowledges the support of a Foundation for Polish Science Scholarship for Young Researchers.

REFERENCES

[1] P. Targowski, M. Góra, and M. Wojtkowski, "Optical coherence tomography for artwork diagnostics," *Laser Chemistry*, vol. 2006, Article ID 35373, 2006.

[2] J. M. Dulieu-Barton, L. Dokos, D. Eastop, F. Lennard, A. R. Chambers, and M. Sahin, "Deformation and strain measurement techniques for the inspection of damage in works of art," *Reviews in Conservation*, vol. 6, pp. 63–73, 2005.

[3] D. Ambrosini and D. Paoletti, "Holographic and speckle methods for the analysis of panel paintings. Developments since the early 1970s," *Reviews in Conservation*, vol. 5, pp. 38–48, 2004.

[4] C. Young, "Quantitative measurement of in-plane strain of canvas paintings using ESPI," in *Applied Optics Division*, pp. 79–84, Institute of Physics, IOP, Brighton, UK, 1998.

[5] C. Young, "Measurement of the biaxial properties of nineteenth century canvas primings using electronic speckle pattern interferometry," *Optics and Lasers in Engineering*, vol. 31, no. 2, pp. 163–170, 1999.

[6] C. Young, "The mechanical requirements of tear mends," in *Alternatives to lining, BAPCR & UCIK Conference*, pp. 55–58, September 2003.

[7] C. Young, R. Hibberd, and P. Ackroyd, "An investigation into the adhesive bond and transfer of tension in lined canvas paintings," in *Proceedings of the 13th Triennial Meeting of the ICOM Committee for Conservation (ICOM-CC '02)*, pp. 370–378, Rio de Janeiro, Brazil, September 2002.

[8] C. Young and R. Hibberd, "The role of canvas attachments in the strain distribution and degradation of easel paintings," in *Tradition and Innovation: Advances in Conservation, Contributions to the IIC Melbourne Congress*, pp. 212–220, London, UK, October 2000.

[9] R. Varoli-Piazza, R. Rosicarello, M. Giorgi, and J. Bridgland, "The use of photogrammetry in determining the correct method of displaying a textile artefact: the cowl of St. Francis of Assisi," in *Proceedings of the 11th Triennial Meeting of the ICOM Committee for Conservation (ICOM-CC '96)*, pp. 726–731, Edinburgh, Scotland, September 1996.

[10] B. Rouba, "Płótna jako podobrazia malarskie (canvases as painting supports)," *Ochrona Zabytków*, vol. 38, pp. 227–244, 1985.

[11] B. Rouba, "Die Leinwandstrukturanalyse und ihre Anwendung für Gemäldekonservierung," *Restauratorenblätter*, vol. 13, pp. 79–90, 1992.

[12] B. Rouba, *Podobrazia płócienne w procesie konserwacji (Canvas Painting Supports in the Process of Conservation)*, Wydawnictwo UMK, Toruń, Poland, 2000.

[13] G. A. Berger and W. H. Russell, *Conservation of Paintings*, Archetype, London, UK, 2000.

[14] B. Rouba, "Rückseitenschutz für Leinwandbilder - eine Methode von Eigenschafteenuntersuchungen," in *Proceedings of the 4th International Conference of Non-Destructive Testing of Works of Art*, pp. 657–669, Berlin, Germany, October 1994.

[15] M. Góra, P. Targowski, A. Rycyk, and J. Marczak, "Varnish ablation control by optical coherence tomography," *Laser Chemistry*, vol. 2006, Article ID 10647, 2006.

[16] C. R. T. Young and R. D. Hibberd, "Biaxial tensile testing of paintings on canvas," *Studies in Conservation*, vol. 44, no. 2, pp. 129–141, 1999.

[17] A. Guzowska, "Przygotowanie płócien dublażowych (preparation of lining supports)," M.A. thesis, Department of Conservation of Paintings and Polychrome Sculpture, Nicolaus Copernicus University, Toruń, Poland, 1996, B. Rouba, Advisor.

[18] L. Tymińska, "Uzupełnianie ubytków w podobraziach płóciennych—próba opracowania nowej metody z wykorzystaniem płynnej masy włóknistej (Filling voids in canvas painting supports—experiment on developing a new method with the use of liquid fibrous pulp)," M.A. thesis, Department of Conservation of Paintings and Polychrome Sculpture, Nicolaus Copernicus University, Toruń, Poland, 2002, M. Roznerska and B. Rouba, Advisors.

[19] P. Targowski, T. Bajraszewski, I. Gorczyńska, et al., "Spectral optical coherence tomography for nondestructive examinations," submitted to *Optica Applicata*.

Hindawi Publishing Corporation
Laser Chemistry
Volume 2006, Article ID 68679, 6 pages
doi:10.1155/2006/68679

Research Article

Optical Coherence Tomography for Examination of Parchment Degradation

Michalina Góra,[1] Michael Pircher,[2] Erich Götzinger,[2] Tomasz Bajraszewski,[1] Matija Strlic,[3] Jana Kolar,[4] Christoph K. Hitzenberger,[2] and Piotr Targowski[1]

[1] *Institute of Physics, Nicolaus Copernicus University, ul. Grudziądzka 5, 87-100 Toruń, Poland*
[2] *Centre for Biomedical Engineering and Physics, Medical University of Vienna, Waehringerstr. 13, A-1090 Vienna, Austria*
[3] *Faculty of Chemistry and Chemical Technology, University of Ljubljana, Aškerčeva 5, SI-1000 Ljubljana, Slovenia*
[4] *National and University Library, Turjaška 1, SI-1000 Ljubljana, Slovenia*

Received 20 September 2006; Revised 20 November 2006; Accepted 22 November 2006

Recommended by Costas Fotakis

A novel application of Optical Coherence Tomography utilizing infrared light of 830 nm central wavelength for non invasive examination of the structure of parchment, some covered with iron gall ink, is presented. It is shown that both the parchment and the ink applied are sufficiently transparent to light of this wavelength. In the study, Spectral OCT (SOCT) as well as Polarisation Sensitive OCT (PS-OCT) techniques were used to obtain cross-sectional images of samples of parchment based on scattering properties. The second technique was additionally employed to recover the birefringence properties and the optical axis orientations of the sample. It was shown that freshly produced parchment exhibits a degree of birefringence. However, this property declines with ageing, and samples of old parchment completely depolarise the incident light.

1. INTRODUCTION

For more than a millennium, iron gall ink was among the most frequently used inks in Western civilization [1]. Some of the most important artworks by Rembrandt, J. S. Bach, Leonardo da Vinci, Victor Hugo, or Hans Andersen, to name but a few, were written or drawn with it. In general, the ink was used on many writing materials, very often on paper, but also on papyrus, parchment or vellum, for example, the Book of Kells, a medieval manuscript of extraordinary beauty and importance.

While many different ink recipes have been passed down to us, this ink consisted of three main ingredients: vitriol (predominantly iron(II) sulphate), oak galls (from which gallotannins were extracted) and binder (gum Arabic). Once applied, the ink rapidly turned from almost colourless to blue.

However, during ageing, the colour of iron gall inks continuously changes, mirroring the chemical processes taking place. Namely, the first-formed blue ink is chemically unstable and in addition, the ink components, mainly acids and iron ions, induce degradation of the support [2]. With time, the ink and support degradation products prevail and lend the ink its brown appearance, typical of many historical documents. However, the degradation process is an on-going one, and eventually the support may be corroded through its entire thickness, which may lead to extensive loss of both material and information.

It is therefore vital that we be able to detect and analyse the degradation processes, and whereas there are a number of analytical methods used in studies of paper degradation [1, 3], analysis of parchment remains difficult due to its inhomogeneity and complex structure. Collagen fibres in parchment undergo degradation, which eventually leads to almost complete loss of fibre structure. At this stage, if in contact with water, a gelatinous substance is formed and the original parchment mechanical properties are lost.

Analysis of parchment usually involves methods based on visual and microscopic, as well as chemical and physical, techniques [4]. Most often used are thermal analytical methods and X-ray diffraction. Microthermal analysis has been used to obtain information on the topography and thermal conductivity of sample areas of 100 μm [5]. The X-ray diffraction of collagen has provided information on

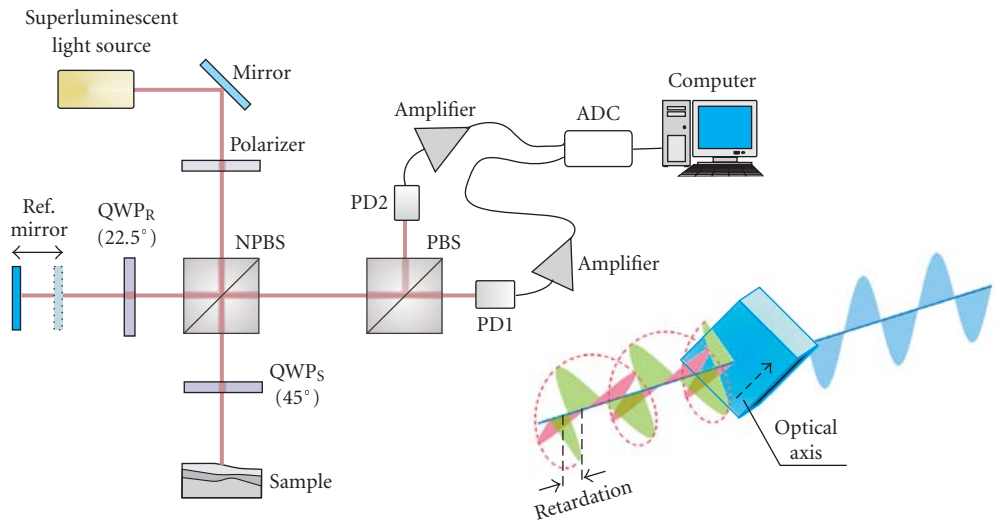

Figure 1: Schematic of the 0.83 μm PS-OCT system (QWP—quarter wave plate, NPBS—nonpolarizing beam splitter, PBS—polarizing beam splitter, PD—photodetector, ADC—analogue to digital converter, REF. MIRROR—reference mirror).

the molecular organization of individual collagen molecules, while small angle X-ray diffraction has been used as a means of monitoring changes in the physical organisation of collagen within a parchment sample [6]. Differential scanning calorimetry (DSC) and thermogravimetry (TGA) were employed to study collagen temperature denaturation, and these results were confirmed by small angle X-ray scattering [7]. X-ray diffraction was also used to study changes in the axial packing of collagen molecules due to dehydration [8]. The mechanical behaviour of parchment through its shrinkage temperature has been described by Cohen et al. [9]. All these methods concentrate on determination of specific chemical or mechanical bulk parameters referred to the whole thickness of the material. Here, we present a record of the first attempt to use optical coherence tomography for nondestructive in situ structural analysis of parchment.

2. EXPERIMENT

Parchment is a particularly difficult material to study due to its complex inhomogeneous structure. Infrared optical coherence tomography (OCT) at around 800 nm is well suited to this application, since both the parchment and the ink absorb light of these wavelengths rather moderately. A more detailed description of the OCT method can be found elsewhere in this volume [10]. Briefly, the method utilizes the interference of light of high spatial coherence (to ensure high sensitivity of imaging) together with very low temporal coherence (to increase in-depth resolution). To reveal the internal structure of the object a narrow beam of such light penetrates it and is scattered from structural elements. This scattered light is collected back by the same optics and then brought to interference with a reference beam in a Michelson interferometer. The positions of scattering centres or interfaces inside the object along the beam (an A-scan) is recovered from the detected signal. A cross-sectional image of the material (B-scan) is compiled from adjacent A-scans.

3. MATERIALS AND METHODS

In this study, two OCT instruments were used: a spectral OCT system (also described in detail in this volume [11]) utilizes a light source of 835 nm central wavelength and a bandwidth of 50 nm. This leads to a theoretical axial resolution of 6 μm in the medium, of refractive index 1.5. The transverse resolution was 15 μm. The second OCT system, a time-domain polarization sensitive OCT (PS-OCT) system (Figure 1), was commissioned in the Centre for Biomedical Engineering and Physics of the Medical University of Vienna [12]. This instrument, in addition to the ordinary OCT images showing distributions of scattering centres, is also capable of imaging the distribution of retardations and optical axis orientations. These last two parameters describe the birefringence of the sample [13]. In such a time-domain instrument, in-depth scanning is accomplished by translation of the reference mirror. A polarizer and quarter-wave plate (QWP 45°) in the object arm convert the source beam into a circularly polarized one. After scattering in a nonbirefringent sample, the light is still circularly polarized, but if in its path within the sample there are some birefringent regions, the emerging light is elliptically polarized. This light is directed to the detecting arm, where it is spit into two orthogonally plane-polarized components which interfere with corresponding components returning from the reference arm. Simultaneous balanced detection of these two interference signals permits recovery of three images (see Figure 3 in Section 4): the intensity representation, which is equivalent to the image obtained from the ordinary OCT instrument, delineates the distribution of scattering centres along the

Figure 2: Samples used for examination: (a) preliminary samples and their cross-sectional views—on the right: sample covered with iron gall ink; on the left: a reference sample without ink; (b) samples of historical parchment with gall ink inscriptions.

probing beam; the retardation and optical axis orientation images characterize the polarization properties of the sample. Briefly, the retardation image reflects the phase difference between the two orthogonal polarization components, while the optical axis orientation image defines their orientation in space (see the insert in Figure 1 for an explanatory example). The resolution of this instrument is similar to that of the SOCT one.

Polarization-sensitive OCT has been used for examination of human skin for several years [14]. As revealed by Pierce et al. [15], the double-path retardation rate varies from 0.25 to 0.6 deg/μm in human skin, depending on its location. The authors point to collagen as the major component of skin responsible for its birefringence. Three dimensional PS-OCT images of human skin have been presented by Pircher et al. [16]. Their results reveal the birefringent nature of the stratum corneum—the outermost layer of the epidermis.

It is reasonable to assume that similar birefringence might be observed in parchment, because it is also composed largely of collagen fibres. However, many factors during the processing of skin to parchment may influence this property. Nevertheless, it is worthwhile to investigate whether or not parchment may retain some ability to polarize light. PS-OCT was used to check this hypothesis. Two kinds of sample were employed in this study:

(i) artificially degraded samples of contemporary parchment (Figure 2(a)),
(ii) fragments of an old manuscript of unknown origin and date (Figure 2(b)).

Samples of calfskin ($\sim$0.35 mm thick) were taken for preliminary study. Although skin, like parchment, is a very inhomogeneous material, we tried for these studies to select a part of the skin which had no macroscopically noticeable features to ensure that all the samples we prepared were as similar as possible. The samples were further processed by applying iron gall ink (composition as in [17]), and exposing the sample to accelerated degradation for 3 weeks at 80°C, 65% relative humidity. It is as yet unsure to what extent this treatment correlates with natural ageing of parchment. However, it is known that heating parchment to an elevated temperature promotes its chemical degradation, and our primary aim was to investigate the differences between degraded and original material.

Fragments of the historical parchment of unknown origin ($0.13 \div 0.18$ mm thick) were supplied by the National and University Library of Slovenia.

4. RESULTS AND DISCUSSION

All samples were investigated with both instruments, and representative results are shown.

Figure 3 displays intensity profiles (top row), retardation (middle row), and optic axis orientation images (bottom row). In the intensity images, backscattered intensity is plotted as a function of position on a logarithmic scale. Illumination is from above. In the fresh sample (left column), a highly reflective superficial layer is observed, followed by a hypo-reflective (dark) layer and a stronger backscattering layer. Zero or low retardation is observed in the topmost layer (blue colour in the retardation image), while the colour transition, via green to yellow, indicates some birefringence in the deeper layers. Also in the deeper layers, a predominating range of optic axis orientation is observed (yellow-green to orange). In the degraded sample without ink (middle column), the hypo-reflective layer beneath the surface is very shallow, and the material appears to have a higher birefringence (steeper transition from blue to yellow with depth). The degraded sample with ink (right column) seems to have a structure with properties in between those of the other samples.

The results obtained with the model artificially degraded samples were verified with the historical samples of

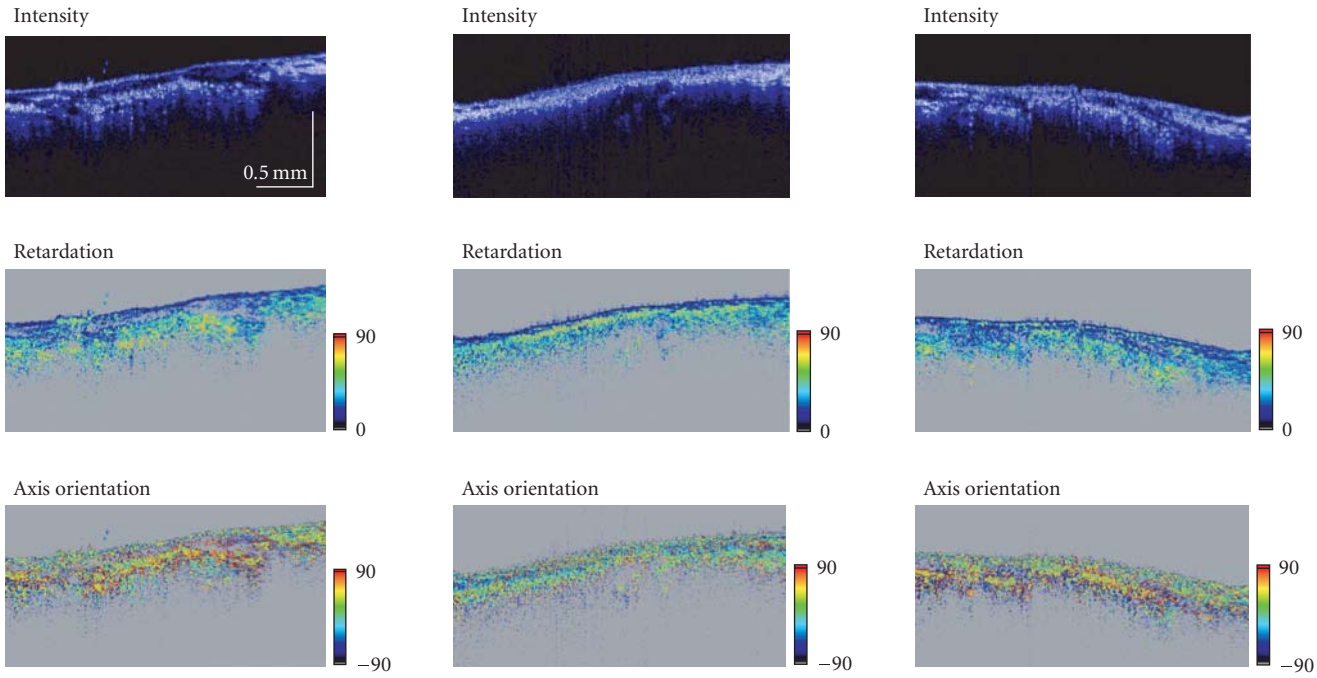

(a) Fresh sample with ink applied.

(b) Samples degraded at 80°C, 65% relative humidity for 3 weeks without ink applied.

(c) Samples degraded at 80°C, 65% relative humidity for 3 weeks with ink applied.

Figure 3: PS-OCT tomograms of parchment samples obtained before and after artificial ageing. All images are presented on the same scale. It can be seen that the fresh sample shows stronger birefringence.

Figure 4: Macro photograph of the sample of historical parchment. Traces of water damage are visible.

parchment (Figure 2(b)). These items carried traces of fire and water spillage (Figure 4). The SOCT tomograms were taken across areas containing letters (squares in Figures 2(b), and 5). PS OCT examination (not shown) reveals complete depolarization of backscattered light.

As can be seen from the tomograms in Figure 5, this sample of parchment reveals much less structural details than the model one under OCT examination. It is not yet conclusive as to whether or not this feature is due to the age of the sample or to its particular properties. En-face images (Figures 5(a), 5(c)) are obtained from OCT data by integration of the signal over the whole depth of imaging. Due to the transparency of iron gall ink to the light used, the letter "a," well defined in the original parchment, is hardly visible, if at all, in Figure 5(a), and is outlined for better differentiation. Much more visible are water stains (dark areas), in which regions the tomograms indicate a thick, homogenous layer (possibly of glue) at the surface (Figure 5(b)).

The analysis of the tomograms shown in Figure 5(d) is more conclusive, due to the fact that water stains cover only the upper part of the area examined, and not interfere with areas covered by ink. Thus, it can be seen that the areas covered by ink are a little more textured than their surroundings (compare Figure 5(d)3 and Figure 5(d)4). This may indicate some structural change caused by the ink.

5. CONCLUSIONS

Optical coherence tomography at around 800 nm is capable of imaging the internal structure of parchment. For this wavelength, due to sufficient transparency of the ink thereon, it is possible to observe nondestructively the degradation of historical parchment below iron gall ink writing for the first

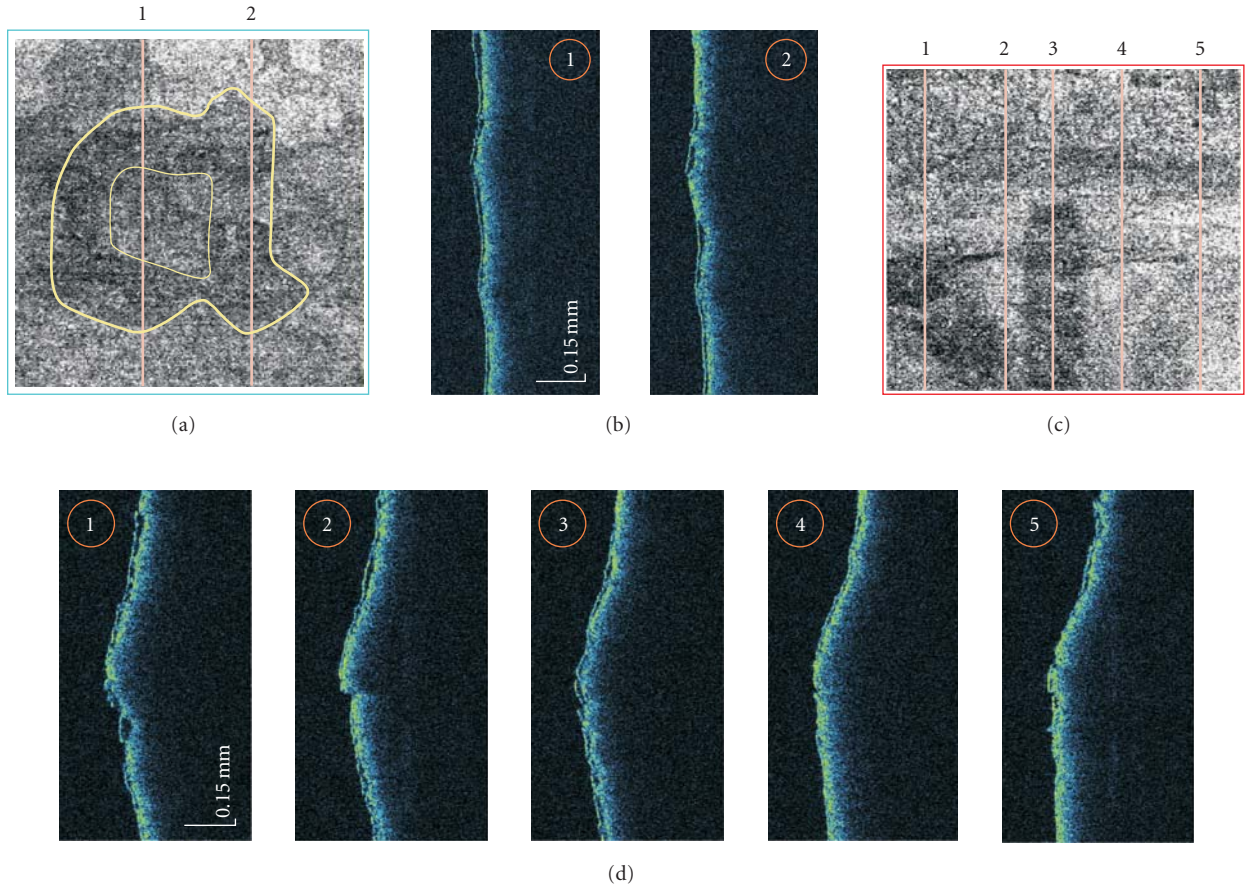

FIGURE 5: SOCT tomograms of samples of old parchment. Lines (a, c) indicate position of OCT images (c, d, resp.). Illumination is from the left.

time. Some evidence of structural degradation under the ink layer has been found.

Additionally, it was shown that freshly produced parchment exhibits some birefringence. However, this property declines with degradation, and samples of old parchment completely depolarize the incident light.

This last finding as well as the range and interpretation of the structural effects caused by the presence of the ink need further investigation.

ACKNOWLEDGMENTS

Financial support from the Oesterreichische Akademische Austausch-dienst (OEAD) and the Polish Ministry of Science (joint project 6/2005/2006 and research project 2 H01E 025 25) is gratefully acknowledged. The fifth author acknowledges the support of the Slovenian Research Agency (programme P1-0153).The fifth and sixth authors also acknowledge the support of the Ministry of Higher Education, Science and Sport of Slovenia, project Eureka E!3843.The fourth author gratefully acknowledges the support of a Foundation for Polish Science Scholarship for young researchers. The authors gratefully acknowledge the assistance of Dr. Z. Rozłucka, who made the cross-sectional photographs for Figure 2(a). The authors wish to thank Dr. Robert Dale for many valuable discussions.

REFERENCES

[1] J. Kolar and M. Strlic, *Iron Gall Inks. On Manufacture, Characterisation, Degradation and Stabilisation*, National and University Library, Ljubljana, Slovenia, 2006.

[2] J. Kolar, A. Štolfa, M. Strlic, et al., "Historical iron gall ink containing documents—properties affecting their condition," *Analytica Chimica Acta*, vol. 555, no. 1, pp. 167–174, 2006.

[3] M. Strlic and J. Kolar, *Ageing and Stabilisation of Paper*, National and University Library, Ljubljana, Slovenia, 2005.

[4] R. Larsen, *Microanalysis of Parchment*, edited by R. Larsen, Archetype, London, UK, 2002.

[5] M. Odlyha, N. S. Cohen, G. M. Foster, A. Aliev, E. Verdonck, and D. Grandy, "Dynamic mechanical analysis (DMA), ^{13}C solid state NMR and micro-thermomechanical studies of historical parchment," *Journal of Thermal Analysis and Calorimetry*, vol. 71, no. 3, pp. 939–951, 2003.

[6] C. J. Kennedy, K. Nielsen, L. Ramsay, and T. J. Wess, "Analysis of collagen structure in parchment by Small angle X-ray diffraction," *Fibre Diffraction Review*, vol. 11, pp. 117–118, 2003.

[7] D. Fessas, M. Signorelli, A. Schiraldi, et al., "Thermal analysis on parchments I: DSC and TGA combined approach for heat

damage assessment," *Thermochimica Acta*, vol. 447, no. 1, pp. 30–35, 2006.

[8] T. J. Wess and J. P. Orgel, "Changes in collagen structure: drying, dehydrothermal treatment and relation to long term deterioration," *Thermochimica Acta*, vol. 365, no. 1-2, pp. 119–128, 2000.

[9] N. S. Cohen, M. Odlyha, and G. M. Foster, "Measurement of shrinkage behaviour in leather and parchment by dynamic mechanical thermal analysis," *Thermochimica Acta*, vol. 365, no. 1-2, pp. 111–117, 2000.

[10] P. Targowski, M. Góra, and M. Wojtkowski, "Optical Coherence Tomography for Artwork Diagnostics," in this volume.

[11] M. Góra, P. Targowski, A. Rycyk, and J. Marczak, "Varnish ablation control by Optical Coherence Tomography," in this volume.

[12] M. Pircher, E. Götzinger, R. Leitgeb, and C. K. Hitzenberger, "Transversal phase resolved polarization sensitive optical coherence tomography," *Physics in Medicine and Biology*, vol. 49, no. 7, pp. 1257–1263, 2004.

[13] C. K. Hitzenberger, E. Götzinger, M. Sticker, M. Pircher, and A. Fercher, "Measurement and imaging of birefringence and optic axis orientation by phase resolved polarization sensitive optical coherence tomography," *Optics Express*, vol. 9, no. 13, pp. 780–790, 2001.

[14] C. E. Saxer, J. F. De Boer, B. Hyle Park, Y. Zhao, Z. Chen, and J. S. Nelson, "High-speed fiber-based polarization-sensitive optical coherence tomography of in vivo human skin," *Optics Letters*, vol. 25, no. 18, pp. 1355–1357, 2000.

[15] M. C. Pierce, J. Strasswimmer, B. Hyle Park, B. Cense, and J. F. De Boer, "Birefringence measurements in human skin using polarization-sensitive optical coherence tomography," *Journal of Biomedical Optics*, vol. 9, no. 2, pp. 287–291, 2004.

[16] M. Pircher, E. Götzinger, R. Leitgeb, and C. K. Hitzenberger, "Three dimensional polarization sensitive OCT of human skin in vivo," *Optics Express*, vol. 12, no. 14, pp. 3236–3244, 2004.

[17] J. Kolar and M. Strlic, "Evaluating the effects of treatments on iron gall ink corroded documents: a new analytical methodology," *Restaurator*, vol. 25, no. 2, pp. 94–103, 2004.

Hindawi Publishing Corporation
Laser Chemistry
Volume 2006, Article ID 10647, 7 pages
doi:10.1155/2006/10647

Research Article

Varnish Ablation Control by Optical Coherence Tomography

Michalina Góra,[1] Piotr Targowski,[1] Antoni Rycyk,[2] and Jan Marczak[2]

[1] *Institute of Physics, Nicolaus Copernicus University, ul. Grudziadzka 5, 87 100 Toruń, Poland*
[2] *Institute of Optoelectronics, Military University of Technology, ul. Kaliskiego 2, 00 908 Warszawa, Poland*

Received 15 September 2006; Accepted 7 November 2006

Recommended by Costas Fotakis

Preliminary results of the application of optical coherence tomography (OCT), in particular in its spectral mode (SOCT) to the control of a varnish ablation process, are presented. Examination of the ablation craters made with an Er:YAG laser allows optimization of the laser emission parameters controlling fluence with respect to efficiency and safety of the ablation process. Results of measurements of ablation crater depth as a function of the number of pulses for a given fluence are presented for selected resins. This validates the applicability of SOCT to calibration of ablation conditions for the particular laser-varnish-paint layer combinations, and of its usage in planning the varnish ablation procedure. These results also imply that a review of conventional ablation thresholds is called for. Applicability of the SOCT technique to contemporaneous in situ monitoring of the range of varnish ablation is discussed.

1. INTRODUCTION

The cleaning of painted surfaces is one of the most crucial operations in art conservation. The protective varnish layer must be removed, if it has turned yellow or opaque, or it covers old, darkened retouchings which are to be removed during the conservation process. Extremely high precision and selectivity is essential for this task in order to preserve the original paint layers without modifying their original colours. Among traditional methods of paint removal, the mechanical one is the safest, but requires undue patience, especially when it must be applied either to a very thin and inhomogeneous layer or to foreign deposits. Chemical methods based on toxic solvents are very difficult to control (even when they are applied in the form of swab or gel), because the solvent may penetrate the paint layer and cause risk of damage during the next steps of conservation. Furthermore, the materials that should be removed are, in the great majority of cases, insoluble in media that are tolerated by paint layers. In addition, substances that are not harmful to the paint layer are usually not aggressive enough to remove the varnish layer.

According to contemporary methods of art conservation, the most desirable requirement is contemporaneous control of varnish removal. This complicated task is difficult to achieve with the traditional empirical methods of art restoration.

Laser techniques are becoming important tools in the conservation (restoration, diagnostic, and protection) of cultural heritage. Research on laser cleaning of paintings and icons by an excimer laser was initiated at the Foundation for Research and Technology-Hellas in Greece [1]. The interested reader can find a comprehensive literature on conservation techniques based on the application of lasers in the proceedings of LACONA conferences I to VI. The cleaning of works of art and historical objects with lasers allows selective removal of undesirable layers, leaving the original paint layer intact [1–4]. A significant problem connected with laser ablation is online monitoring and in situ control during each stage of the laser cleaning. A very useful technique is laser induced breakdown spectroscopy (LIBS) [5, 6] in which the chemical composition of the plasma produced is spectroscopically analyzed, and traces of paint components indicate that the cleaning beam has reached the paint layer. Contemporaneously with matters related to monitoring the cleaning process, phenomena occurring in ablated material, such as the formation of microcracks, defects, and other structural changes, are being investigated. Other nondestructive optical methods, for instance, holographic interferometry [7], have already been successfully used for this purpose.

In this contribution, the preliminary results of the application of optical coherence tomography (OCT) to the control of a varnish ablation process are presented. The OCT method allows noncontact and nondestructive imaging of semitransparent objects. It enables fast and convenient calibration of ablation conditions for the particular laser-varnish combination. Moreover, the technique provides information on the volume of removed material and the thickness, structure, and quality of the remaining varnish layer. This is essential for control of the ablation depth. In this paper, the results of ablation of different varnishes by the Er:YAG laser (working in the so-called short free-running regime) are presented.

2. EXPERIMENT

The use of the laser for varnish removal needs precise optimization of its conditions. Ablation with minimum thermal damage of adjacent areas depends on the absorption parameters of the material, together with the laser pulse energy and duration, and the thermal relaxation time of the material, that is, the time needed for diffusion of heat in the substance. Additionally, multiple scattering in matt surfaces, when present, significantly increases absorption of the laser radiation. Therefore, the major parameter of the laser pulse to be established is the radiation fluence. This parameter should be determined experimentally for each combination of varnish and paint layers. This test is usually performed near the edge of the painting. Unfortunately, the parameters obtained within the test area are not usually optimal for other areas. This necessitates a method which may ultimately be used for contemporaneous monitoring of the ablation process in situ.

To assay the ability of OCT to monitor the varnish removal process, model samples of varnish layers were prepared by applying selected resins to fused silica plates (see samples section). Without wetting the surface, a cumulative number of impulses of the same fluence were applied to consecutive locations in the sample. As a result, a set of graded craters was produced. Generally, two kinds of OCT analysis of ablation craters are possible: qualitative, when it is mainly the shape of craters in varnish layer (surface map) which is recovered, and quantitative, when additionally the depths of the ablation craters are measured. Together, these enable estimation of the material removed. Independently, scanning electron microscope (SEM) images (Novoscan 30, Zeiss, Germany) of sample surfaces were obtained to compare to the surface maps generated from volume OCT data. It is worthwhile to note that, since samples have to be gold-plated for this purpose and examined in vacuum, the SEM method cannot be applied in situ.

3. MATERIALS AND METHODS

3.1. Er:YAG laser system

An essential prerequisite for laser cleaning is the proper choice of laser wavelength. This depends on the absorption coefficient of the material to be ablated. In the experiments

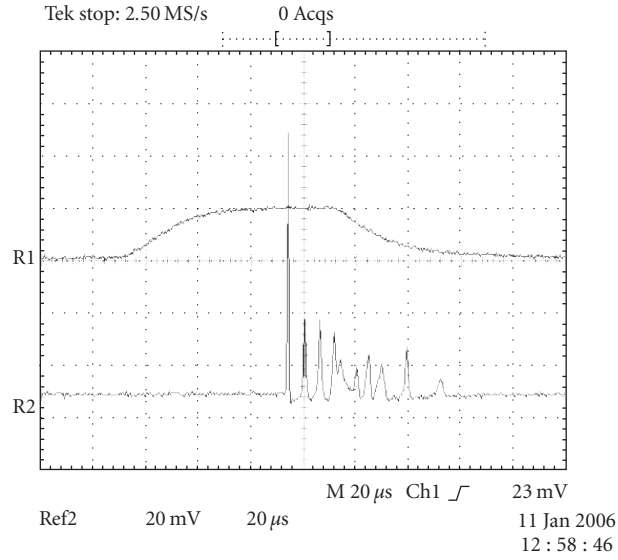

Figure 1: Time course of the pumping impulse (upper curve), and of the laser pulse (burst pulse) which usually consists of dozen or so pulses of free-running generation, each lasting for about 1 microsecond.

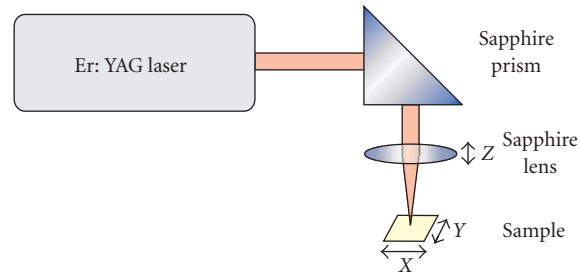

Figure 2: Diagram of the Er:YAG laser setup used in this study.

described, an infrared Er:YAG laser working at a wavelength of 2.936 μm was used to ablate various varnish layers from fused silica plates. Radiation of this wavelength is strongly absorbed by the OH bond vibration (the absorption coefficient can reach a value of as high as $10^5\,\mathrm{cm}^{-1}$), so that the depth of penetration of light into the treated medium may be extremely small [8, 9]. OH groups can be introduced onto the surface of layers to be removed as a liquid, for example, water or alcohol, film. However, this treatment (called wetting) has not been used in the presented study.

The Er:YAG laser was working in the short free-running mode (or burst mode), in which several impulses of free generation were emitted, each of them lasting for about 1 microsecond, the total duration of the burst being less than 80 microseconds (see Figure 1). The total output energy of the laser was adjustable, but always kept below 80 mJ. The fluence can be controlled by means of the focusing optics (prism and lens, both made of sapphire, Figure 2).

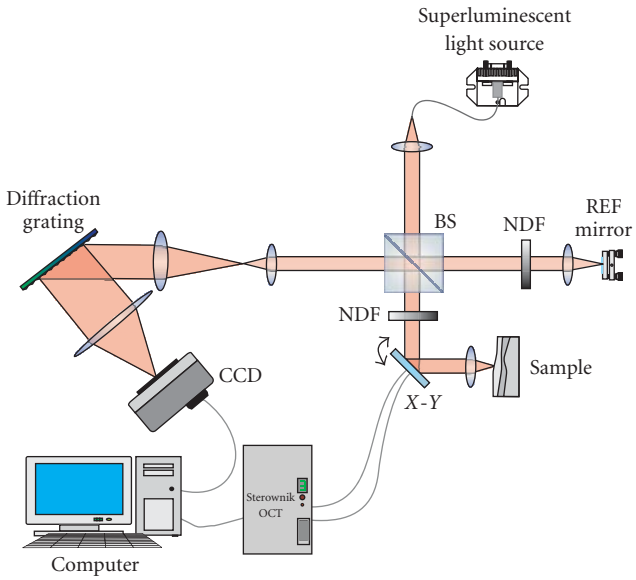

FIGURE 3: Diagram of the SOCT instrument used in the study: BS—beam splitter, NDF—neutral density filter, CCD-CCD line-scan camera, X-Y-galvanometric scanner.

3.2. Optical coherence tomography

Optical coherence tomography (OCT) is a new, fast-developing technique for noncontact, nondestructive imaging of semitransparent objects. In this method, the positions of scattering and/or reflecting interfaces in the internal structure of the object along the penetrating beam are obtained. OCT has found its main applications in medicine, but it has also been successfully used in materials science, particularly for museum objects. Among these, it has already been shown that OCT is capable of imaging varnish layers [10–12]. A comprehensive review of this last application, as well as a general idea of operational procedures, are given elsewhere in this volume [13].

The Spectral OCT (SOCT) system shown schematically in Figure 3 is a bulk optics instrument based on a Michelson interferometer setup. The superluminescent diode (Superlum Ltd., Russia) emitting light with a central wavelength of 835 nm and spectral width (FWHM) of 50 nm was used as a light source. The beam of light, of high spatial but low temporal coherence, is split into two interferometric arms with the aid of a 50 : 50 nonpolarising beam-splitting cube BS. One arm is terminated by the reference mirror kept in a fixed position. The other, namely, the object arm, comprises a set of two transversal scanners X-Y (Cambridge Technology Inc., USA) which are used for scanning the probing beam across the object. The beam is focused on the object by a lens L and penetrates the object. Some of it is scattered and/or reflected back from elements in its structure, and this is finally collected by the same optics L, and returned to the beam-splitter BS. It is then combined with the light returning from the reference arm. The resulting interference signal is analyzed and registered by a spectrometer (comprising a holographic diffraction grating: 1800 grids, Spectrogon AB, Sweden, and a CCD line scan camera: 1024 pixels, 8 bit A/D conversion, Dalsa Corporation, Canada). The detection conditions were set up to the shot-noise limited mode in order to utilise whole dynamic range of the CCD camera. The spectral fringe patterns registered by this detector are then transferred to a personal computer. The fringe pattern signal is then reverse Fourier transformed into one line of a tomogram (an A-scan). The exposure time per A-scan is usually 30 microseconds.

The axial resolution of the system is $\sim 6\,\mu$m in these media which have refractive indices ranging from 1.3 to 1.5. The transversal resolution is kept below $15\,\mu$m. In order to obtain either a 2D slice (B-scan) or a 3D (volume) tomogram, the beam is scanned transversally by galvanometric scanners X-Y.

The total data collection time for a B-scan composed of 5000 A-scans is thus 0.15 second, and about 5 seconds is required for 3D (volume) data.

The signal is visualised in real time as a cross-sectional view and stored for postprocessing. The numerical processing of the data, besides the reverse fast Fourier transform, essential to the SOCT method, includes: subtraction of noninterference background, spectral shaping [14], and numerical dispersion correction [15].

In the 2D OCT tomograms or B-scans (see Figures 6(e), 6(f), and 7 in the results section), the intensity of light reflected or scattered from the interfaces along the penetrating beam is coded in a false-colour scale: warm colours (red and yellow) indicate a high scattering level of the probing light, while the cold ones (blue and black) indicate low scattering levels. Light is incident from the top, and the narrow line indicates the strong reflecting surface of intact varnish. Areas altered by the ablation process produce multiple scattering and are visible as fuzzy regions of mixed colour.

The OCT volume data may be used, *inter alia*, to recover the surface profile of the object examined (Figures 6(c) and 6(d)). In this process, the position of the first nonzero signal in each A-scan, corresponding to the first scattering boundary (the air-object interface), is automatically determined.

3.3. Samples

For the OCT experiments, five resins were selected to model varnishes of different properties: polyester resin in styrene with and without SiO_2 as matting agent, vinyl resin, polyurethane resin, and epoxy resin. All resins were applied to fused silica plates (Vitrosil 005^{TM}, one inch diameter and two millimetres thick). The transmission of the plate is $\sim$ 91% at 2,936 μm. The laser energy meter, placed after the plate, was used to indicate independently the total ablation of the resin.

4. RESULTS AND DISCUSSION

4.1. Estimation of the ablation conditions

To establish safe conditions for the removal of the varnish layer (Winsor & Newton Matt Varnish) from wooden

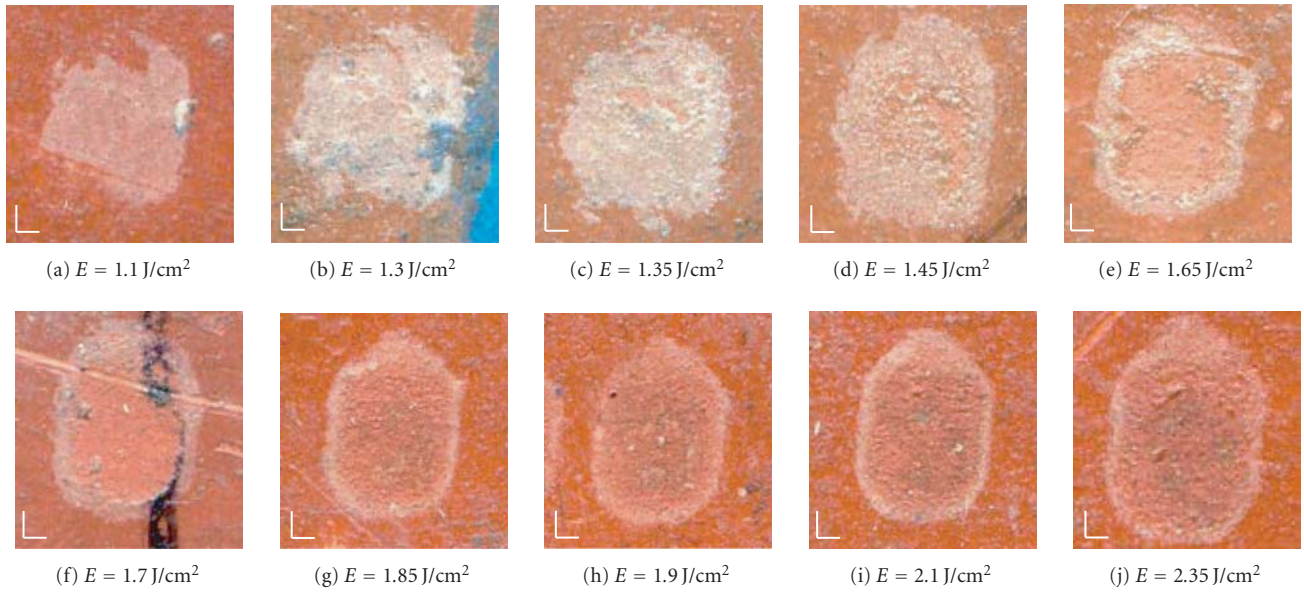

(a) $E = 1.1\,\mathrm{J/cm^2}$ (b) $E = 1.3\,\mathrm{J/cm^2}$ (c) $E = 1.35\,\mathrm{J/cm^2}$ (d) $E = 1.45\,\mathrm{J/cm^2}$ (e) $E = 1.65\,\mathrm{J/cm^2}$

(f) $E = 1.7\,\mathrm{J/cm^2}$ (g) $E = 1.85\,\mathrm{J/cm^2}$ (h) $E = 1.9\,\mathrm{J/cm^2}$ (i) $E = 2.1\,\mathrm{J/cm^2}$ (j) $E = 2.35\,\mathrm{J/cm^2}$

Figure 4: Illustration of the reaction of the varnish and underlying paint layer to different laser fluences. Bars indicate 1 mm in both directions.

Figure 5: Result of ablation of varnish (Winsor & Newton Matt Varnish) over different underlying paint layers using the same fluence ($1.7\,\mathrm{J/cm^2}$).

Table 1: Ablation thresholds estimated by inspection of the sample surface.

Resin	Ablation threshold $\mathrm{J/cm^2}$
Polyester resin in styrene with SiO_2 as a matting agent	3.3
Polyester resin in styrene without matting agent	3.3
Vinyl resin	2.9
Polyurethane resin	4.3
Epoxy resin	2.9

polychrome, a sequence of test ablations was performed. In Figure 4, the results of single-pulse ablations with fluences ranging from $1.1\,\mathrm{J/cm^2}$ (the ablation threshold) to $2.35\,\mathrm{J/cm^2}$ are presented. Inspection of the ablation spots leads to estimation of the optimal range of fluences as between $1.45\,\mathrm{J/cm^2}$ and $1.7\,\mathrm{J/cm^2}$. On exceeding $1.7\,\mathrm{J/cm^2}$, carbonization of the paint layer sets in.

However, as can be seen in Figure 5, the fluence suitable for varnish removal from the red paint is not sufficient in a different area of the object, where the underlying paint is green. Therefore, each such different area of the object should be treated individually to avoid unnecessary damage.

For all model samples, the ablation threshold was estimated by inspection of the effects of a single pulse on the sample surface. The fluence was increased until a change in the resin surface was visible. The results are summarised in Table 1.

4.2. OCT assay of the ablation process

To prepare objects for OCT examination, a set of graded craters was produced by directing cumulative numbers of impulses of the same fluence to consecutive locations in the sample (as described in Section 2). In these experiments, two sets of craters were created for each sample: one with a fluence of $4\,\mathrm{J/cm^2}$ (Figure 6(a)), the other with a fluence of $7\,\mathrm{J/cm^2}$ (Figure 6(b)).

As can be seen from Figure 6, there is excellent correspondence between the microphotographs and the surface profiles obtained with OCT. However, extra useful information may be obtained from the OCT tomograms. Firstly, the surface profile is clearly visible, allowing tracking of the ablation process: the depth of crater was chosen as an indicator of progress. Secondly, the range of alteration of the structure of material under the crater surface is seen—this feature is not accessible with SEM. Thirdly, it is clearly visible when the whole layer is burnt through (Figure 7).

The results obtained for all of the samples are summarised in Figure 8. As can be seen from the diagram, the depth of crater usually increases almost linearly with the number of pulses. In that case, it is possible to calculate the number of pulses necessary exactly to ablate the required layer of varnish.

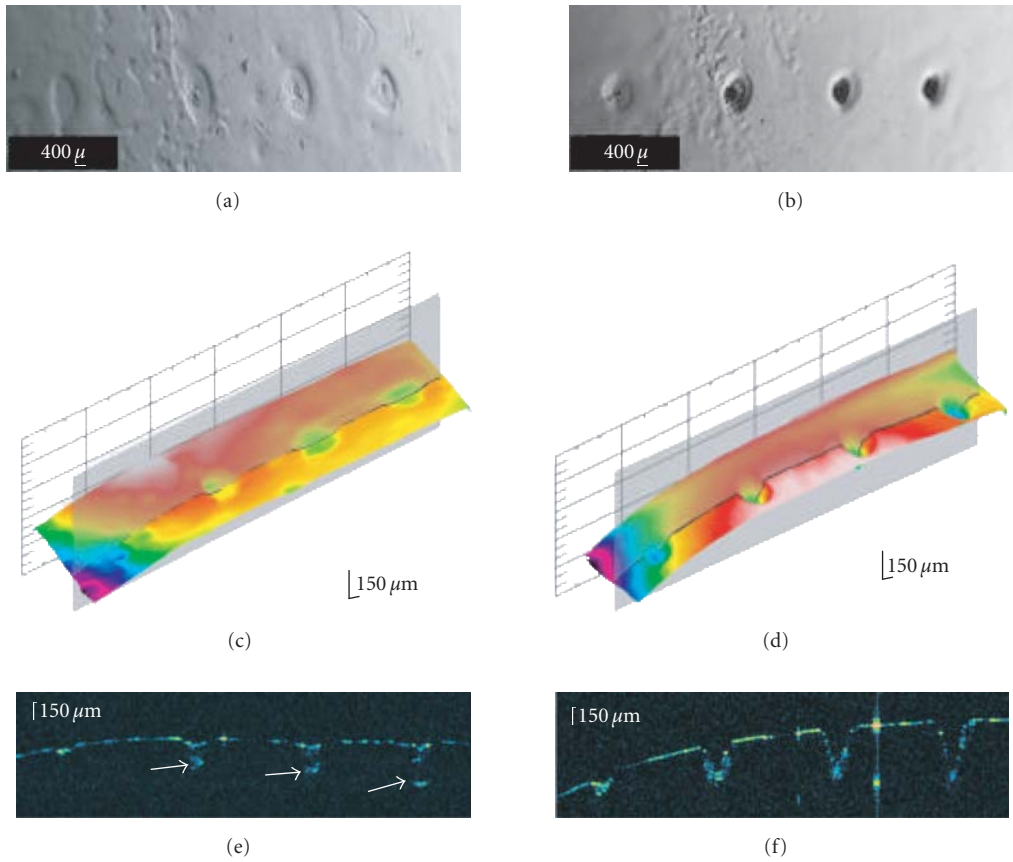

FIGURE 6: Testing of ablation conditions of Polyester resin in styrene without matting agent with two irradiation fluences: (a,c,e) 4 J/cm^2 and (b,d,f) 7 J/cm^2. In both cases, craters were formed by accumulation of 1, 2, 5, and 10 laser pulses (from the left to the right). Upper panels: SEM surface microphotographs; middle panels: surface maps recovered from OCT data—gray planes indicate positions where the OCT tomograms were taken; lower panels: the OCT tomograms (B-scans). Notice the expanded vertical scale for both the OCT surface maps and the OCT tomograms.

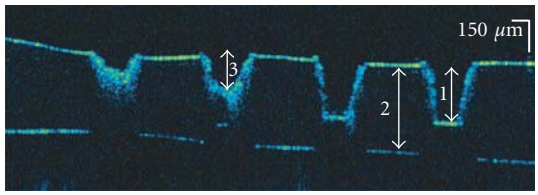

FIGURE 7: The OCT tomogram of the ablation of polyester resin in styrene with SiO_2 as a matting agent using a fluence of 7 J/cm^2. Craters were formed by accumulation of 1, 2, 5, and 10 laser pulses (from the left to the right). Craters formed by 5 and 10 pulses reach the substrate surface, and determination of putative crater depth is not possible. Notice the discrepancy between the thickness of the resin layer in the craters (1) and in the resin itself (2). This arises because of refraction in the resin, and vertical distances recovered by OCT are optical ones. The bars indicate distances in the air, to define properly the crater depth (3).

However, for some media (here, the polyester resin with or without the matting agent) pulses of higher fluence create deeper ablation craters, whereas consecutive pulses of low fluence do not increase the crater depth. On the other hand, the presence of a shallow crater in these cases indicates that some thermal process has occurred (Figures 6(a), 6(c), and 6(e)): the varnish material only melts, then resolidifies. This process causes some changes to the structures underneath the crater which can be seen as regions of higher scattering in the OCT tomograms (Figure 6(e), arrows). The presence of such microdefects underneath the surface of the target material has previously been reported by Bonarou et al. [7]. However, it is worthwhile to note that this graded growth of structural defects with increasing number of laser pulses occurs also below threshold, when the varnish surface remains almost intact. It seems that, even though the value of the fluence is higher then the conventional ablation threshold given in Table 1, ablation does not in fact occur. Therefore, the ablation threshold obtained in the conventional way for this resin is probably underestimated.

5. CONCLUSIONS

The cleaning of painted surfaces is one of the most critical operations in art conservation. The application of lasers

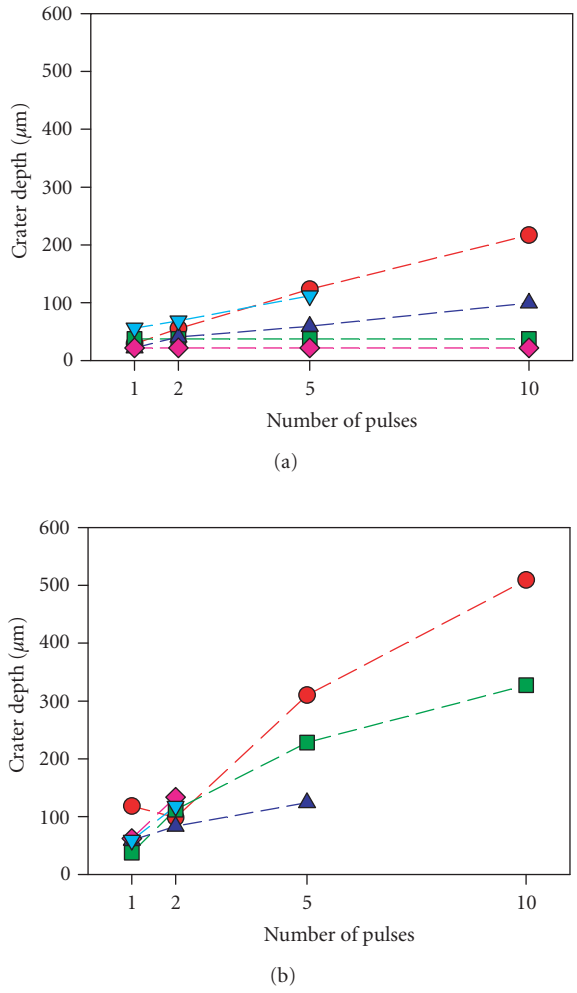

FIGURE 8: Depth of ablation craters obtained with cumulative number of pulses of fluence (a) 4 J/cm^2 and (b) 7 J/cm^2. ♦ polyester resin in styrene with SiO_2 as matting agent; ■ polyester resin in styrene without matting agent; ▲ vinyl resin; ▼ polyurethane resin; ● epoxy resin.

for this task requires precise optimization of the operating conditions. However, these conditions may differ in different parts of the object. The OCT method presented enables fast and convenient calibration of ablation conditions for particular laser-varnish-paint layer combinations, and it may be used to plan the varnish ablation procedure. It also permits nondestructive, in situ estimation of ablation speed and/or instantaneous monitoring of the thickness of remaining material. This is essential for the control of the ablation range. The spectral modality of the OCT technique (SOCT) best suites this task due to its high speed. In SOCT, the major limitation is the data processing speed if real-time monitoring is of the essence. Current moderately priced personal computers permit image processing at the rate of up to 10 medium resolution frames per second. This appears to be fast enough for the lasers used for ablation, which have pulse or burst repetition rates of up to a few Hz. It is therefore expected, despite its physical limitations, that SOCT will be instrumental for instantaneous, in situ control of varnish ablation.

ACKNOWLEDGMENTS

This work was supported by Polish Ministry of Science Grant 2 H01E 025 25. Authors wish to thank Dr. Robert Dale for very valuable discussions and Dr. Janusz Szatkowski for SEM images.

REFERENCES

[1] C. Fotakis, D. Anglos, C. Balas, et al., "Laser technology in art conservation," in *OSA TOPS on Lasers and Optics for Manufacturing*, A. C. Tam, Ed., vol. 9, pp. 99–104, Optical Society of America, Washington, DC, USA, 1997.

[2] J. F. Asmus, "Light cleaning: laser technology for surface preparation in the arts," *Technology and Conservation*, vol. 3, no. 3, pp. 14–18, 1978.

[3] M. Cooper, Ed., *Laser Cleaning in Conservation: An Introduction*, Butterworth Heinemann, Oxford, UK, 1998.

[4] J. Marczak, "Renovation of works of art by laser radiation," *Przegląd Mechaniczny*, vol. 15-16, pp. 37–40, 1997.

[5] D. Anglos, S. Couris, and C. Fotakis, "Laser diagnostics of painted artworks: laser-induced breakdown spectroscopy in pigment identification," *Applied Spectroscopy*, vol. 51, no. 7, pp. 1025–1030, 1997.

[6] Final Report CRAFT project ENV4-CT98-0787, "Advanced workstation for controlled laser cleaning of artworks," http://www.art-innovation.nl/.

[7] A. Bonarou, L. Antonucci, V. Tornari, S. Georgiou, and C. Fotakis, "Holographic interferometry for the structural diagnostics of UV laser ablation of polymer substrates," *Applied Physics A: Materials Science and Processing*, vol. 73, no. 5, pp. 647–651, 2001.

[8] A. de Cruz, M. L. Wolbarsht, and S. A. Hauger, "Laser removal of contaminants from painted surfaces," *Journal of Cultural Heritage*, vol. 1, supplement 1, pp. 173–180, 2000.

[9] A. Andreotti, P. Bracco, M. P. Colombini, et al., "Novel applications of the Er:YAG laser cleaning of old paintings," http://www.art-restorers-ass.nl/.

[10] P. Targowski, B. Rouba, M. Wojtkowski, and A. Kowalczyk, "The application of optical coherence tomography to nondestructive examination of museum objects," *Studies in Conservation*, vol. 49, no. 2, pp. 107–114, 2004.

[11] H. Liang, M. G. Cid, R. G. Cucu, et al., "En-face optical coherence tomography—a novel application of non-invasive imaging to art conservation," *Optics Express*, vol. 13, no. 16, pp. 6133–6144, 2005.

[12] I. Gorczyńska, M. Wojtkowski, M. Szkulmowski, et al., "Varnish thickness determination by spectral optical coherence tomography," in *Proceedings of the 6th International Congress on Lasers in the Conservation of Artworks LACONA VI, Vienna, Austria 2005*, J. Nimmrichter, W. Kautek, and M. Schreiner, Eds., Springer, Berlin, Germany, 2006.

[13] P. Targowski, M. Góra, and M. Wojtkowski, "Optical coherence tomography for artwork diagnostics," *Laser Chemistry*, vol. 2006, Article ID 35373, 2006.

[14] M. Szkulmowski, M. Wojtkowski, P. Targowski, and A. Kowalczyk, "Spectral shaping and least square iterative deconvolution in spectral OCT," in *Coherence Domain Optical*

Methods and Optical Coherence Tomography in Biomedicine VIII, vol. 5316 of *Proceedings of SPIE*, pp. 424–431, San Jose, Calif, USA, January 2004.

[15] B. Cense, N. A. Nassif, T. C. Chen, et al., "Ultrahigh-resolution high-speed retinal imaging using spectral-domain optical coherence tomography," *Optics Express*, vol. 12, no. 11, pp. 2435–2447, 2004.

Hindawi Publishing Corporation
Laser Chemistry
Volume 2006, Article ID 39046, 11 pages
doi:10.1155/2006/39046

Research Article

Multianalytical Study of Laser Pulse Duration Effects in the IR Laser Cleaning of Wall Paintings from the Monumental Cemetery of Pisa

A. Andreotti,[1] M. P. Colombini,[1] A. Nevin,[2,3] K. Melessanaki,[2] P. Pouli,[2] and C. Fotakis[2,4]

[1] *Dipartimento di Chimica e Chimica Industriale, Università di Pisa, Via Risorgimento 35, 56126 Pisa, Italy*
[2] *Institute of Electronic Structure and Lasers (IESL), Foundation for Research and Technology-Hellas (FORTH), P.O. Box 1385, 71110 Heraklion, Crete, Greece*
[3] *Courtauld Institute of Art, University of London, Somerset House, Strand WC2R 0RN, London, UK*
[4] *Department of Physics, University of Crete, P.O. Box 2208, 71003 Heraklion, Crete, Greece*

Received 15 September 2006; Revised 13 December 2006; Accepted 13 December 2006

Recommended by Wolfgang Kautek

The feasibility of laser cleaning for the removal of a variety of surface deposits from fragments of real wall paintings from the monumental cemetery of Pisa using Nd:YAG at 1064 nm at (μs), (ns), and (ps) regimes is presented. Multianalytical investigations of the samples from irradiated surfaces of fragments were carried out in order to characterize the original and added materials and to detect any laser-induced alterations; analysis included scanning electron microscopy (SEM), Fourier transform infrared spectroscopy (FTIR), laser-induced breakdown spectroscopy (LIBS), pyrolysis-gas chromatography-mass spectrometry (PY-GC-MS), and gas chromatography-mass spectrometry (GC-MS). The presence of nitrocellulose and pure lead contaminations on the surface of the samples has been identified. Assessment of the laser cleaning has highlighted the importance of the optimization of laser parameters, specifically pulse duration and fluence at the specified wavelength.

1. INTRODUCTION

The use of lasers to selectively remove unwanted materials from sensitive surfaces is well studied and has extensive applications [1], including the conservation of cultural heritage. Over the last decade, lasers have been used as a highly controllable cleaning tool for the removal of dirt and various layers; numerous successful case studies on the laser cleaning of a variety of materials have been reported and include stone, varnished icons and paintings, metals, and paper [2, 3]. Laser cleaning of paintings and polychromy requires a careful selection of laser parameters: wavelength, pulse duration, fluence, repetition rate, and number of pulses. Most importantly, the removal of dirt or other unwanted materials from the surface of a painting must not result in damage, chemical modifications, or otherwise compromise the integrity of the original material. Laser-induced pigment alterations have been indicated as problematic in various studies of the cleaning of wall paintings [4, 5] and this has led to a series of model investigations of the physiochemical parameters that may induce and influence alterations [6–8]. In addition, investigations of the photothermal reactions on polymer-based materials have been studied in a variety of model systems [9, 10] and on varnishes [11].

Particular advantages are associated with the use of ultrashort laser pulses where limited photochemical modifications and thermal diffusion occur at the laser-substrate interface. However, cleaning using ultra-short laser pulses is complicated and not yet well defined [12] and such sources are of limited availability.

Studies on the laser cleaning of both model systems [4, 13, 14] and real samples [5, 13, 14] of paintings have investigated various laser wavelengths (Er:YAG at 2.94 μm, Nd:YAG at 1064 nm) and different pulse durations (μs and ns, resp.). The aim of this work is to assess the feasibility of the use of laser cleaning for the removal of surface deposits from fragments of real wall paintings from the monumental cemetery of Pisa using Nd:YAG laser irradiation at 1064 nm with pulse durations of μs, ns, and ps.

The cycle, painted from the late medieval until early renaissance, is considered one of the finest Italian wall

(a) (b)

Figure 1: Images under visible radiation of (a) fragment 1 and (b) fragment 2.

paintings, executed by artists including Taddeo Gaddi, Benozzo Gozzoli, and Bonamico Buffalmacco. The exterior wall paintings were exposed to inevitable fluctuations in temperature and humidity; their condition is further complicated by restorations from the 19th and early 20th centuries during which various modern materials including nitrocellulose were applied to the surface of the paintings. Second World War damage led to fire, which caused further contamination of the surface of the paintings with ash, soot, and molten lead from the roof.

In order to evaluate the influence of pulse duration on cleaning of the wall paintings, tests were carried out on representative fragments of the paintings to remove different patterns of surface dirt. The fragments choosen for the laser cleaning investigations were systematically studied for a thorough characterization of the contaminant and original paint layer (binding media and pigments).

Moreover, to assess the long-term effects of laser action on the substrate, organic material was analyzed six months after laser irradiation tests.

2. EXPERIMENTAL

The precious fragments of the wall paintings from the monumental cemetery were examined in the following order. First, samples were photographed and their condition was recorded. Selected areas were sampled for transmission FTIR analysis (diamond cell) for the characterization of the surface coating. Further, samples were prepared in cross-section for examination using optical microscopy followed by scanning electron microscopy with energy-dispersive X-ray emission (SEM-EDX) for both elemental analysis and high-resolution imaging. Microdestructive analysis was carried out for elemental depth-profiling using laser-induced breakdown spectroscopy in selected points. Pyrolysis-silylation gas chromatography-mass spectrometry (Py-silylation/GC-MS) and GC-MS [15, 16] were used for the characterization of the organic material before the laser treatment; following laser cleaning, the ablated material was analyzed to assess possible photothermal modifications of surface coatings. Finally, laser-cleaned areas were subjected to colorimetric control under the microscope and samples were taken and prepared in cross-section for examination using optical and scanning electron microscopy.

3. METHODOLOGY AND METHODS

3.1. Samples

The study focused on two representative fragments from the monumental cemetery of Pisa for the assessment of the most suitable laser parameters for the removal of surface treatments (*patinas*) and encrustations. The fragments which are painted over a red background come from decorative sections of the painting and contain a floral motif and creeping vine leaf, as shown in Figure 1.

3.2. Laser instrumentation

The fundamental frequency (at 1064 nm) of the following Nd:YAG laser systems at various pulse durations has been used:

(1) a fibre-coupled short free-running laser system (El. En., EOS 1000) emitting pulses of 120–1000 mJ output energy and pulse duration in the range of 50–130 μs;

(2) a Q-switched laser system (SPECTRON, SL805) emitting pulses of 15 ns and maximum output energy of 450 mJ;

(3) a Q-switched laser system (EKSPLA, SL312) with pulses up to 120 mJ and 150 ps duration.

For a systematic study of the laser cleaning parameters, this investigation has been limited to laser cleaning at a single wavelength (1064 nm) with different pulse durations (μs, ns, and ps). Laser-assisted removal of the surface dirt, past treatments, and encrustations was carried out with different energy density values as well as a variable number of pulses. The pulse repetition was kept at slow values (2–4 Hz) in order to follow and control the removal process. The application of water as a wetting agent has also been considered. Selected tests are reported in Table 1. (See Section 4.2) for fragment 1 and fragment 2.

3.3. Analytical techniques

The following instrumental techniques have been used to analyze samples of the fragments, to characterize the original and added materials and to detect any laser-induced alterations:

(1) FT-IR spectrophotometer (Perkin Elmer, USA), mod. Spectrum GX I, interfaced with a FT-IR autoimage system microscope (Perkin Elmer USA);

(2) low-vacuum scanning electron microscope JSM 5600 (JEOL, Tokyo, Japan), equipped with energy-dispersive X-ray emission—system Oxford Link ISIS for spot analysis. Backscattered electron images of the cross-section were taken at 20 kV;

(3) a nanosecond Q switched Nd:YAG laser (pulse duration ca. 10 ns) using the third harmonic (355 nm) for laser induced breakdown spectroscopy (LIBS). The laser beam focused on the sample surface by means of a 50 mm focal length planoconvex quartz lens and a single laser pulse measurement was performed. Typical laser pulse energy values ranged from 2 to 4 mJ with a spot diameter on the sample of approximately 100–150 μm. The spectrum was recorded with an intensified CCD detector (Andor Technologies, DH520-18F-01 with an EEV30-11 sensor). The gating pulse applied to the intensifier was delayed 200–500 ns with respect to the laser pulse and has a temporal width of 500–1000 ns [17, 18];

(4) pyrolyser operating in constant temperature mode (Pyrojector II, SGE, Austin, Tex, USA), connected to the PTV injector of the GC system gas chromatograph. The pyrolyses were performed with "in situ" hexamethyldisilazane silanization [15];

(5) 5890 series II gas-chromatograph (Hewlett Packard, Palo Alto, Calif, USA) coupled with a quadrupole mass spectrometric detector mod. 5971A (electron impact 70 eV, ion source temperature 180°C, interface temperature 280°C).

4. RESULTS AND DISCUSSION

4.1. Characterization of the materials

The diagnosis of the constituents of works of art is of primary importance before starting the laser cleaning; the fragments of the wall painting were covered with surface deposits and encrustations of unknown origin, and hence it was necessary to identify the contaminant materials. Therefore, thorough analysis with different techniques were carried out, in order to plan the laser tests on the basis of the materials present in the selected areas of the fragments. A careful investigation of the inorganic materials was performed by cross-section analysis of the fragments under the microscope, SEM-EDX, and LIBS analysis, while the characterization of the organic material and their degradation products was carried out using FT-IR, PY-GC-MS, and GC-MS.

4.1.1. Inorganic material

A representative cross-section is shown in Figure 2. The complexity is evident, a deposit of a metal is visible on the surface

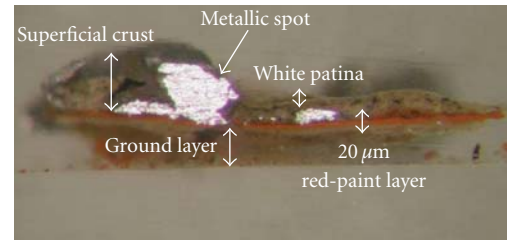

Figure 2: Cross-section from fragment 2.

of the red-paint layer of about 20 μm or less; moreover a thick grey layer is observed as a thick crust over the paint layer, and over it a very thin white layer is present. Below the red paint, the ground preparation of about 50 μm is present.

SEM-EDX analysis permitted the identification of the inorganic constituents of the different layers. Specifically, the metallic material deposited on the surface of different fragments is lead, as confirmed by the LIBS analysis; the presence of lead on the surface of the fragment is due to fires following Second War World bombing, during which the lead roof melted, and molten lead fell onto the surface of the wall paintings. The SEM-EDX analysis of the shiny metal spot, particularly apparent in the back scattered electron image is reported in Figure 3 together with the LIBS spectrum. The LIBS analysis was carried out on many metallic grey spots present on much of the surface of both the samples; the observed spots vary from small droplets to larger stains of metallic lead, with a diameter varying from about 0.5 cm to 8 cm.

The SEM-EDX analysis also highlighted the presence of iron oxide in the red-paint layer, identified as red ochre, which was further confirmed by LIBS analysis. In Figure 4, a spectrum of the red pigment in fragment 2 is presented. Moreover, LIBS provided elemental confirmation of red and yellow ochres, iron containing pigments in the different fragments, as well as the presence of a copper-based green pigment.

As a further example of the characterization of the inorganic materials found in the fragments, in Figure 5 the SEM-EDX analysis of the thick grey crust found on top of the red-ochre layer is given: it consists predominantly of calcium carbonate, carbon-black, and calcium sulphate, and in the electron image the needle-like shape of the calcium sulphate (gypsum) is clearly visible.

4.1.2. Organic material

The thin white layer observed as an opaque layer over the thick crust in the cross-section from fragment 2, but also widespread on the surface of fragment 1, was further identified using micro-FT-IR in the diamond cell. A comparison of the spectrum with that of the naturally aged reference material nitrocellulose, seen in Figure 6, indicates strong similarities between the compounds. The semitransparent adhesive nitrocellulose was likely applied to the painting in conservation treatments dating to 1947.

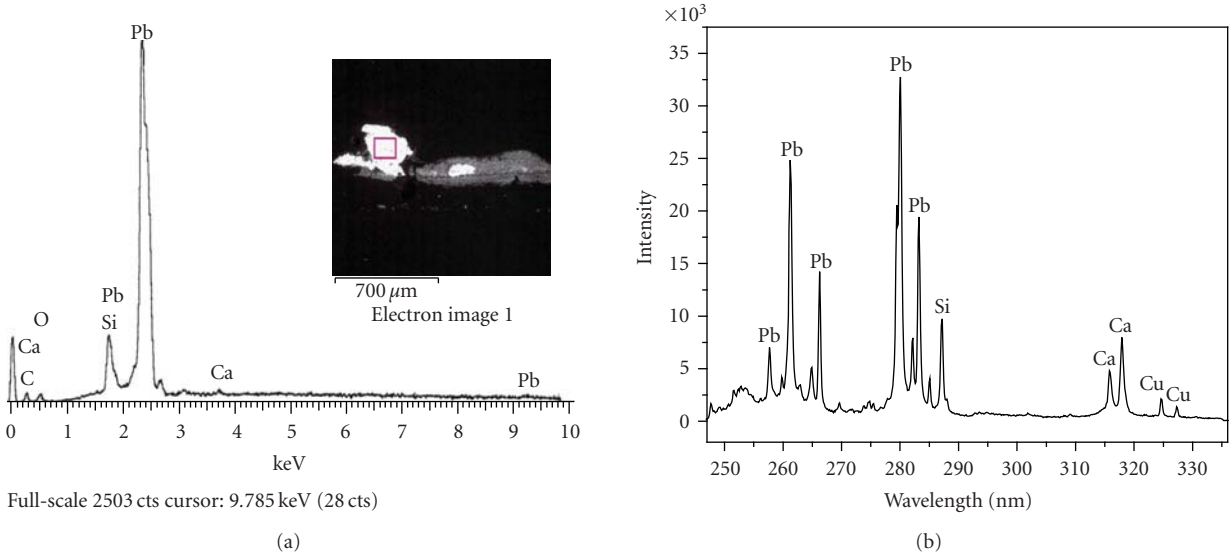

Figure 3: Fragment 2, (a) SEM-EDX of the area indicated in red on the electron image and (b) LIBS analyses on a metallic shiny spot.

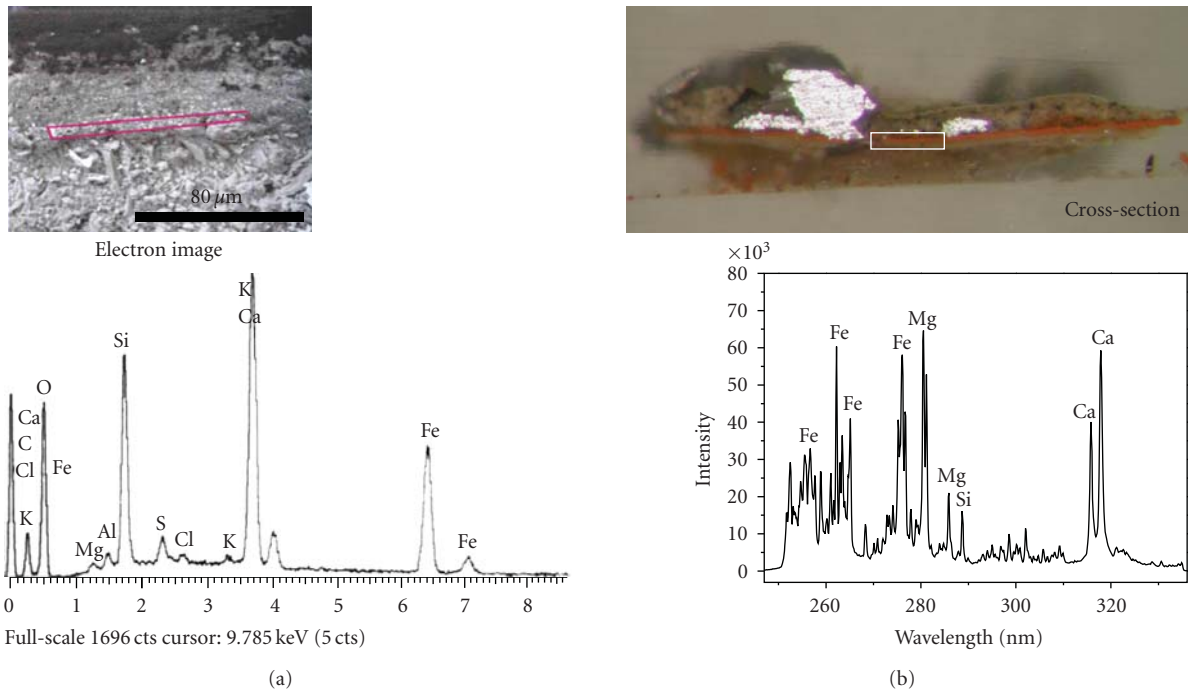

Figure 4: Fragment 2, (a) SEM-EDX of the area outlined in red in the electron image, which corresponds to the area indicated in white on the cross-section and (b) LIBS analyses of the red pigment.

The adhesive is characterized by vibrational bands corresponding to NO_2-O asymmetric stretching bands at 1718 cm^{-1}, 1654 cm^{-1}, and 839 cm^{-1} and a symmetric one at 1282 cm^{-1}. Additional modes are associated with aliphatic C−H stretching bands at 2800–3200 cm^{-1} and O−H stretching at 3200–3400 cm^{-1}. The fingerprint region has distinct stretching bands at 1377 cm^{-1} (C−NO_2), 1161 cm^{-1} (C−OH), and 1066 cm^{-1} (C−OH). Interferences from calcium carbonate are observed in the sample which has a peak at approximately 1428 cm^{-1} which corresponds to the C−O ν_3 stretching vibration.

However, for a more specific characterization of the organic material from the two fragments, PY-GC-MS with silanization "in situ" followed by GC-MS was used. An

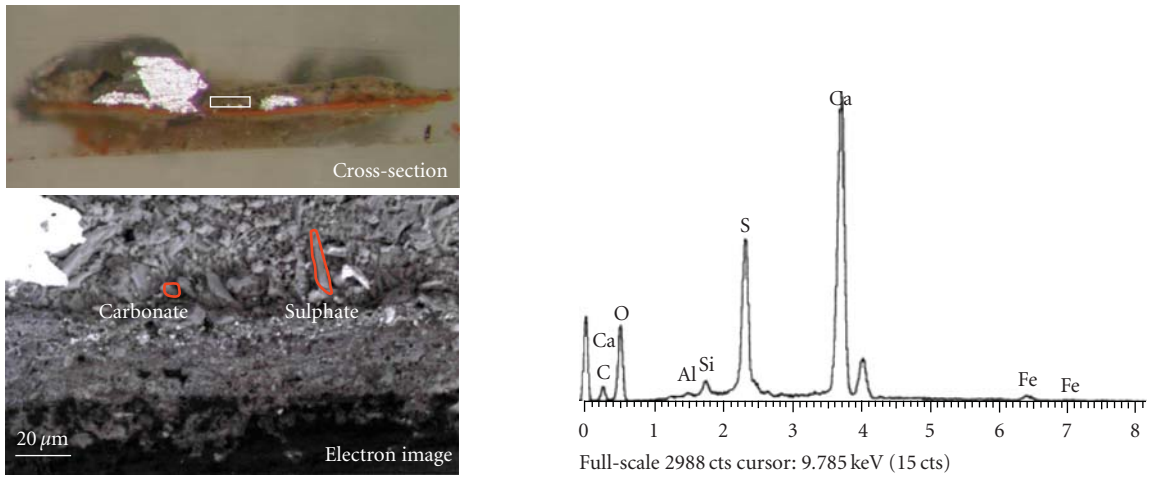

Figure 5: Fragment 2, SEM-EDX of the crystal of calcium sulphate outlined in red in the electron image (corresponding to the area indicated in white on the cross-section) analysis of the superficial crust.

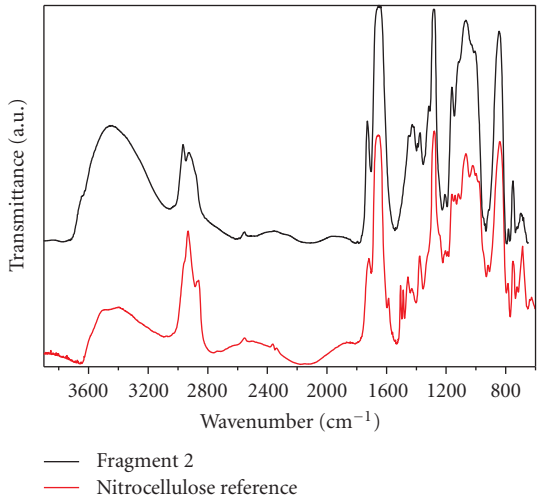

Figure 6: Fragment 2, FT-IR spectra of the white patina.

example of the pyrogram of the superficial white patina from fragment 1 is reported in Figure 7. The extract ions of m/z 217 and 204, characteristic of carbohydrates, indicate the presence of levoglucosane and other sugars, thus confirming the FT-IR identification of the white patina as nitrocellulose. In fact, the most specific pyrolysis product of cellulose is levoglucosane, the anhydro-sugar of glucose. Moreover, the PY-GC-MS investigation of the binding media of the wall painting has indicated the presence of pyrrole, a specific marker of animal glue.

The presence of this proteinaceous material was further confirmed by GC-MS analysis, as shown following statistical treatment using principal component analysis (PCA) [16] of the percentage of amino acids of the proteinaceous fractions collected from fragments 1 and 2 (see Figure 8). Moreover, the study of the lipidic fractions shows the presence of a lipidic material, likely egg due to the presence of traces of cholesterol.

However these products have been found only in trace quantities and they were not widespread in all the fragments analyzed; results therefore suggest that the painting technique was mainly "a fresco" and that the animal glue and egg are probably present as restoration materials.

The different results obtained from the variety of analyses of the superficial layers indicate that they are mainly composed of nitrocellulose and black crusts of heterogeneous materials including metallic lead. The proteinaceous material identified as animal glue and traces of egg likely belong to past restorations, including those from the 19th century; these materials may have penetrated the original matrix, and therefore cannot be removed. The main problem related to the laser cleaning of these wall paintings is not only their compromised condition and the complexity of added materials including deteriorated restoration products and widespread depositions of dirt, but rather the presence of red and yellow ochres and copper pigments, which are well known for their sensitivity to pigment alterations following laser irradiation.

4.2. *Laser cleaning: assessments and evaluations*

Removal of the superficial white patina of nitrocellulose, the thick encrustation, and metallic lead is particularly problematic since all materials are well attached to the upper pigment layers, and are widely distributed on the surface of both fragments. Laser cleaning of the different contaminants using a variety of different pulse fluences and pulse durations was explored in order to identify the most suitable parameters for each type of material and to evaluate the problems associated with different cleaning regimes. Laser parameters employed in the cleaning tests on fragments 1 and 2 are reported in Table 1, together with brief observations of the laser cleaning results after evaluation under the binocular microscope.

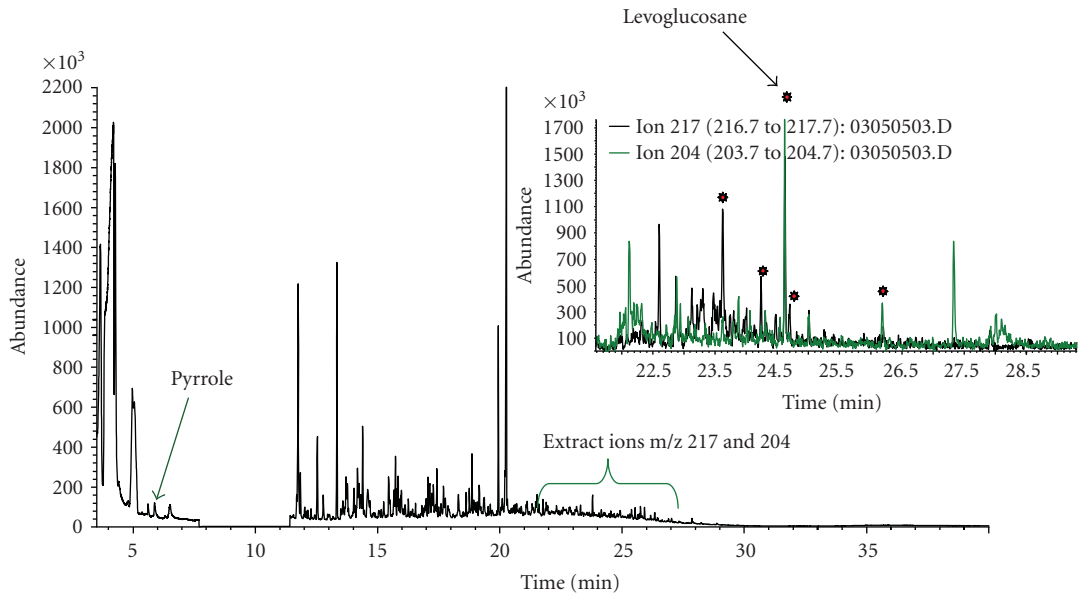

Figure 7: Fragment 1, pyrogram of the superficial crust.

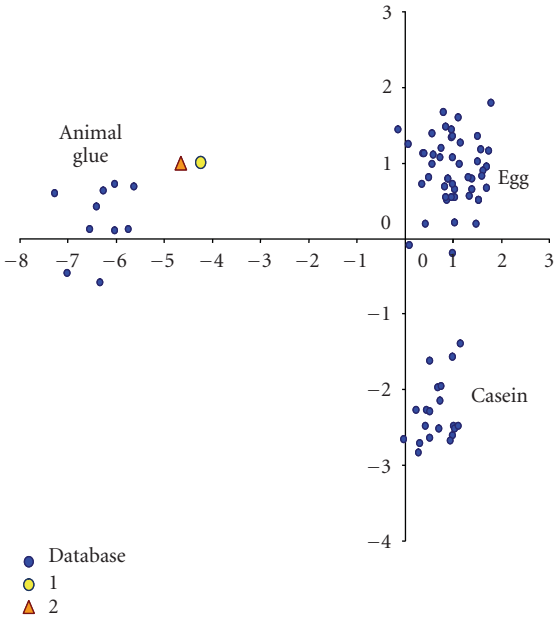

Figure 8: PCA of the amino acids percentage content of the proteinaceous fraction of samples from fragments 1 and 2.

4.2.1. Removal of the white surface patina

The thin white patina appears to have been successfully removed from fragment 1 with all the laser systems, as visible in macrophotographs seen in Figure 9(a) for the μs laser application of a single pulse at 1.4 J/cm^2, Figure 9(b) for ns laser application of a single pulse at 0.2 J/cm^2, and Figure 9(c) for ps laser application of three pulses at 0.3 J/cm^2.

Similarly good results were observed in fragment 2, as seen in Figure 10; however in this case, in the areas cleaned, the layer of nitrocellulose was slightly different (thicker) but nonetheless similar in behavior to that observed on the surface of fragment 1 (Figure 9).

With the μs laser system, the patina was generally removed using fluences lower than 9 J/cm^2, but unfortunately in a few areas of the fragment, the layer of the patina was thicker, and the application of a single pulse at 11 J/cm^2 caused browning of the red underlying pigment, a particular problem for the cleaning of areas of sensitive pigments. However, an optimal removal test (2.8 J/cm^2, 2 pulses) is reported in Figure 10(a) in which no pigment alterations are observed. With the ns laser, a good removal of the patina was also obtained, without any visible browning of the pigment. A spot test (0.3 J/cm^2, 1 pulse) is reported in Figure 10(b). The photomechanical effects of the picoseconds laser, as compared with lasers of longer pulse duration, permit a controlled removal of the white surface patina. Following ablation, the surface film becomes detached and lifts from the surface of the fragment without removing any pigment particles, and no pigment alterations are observed. One of the spot tests (0.2 J/cm^2, 5 pulses) is reported in Figure 10(c). Additionally, with the ps laser, the superficial patina has been completely removed as confirmed by the PY-GC-MS analysis of a sample from fragment 2 taken of the area following cleaning, in which no traces of the surrounding nitrocellulose were found. The especially sensitive technique hence confirms the complete removal of the surface coating from the sample. Additionally, analysis of removed material indicates that during ablation no molecular changes of the surface coating are detected. In general, cleaning of similar areas using μs pulses requires a higher fluence than that needed for ns and

Table 1: Laser parameters adopted in the cleaning tests on fragments 1 and 2 and laser cleaning results (the abbreviations outside of the parentheses indicate the following: A indicates alteration of the pigment, G indicates good removal, I indicates ineffective removal, L indicates loss of pigment, P indicates partial removal. Within parentheses, the area treated with the laser is given and corresponds to C: grey crust, W: white surface film/patina).

Laser	Fragment 1				Fragment 2			
	Laser parameters				Laser parameters			
	Spot number	Fluence (J/cm^2)	Number of pulses	Cleaning results	Spot number	Fluence (J/cm^2)	Number of pulses	Cleaning results
Short free-running Nd:YAG laser (250 μs)	1	8.5	2	L (C)	1	0.7	2	P (C)
	2	7.1	1	L (C)	2(Figure 12(b))	13	1	G (C)
	3	1.4	1	G (C)	3	11	1	G (C)
	4(Figure 9(a))	1.4	1	G (W)	4	9.9	1	G (C)
	5(Figure 13)	2.8	5	G (C)	5	8.5	1	P (C)
	6(Figure 13)	2.8	18	G (C)	6	7.1	1	P (C)
	7(Figure 13)	2.1	50	G (C)	7	5.7	1	I (C)
	—	—	—	—	8	5.7	1	I (C)
	—	—	—	—	9(Figure 12(a))	8.5	4	P (C)
	—	—	—	—	10	8.5	2	P (C)
	—	—	—	—	11	8.5	6	L (C)
	—	—	—	—	12(Figure 11(a))	14	1	G (C)
	—	—	—	—	13(Figure 11(a))	14	1	G (C)
	—	—	—	—	14(Figure 11(a))	14	1	G (C)
	—	—	—	—	15(Figure 11(a))	14	3	G (C)
	—	—	—	—	16	14	1	G (C)
	—	—	—	—	17	14	1	G (C)
	—	—	—	—	18	14	1	G (C)
	—	—	—	—	19(Figure 12(c))	13	1	A (C)
	—	—	—	—	20	11	1	A (W)
	—	—	—	—	21	10	1	G (W)
	—	—	—	—	22	8.5	1	G (W)
	—	—	—	—	23	7.1	1	G (W)
	—	—	—	—	24	5.7	1	G (W)
	—	—	—	—	25	4.3	2	G (W)
	—	—	—	—	26(Figure 10(a))	2.8	2	G (W)
	—	—	—	—	27	1.4	1	G (W)
Q-switched Nd:YAG laser (20 ns)	1	0.2	2	L (W)	1(Figure 11(b))	1.4	3	L (C)
	2	0.2	1	G (W)	2(Figure 11(b))	1.4	2	P (C)
	3	0.2	3	G (W)	3(Figure 11(b))	1.4	30	P (C)
	4(Figure 9(b))	0.2	1	G (W)	4(Figure 11(b))	2.0	20	P (C)
	5	0.3	1	G (W)	5	2.0	5	P (L)
	6	0.3	2	G (W)	6(Figure 10(b))	0.3	1	G (W)
	7	0.3	6	G (C)	7	2	50	P (L)
Q-switched Nd:YAG laser (500 ps)	1	0.2	10	P (W)	1	0.2	23	P (C)
	2	0.3	5	G (W)	2	0.3	10	P (C)
	3	0.2	5	I (W)	3(Figure 11(c))	0.7	27	G (C)
	4	1.1	16	P (C)	4	1.1	18	L (C)
	5	0.2	1	I (C)	5	0.7	1	G (W)
	6	0.3	3	I (C)	6	0.2	3	G (W)
	7(Figure 9(c))	0.3	3	G (W)	7(Figure 10(c))	0.2	5	G (W)
	8	0.7	1	P (C)	—	—	—	—
	9	0.6	1	P (C)	—	—	—	—
	10	1.1	1	P (C)	—	—	—	—
	11	1.6	1	P (C)	—	—	—	—
	12	0.6	6	G (C)	—	—	—	—

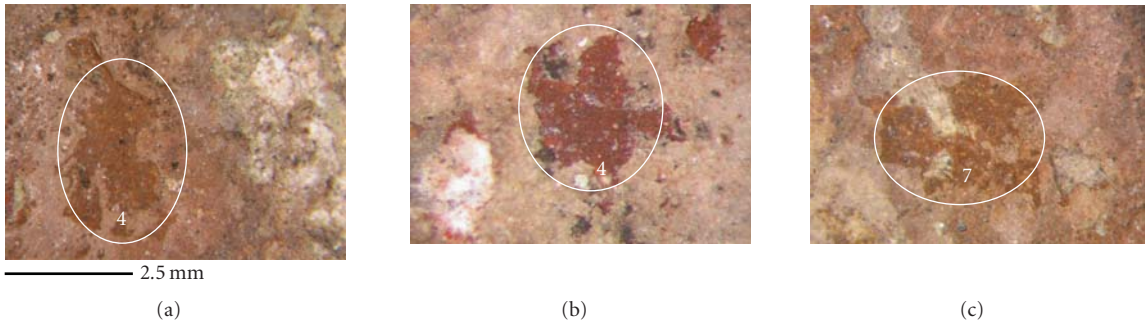

Figure 9: Fragment 1; removal of the white patina with μs (a), ns (b), and ps (c) laser radiations; the numbers within the circles correspond to the laser parameters employed as reported in Table 1.

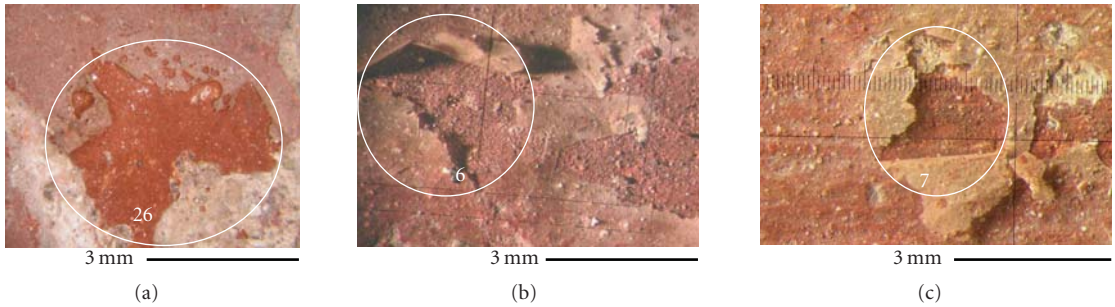

Figure 10: Fragment 2; removal of the white patina with μs (a), ns (b), and ps (c) laser radiations; the numbers indicated within the circles correspond to the laser parameters employed as reported in Table 1.

ps, but in the optimum conditions, it is possible to effectively clean without damage to the pigment layer.

4.2.2. *Removal of the superficial thick crust of deposited metallic lead*

The removal of lead deposits and crusts is compromised as the molten lead from the roof likely caused pigment alterations due to the high temperature interactions with the surface; in addition, the lead droplets were strongly adhered to the surface of the paintings.

With one pulse of the μs laser at fluence 14 J/cm^2 on a wet surface, the lead crust was removed without any observable damage to the underlying pigments. The predominant photothermal effects of the laser radiation with longer pulses induced melting, rather than the mechanical ablation of the lead, thus allowing its gradual removal from the red-paint layer. In Figure 11(a), a laser-cleaned area where a thick drop of lead was originally present is reported (14 J/cm^2, 1–3 pulses, see Table 1 for more detailed laser parameters). In contrast to the μs cleaning, the application of consecutive pulses of the ns laser resulted in the removal of only a superficial part of the lead. In fact, the thicker crust of lead may be detached only under extreme cleaning conditions (e.g., higher number of pulses or higher fluences) but with concomitant removal of the original red pigment layer. In Figure 11(b), it is clearly visible that the grey lead encrustation was effectively rendered shiny or thinned by consecutive laser pulses at 1.4 J/cm^2 or 2 J/cm^2 (spot numbers 2-3-4, 2–30 pulses, see Table 1 for more detailed laser parameters). However, in spot number 1 (1.4 J/cm^2, 3 pulses, see Figure 11(b)), the removal of lead is accompanied by the loss of part of the pigment layer, probably due, in addition to the photomechanical effects, to a local decohesion of the paint layer to the plaster. With the ps laser, instead, removal of lead was quite satisfactory (see Figure 11(c), 0.7 J/cm^2, 27 pulses), however further studies should be performed to confirm the result, as the lead stains at the tested areas were rather thin.

It is stressed that for the removal of hard thick encrustations, the application of consecutive pulses at lower fluences was generally more successful than that of one single pulse at higher fluences. As an example of this issue, three macrophotographs of the μs laser spots are reported in Figure 12. Using the same μs laser, with the application of four consecutive pulses of μs duration at 8.5 J/cm^2 resulted in a rather promising crust removal, while a part of the lead drop still remained after treatment (Figure 12(a)). Therefore it was decided to test one single laser pulse at higher fluence (13 J/cm^2) and the drop of lead was completely removed with no damage to the underlying pigment (Figure 12(b)). On the other hand, when a single pulse of the same fluence (13 J/cm^2) was applied to an area where the stain of lead was thinner, the stain was removed, but the red pigment was clearly altered (Figure 12(c)).

From these comparative studies, it can be concluded that with increasing laser intensities, the removal efficiency is

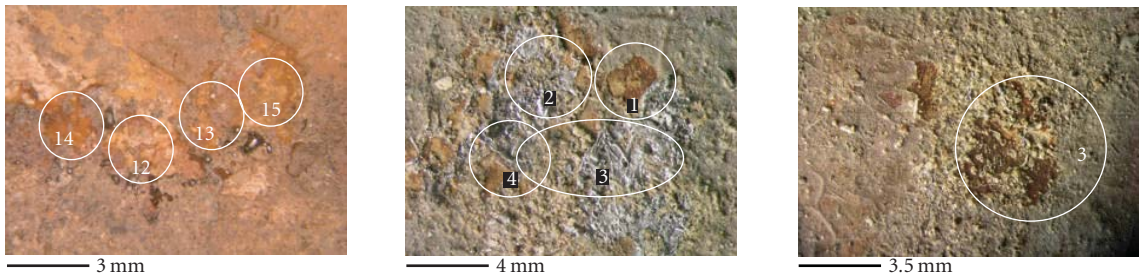

(a) (b) (c)

Figure 11: Fragment 2, removal of the superficial crust with lead deposits with μs (a), ns (b), and ps (c) laser radiations; the numbers correspond to the laser parameters reported in Table 1.

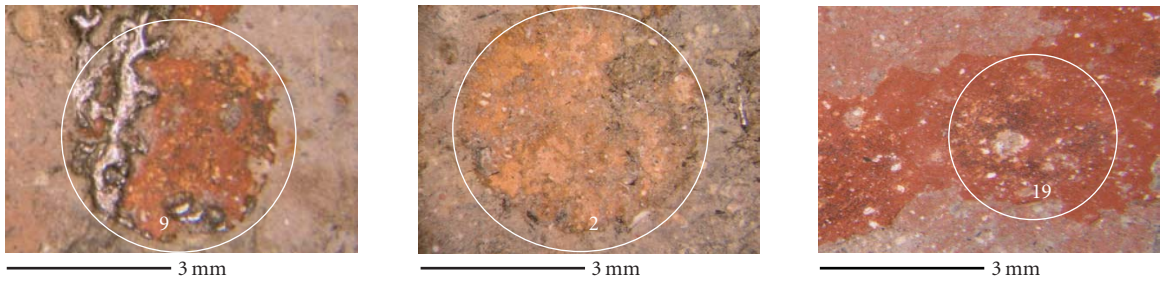

(a) (b) (c)

Figure 12: Fragment 2, laser cleaning tests (in the μs regime) to remove the superficial crust with lead deposits: four consecutive pulses at 8.5 J/cm^2 were not able to completely remove the metallic lead deposit (a); only one pulse at higher fluence values efficiently removed a relatively thick lead stain (b), while in the case of a thinner lead stain, the result was not successful (c); the numbers correspond to the laser parameters reported in Table 1.

increased for both ns and ps lasers. Significantly higher laser fluences are needed to remove the thicker layers of encrustation in all cleaning regimes (μs, ns, and ps), but side effects include the detachment of the fragile underlying pigment layer with the ns and ps regimes and a higher possibility of inducing pigment color alteration with μs laser pulses.

A further example of laser cleaning of a larger area indicates the type of results obtained with careful treatment. The thick black crusts present in some areas of fragment 1 exhibit very strong adhesion to the pigments; cleaning with lasers was able to only partially remove the crust from the paint layer. The best results were obtained with the laser of longer pulse duration, as shown in Figure 13 for the cleaning of a larger area (spot numbers 5-6-7, fluence in the range of 2-3 J/cm^2; 5–50 consecutive pulses, see Table 1 for more detailed laser parameters).

5. CONCLUSIONS

Particularly important, as exemplified in this study, is the heterogeneity of the surface of the samples studied; with variation in condition, state of conservation, thickness, and type of contaminant and restoration materials, it is impossible to specify optimal conditions for laser cleaning of the entire fragments. In fact, tests illustrate the necessity to optimize laser cleaning for each type of area and the requirement to assess the cleaning results using different and complementary analyses. A good compromise between fluence and the number of pulses always needs to be determined, and the use of lasers for cleaning of wall paintings may be well complimented by other traditional methods for cleaning, as it is not always possible to completely remove surface dirt using laser ablation alone.

Following extensive testing, the optimal conditions for the laser cleaning of specific layers/crusts on the studied fragments of the wall paintings from the monumental cemetery of Pisa were determined. Long-pulse laser radiation, with fluences lower than 7 J/cm^2, provided controlled removal of different patinas. In cases of thicker layers, good results were generally obtained with fluence lower than 14 J/cm^2 and best results were obtained by increasing the number of consecutive laser pulses at a lower fluence, instead of using fewer pulses at a higher fluence, in order to avoid pigment colour alteration. Ablation using the μs laser offers the possibility to remove the drops of lead present on the surface, without damaging the fragile underlying pigment. Wetting of the surface with aqueous solutions before applying the radiation was found to enhance the cleaning. In addition, the novel application of ultrashort pulses of ps duration to the cleaning of wall paintings was considered with very encouraging results,

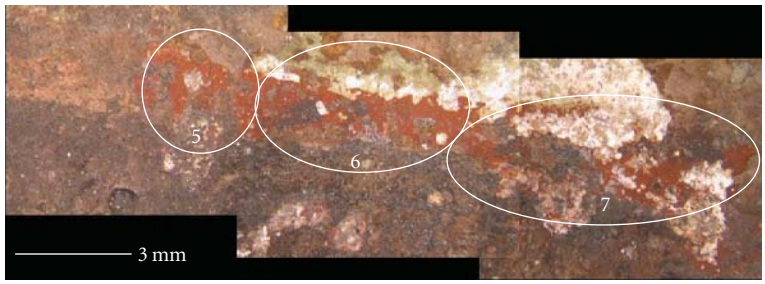

Figure 13: Fragment 1: removal of a larger area of thick black crust with the μs laser; the numbers correspond to the laser parameters reported in Table 1.

providing increased control and minimal observed alteration to the substrate, with fluences lower than 0.7 J/cm^2.

Analysis of laser-cleaned areas was undertaken using molecular spectroscopy. Further, the efficacy of the cleaning was monitored following treatment by examination of samples in cross-section. For the optimized laser parameters adopted, no alteration products were detected. Finally, microscopic observations of the surface and PY/GC/MS analysis of the samples suggested an efficient removal of the different encrustations and of the white patina. In addition, the gas chromatographic analysis has indicated that by using the optimized laser parameters for the different laser systems, no degradation products of the organic materials were detected and that a gradual thinning of the superficial layer is possible by operating under controlled laser parameters. Positive results were associated with each laser employed; however differences in the materials found on the surface of the fragments and different responses to the lasers used yielded significant variations in optimum cleaning conditions. This highlights the importance of further study of mechanisms of laser materials interactions, in order to foster a synergistic approach to the optimization and assessment of laser techniques to the multifacetted problems encountered in the cleaning of wall paintings.

ACKNOWLEDGMENTS

This work was performed at the Ultraviolet Laser Facility operating at IESL-FORTH and has been supported in part by the European Commission through the Research Infrastructures activity of FP6 ("Laserlab-Europe" RII3-CT-2003-506350). The third author is supported with a fellowship from the "ATHENA" EST Marie Curie Project (MEST-CT-2004-504067) at IESL-FORTH. The authors fully acknowledge Dr. Clara Baracchini (Soprintendenza ai Beni Architettonici e al Paesaggio, al Patrimonio Storico Artistico e Demoantropologico, Pisa, Italy) for providing the wall painting samples and for the historical discussion.

REFERENCES

[1] B. Luk'yanchuk, *Laser Cleaning*, World Scientific, Singapore, 2002.

[2] M. I. Cooper, *Laser Cleaning in Conservation: An Introduction*, Butterworth-Heinemann, Oxford, UK, 1998.

[3] C. Fotakis, D. Anglos, S. Georgiou, V. Tornari, and V. Zafiropulos, *Lasers in the Preservation of Cultural Heritage; Principles and Applications*, edited by R. G. W. Brown and E. R. Pike, Taylor and Francis, New York, NY, USA, 2006.

[4] L. Shekede, "Lasers: a preliminary study of their potential for the cleaning and uncovering of wall paintings," in *Restauratorenblätter, Sonderband - Lacona I, Laser in the Conservation of Artworks*, pp. 51–56, Mayer, Vienna, Austria, 1997.

[5] E. Dragasi, N. Minos, P. Pouli, C. Fotakis, and A. Zanini, "Laser cleaning studies on wall paintings; a preliminary study of various laser cleaning regimes," to apper in *Proceedings of Lasers in the Conservation of Artworks, LACONA 6*.

[6] P. Pouli, D. C. Emmony, C. E. Madden, and I. Sutherland, "Analysis of the laser-induced reduction mechanisms of medieval pigments," *Applied Surface Science*, vol. 173, no. 3-4, pp. 252–261, 2001.

[7] M. Chappé, J. Hildehagen, K. Dickmann, and K. Bredol, "Laser irradiation of medieval pigments at IR, VIS and UV wavelengths," *Journal of Cultural Heritage*, vol. 4, supplement 1, pp. 264–270, 2003.

[8] V. Zafiropoulos, C. Balas, A. Manousaki, et al., "Yellowing effect and discoloration of pigments: experimental and theoretical studies," *Journal of Cultural Heritage*, vol. 4, supplement 1, pp. 249–256, 2003.

[9] M. Lassithiotaki, A. Athanassiou, D. Anglos, S. Georgiou, and C. Fotakis, "Photochemical effects in the UV laser ablation of polymers: implications for laser restoration of painted artworks," *Applied Physics A: Materials Science and Processing*, vol. 69, no. 3, pp. 363–367, 1999.

[10] G. Bounos, A. Athanassiou, D. Anglos, S. Gheorgiou, and C. Fotakis, "Product formation in the laser irradiation of doped poly(methyl methacrylate) at 248 nm: implications for chemical effects in UV ablation," *Journal of Physical Chemistry B*, vol. 108, no. 22, pp. 7052–7060, 2004.

[11] V. Zafiropulos, "Laser ablation in cleaning of artworks," in *Laser Cleaning*, B. Luk'yanchuk, Ed., chapter 8, pp. 343–392, World Scientific, Singapore, 2002.

[12] P. Pouli, G. Bounos, S. Georgiou, and C. Fotakis, "Femtosecond laser cleaning of painted artefacts; is this the way forward?" to appear in *Proceedings of Lasers in the Conservation of Artworks, LACONA 6*.

[13] P. Bracco, G. Lanterna, M. Matteini, et al., "Er: YAG laser: an innovative tool for controlled cleaning of old paintings: testing and evaluation," *Journal of Cultural Heritage*, vol. 4, supplement 1, pp. 202–208, 2003.

[14] M. P. Colombini, A. Andreotti, G. Lanterna, and M. Rizzi, "A novel approach for high selective micro-sampling of organic

painting materials by Er: YAG laser ablation," *Journal of Cultural Heritage*, vol. 4, supplement 1, pp. 355–361, 2003.

[15] I. Bonaduce and M. P. Colombini, "Characterisation of beeswax in works of art by gas chromatography—mass spectrometry and pyrolysis—gas chromatography—mass spectrometry procedures," *Journal of Chromatography A*, vol. 1028, no. 2, pp. 297–306, 2004.

[16] A. Andreotti, I. Bonaduce, M. P. Colombini, G. Gautier, F. Modugno, and E. Ribechini, "Combined GC/MS analytical procedure for the characterization of glycerolipid, waxy, resinous, and proteinaceous materials in a unique paint microsample," *Analytical Chemistry*, vol. 78, no. 13, pp. 4490–4500, 2006.

[17] D. Anglos, "Laser-induced breakdown spectroscopy in art and archaeology," *Applied Spectroscopy*, vol. 55, no. 6, pp. 186A–205A, 2001.

[18] D. Anglos, "Laser-Induced Breakdown Spectroscopy (LIBS): cultural heritage applications," in *Lasers in the Preservation of Cultural Heritage; Principles and Applications*, R. G. W. Brown and E. R. Pike, Eds., chapter 3, pp. 53–94, Taylor and Francis, New York, NY, USA, 2006.

Hindawi Publishing Corporation
Laser Chemistry
Volume 2006, Article ID 85324, 7 pages
doi:10.1155/2006/85324

Research Article

A Comprehensive Study for the Laser Cleaning of Corrosion Layers due to Environmental Pollution for Metal Objects of Cultural Value: Preliminary Studies on Artificially Corroded Coupons

A. Siatou,[1] D. Charalambous,[1] V. Argyropoulos,[1] and P. Pouli[2]

[1] *Department of Conservation of Antiquities and Works of Art, Technological Educational Institute of Athens, Ag. Spyridonos str., 122 10 Aigaleo, Greece*
[2] *Institute of Electronic Structure and Lasers, Foundation for Research and Technology-Hellas, P.O. Box 385, Heraklion, 71110 Crete, Greece*

Received 15 September 2006; Revised 13 December 2006; Accepted 14 December 2006

Recommended by Wolfgang Kautek

This paper is focused on the systematic investigation of the layer-by-layer removal of corrosion products on artificially corroded metal coupons aiming to introduce a methodology for the optimum laser cleaning approach of historical metal objects. Thus, it is very important to determine the chemical composition of the studied surfaces before and after irradiation. A series of laser cleaning studies has been performed on test coupons (reference and artificially corroded). Wavelength and pulse duration effects are investigated. Initial studies were focused on the use of infrared (1064 nm) and ultraviolet (355 nm and 248 nm) radiations of nanosecond (*ns*) pulse duration. Damage and removal threshold values were determined for the substrates and the corrosion layers, respectively. The irradiated surfaces are evaluated microscopically under the optical and the scanning electron microscope, while the mineralogical and chemical composition of the various layers is determined with X-ray diffraction and SEM-EDAX analyses, respectively. The results obtained are providing a comprehensive approach for understanding the main mechanisms that are significant in the different laser cleaning regimes, while the optimum cleaning methodologies for the studied materials are being established.

1. INTRODUCTION

The goal of this work is to find the best method for cleaning iron, copper, and silver alloy historical museum objects, which often require controlled cleaning of the surface from corrosion products without affecting the metal substrate [1, 2]. These museum objects often have decorative surface details such as engravings, granulation, inlays, gilding, niello, and so forth, but corrosion due to the atmosphere has tarnished or oxidized these surfaces [3]. For museum display, it is often necessary to remove tarnished or oxidized corrosion, while it is important not to affect either the metal substrate (minimal scratching) or the surface decoration. Such controlled mechanical cleaning is difficult with traditional hand or electrically powered tools commonly used by professional conservators-restorers (C-Rs). C-Rs are always in search for optimum methods of cleaning such fine surface detail in a controlled manner. Laser cleaning is able to provide an adequate cleaning of historical objects.

Nowadays lasers are used widely in analysis, monitoring, and conservation of cultural heritage objects (see [4]). Their unique properties are being responsible for high control, selectivity, minimal contact, and versatility; attributes that are essential for any conservation intervention on such valuable objects. In metal conservation, there have been plenty of studies aiming to use lasers for the removal of different corrosion layers, encrustations, and coatings from various metal surfaces with mixed results (see [5–8]). Still many issues are not yet resolved and thus the application of lasers in metal conservation is not universally accepted. Such issues include the preservation of the original surface, the understanding of the formation of unwanted laser-induced alteration layers, the final morphology of the irradiated surfaces, and the establishment of a methodology for the everyday

Table 1: The composition of the reference samples and the artificial corrosion layers.

Reference samples		Artificially corroded layers		
Type of metal	Composition (%)	Corrosion products	Color	Description
Iron alloy	Fe: 97.84 ± 0.15 C: 0.81 ± 0.14 Mn: 1.25 ± 0.04 Cr: 0.09 ± 0.03	Goethite, α-FeO(OH) and/or akageneite, β-FeO(OH)	Yellow-brown	Dark brown to orange corrosion spots evenly distributed on the surface
Copper alloy	Cu: 84.52 ± 0.75 Zn: 5.69 ± 0.21 Pb: 4.83 ± 0.54 Sn: 4.87 ± 0.25 (trace elements-average: 0.004 Mn, 0.056 Fe, 0.06 Ni, 0.002 Si)	Copper(II)hydroxide nitrate, $Cu_2NO_3(OH)_3$ Copper(II)oxide, CuO (cuprite)	Green Black	Uniform green corrosion layer At some places, a black or dark brown layer of oxide is visible underneath the green corrosion
Silver alloy	Ag: 95.62 ± 0.15 Cu: 4.19 ± 0.14 Mg: 0.19 ± 0.07	Silver(II)sulphide, Ag_2S	Black	Tarnishing (uniform black corrosion product at the entire surface)

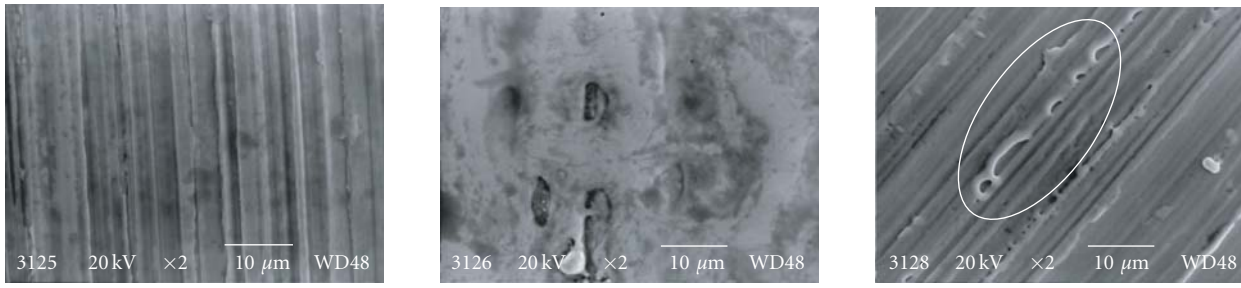

(a) (b) (c)

Figure 1: Determination of the damage threshold with Nd:YAG laser pulses at 1064 nm on iron reference sample. At high fluences (5.7 J/cm^2), the grinding lines of the reference surface are completely destroyed (melted), while at the damage threshold (0.9 J/cm^2) melting is limited and occurs only at the edges of the grinding lines. SEM photos under 2000 magnification, scale marker length: 10 μm.

implementation of laser cleaning in the conservation practice.

The above studies have been mainly investigating the effects that the radiation of various laser systems at different wavelengths with nanosecond (*ns*) pulse duration may cause. Recently, the use of ultrashort laser pulses to clean metal surfaces was reported with very interesting results [9]. Such lasers may be a viable solution to many of the above mentioned unclear issues in metal conservation as they offer unique advantages in comparison to the *ns* laser systems; such as minimal thermally and chemically induced alterations, higher spatial confinement, control, and so forth [10].

2. EXPERIMENT

This work aims to investigate in a systematic way how the wavelength and pulse duration may affect the laser-assisted removal of various corrosion layers formed on historical metal objects exposed to urban environment. Artificially corroded samples of iron, copper, and silver alloys are being used for the evaluation of the different laser cleaning regimes and methodologies. Damage and removal threshold values are determined both for the metal substrate and the corrosion layers, while physicochemical analysis on the irradiated surfaces aims to detect any laser-induced alterations. The specific objective is to determine the fluence values adequate to remove corrosion products from the different metal substrates, in a controlled manner, without altering the object's original surface or damaging the metal substrate.

The project's plan includes the study of both infrared (1064 nm) and ultraviolet (355 nm and 248 nm) laser radiations at various pulse durations (microsecond, μs, nanosecond, *ns*, and picosecond, *ps*). The initial results presented herein were focused on the study of all the wavelengths (1064 nm, 355 nm, and 248 nm) in the *ns* regime.

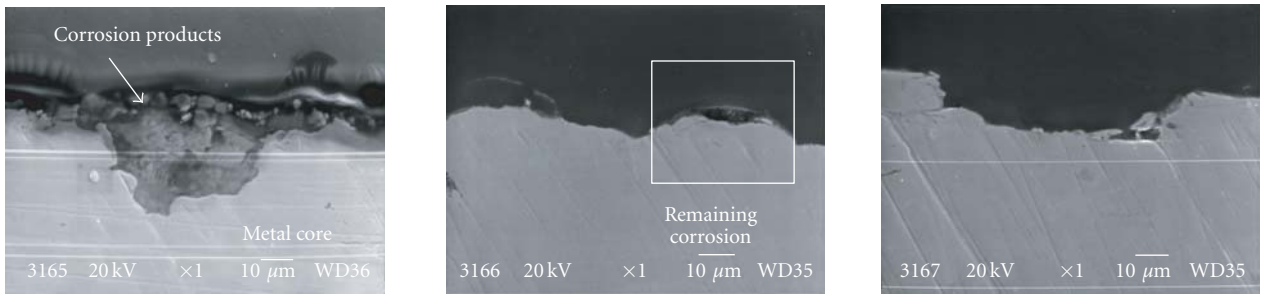

(a) (b) (c)

Figure 2: Cross-sections of the artificially corroded iron sample: (a) the corrosion products are formed both inwards and outwards the metal core, (b) mechanical cleaning may leave traces of corrosion, and (c) laser cleaning at the determined ablation threshold (0.4 J/cm^2) removes efficiently all the corrosion without affecting the metal substrate. SEM photos under 2000 magnification, scale marker length: 10 μm.

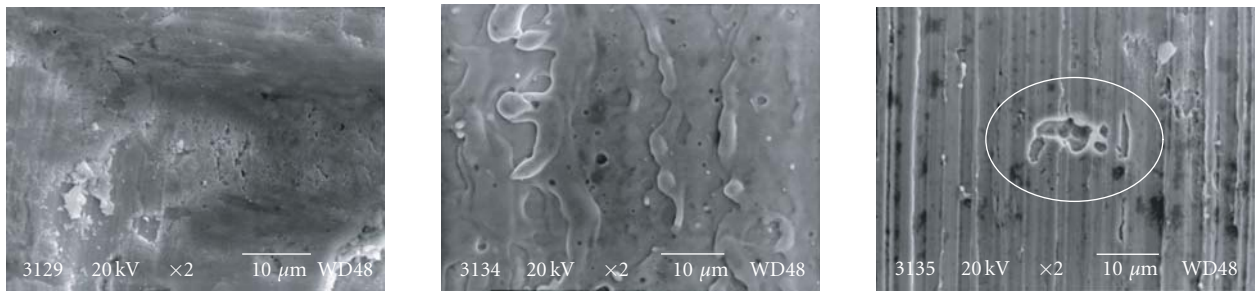

(a) (b) (c)

Figure 3: Determination of the ablation threshold with Nd:YAG laser pulses at 1064 nm on artificial corrosion on iron (a). At high fluences (5.7 J/cm^2), the grinding lines of the reference surface are completely destroyed (melted) (b), while at the damage threshold (0.4 J/cm^2) melting is limited (c) and the corrosion is efficiently removed. SEM photos under 2000 magnification, scale marker length: 10 μm.

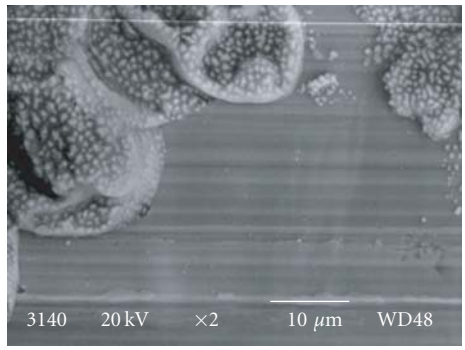

Figure 4: Ultraviolet pulses (KrF excimer laser at 248 nm) could not remove the corrosion layer, while further alteration of the corroded surfaces occurs. SEM photos under 2000 magnification, scale marker length: 10 μm.

Due to the nature of the studied corrosion layers (pulverant and/or randomly distributed corrosion spots) and substrates (metal surfaces) it was not possible to establish in a systematic way the amount of ablated material per pulse for a series of different fluence values and thus determine from the corresponding graph the ablation threshold for each studied material [11]. Instead, the determination of the damage threshold on the metal substrate and the ablation threshold of the artificial corrosion layer was based on the presence of any melting or discoloration feature observed on the studied surface upon its irradiation with a single laser pulse as a function of increasing fluence values. Figure 1 shows a series of SEM photos indicating the determination process of the damage threshold on reference iron coupon. The grinding lines of the reference surface (see Figure 1(a)) are completely destroyed upon irradiation with Nd:YAG laser pulses at 1064 nm at relatively high fluence values (5.7 J/cm^2), where intense melting occurs. Instead, at 0.9 J/cm^2, melting is limited and observed only at the edges of the grinding lines, and thus this fluence value is considered as the ablation threshold of the iron core metal.

3. MATERIALS AND METHODS

3.1. Samples

Test samples representing the composition and the corrosion of historical metal artifacts were prepared. The three types of metal substrates studied were (a) iron (low carbon steel), (b)

Table 2: The humid-dry cycles used to create corrosion on iron.

Time (hours)	Temperature (°C)	Relative humidity (%)
24	30	100
24	Variable 25–30	Variable 50–60
24	30	100

Table 3: The parameters of the employed laser systems.

Laser system	Type	Wavelength (nm)	Pulse duration
BMI series 5022 DNS 10	Q-switched Nd:YAG	1064	5–7 ns
		355	5–7 ns
TUI model Braggstar 200	KrF excimer	248	10 ns

copper (cast bronze), and (c) 950° silver alloys. The detailed information on the composition of the reference surfaces is presented in Table 1.

Artificial corrosion was then produced on the metal surface using the following different methodologies according to the substrate:

(A) iron alloy coupons were corroded in a "voetsch industrietechnik (VC 4034)" climatic chamber using humid-dry cycles. The methodology used was based on the artificial corrosion of similar coupons prepared by Heritage Malta[1] and are given in Table 2. This type of artificial corrosion creates localized corrosion spots randomly distributed on the iron surface;

(B) bronze coupons were corroded by direct application on the surface of a $Cu(NO_3)_2 + NH_4OH$ solution, as suggested in [12]. A cold solution of $Cu(NO_3)_2 + NH_4OH$ was applied by brushing directly onto the heated metal surface at several time intervals. The bronze coupons were then dried in room condition. The corroded surface is uniformly covered with a layer of green corrosion products (copper(II)hydroxide nitrate);

(C) silver exposed to urban or indoor environment, as most historical objects are, tarnishes due to the sulfur containing atmosphere, forming a black layer of silver sulfide on the objects surface [3, 13]. For the artificial corrosion of silver, we created an atmosphere containing sulfur ions in a closed chamber by acidifying sodium sulfide (Na_2S). After one-day exposure, an evenly distributed black layer was created on the silver surface.

The aim is the total removal of the corrosion products on iron and silver and the removal of the green corrosion layer on bronze, without any alteration (both in color and surface morphology) to the underlying metal surface.

[1] Heritage Malta (HM), Old Royal Naval Hospital, Bighi,CSP 12, Kalkara, Malta.

3.2. Laser irradiation

Irradiation studies were carried out using the following laser systems:

(i) A modified Q-switched Nd:YAG laser (BMI, series 5022 DNS 10) with pulse duration in the range of 5–7 ns and maximum repetition rate of 10 Hz. The system emits both the fundamental wavelength (at 1064 nm) and its third harmonic (at 355 nm) at maximum energy outputs of 1000 mJ and 300 mJ, respectively.

(ii) A compact excimer laser (TUI laser, Braggstar 200 model) operating at 248 nm (KrF). The system produces pulses (10 ns) with maximum energy of 16 mJ.

All laser beams were focused by means of a fused silica plano-convex lens ($f = +100$ mm) on the sample surface. Optical attenuators introduced in the beam path in various angles were employed to adjust the energy output of each laser beam. The parameters of the employed systems are presented in Table 3.

The complementary application of wetting solutions (water and/or ethanol) was also considered. As there was no obvious difference in the behavior of the two wetting agents, ethanol was chosen because it is inert with the metal surface while water may cause further corrosion to the metal, that is, flash rusting on iron. Its application on the corroded bronze samples was found to enhance the cleaning process and remove the corrosion products in a homogeneous way without discoloration phenomena. On the other hand, no obvious difference was observed on iron samples while it was believed to cause the formation of bluish coloration on the surface of silver.

3.3. Analytical techniques

The surface morphology of the irradiated samples was studied using a stereomicroscope (SM), while specially prepared samples embedded in resin which were examined under reflected polarized light by means of a Nikon ECLIPSE ME

Table 4: Laser cleaning tests on iron.

Laser system	Wavelength λ(nm)	Damage threshold for the metal substrate (J/cm^2)	Ablation threshold for the corrosion products (J/cm^2)	Comments
Nd:YAG	1064	0.90	0.35	Suggested cleaning at 0.6–0.8 J/cm^2
Nd:YAG	355	0.4	0.2	The corrosion products are altered when many pulses are applied
KrF excimer	248	The metal is not affected at the studied fluences (0.1–0.5 J/cm^2)		

Table 5: Laser cleaning tests on copper.

Laser system	Wavelength λ(nm)	Damage threshold for the metal substrate (J/cm^2)	Ablation threshold for the green corrosion layer (J/cm^2)	Comments
Nd:YAG	1064	0.4	0.3-0.4	Suggested cleaning at 0.3 J/cm^2
Nd:YAG	355	0.2	0.2	Insufficient removal/discoloration of corrosion products
KrF excimer	248	The metal is not affected at the studied fluences (0.1–0.5 J/cm^2)		

600 microscope (OM) equipped with a HITACHI KP-CS 71 digital camera. The cross-sections were studied in various magnifications (5x, 10x, 20x) aiming to determine the interface between the corrosion layer and the authentic surface and thus deciding the cleaning limit. A JEOL JSM-840 scanning electron microscope (SEM) was employed to study any laser induced alterations to the original surface.

X-ray diffraction analysis (XRD) was used to identify the chemical composition of the various corrosion layers as well as possible changes in the chemistry of the irradiated surfaces. Analysis was performed by a RIGAKU, RINT 2000 series powder diffractometer, using Cu Ka1 radiation (1,5405 Å). Measurements were carried out in the range $3^\circ < 2 < 70^\circ$ with a step of 0.02°.

4. RESULTS AND DISCUSSION

4.1. Iron

Figure 2 shows a series of cross-sections on artificially corroded iron: Figure 2(a) shows the formation of corrosion spots both inwards and outwards the original surface, Figure 2(b) shows their insufficient removal by mechanical means (traces of corrosion products are still left on the surface), and Figure 2(c) shows their total removal by laser application (there are no traces of corrosion products left).

The results of the irradiation tests are summarized in Table 4. The Q-switched Nd:YAG laser system emitting pulses of ns pulse duration at 1064 nm was found to be able to remove corrosion products of iron in-depth without affecting the metal core. The selection of the ablation threshold on the corrosion is presented in Figure 3.

On the opposite, ultraviolet radiation both at 355 nm and 248 nm was insufficient to remove the corrosion spots while causing further alteration (blackening) (see Figure 4). The chemistry of the blackened surfaces is under investigation.

4.2. Bronze

Two distinctive corrosion layers are observed on the bronze coupons: a thick green corrosion layer ($Cu_2NO_3(OH)_3$) that uniformly covers the entire surface (Figure 5(a)) and under this a dark oxide layer (CuO). Considering that this dark oxide layer acts as a barrier that protects the underlying metal surface from further corrosion [1] it was decided to remove only the green corrosion layer while keeping the oxide layer intact.

The results of the irradiation tests are summarized in Table 5. Similarly to the iron case, the infrared radiation at 1064 nm emitted from the Nd:YAG laser at fluences in the range of 0.3-0.4 J/cm^2 was able to efficiently remove the green corrosion layer without any alteration to the underlying oxide layer (see Figure 5(b)). It was also shown that the application of a thin layer of ethanol enhances the cleaning process.

On the other hand, irradiation tests with ultraviolet wavelengths resulted in an apparent discoloration (towards yellow) of the green corrosion layer (see Figure 5(c)). The chemistry of the yellow-discolored layers is under investigation.

4.3. Silver

The silver sulfide (Ag_2S) layer formed on the coupons surface is very adherent and thus difficult to remove. Our aim is to reach the original surface and expose the shining silver surface. However, this task is difficult since silver is very sensitive to laser irradiation causing melting on the surface with all wavelengths.

Table 6: Laser cleaning tests on silver.

Laser system	Wavelength λ(nm)	Damage threshold for the metal substrate (J/cm^2)	Ablation threshold for the corrosion layer (J/cm^2)	Comments
Nd:YAG	1064	1.5	n/a	Melting of the corroded metal occurs even at 0.1 J/cm^2
Nd:YAG	355	0.55	0.20	Removal of a superficial corrosion layer, discoloration (whitening) of the surface
KrF excimer	248	The metal is not affected at the studied fluences 0.1–0.5 J/cm^2	0.25	Removal of a superficial corrosion layer without any damage to the substrate

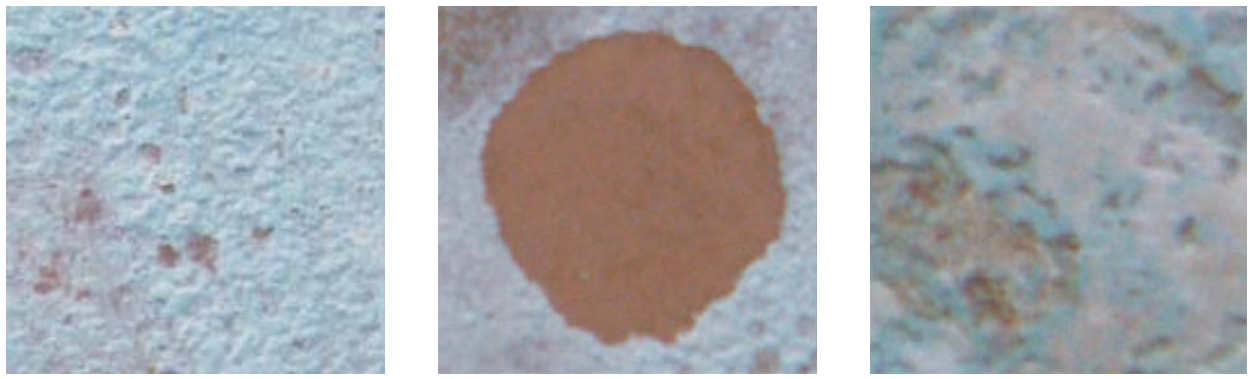

(a) (b) (c)

Figure 5: (a) Uniform formation of green corrosion products on bronze samples, (b) removal of the green corrosion layer at 1064 nm, fluence value equal to the threshold (0.3 J/cm^2), (c) discoloration (yellowing) of the green corrosion product at 355 nm (0.2 J/cm^2). Horizontal dimension: 5 mm.

The best case scenario is the removal of a superficial corrosion layer using UV irradiation. This can be achieved with a KrF excimer laser emitting pulses of *ns* duration at 248 nm, since at 355 nm whitening appears on the surface and the metal becomes dull. The results of the irradiation tests on the silver samples are presented in Table 6.

4.4. Overall comments/discussion

From the above-shown preliminary results, focused on the study of infrared and ultraviolet wavelengths (1064 nm, 355 nm, and 248 nm) in the *ns* regime, it is clear that many issues still have to be answered. Infrared radiation at 1064 nm with *ns* pulse duration emitted from a Q-switched Nd:YAG laser was found to be able to remove artificially grown corrosion spots on iron and relatively thin corrosion products from bronze coupons with quite satisfactory results. Still their application in real objects with thicker, harder, and more inhomogeneous corrosion layers should be considered. Similarly, ultraviolet laser pulses at 248 nm emitted from a KrF excimer laser were found to be able to remove tarnish from silver quite satisfactory, still the final surface lacks its initial glossy appearance. Studies are now performed with laser systems with shorter pulse widths and the initial results are very satisfactory. The thorough and comparative evaluation of these studies may answer many of the unsolved issues in metal conservation and will indicate the appropriate laser parameters for the cleaning of each individual problem.

ACKNOWLEDGMENTS

This project was funded by the European Social Fund and National Resources-(EPEAEK II) ARCHIMEDES, entitled "The application of new technologies for the cleaning of archaeological and historical metal objects; investigation of the possibility of applying laser technology and electrolytic methods." The authors would like to thank the Greek Center of Metal Research (ΕΛ.Κ.Ε.ΜΕ) for the artificial ageing of the iron alloy coupons.

REFERENCES

[1] J. M. Cronyn, *The Elements of Archaeological Conservation*, Routledge, Taylor and Francis, London, UK, 1990, edition 2001.

[2] R. Bertholon and C. Relier, "Les métaux archéologiques," in *La conservation en archéologie. Méthodes et pratique de la*

conservation-restauration des vestiges archéologiques, Masson, Paris, France, 1990.

[3] L. Selwyn, *Metals and Corrosion: A Handbook for the Conservation Professionals*, Canadian Conservation Institute, Ottawa, Canada, 2004.

[4] C. Fotakis, D. Anglos, V. Zafiropulos, S. Georgiou, and V. Tornari, *Lasers in the Preservation of Cultural Heritage: Principles and Applications*, Edited by R. G. W. Brown and E. R. Pike, Taylor and Francis, New York, NY, USA, 2006.

[5] C. A. Cottam and D. C. Emmony, "TEA-CO_2 laser surface processing of corroded metals," *Corrosion Science*, vol. 41, no. 8, pp. 1529–1538, 1999.

[6] P. Mottner, G. Wiedemann, G. Haber, W. Conrad, and A. Gervais, "Laser cleaning of metal surface-laboratory investigations," in *Proceedings of the International Conference LACONA V Lasers in the Conservation of Artworks*, vol. 100 of *Springer Proceedings in Physics*, pp. 79–86, Osnabrueck, Germany, September 2005.

[7] Y. Koh and I. Sárady, "Cleaning of corroded iron artefacts using pulsed TEA CO_2- and Nd:YAG-lasers," *Journal of Cultural Heritage*, vol. 4, supplement 1, pp. 129–133, 2003.

[8] R. Pini, S. Siano, R. Salimbeni, M. Pasquinucci, and M. Miccio, "Tests of laser cleaning on archeological metal artefacts," *Journal of Cultural Heritage*, vol. 1, supplement 1, pp. S129–S137, 2000.

[9] T. Burmester, M. Meier, H. Haferkamp, S. Barcikowski, J. Bunte, and A. Ostendorf, "Femtosecond laser cleaning of metallic cultural heritage and antique works," in *Proceedings of the International Conference LACONA V Lasers in the Conservation of Artworks*, vol. 100 of *Springer Proceedings in Physics*, pp. 61–69, Osnabrueck, Germany, September 2005.

[10] D. Bäuerle, *Laser Processing and Chemistry*, Springer, Berlin, Germany, 2000.

[11] S. Georgiou, "Overview of laser processing and cleaning methods," in *Lasers in the Preservation of Cultural Heritage: Principles and Applications*, chapter 6, Taylor and Francis, New York, NY, USA, 2006.

[12] R. Hughes and M. Rowe, *The Colouring Bronzing and Patination of Metals*, Thames and Hudson, London, UK, 1991.

[13] I. Singh, P. Sabita, and V. A. Altekar, "Silver tarnishing and its prevention—a review," *Anti-Corrosion Methods and Materials*, vol. 30, no. 7, pp. 4–8, 1983.

Hindawi Publishing Corporation
Laser Chemistry
Volume 2006, Article ID 90279, 9 pages
doi:10.1155/2006/90279

Review Article

Laser Cleaning of Easel Paintings: An Overview

Rui Bordalo,[1] Paulo J. Morais,[1] Helena Gouveia,[1] and Christina Young[2]

[1] *Instituto de Soldadura e Qualidade, 2740 120 Porto Salvo, Portugal*
[2] *Courtauld Institute of Art, London WC2R ORN, UK*

Received 22 September 2006; Revised 30 November 2006; Accepted 30 November 2006

Recommended by Marta Castillejo

The application of laser cleaning to paintings is relatively recent despite its use on stone-based materials for over 30 years. The cleaning of paintings is of high importance, because it is the least reversible invasive intervention, as well as the most usual of all conservation treatments. Paintings are multilayer system of heterogeneous nature, often very sensitive and inherent difficult to clean. Being a noncontact method, laser cleaning has advantages compared to alternative techniques. Over the last decade, there have been important research studies and advances. However, they are far from sufficient to study the effects on painting materials and to establish the best parameters for each material under investigation. This paper presents a historical overview of the application of laser technology to the cleaning of paintings giving special emphasis on the research of the last decade. An overview of the current research into the interaction between the radiation and the different painting materials (varnish, pigments, and medium) is also given. The pigment's mechanisms of discoloration and the presence of media as a variable factor in the discoloration of pigments are discussed.

1. THE LASER IN PAINTINGS CONSERVATION

The most widely used traditional techniques employ mechanical or chemical cleaning. The use of solvents applied over the surface may affect the pigments and medium in a nondesirable and nonreversible way because it is difficult to control penetration into the paint layers [1]. Gel formulations to control penetration can lead to problems of clearance from the surface. The integrity of the artwork can be also jeopardised because many layers to be removed are partially or totally insoluble in solvents. Mechanical action typically using a scalpel is another option but it presents an obvious danger by its physical action over the layers which can lead to the damage of the texture. The control of these techniques is in part dependant on the skill of the conservator and there is a border line between optimum cleaning and overcleaning.

Laser technology has great potential in the development of safer procedures for conservation because of its controllability and reproducibility. The application of laser technology to the paintings conservation field started in the earlier 1990s. This technology has always attracted much interest as it became the first technique that did not interact physically with the artwork, and thus was in accordance with the conservation principle of "minimum intervention." Lasers can remove layers that conventional techniques cannot remove safely [2]. For example, in the case of organic polymeric materials, excimer lasers are capable of removing layers with the resolution of 0.1 to 2.0 μm per pulse [3]. However, laser cleaning is an intrusive technique and should be used with good control methodologies. In general, every laser is effective, selective, and safe when used within certain parameters. For painted artworks, laser cleaning is one of the most delicate applications and requires a thorough study of the laser induced thermal, photochemical, and photomechanical effects in order to avoid damage of the paint layer.

1.1. Types of laser used in laser cleaning of paintings

Excimer laser

The term excimer is short for *excited dimer* and refers to the chemical medium of the laser: rare gas-halide mixtures. The excimer laser emits primarily in the UV region, at $\lambda = 193$ nm (ArF), $\lambda = 248$ nm (KrF), $\lambda = 308$ nm (XeCl), and $\lambda = 351$ nm (XeF). Excimer lasers are very effective due to the high absorptivity of materials characteristically employed in paintings causing minimal light penetration on the layers. Research has shown that 248 nm is the most promising wavelength for varnish and over paint layer removal [4–6].

The UV is strongly absorbed by the functional groups of the varnish and its degradation products.

Nd: YAG laser

Nd: YAG is the standard laser system for stone cleaning applications. Nd:YAG is an acronym for *neodymium-doped: yttrium aluminium garnet* (Nd: $Y_3Al_5O_{12}$) and emits typically on the near infrared region (NIR) at $\lambda = 1064\,\text{nm}$ (ω). More recently, this type of lasers have been developed to emit radiation at $\lambda = 532\,\text{nm}$ (2ω), $\lambda = 355\,\text{nm}$ (3ω), $\lambda = 266\,\text{nm}$ (4ω), and $\lambda = 213\,\text{nm}$ (5ω) multiples of the fundamental wavelength [7]. The infrared radiation tends to induce photothermal effects, capable of breaking bonds of inorganic materials. Although it is less efficient with organic materials because its energy is insufficient to break the covalent bonds, this type of lasers can lead to excellent results on the cleaning of painted artworks [8].

Er: YAG laser

This is the most recent laser tested for the cleaning of paints with successful results [9]. Er: YAG is an acronym for *erbium-doped: yttrium-aluminium-garnet* (Er: $Y_3Al_5O_{12}$). It generates a wavelength of 2.94 μm in the midinfrared region which is highly absorbed by OH bonds (in aqueous liquids). Consequently, the laser beam is quickly absorbed achieving very superficial ablation depths. Theoretically, the efficiency of the laser ablation is directly proportional to the amount of OH groups present in the materials. These OH bonds, when not present on the original material, can be obtained by the addition of hydroxylated liquids, which can also help to limit the radiation and heat penetration.

1.2. Historical overview into laser cleaning of paintings

Following their pioneering work with laser cleaning of stone, Asmus et al. studied the possibility of using laser technology to remove lime layers to uncover a mural painting by Leonardo da Vinci [10]. Although not published, the first paper reported about the potential application of the laser technology to the cleaning of easel paintings dates from 1981 [11]. It consisted in a preliminary study of the removal of varnish and dirt using two lasers working at 308 nm. Several undesirable consequences thought to be caused by the irradiation, nevertheless it was concluded that there was potential for laser technology with the need of further research. In 1986, some cleaning of mural paintings was attempted [12]. It was only in 1992 that the first paper was published reporting a scientific study about the use of excimer laser on easel paintings [13]. The investigation was based on the applicability of UV radiation on the ablation of varnishes and other deposits from painted surfaces. It was stated that the composition of both paint layer and dirt or over paint layers were of the most importance in order to determine the best laser parameters. It was also advanced, for the first time, the necessity to develop a database for a generalisation of the cleaning process due to the direct dependence of the laser parameters on the surface layer characteristics.

Since 1993, the Foundation for Research and Technology Hellas (FORTH) has conducted studies about laser development in order to assess their potentialities and limits on artwork cleaning applications. These studies included laser cleaning of surface layers and over paint, analysis of medium and pigments, imaging techniques for structural diagnostics, and authentication techniques.

In 1995, the first edition of the international workshop LACONA (lasers in the conservation of artworks) was organised to discuss the emergent application of laser technology to conservation. Its success turned this workshop into an international biannual conference in this field of research. Since then, lasers became better known to conservators and it consolidated the interest by the establishment of several research groups in Europe with several different material interests.

Cooper [14] published the first book entirely dedicated to laser cleaning of artworks in general. It includes an explanation of the laser principles and of the laser types. Despite the fact of being focused on sculpture on its several supports, mainly stone and metal, it includes a chapter especially dedicated to the developing laser cleaning of paintings [4]. Since then, and as the best of the author's knowledge, there was no newer published review of the literature concerning the laser application to paintings.

So far the only equipment built specifically for laser cleaning of paintings is a excimer laser, developed by a European consortium under an EU project between 1999 and 2001, which was one of the most relevant and comprehensive studies ever made [15, 16]. However, portable and flexible lasers for the cleaning of painted artworks are still not commercially available to the restorers. The main focus of the EU research project was the interaction of UV radiation on varnish and pigments in egg tempera medium and on the molecular changes to these materials by the UV radiation was investigated.

Over the last decade, several studies have been focused on the effect of UV radiation and also of infrared light and other regions of the electromagnetic spectrum on pigments and other paint materials [4, 7, 8, 17–21].

2. THE LASER RADIATION EFFECT IN PAINTING MATERIALS

A representative painting consists of a support or substrate (canvas, wood, or stone), a ground layer and several paint layers, each one of approximately 20 to 50 μm thickness, deposited over the former. The paint layer is a mixture of pigments and a medium to aggregate the pigments. Traditionally, the media is either egg tempera or oil (commonly linseed, walnut, and poppyseed). Furthermore, varnish used to be applied over the painting to serve as a protective layer and to provide colour saturation. A typical layer of varnish is about 50 to 80 μm thickness. During the aging process, two processes occur at the same time: three-dimension polymerisation and natural oxidation [22].

Several paint materials samples have been prepared by different authors to be tested by laser radiation, which range from pigments compressed into pellets to real paintings. In order to proceed with the cleaning, the laser radiation is fired into the layer to ablate, and once the protection layer has been removed (if present) the radiation will penetrate the paint layer if not prevented or controlled. This penetration into the paint layer can induce discoloration of the paint depending on the pigment material affected by the laser radiation. Discoloration of pigments is a serious problem; it can affect polychromies after laser irradiation depending on factors such as the nature of the material and the type and intensity of the laser used. It was suggested that photochemical modifications could occur from the radicals, and ions originated from the ablation could produce photo-oxidation products [23].

In order to prevent pigment discoloration, it has been proposed in [6, 24] that a thin layer of varnish should be left to avoid the radiation penetration into the paint layer. The study included several kinds of varnishes normally used and the energy transmitted by the laser was measured in relation to the ablation depth with an excimer laser at 308 nm. It was verified that fresh varnish is more transparent to UV light than older varnish. It was also suggested in the same study that for fresh varnish, after the first laser incidence, the surface suffers some modification and changes its absorption properties; the second incidence is more strongly absorbed and the material is ablated; furthermore, shots will irradiate fresh varnish. It was shown that freshly prepared varnish could not be representative of artificially or naturally aged varnish because of its different ablation/absorption behaviour.

On direct irradiation over paint material without protective varnish, several oxidation products were found and are explained due to a photodissociation of the pigments and that the radicals reacts with the oxygen present on the atmosphere or with the medium [25]. Although some studies suggested that the mechanism responsible for the discoloration of pigments was oxidation [26], latter studies suggested reduction as responsible for the blackening [27]. This process could be explained by a punctual scarcity of oxygen caused by the dense plasma which could lead to some compound's decomposition. Oxidation was also suggested as possible to occur after the irradiation is over and the heat dispersed.

2.1. The laser radiation effect on varnishes

Chemically, varnishes are normally tetracyclic or pentacyclic organic compounds with carbonyl or hydroxyl groups [22]. The UV radiation is strongly absorbed by the several varnish functional groups and its degradation products. Thus, general studies of UV laser effects on polymers/organic compounds have been used as starting point to the study of varnishes. Following these studies, Georgiou et al. [28] states that photochemical effects could be expected for the ions and radicals produced by the ablation process to be reactive and that photooxidation could take place during irradiation or in the long term. The same authors found chemical differences when comparing dammar and mastic varnishes under irradiation of 248 nm wavelength. The fact that dammar is characteristically a much weaker absorber to 248 nm than mastic seems to justify the related differences. It was also stated that depolymerization or cross-linking could occur. On a preliminary work, performed by Madden et al. [29], a set of 35 different materials, including varnishes, was studied. It was demonstrated that the reaction of both polymers and oligomers to laser radiation depends on their chemistry and preparation.

A study performed by Zafiropulos et al. [26] made some important findings on varnish irradiation. It was experimentally demonstrated that when the fluence increases the efficiency also increases until a maximum is achieved [15, 26]. This point is referred as the saturation point in the light absorption on the most superficial layers; at higher fluence the irradiation is transformed into thermal energy. Other important work on excimer laser ablation of varnishes (dammar, mastic, and copal oil) was performed by Theodorakopoulos [30]. His study focused on the organic chemistry of the aged coatings as a function of depth. It was demonstrated that the removal of 10–15 μm from the degraded surface layer of varnish causes no damage to the remaining film as was proven by the decreasing gradients in degrees of condensation, oxidation, and polarity [30].

2.2. Laser radiation effect on binding media

Although the interaction between traditional binding media and laser radiation has been the focus of some research, the amount of this work when compared with the research of pigment discoloration is small. The involved mechanism on the deterioration of the medium by laser radiation has not yet been full understood even though several theories have been proposed.

2.2.1. Laser radiation effect on egg tempera

The interaction of the radiation on egg tempera has been investigated by Teule et al. [17]. Chemical changes or physical effects such as discoloration have been observed when using an excimer-based laser ($\lambda = 248$ nm). The main problem found was the oxidation of the binding media although it was limited to the surface of the samples (<2 μm). The same conclusion was reached by Castillejo et al. [31] during a laser cleaning tests with KrF laser. The oxidation seems to be influenced by the presence of certain inorganic pigments. The analyses showed that unpigmented egg tempera samples after irradiation presented a low degree of chemical change. Comparison of the results between the organic and the inorganic samples on the same binding medium showed that in the presence of inorganic pigments there are alterations of the pigment and degradation and charring of the binding medium. The authors concluded that this can be attributed to oxidation and cross-link phenomena.

2.2.2. Laser radiation effect on oil

In preliminary work, Schnell et al. [32] prepared linseed oil samples containing different pigments. The authors irradiated samples containing pigments with low discoloration threshold with radiation at 1064 nm wavelength using $\sim$0.6 J/cm^2. The reaction products were analysed by nuclear magnetic resonance (NMR) spectroscopy. Glycerin, alkenes, alkanes, and aldehydes were detected in the gas phase and other nonidentified low-molecular products. It was suggest that the emitted gases were cooled down very fast due to adiabatic expansion induced by short pulses and therefore oxidation was prevented by the reducing atmosphere [32].

Bracco et al. [18] investigated the use of Er: YAG lasers on mock-up paintings. The gas chromatography-mass spectrometry (GC-MS) analysis revealed that between the ablated material and the untreated surfaces only minor alterations in the composition were noticeable. These alterations consisted basically in the decrease of the oleic acid content on the resinous and oil-resinous varnishes and a slight decrease of the hydroxylic components of the ablated materials. Fourier transform infrared spectroscopy (FTIR) analysis showed no change of composition before and after the irradiation, except some minor variations in the amounts of several polar substances and some small wavelength shifts of the absorption bands of esters from the ablated materials from resin and oil-resin varnishes [18, 33]. Zafiropulos et al. [26] looked at the possibility of cross-linking of oil. The authors found that after a successful partial removal of a varnish there was cross-linking of the underlying oil medium.

2.2.3. Laser radiation effect on acrylics

Acrylics are synthetic resins made by polymerising esters of acrylic acids. Real et al. [34] performed tests to remove over paints and other materials from acrylic substrates with 248 nm excimer laser, although his study did not cover the laser effect on acrylic paint. Using a fluence of 1.3 J/cm^2, the over paints were removed and also some of the acrylic layer, inducing a greyish discoloration. With a fluence of 0.21 J/cm^2, the over paints were removed but the acrylic layer appeared undamaged under the microscope.

2.3. Laser radiation effect on the pigments

The first study to consider the effect of laser radiation (Nd: YAG, excimer and dye) on pigments was done by Shekede [35–37]. It was essentially a qualitative study focused on the visual effects and how they were assessed. It was found that the removal of a coating produced changes on the underlying layer independently of the media type, coating material, or wavelength used. Generally, the studies made up to 1999 were not able to determine the physical/chemical changes that pigment discoloration introduced. Since then, some studies have been performed to assess this issue although a detailed comprehension of the discoloration has not been yet achieved. Some authors attribute pigment discoloration to chemical decomposition, phase changes [27, 38–40], or physical effects, such as melting [32].

Recent research using X-ray diffraction (XRD) on pigments attempted to understand pigment discoloration process [39]. The results showed crystalline phase and chemical composition changes and the authors suggested a structural modification within the volume of the pigment's particles near to the ablation threshold (i.e., minimum energy required for ablation). Pouli and Emmony [20] studied the reaction of some pigments to Nd: YAG radiation by the application of X-ray photoelectron spectroscopy (XPS) and Auger electron spectroscopy (AES) to the altered surfaces and XRD to irradiated pigment pellets and compared the obtained results with heated samples. XRD curves did not yield new peaks which were explained by the amorphous nature of the reaction products or by the superficial alteration. Although there was discoloration of the pigment, the surface analysis showed similar results before and after laser irradiation [20].

It is known that the presence of a medium does affect the degree of discoloration of some pigments [19, 41]. The influence of the binding media nature on the discoloration of the paint layer is clearly evident in a study performed by Gordon Sobott et al. [38] which prepared samples of several pigments in different binding media. It has also been reported that binders are less sensitive than inorganic pigments when irradiated with 1064 nm radiation [32].

In a recent study, Chappé et al. [8] compared the influence of several laser wavelengths on ten inorganic and one organic pigments. It was concluded that in general the highest discoloration threshold occurs at 1064 nm. Nevertheless, it was also found that the samples show as well a high sensitivity to laser radiation at 355 nm and 266 nm. It was also concluded that the chemical reaction which by the pigments suffer the discoloration was due to laser induced heat. Sansonetti and Realini [19] studied Nd: YAG laser irradiation over samples prepared with six inorganic pigments and with linseed oil and gypsum as binders. It was observed that for the pigmented oil samples the lower fluence (0.1 J/cm^2) preserved the surface morphology while at the intermediate fluence (1 J/cm^2) some variation was observed and at the higher fluence (3 J/cm^2) the layers were ablated. Regarding the chromatic analysis, a change was observed for the low and intermediate fluences, although the low fluence only produced minor variation in lightness ($\Delta L < 1$). At the intermediate fluence, chromatic changes were always produced according the total colour variation ($\Delta E > 5$). It was shown by the authors that the chromatic changes are not directly proportional to the used fluences.

As confirmed by several sources [17], the intensity of fluorescence emission is considerably decreased after UV laser irradiation, which can be evidence of the binding medium degradation or due to the presence of impurities. The degradation of the medium may induce an alteration to the optical properties and contribute to pigment discoloration.

2.3.1. Lead pigments

Lead white ($2PbCO_3 \cdot Pb(OH)_2$)

Its darkening upon laser radiation has been attributed to the formation of plattnerite (PbO_2) as an alteration product

resulting from oxidation [42, 43], but more recently it has been attributed also to reduction phenomena [40]. Pouli and Emmony [20] demonstrated that under laser irradiation the pigment suffered only from a temporary blackening. The reduction assumption is supported by AES analysis which indicated the presence of elemental carbon after laser incidence [20] and by XPS analysis which revealed an increase of the amount of lead relatively to oxygen [40]. The temporary blackening [27] could be explained by the exposure to the air humidity and to CO_2 which induces the formation of carbonate-hydroxide complex above the PbO surface [27, 40, 44]. A study by Cooper et al. [41] suggested that presence of binding media affects the discoloration degree of the pigment, which was attributed to the conversion of basic lead carbonate into elemental lead on the surface.

Red lead or minium (Pb_3O_4)

This pigment is naturally unstable inducing a blackening mainly due to the transformation into Plattnerite (PbO_2) or galena (PbS) [45, 46]. Pouli and Emmony [20] performed heat tests of red lead, which showed to transform into yellow lead. As similarly with lead white, the incidence of laser radiation induced temporary darkening. Chappé et al. [8] refers that under laser irradiation the colour change occurs first to metallic-grey and with increasing energy density it changes back into orange probably due to a photochemical interaction. Like lead white, it has been found that graphite (C) and pure metal (Pb) [34] regained its original colour over one week. Gordon Sobott et al. [38] studied the pigment behaviour with different binding media and wavelengths and it was concluded that the discoloration could be attributed to the formation of lead oxides.

Yellow lead or massicot (PbO)

Pouli and Emmony [20] addressed laser induced discoloration of this pigment. They have showed that the pigment has a high decomposition temperature of over 1000°C. Although XRD analysis indicates no change on the direct heating tests, it was suggested that the observed blackening induced by laser radiation could be explained by the reduction of PbO to metallic lead.

Lead chromate or red chrome ($Pb(OH)_2 \cdot PbCrO_4)_2$

Gordon Sobott et al. [38] verified that under 248 nm wavelength radiation lead chromate became black up to 0.25 J/cm^2, and above 0.375 J/cm^2 pigment particles were removed.

Naples yellow ($BiVO_4$, $Pb(SbO_3)_2$ or $Pb(SbO_4)_2$)

Chappé et al. [8] studied this pigment (lead antimonate) showing that the discoloration is most evident at 355 nm and the colour change is probably due to a photochemical interaction. Pigment reduction seems to be typical of this pigment [31].

Chrome yellow (PbCrO4)

It has been suggested [31] that pigment reduction is typical of this pigment the same way as for the Naples yellow. Gordon Sobott et al. [38] verified that with 1064 nm wavelength the pigment reacted only slightly while with 248 nm it turned black.

2.3.2. Cobalt pigments

Cobalt blue ($CoO \cdot Al_2O_3$)

Chappé et al. [8] reported colour changes with the four harmonics of Nd: YAG laser, although it was concluded that this pigment is relatively stable under laser radiation. The measured discoloration thresholds were $\sim$0.5 J/cm^2 at $\lambda = 1064$ and 532 nm and 0.1 J/cm^2 at $\lambda = 355$ and 255 nm.

Smalt (potassium glass with cobalt oxide)

Gordon Sobott et al. [38] studied the effect of Nd: YAG laser on smalt mixed with several binding media (lime, casein, and linseed oil). It was demonstrated that smalt did not reveal any discoloration but suffers mechanical damage [35, 38].

2.3.3. Iron pigments

Yellow ochre (goethite, $Fe_2O_3 \cdot H_2O$)

Athanassiou et al. [47] has noticed that after UV laser irradiation the composition of this pigment changed from goethite to haematite (Fe_2O_3). Gaetani and Santamaria [48] have not verified any transition from yellow to red ochre (red ochre is prepared by heating yellow ochre). Sansonetti and Realini [19] reported that under low fluence at 1064 nm there was colour change although no morphological alteration was observed. The author also verified that at an intermediate fluence the oil layer was damaged. XRD showed that after laser irradiation there was a decrease of goethite [FeO(OH)] and an increase of Fe_2O_3, among other nonspecified variety of components [39].

Brown ochre (Fe_2O_3, $Fe_2O_3 \cdot nH2O$)

Chappé et al. [8] reported some colour changes into black. This pigment revealed to be very unstable and it was classified as suitable only for laser cleaning at 532 and 1064 nm wavelengths.

Raw sienna (goethite, FeO(OH))

Raw sienna is an iron-oxide pigment and it is quite transparent being easily affected by changes of the binder. Pouli and Emmony [20] found that it has a similar behaviour when compared with yellow ochre. Heat testing revealed that they transformed into red iron oxide (haematite).

Burnt sienna (haematite, Fe_2O_3)

This pigment was briefly studied by Pouli and Emmony [20] which performed laser testing with Nd: YAG at 1064 nm wavelength. The pigment revealed a slight darkening after 3 pulses with 0.3 J/cm^2 of fluence.

Red ochre (Fe_2O_3)

Sansonetti and Realini [19] prepared red ochre samples with linseed oil and gypsum as binders. It was observed that under a low fluence the oil samples suffered a colour change although no corresponding morphological alterations were observed and that the intermediate fluence caused total ablation. It was observed a strong discoloration and morphological alterations in the gypsum sample using the lowest fluence.

Green earth (complex aluminosilicate minerals)

Gordon Sobott et al. [38] verified the reaction threshold for green earth at 81.9 J/cm^2 when mixed with linseed oil and a severe ablation of the paint layer at 135.4 J/cm^2. The same study determined the absorption minimum of green earth at 536 nm.

2.3.4. Copper pigments

Malachite ($CuCO_3 \cdot Cu(OH)_2$)

Chappé et al. [8] defined it as highly sensitive to laser radiation changing its colour from green to black upon irradiation. Discoloration was attributed to the formation of oxides of copper. XRD analysis revealed the formation of $Cu_2CO_3(OH)_2$ and CuO [20]. Pouli et al. [27] suggested that the discoloration is due to the decomposition of copper carbonate and copper hydroxide components into copper oxide (black). Gordon Sobott et al. [38] indicates decomposition into copper oxide, carbon oxide, and water upon laser irradiation above the reaction threshold. As suggested by Teule et al. [17], the colour change of malachite can be due to the alteration to tenorite (CuO) and cuprite (Cu_2O).

Verdigris ($Cu(C_2H_3O_2)H_2O$)

Laser irradiation tests revealed that this pigment did not suffer any discoloration [20, 27]. Furthermore, the increase of fluence or pulse number resulted in spallation rather then discoloration [28]. XPS was reported as not being able to find chemical changes. It was suggested to try other approaches in order to certify that no changes are occurring.

Azurite ($2CuCO_3 \cdot Cu(OH)_2$)

Gordon Sobott et al. [38] verified the appearance of cuprite which indicates decomposition into copper oxide and carbon oxide upon laser irradiation above the reaction threshold. A similar reaction was verified on malachite.

2.3.5. Other metal oxide pigments

Chromium oxide (Cr_2O_3)

Sansonetti and Realini [19] refers to colour change under low fluence (<0.1 J/cm^2) but no morphological alteration was observed. Under intermediate level of fluence it was observed loss of material. Chappé et al. [8] found the pigment as stable under the four harmonics of Nd: YAG laser although discoloration was verified from a dark-green into grey. The measured discoloration threshold was 0.17 J/cm^2 for $\lambda = 1064$ nm and $\sim$0.1 J/cm^2 for $\lambda = 532$, 355, and 266 nm.

Zinc white (ZnO)

Chappé et al. [8] reported colour changes into grey upon laser irradiation due to the reduction of ZnO into Zn, according the authors. It is also reported that the discoloration reverses to white after a week. After laser irradiation at 0.6 J/cm^2 (at 1064 nm) discoloration into brown/grey was reported [32]. Environmental scanning electron microscope (ESEM) analysis revealed melting points of 1 micron thick or less, being the melting point of ZnO 1975°C.

Titanium white (TiO_2)

This pigment turned into a bluish grey tone using 0.6 J/cm^2 (at 1064 nm) of fluence [32]. Although the melting point of TiO_2 is 1855°C, ESEM revealed melting points on the incidence area. It was advanced that the discoloration could be caused either by physical effects through the increase of the particle size, or by the chemical decomposition of the metal oxides [32].

2.3.6. Other pigments

White gypsum ($CaSO_4 \cdot 2H_2O$)

It was studied by Sansonetti and Realini [19] who refers to white gypsum as very stable showing no chromatic or morphologic changes until 3 J/cm^2 of fluence is used.

Black bone (C)

Sansonetti and Realini [19] reported Nd: YAG laser irradiation of 0.1 and 1 J/cm^2 on bone black pigment with oil and gypsum medium. On the oil samples, the low fluence induced no morphological or chromatic alteration while some changes were observed (grooves with corroded edges on the surface) with intermediate fluence.

Vermilion or cinnabar (HgS)

Vermilion is in a metastable equilibrium of two isometric phases, red hexagonal cinnabar (α-HgS), and black cubic (α'-HgS) metacinnabar [20]. This pigment changes its red colour to black by a light-induced phenomenon probably due to a

photochemical interaction [49]. Although these phases have the same chemical composition and molecular weight, they have different properties. Pouli and Emmony [20] reported that its discoloration is permanent when using laser irradiation at 0.3–0.5 J/cm^2. AES and XPS showed an increase of carbon and of the Hg/S ratio. It was suggested that this was explained by the formation of black mercuric sulphide (Hg_2S). Abraham et al. [50] advanced the possibility that the discoloration was due to conversion to meta-cinnabar which was confirmed when it was found that under laser radiation cinnabar changed from a red hexagonal crystal structure into a grey-black metacinabar cubic structure [8, 39]. This modification is almost independent of the wavelength. However, XPS analysis suggested the presence of Hg_2S and Hg after irradiation and that this chemistry change contradicts the previous hypothesis justified by the fact that such modification would not affect the Hg/S ratio and would not introduce new species of Hg [27]. Furthermore, scanning transmission electron microscopy (STEM) analysis confirmed no change in the crystal shape. However, Schnell et al. [32] revealed in their study that cinnabar was the only pigment to suffer a phase change, which was detected by XRD.

Ultramarine ($Na_{8-10}Al_6Si_6O_{24}S_4$)

Sansonetti and Realini [19] refer a discoloration (on oil samples) at a low fluence (0.1 J/cm^2), which is stable until an intermediate fluence (1 J/cm^2) is used. No morphological changes were observed by the authors with this range of fluence when using a microscope. The same author observed a good morphological resistance under laser irradiation independently of the used fluence on gypsum samples. However, it was observed a strong colour change under the lowest fluence although it was not proportional to the used fluence. It was verified by Chappé et al. [8] that ultramarine pigment is a highly stable pigment. The pigment, upon laser irradiation, only showed some degree of discoloration (from dark blue into white) after some high threshold is reached. Thus, it was classified as suitable for laser cleaning with each of the four Nd: YAG laser wavelengths. It was advanced the possibility that the observed discoloration could be motivated by the presence of a mineral (Nosean) although its presence could not be definitively proved.

2.3.7. Organic pigments

The samples that have been presently studied have shown a high degree of stability under intense laser treatment [31]. The ablation of organic material leads to the formation of a thin layer of char that covers the paint surface. Castillejo et al. [31] have demonstrated that this layer is not produced in the absence of inorganic materials in the paint. This seems to indicate that the pigment particles mediate the char formation through an energy transfer mechanism.

Madder lake (Al-Ca complex salt of alizarin)

Under laser irradiation, this organic material changes its red colour to white. This discoloration was observed in all the Nd: YAG laser wavelengths tested with the exception of 1064 nm where the threshold was higher. No chemical explanation could be given.

Curcumin ($C_{21}H_{20}O_6$)

Castillejo et al. [31] determined that the colour of this organic pigment remained practically unaltered under UV excimer laser radiation (248 nm) using low fluence of irradiation (0.11 J/cm^2). However, at higher fluence (0.4 J/cm^2) the pigment reveals a slight discoloration.

3. REAL EASEL PAINTING TESTS

Apart from the tests in samples and mock-ups, real paintings have been used to test laser cleaning. Teule et al. [2] performed the study of the treatment of two oil paintings severely damaged in a fire using an excimer laser. Both paintings presented several hard problems that were not possible to treat by conventional techniques. The first painting had suffered discoloration due to high temperatures and soot that was located on the top of the paint layer, while on the second painting heat caused detachment of the paint from the support and hard and brittle blisters were formed. Tests with solvents were performed but none was able to remove the layer successfully without damage on the paint layer. Furthermore, it would also result on the penetration of soot particles into the painting. Physical contact was not advisable as it would cause delamination of the paint layer as well. In the first case, a moderate fluence of 0.38 J/cm^2 was applied while the second painting was irradiated at 0.41 J/cm^2. No discoloration of the paint layer was visible and the surface texture remained intact as well. Similar work on another painting was also described by Teule et al. [17]. The main problem in this case was a yellowed varnish. The painting presented also some burnt retouching due to past interventions. In order to proceed to a relining, it was required the removal of these interventions as well of the varnish. The use of solvents was not desirable as it would have deeply penetrated the dry paint layers. An energy fluence of 0.43 J/cm^2 was then used to remove successfully the retouchings and fillings. During the process, the original paint layer was irradiated with a 248 nm excimer laser and no discoloration or change was detected. However, the lead white that had been used on the retouch turned grey, although it is mentioned that it did regenerate. In order to prevent pigment discoloration, it has been proposed [24, 28] that a thin layer of varnish should be left in order to avoid the radiation penetration into the paint layer. As mentioned by Hill et al. [24], this layer should have a thickness of the order, or greater than, of the optical penetration depth.

An Nd: YAG laser was also already used to clean an icon covered by candle soot and dirt over sensitive silver layer and an uncharacterized yellow layer [7]. It was found that the wavelength of 355 nm was the most efficient wavelength to the removal of the soot and dirt without damaging the underlying layers.

It has also been reported [18] that several real easel paintings were cleaned using Er: YAG laser. The laser was used to

gradually remove an egg-tempera over paint which showed to be of difficult removal by both solvent and mechanical cleanings. It was stated that the layer was removed with success without affecting the original layer despite no online characterisation technique is mentioned.

The potential of the laser to remove overpaintings from a contemporary painting was assessed by McGlinchey et al. [51]. On this study, it was used mock-up samples for a first assessment and later the real painting with Nd:YAG and excimer lasers. The overcleaning removal was successful and it was concluded that the laser irradiation were viable for small areas.

4. CONCLUSION

Laser research is nowadays focused on the development and enhancement of the controllable removal of layers, either protective layers, such as varnishes, or over paint layers. The direct incidence of laser radiation into the paint layer usually induces discoloration of the paint materials, which depends on factors such as the nature of the material and type and intensity of the used laser. The discoloration mechanism has been studied and it has been concluded that it is due to oxidation and reduction phenomena depending from the irradiated material. A complete knowledge of the interaction between the laser radiation and pigments, binding medium and varnish involved is necessary before the actual cleaning procedure. Further research on samples is necessary in order to fully understand the interaction laser material.

ACKNOWLEDGEMENT

The authors would like to thank Fundação para a Ciência e a Tecnologia for the Ph.D. scholarship (SFRH/BD/16759/2004) of Rui Bordalo.

REFERENCES

[1] A. Phenix and K. Sutherland, "The cleaning of paintings: effect of organic solvents on oil paint films," *Reviews in Conservation*, no. 2, pp. 47–59, 2001.

[2] J. M. Teule, U. Ullenius, I. Larsson, et al., "Controlled laser cleaning of fire-damaged paintings," in *Proceedings of the 13th Triennial Meeting of the Committee for Conservation of the International Council of Museums (ICOM-CC '02)*, pp. 252–256, Rio de Janeiro, Brazil, September 2002.

[3] C. Fotakis, "Lasers for art's sake," *Optics and Photonics News*, vol. 6, no. 5, pp. 30–35, 1995.

[4] V. Zafiropulos and C. Fotakis, "Lasers in the conservation of painted artworks," in *Laser Cleaning in Conservation: An Introduction*, M. Cooper, Ed., chapter 6, pp. 79–90, Butterworth-Heinemann, Oxford, UK, 1998.

[5] I. Gobernado-Mitre, A. C. Prieto, V. Zafiropulos, Y. Spetsidou, and C. Fotakis, "On-line monitoring of laser cleaning of limestone by laser-induced breakdown spectroscopy and laser-induced fluorescence," *Applied Spectroscopy*, vol. 51, no. 8, pp. 1125–1129, 1997.

[6] V. Zafiropulos, "Laser ablation in cleaning of artworks," in *Optical Physics, Applied Physics and Material Science: Laser Cleaning*, B. S. Luk'yanchuk, Ed., pp. 343–392, World Scientific, Singapure, 2002.

[7] J. Hildenhagen and K. Dickmann, "Nd: YAG laser with wavelengths from IR to UV (ω, 2ω, 3ω, 4ω) and corresponding applications in conservation of various artworks," *Journal of Cultural Heritage*, vol. 4, supplement 1, pp. 174s–178s, 2003.

[8] M. Chappé, J. Hildenhagen, K. Dickmann, and M. Bredol, "Laser irradiation of medieval pigments at IR, VIS and UV wavelengths," *Journal of Cultural Heritage*, vol. 4, supplement 1, pp. 264s–270s, 2003.

[9] A. De Cruz, M. L. Wolbarsht, and S. A. Hauger, "Laser removal of contaminants from painted surfaces," *Journal of Cultural Heritage*, vol. 1, no. 2, pp. S173–S180, 2000.

[10] J. F. Asmus, D. L. Westlake, and H. T. Newton, "Laser technology for the divestment of a lost Leonardo da Vinci mural," *Journal of Vacuum Science and Technology*, vol. 12, no. 6, pp. 1352–1355, 1975.

[11] L. Carlyle, "Laser interactions with paintings: results and proposals for further study," Unpublished Report, The Canadian Conservation Institute, Ottawa, Canada, 1981.

[12] J. F. Asmus, "More light for art conservation," *IEEE Circuits and Devices Magazine*, vol. 2, no. 2, pp. 6–14, 1986.

[13] E. Hontzopoulos, C. Fotakis, and M. Doulgeridis, "Excimer laser in art restoration," in *9th International Symposium on Gas Flow and Chemical Lasers*, C. Fotakis, C. Kalpouzos, and T. G. Papazoglou, Eds., vol. 1810 of *Proceedings of SPIE*, pp. 748–751, Heraklion, Greece, September 1993.

[14] M. Cooper, Ed., *Laser Cleaning in Conservation*, Butterworth-Heinemann, Oxford, UK, 1998.

[15] M. Cooper, Ed., *Laser Cleaning in Conservation: an Introduction*, Butterworth-Heinemann, Oxford, UK, 1998.

[16] J. H. Scholten, V. Zafiropulos, A. Petrakis, M. den Leeuw, P. T. Rutgers, and M. P. Koster, "The development of a professional laser cleaning station for paintings," submitted to Restauratorenblätter, Sonderband, for the Proceedings of Lacona II.

[17] R. Teule, H. Scholten, O. F. van den Brink, et al., "Controlled UV laser cleaning of painted artworks: a systematic effect study on egg tempera paint samples," *Journal of Cultural Heritage*, vol. 4, supplement 1, pp. 209s–215s, 2003.

[18] P. Bracco, G. Lanterna, M. Matteini, et al., "Er: YAG laser: an innovative tool for controlled cleaning of old paintings: testing and evaluation," *Journal of Cultural Heritage*, vol. 4, supplement 1, pp. 202s–208s, 2003.

[19] A. Sansonetti and M. Realini, "Nd: YAG laser effects on inorganic pigments," *Journal of Cultural Heritage*, vol. 1, no. 2, pp. S189–S198, 2000.

[20] P. Pouli and D. C. Emmony, "The effect of Nd: YAG laser radiation on medieval pigments," *Journal of Cultural Heritage*, vol. 1, no. 2, pp. S181–S188, 2000.

[21] R. Salimbeni, "Laser techniques in conservation: an example of sustainable innovation in full development in Europe," in *International Conference on Lasers, Applications, and Technologies 2005: Laser Sensing, Imaging, and Information Technologies*, vol. 6162 of *Proceedings of SPIE*, pp. 11 pages, St. Petersburg, Russia, May 2006.

[22] E. René de la Rie, "Photochemical and thermal degradation of films of dammar resin," *Studies in Conservation*, vol. 33, pp. 53–70, 1988.

[23] J. H. Scholten and D. A. Schipper, "Advanced workstation for controlled laser cleaning of paintings," in *Laser Techniques and Systems in Art Conservation*, vol. 4402 of *Proceedings of SPIE*, pp. 121–129, Munich, Germany, June 2001.

[24] A. E. Hill, T. Fourrier, J. Anderson, A. Athanassiou, and C. Whitehead, "Measurement of the light absorption length of

308nm pulsed laser light in artificially aged varnishes," in *Proceedings of the 12th Triennial Meeting of the Committee for Conservation of the International Council of Museums (ICOM-CC '99)*, pp. 299–303, Lyon, France, August-September 1999.

[25] S. Georgiou, V. Zafiropulos, V. Tomari, and C. Fotakis, "Mechanistic aspects of excimer laser restoration of painted artworks," *Laser Physics*, vol. 8, no. 1, pp. 307–312, 1998.

[26] V. Zafiropulos, A. Galyfianaki, S. Boyatzis, A. Fostiridou, and E. Ioakimoglou, "UV-laser ablation of polymerized resin layers and possible oxidation process in oil-based painting media," in *Optics and Lasers in Biomedicine and Culture*, S. Fotakis, C. Kalpouzos, and T. G. Papazoglou, Eds., vol. 5, pp. 115–122, Springer, Berlin, Germany, 2000.

[27] P. Pouli, D. C. Emmony, C. E. Madden, and I. Sutherland, "Studies towards a thorough understanding of the laser-induced discoloration mechanisms of medieval pigments," *Journal of Cultural Heritage*, vol. 4, supplement 1, pp. 271s–275s, 2003.

[28] S. Georgiou, V. Zafiropulos, D. Anglos, C. Balas, V. Tornari, and C. Fotakis, "Excimer laser restoration of painted artworks: procedures, mechanisms and effects," *Applied Surface Science*, vol. 127–129, pp. 738–745, 1998.

[29] O. Madden, M. Abraham, S. Scheerer, and L. Werden, "The effects of laser radiation on adhesives, consolidants and varnishes," in *Proceedings of the 5th International Conference on Lasers in the Conservation of Artworks (Lacona V '03)*, K. Dickmann, C. Fotakis, and J. F. Asmus, Eds., vol. 100 of *Springer Proceedings in Physics*, pp. 247–254, Osnabrück, Germany, September 2005.

[30] C. Theodorakopoulos, *The excimer laser ablation of picture varnishes: an evaluation with reference to light-induced deterioration*, Ph.D. thesis, RCA/AMOLF, London, UK, 2005.

[31] M. Castillejo, M. Martín, M. Oujja, et al., "Evaluation of the chemical and physical changes induced by KrF laser irradiation of tempera paints," *Journal of Cultural Heritage*, vol. 4, supplement 1, pp. 257s–263s, 2003.

[32] A. Schnell, L. Goretzki, and C. Kaps, "Nd-YAG laser irradiation of pigments and binders in paint layers," in *Proceedings of 8th European Congress and Exhibition on Advanced Materials and Processes (EUROMAT '03)*, Lausanne, Switzerland, September 2003.

[33] M. P. Colombini, A. Andreotti, G. Lanterna, and M. Rizzi, "A novel approach for high selective micro-sampling of organic painting materials by Er: YAG laser ablation," *Journal of Cultural Heritage*, vol. 4, supplement 1, pp. 355s–361s, 2003.

[34] W. A. Real, I. Zergioti, Y. Spetsidou, and D. Anglos, "Use of KrF excimer laser for cleaning fragile and problematic paint surfaces," in *Proceedings of the 11th Triennial Meeting of the Committee for Conservation of the International Council of Museums (ICOM-CC '96)*, J. Bridgland, Ed., pp. 303–309, Edinburgh, Scotland, September 1996.

[35] L. Shekede, "Lasers: a preliminary study of their potential for the cleaning and uncovering of wall paintings," Diploma Project, Wall Paintings Departement, Courtauld Institute of Art, London, UK, 1994.

[36] L. Shekede, "The effects of laser radiation on polychromed surfaces," in *Post-Prints of the Analysis of Pigments and Plasters, The United Kingdom Institute of Conservation of Historic and Artistic Works*, pp. 23–25, London, UK, February 1997.

[37] L. Shekede, "Lasers: a preliminary study of their potential for the cleaning and uncovering of wall paintings," in *Proceedings of the 1st International Conference on Lasers in the Conservation of Artworks (LACONA I '95)*, pp. 51–56, Crete, Greece, October 1995.

[38] R. J. Gordon Sobott, T. Heinze, K. Neumeister, and J. Hildenhagen, "Laser interaction with polychromy: laboratory investigations and on-site observations," *Journal of Cultural Heritage*, vol. 4, supplement 1, pp. 276s–286s, 2003.

[39] V. Zafiropulos, C. Balas, A. Manousaki, et al., "Yellowing effect and discoloration of pigments: experimental and theoretical studies," *Journal of Cultural Heritage*, vol. 4, supplement 1, pp. 249s–256s, 2003.

[40] P. Pouli, D. C. Emmony, C. E. Madden, and I. Sutherland, "Analysis of the laser-induced reduction mechanisms of medieval pigments," *Applied Surface Science*, vol. 173, no. 3-4, pp. 252–261, 2001.

[41] M. I. Cooper, P. S. Fowles, and C. C. Tang, "Analysis of the laser-induced discoloration of lead white pigment," *Applied Surface Science*, vol. 201, no. 1–4, pp. 75–84, 2002.

[42] S. Giovanni, M. Matteini, and A. Moles, "Studies and developments concerning the problem of altered lead pigments in wall painting," *Studies in Conservation*, vol. 35, no. 1, pp. 21–25, 1990.

[43] O. van den Brink, *Molecular changes in egg tempera paint dosimeters as tools to monitor the museum environment*, Ph.D. thesis, University of Amsterdam, Amsterdam, The Netherlands, 2001.

[44] V. Zafiropulos, T. Stratoudaki, A. Manousaki, K. Melesanaki, and G. Orial, "Discoloration of pigments induced by laser irradiation," *Surface Engineering*, vol. 17, no. 3, pp. 249–253, 2001.

[45] L. Carlyle and J. H. Townsend, "An investigation of lead sulphide darkening of nineteenth century painting material," in *The United Kingdom Institute of Conservation and the Tate Gallery: Dirt and Pictures Separated Conference*, pp. 40–43, London, UK, 1990.

[46] S. Aze, J.-M. Vallet, and O. Grauby, "Chromatic degradation processes of read lead pigment," in *Proceedings of the 13th Triennial Meeting of the Committee for Conservation of the International Council of Museums (ICOM-CC '02)*, vol. 2, pp. 549–555, Rio de Janeiro, Brazil, September 2002.

[47] A. Athanassiou, A. E. Hill, T. Fourrier, L. Burgio, and R. J. H. Clark, "The effects of UV laser light radiation on artists' pigments," *Journal of Cultural Heritage*, vol. 1, no. 2, pp. S209–S213, 2000.

[48] M. C. Gaetani and U. Santamaria, "The laser cleaning of wall paintings," *Journal of Cultural Heritage*, vol. 1, no. 2, pp. S199–S207, 2000.

[49] J. Plesters, A. Roy, and D. Bomford, "Interpretation of the magnified image of paint surfaces and samples in terms of condition and appearance of the picture," in *Science and Technology in the Service of Conservation*, N. S. Brommelle and P. Smith, Eds., pp. 169–176, IIC, London, UK, 1982.

[50] M. H. Abraham, S. Scheerer, O. Madden, and F. Adar, "Laser-induced chemical changes in art materials," in *Laser Techniques and Systems in Art Conservation*, vol. 4402 of *Proceedings of SPIE*, pp. 68–72, Munich, Germany, June 2001.

[51] C. McGlinchey, C. Stringari, E. Pratt, et al., "Evaluating the effectiveness of lasers for the removal of overpaint from a 20th C minimalist painting," in *Proceedings of the 5th International Conference on Lasers in the Conservation of Artworks (Lacona V '03)*, K. Dickmann, C. Fotakis, and J. F. Asmus, Eds., vol. 100 of *Springer Proceedings in Physics*, pp. 209–216, Osnabrück, Germany, September 2003.

Hindawi Publishing Corporation
Laser Chemistry
Volume 2006, Article ID 42709, 5 pages
doi:10.1155/2006/42709

Research Article

Laser Cleaning and Spectroscopy: A Synergistic Approach in the Conservation of a Modern Painting

K. Melessanaki,[1] C. Stringari,[2] C. Fotakis,[1] and D. Anglos[1]

[1] *Institute of Electronic Structure and Laser (IESL), Foundation for Research and Technology-Hellas (FORTH), P.O. Box 1385, GR71110 Heraklion, Crete, Greece*
[2] *Solomon R. Guggenheim Museum, New York, NY 10128-0173, USA*

Received 15 September 2006; Revised 17 November 2006; Accepted 17 November 2006

Recommended by Marta Castillejo

We present results from preliminary laser cleaning studies performed on a 20th century modern painting, in which laser-induced breakdown spectroscopy (LIBS) was employed for monitoring the progress of material removal. This synergistic approach, that combines laser ablation cleaning with spectroscopic control, is of obvious importance as it offers a reliable means of ensuring proper conservation and could be the basis of a standard protocol for laser-based restoration procedures.

1. INTRODUCTION

Laser cleaning methods have been employed over the past three decades in a number of conservation cases including the removal of surface deposits and/or contamination, corrosion layers, materials from previous conservation treatments and overpaint layers from different types of cultural heritage objects [1–4]. The effectiveness of modern laser cleaning methodologies has been gaining recognition and lasers have been successfully used in quite a few cases of encrustation removal from archaeological and historical stone sculpture and monuments [3–5]. On the other hand, laser cleaning of painted artworks has been demonstrated [3, 4, 6] but its application remains mostly at the research level because materials in paintings are quite diverse and often complex and sensitive, requiring delicate and highly controlled procedures. Currently, research is in progress for understanding the interaction of laser radiation with such complicated structures and the mechanism behind material removal in order to achieve proper conservation.

In all cases of restoration, reliable monitoring tools are necessary that will enable control of the cleaning. Simple means such as the naked eye of an experienced conservator provide control as cleaning is performed but with limited capabilities. On the other hand, more sophisticated analytical tools are available, including different types of microscopy and spectroscopy, but these are used off-line or require sampling. Laser induced breakdown spectroscopy (LIBS) has been proposed and used as a diagnostic tool for monitoring and controlling the laser cleaning process [7–10]. One of the most interesting features of LIBS is its ability to perform depth profile analysis. Revealing the sratigraphy of a painted structure, namely, finding the successive paint layers, is obviously quite important in the characterization of a painting regarding the technique used or the presence of overpaintings or retouching. In the case of laser cleaning, LIBS can be performed in situ by using pulses from the same laser and this way, one is able to monitor the progress of material removal on-line by recording the corresponding spectra [6–9].

Conservation problems in modern paintings are quite diverse and include, for example, degradation of complex materials, for which one often has limited knowledge, or previous unsuccessful restoration treatments. Furthermore, in certain cases the original materials and those to be removed are quite similar and thus setting discrimination boundaries between them is extremely difficult if not impossible. These cases pose a challenging and highly demanding conservation problem and a laser restoration approach might turn out to be useful. Some practical and technological issues in the development of a proper laser cleaning protocol for works of contemporary art are discussed, with respect to the use of on-line depth profiling of the painting.

2. EXPERIMENT

In this paper, we discuss a set of preliminary laser cleaning tests performed at IESL-FORTH, on a 20th century modern painting from the Guggenheim Museum of New York. The painting was part of Ad Reinhardt's "Black Square" series (1966). It had travelled extensively until the early 1980s, suffered various damages, and was completely over-painted with an acrylic emulsion and a transparent "sealant." Removal of these overpaint layers was not possible with standard conservation methods [10, 11] and therefore a collaboration between IESL-FORTH and the Guggenheim Museum was set up to investigate the possibility of laser cleaning. The aim of the work was to establish proper laser cleaning parameters that would give rise to controlled removal of the overpaint layers. More specifically this work presents results from the investigation of the possibility of using LIBS as a monitoring tool during the laser cleaning of modern materials. In principle, on the basis of the characteristic LIB spectra recorded, one may be able to discriminate among different overpaint layers as these are progressively removed. In cases in which the plume emission produced during laser ablation might not be intense enough to yield a clean LIB spectrum, an alternative approach is followed. Single pulses with proper fluence (higher than that used for cleaning) from the same laser are delivered in between successive cleaning scans to probe a small area on the exposed surface. This way, an incremental depth profiling is performed parallel to cleaning that enables one to follow the progress of material removal. The latter approach has been used in this study.

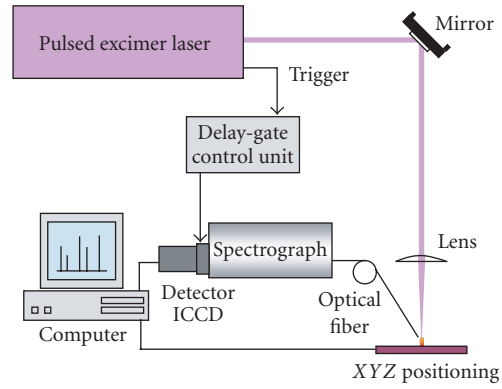

Figure 1: Schematic diagram of experimental setup for laser cleaning and LIBS analysis.

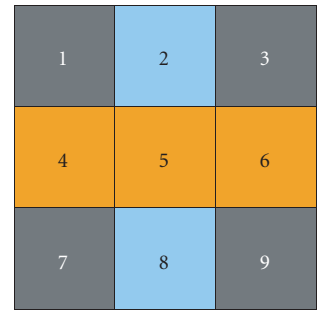

Figure 2: Schematic representation of the colored layers of the overpainting.

3. MATERIAL AND METHODS

A diagram of the experimental set up used for laser cleaning and LIBS analysis of the painting is presented in Figure 1. The painting was mounted on a motorized xyz-stage, controlled by a computer. The stage enabled positioning of the painting close to the focal plane of the laser beam (z-axis) and allowed its precise lateral translation (xy-plane) with respect to the laser beam. A KrF excimer laser emitting at 248 nm (COMPex Lambda Physik, pulse duration: 30 nanoseconds) has been employed for both the cleaning application and the LIBS measurements.

The laser beam is focused on the painted surface by means of a cylindrical planoconvex quartz lens ($f = +300$ mm) that results in illumination of a $3.7 \times 0.4\,\text{cm}^2$ rectangle on the painting surface. The beam is scanned in the direction perpendicular to the long dimension of the focused rectangle, across a preselected area that is typically 1–3 cm long. A set of 5–10 pulses are applied at each individual rectangle. To obtain a homogeneous surface exposure, successive rectangles are overlapped to a degree of 80%. Typical laser fluence for laser cleaning was about $1.1\,\text{J/cm}^2$ while for the LIBS analysis, performed in between successive cleaning scans, the fluence was increased at approximately $2\,\text{J/cm}^2$ by adjusting the focussing lens. The light emitted from the plasma plume was collected with an UV transmitting optical fiber oriented roughly at the center of the illuminated rectangle at an angle of 30° with respect to the normal to the painting surface. The plasma emission was analyzed in a 0.20 m spectrograph (PTI model 01-001AD) equipped with two diffraction gratings of 300 and 1200 grooves/mm and the spectrum was recorded on an intensified CCD detector (Andor Technologies, DH520-18F-01). The plasma emission was recorded with a delay of 500 nanoseconds with respect to the laser pulse with an integration window of 500–1000 nanoseconds.

4. RESULTS AND DISCUSSIONS

Following preliminary tests on replicas (model samples), cleaning trials were carried out on selected areas of the painting. The painting is a $1.55 \times 1.55\,\text{m}^2$ square subdivided to 9 equal squares in a 3×3 arrangement with subtle variations of black. The overpaint structure consisted of symmetrically grouped pigment layer patterns, following the geometry of the original painting (Figure 2).

Analysis of selected cross sections from all 9 squares, by using SEM-EDS and optical and FT-IR microspectrometry, provide some insight into the stratigraphy of the overpaint layers, which is very valuable as a reference for the LIBS results and especially important for the interpretation of monitoring and cleaning results. Cross sections showed that squares 1, 3, 7, and 9 had blue and red paint layers,

Table 1: Indicative stratigraphy obtained from cross-section analysis of squares 2 and 6.

Square 2		Square 6	
Layer*	Components	Layer*	Components
18 17 16 15 14	Acrylic emulsion with low pigment concentration	20 19 18 17 16 15	Acrylic emulsion with low pigment concentration
13	Black paint (black iron oxide, bone black)	14	Black with red paint (red cadmium sulfoselenide, black or red iron oxide)
12	Blue paint (cobalt oxide)	13	Black paint (black iron oxide, bone black)
11	Black paint (black iron oxide, bone black)	12	Black with red paint (red cadmium sulfoselenide, black or red iron oxide, barytes)
10	Blue paint (cobalt oxide)	11	Yellow paint (black iron oxide, bone black, chromium yellow)
9	*Acrylic sealant layer*	10	*Acrylic sealant layer*
8 7	Paint mixture of black and blue (black iron oxide ultramarine blue)	9 8 7 6	Paint mixture of black and blue (black iron oxide, ultramarine blue, barytes)
6 5 4 3 2	Paint mixture of black, blue, and green (black iron oxide, ultramarine blue, chromium green, barytes)	5 4 3 2	Paint mixture of black and blue (black iron oxide, bone black, ultramarine blue, cerulean blue, barytes)
1	Ground layer (titanium dioxide)	1	Ground layer (titanium dioxide)

*Layer numbering starts from the ground layer with the outer layers receiving the highest number.

squares 2 and 8 had blue, and finally squares 4, 5, and 6 had red and yellow paint layers under the final black overpaint. The stratigraphy of squares 2 and 6 that have been examined in detail in this study is given in Table 1.

Single pulse LIB spectra were collected following a certain number of laser cleaning scans over the preselected area. For example, representative spectra obtained during cleaning over square 2, are shown in Figure 3. The spectrum obtained before starting the cleaning, corresponds to material rich in acrylic medium and this is demonstrated by the emission bands of C_2 (excited carbon dimers) at around 476 nm and 512 nm and also by the fact that the emission from neutral Ca (422.67 nm) is stronger than the one arising form Ca ions (393.37 and 396.85 nm). The latter indicates a lower plasma temperature expected for the pigment poor outer acrylic layer that is not strongly absorbing at 248 nm. Following the first cleaning scan (10 pulses), the LIB spectrum indicates the presence of Ca, Fe, Co, Al, Cu, and Na, suggesting that material has been removed down to layers 13/12 or 11/10, which combine black and blue pigments based on iron and cobalt respectively (see Table 1). In addition, the spectrum suggests the presence of a Cu based pigment, which could either be azurite (blue) or malachite (green). It is noted that optical microscopic examination of the cross section sample shows green pigment grains dispersed in the black layers 13 and 11. The strong Ca emission arises most likely from the pigment bone black, $Ca_3(PO_4)_2$. Following 3 cleaning scans with 5 pulses each, we reach a new layer that shows different pigment composition rich in Fe, Al, Ba, Ca, and Na. Emission from Ba indicates the presence of barytes (white pigment or filler based on $BaSO_4$), while the increase of Al and Na emission correlates with the presence of the blue pigment ultramarine blue, $Na_8Al_6Si_6O_{24}S_3$. Most likely these spectra correspond to layers that are just below the acrylic sealant, on the top part of the original paint and signal that cleaning should end before that level.

In square 6, several spectra were also collected during the progress of cleaning that reveal the presence of different layers (Figure 4). Following scan 1, material containing Fe, Ca, and Al is seen, that most likely corresponds to the top layers of the light black acrylic overpaint (20–15). Following scan 3, new emissions show up from Ba, Mn, and Cd besides those from Ca, Al, and Fe. The emission due to Cd correlates with the presence of cadmium red (see Table 1) and suggests that layers 14/13/12 have been reached. The presence of Mn might indicate the use of manganese brown or black. Most

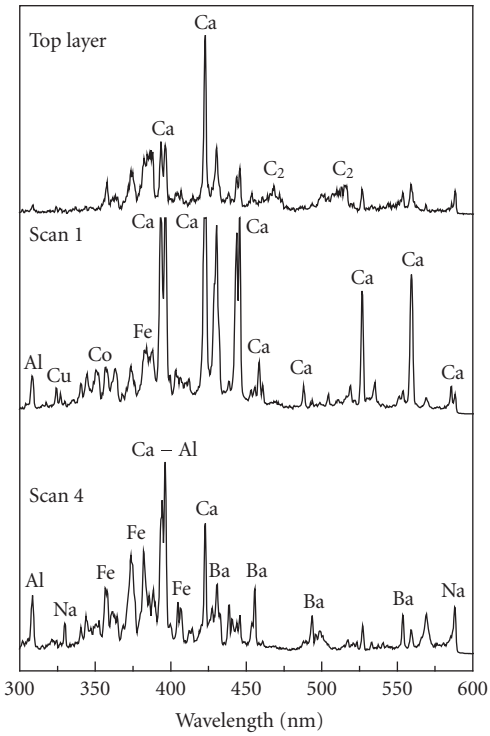

Figure 3: LIBS monitoring of the laser cleaning process at square 2.

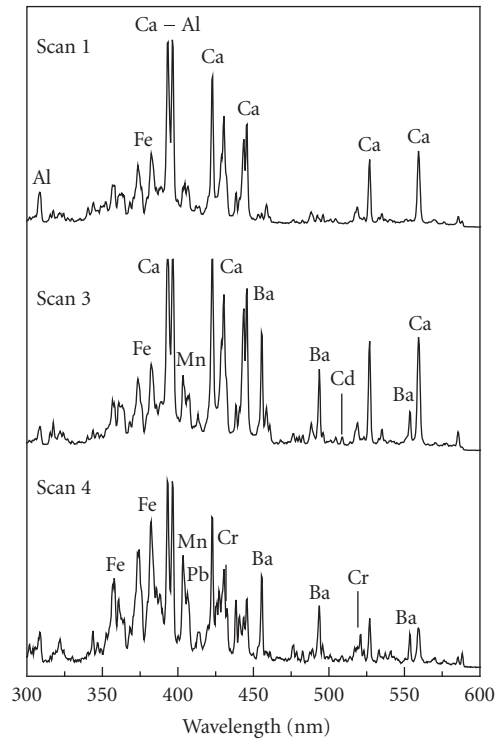

Figure 4: LIBS monitoring of the laser cleaning process at square 6.

importantly, following scan 4, two new emissions from Cr and Pb are observed, which suggest the presence of chrome yellow, $PbCrO_4$, one of the components in layer 11. This is just over the sealant that has been applied on the original paint and therefore determines the cleaning limit.

These results indicate that LIBS offers a potential tool for monitoring laser cleaning of multi-layer paint structures and in certain cases it can be used to signal the end-point of cleaning protecting the original paint. The presence of mixtures of pigments with several components results in rather line-rich spectra and both high resolution and broad spectral coverage are highly desirable. The use of echelle type spectrometers should be promising for such demanding applications of LIBS [12]. Finally, one has to note that an optimum approach to such complex conservation problems is to follow a specific procedure, that includes first detailed analysis and understanding of the materials present followed by controlled conservation innervation. On the basis of these preliminary results, a more extended laser conservation campaign for the painting has been undertaken at Art Innovation (the Netherlands) and results will be reported in the future.

ACKNOWLEDGMENTS

This work has been supported by the Ultraviolet Laser Facility operating at IESL-FORTH and by AXA Art Insurance, that generously donated the painting and funding for the research; special thanks go to Chris McGlinchey at the MoMA, New York.

REFERENCES

[1] J. F. Asmus, G. Guattari, L. Lazzarini, G. Musumeci, and R. F. Wuerker, "Holography in the conservation of statuary," *Studies in Conservation*, vol. 18, no. 2, pp. 49–63, 1973.

[2] K. G. Watkins, J. H. Larson, D. C. Emmony, and W. M. Steen, "Laser cleaning in art restoration: a review," in *Proceedings of the NATO Advanced Study Institute on Laser Processing: Surface Treatment and Film Deposition*, p. 907, Sesimbra, Portugal, July 1994.

[3] M. Cooper, *Laser Cleaning in Conservation: An Introduction*, Butterworth-Heinemann, Oxford, UK, 1998.

[4] C. Fotakis, D. Anglos, V. Zafiropulos, S. Georgiou, and V. Tornari, *Lasers in the Preservation of Cultural Heritage: Principles and Applications*, Taylor & Francis, Philadelphia, Pa, USA, 2006.

[5] P. Pouli, K. Frantzikinaki, E. Papakonstantinou, V. Zafiropulos, and C. Fotakis, "Pollution encrustation removal by means of combined ultraviolet and infrared laser radiation: the application of this innovative methodology on the surface of the Parthenon west frieze," in *Proceedings of the 5th International Conference on Lasers in the Conservation of Artworks (LACONA V)*, vol. 100 of *Springer Proceedings in Physics*, pp. 333–340, Osnabruck, Germany, September 2003.

[6] S. Georgiou, V. Zafiropulos, D. Anglos, C. Balas, V. Tornari, and C. Fotakis, "Excimer laser restoration of painted artworks: procedures, mechanisms and effects," *Applied Surface Science*, vol. 127–129, pp. 738–745, 1998.

[7] D. Anglos, S. Couris, and C. Fotakis, "Laser diagnostics of painted artworks: laser-induced breakdown spectroscopy in pigment identification," *Applied Spectroscopy*, vol. 51, no. 7, pp. 1025–1030, 1997.

[8] D. Anglos, "Laser-induced breakdown spectroscopy in art and archaeology," *Applied Spectroscopy*, vol. 55, no. 6, pp. 186A–205A, 2001.

[9] I. Gobernado-Mitre, A. C. Prieto, V. Zafiropulos, Y. Spetsidou, and C. Fotakis, "On-line monitoring of laser cleaning of limestone by laser-induced breakdown spectroscopy and laser-induced fluorescence," *Applied Spectroscopy*, vol. 51, no. 8, pp. 1125–1129, 1997.

[10] J. H. Scholten, J. M. Teule, V. Zafiropulos, and R. M. A. Heeren, "Advanced workstation for controlled laser cleaning of paintings," in *Optics and Lasers in Biomedicine and Culture*, vol. 5 of *Series of the International Society on Optics Within Life Sciences*, pp. 183–187, Springer, Berlin, Germany, 2000.

[11] C. McGlinchey, C. Stringari, E. Pratt, et al., "Evaluating the effectiveness of lasers for the removal of overpaint from a 20th C minimalist painting," in *Proceedings of the 5th International Conference on Lasers in the Conservation of Artworks (LACONA V)*, vol. 100 of *Springer Proceedings in Physics*, pp. 209–216, Osnabruck, Germany, September 2003.

[12] M. Sabsabi, V. Detalle, M. A. Harith, W. Tawfik, and H. Imam, "Comparative study of two new commercial echelle spectrometers equipped with intensified CCD for analysis of laser-induced breakdown spectroscopy," *Applied Optics*, vol. 42, no. 30, pp. 6094–6098, 2003.

Hindawi Publishing Corporation
Laser Chemistry
Volume 2006, Article ID 81750, 6 pages
doi:10.1155/2006/81750

Research Article

Characterization of Stone Cleaning by Nd:YAG Lasers with Different Pulse Duration

Laura Bartoli,[1] Paraskevi Pouli,[2] Costas Fotakis,[2,3] Salvatore Siano,[1] and Renzo Salimbeni[1]

[1] *Istituto di Fisica Applicata "N. Carrara" (IFAC), Consiglio Nazionale delle Ricerche (CNR), Via Madonna del Piano 10, 50019 Sesto Fiorentino (FI), Italy*
[2] *Institute of Electronic Structure and Lasers (IESL), Foundation for Research and Technology Hellas (FORTH), P.O. Box 1527, 71110 Heraklion, Greece*
[3] *Department of Physics, University of Crete, 71003 Heraklion, Greece*

Received 15 September 2006; Revised 15 December 2006; Accepted 27 December 2006

Recommended by Wolfgang Kautek

The present work is a comparative study on the laser cleaning of stonework using Nd:YAG lasers at different pulse durations. The ablation rate, the degree of cleaning, and the appearance of the treated surface were studied irradiating a simulated sample and a real stone artefact using three different Nd:YAG laser systems with pulse duration of 90 microseconds, 15 nanoseconds, and 150 picoseconds. To our knowledge, the picosecond laser is here used for the first time in stone conservation. Differences in efficiency and in cleaning result are shown and discussed.

1. INTRODUCTION

The use of Nd:YAG lasers as a cleaning tool for the removal of black pollution encrustation from a variety of stonework is well known, as reported in restoration studies. Nevertheless, so far, there has not been a general agreement about the best choice of laser pulse duration.

Up to a few years ago, laser cleaning of stones was mainly carried out using nanosecond (ns) pulse Q-switched (QS) Nd:YAG lasers but several research groups documented problems connected with the aggressiveness [1, 2] and the yellow appearance that QS lasers can induce on certain lithotypes [3–5]. Many technological solutions have been provided to solve the mentioned problems. In particular, the use of short free running (SFR) Nd:YAG laser systems has been proposed [2] to overcome mainly the lack of choice and the aggressiveness of QS laser on fragile stones and to avoid the yellowing of the substrate after the cleaning. In addition, a new class of fiber-coupled long Q-switched laser (LQS), with variable pulse duration from tens to hundreds of ns, has been recently used for the cleaning of metal artworks as well as for stone cleaning with satisfactory results [6].

Recently, the ultra-short laser technology was employed in various material processing applications. Studies have shown that the use of shorter pulse-widths is associated with minimal thermal and chemical induced alterations, while ensuring high spatial confinement and control [7–10]. Initial studies on the use of ultra-short laser pulses in the processing and analysis of objects with cultural and historical importance [11] have shown their unique advantages (minimal photochemical modifications to the remaining material and high precision nearly independent of the optical properties of the substrate) and thus highlight the prospective of their exploitation in demanding applications. This work attempts to assess their viability in stonework conservation and, to our knowledge, the picosecond (ps) regime is here studied for the first time for the laser cleaning of pollution encrustations.

2. EXPERIMENT

In this paper, the pulse duration effect on the laser assisted removal of pollution crusts on stonework is investigated. Laser cleaning tests with three Nd:YAG laser systems emitting infrared pulses (1064 nm) at different pulse duration (μs, ns, ps) were performed on both real black crusts on marble as well as on a reference sample with simulated thick crust. The cleaning result was comparatively assessed on the basis of the removal efficiency (etching rate) and the cleaning result (morphology and coloration of the laser cleaned surfaces).

3. MATERIAL AND METHODS

Three Nd:YAG laser systems at their fundamental wavelength (1064 nm) were used in the present study:

(1) a fiber-coupled SFR laser (El.En. EOS 1000) with a variable pulse duration between 50–130 μs for increasing output energies in the range of 120 up to 1000 mJ/pulse,
(2) a Q-switched system (SPECTRON SL805) emitting pulses of 15 ns and maximum output energy of 450 mJ, and
(3) a Q-switched system (EKPLA SL 312M) with pulses up to 120 mJ and 150 ps duration.

A reference sample simulating thick crust on stone (sample S) was used for comparison purposes. For the encrustation simulation the idea was to imitate the most common accumulation encountered on archaeological objects both in terms of composition and morphology. Therefore, it was attempted to adhere a mixture of pulverised encrustation (collected from real archaeological objects) on marble plates using gypsum as the binding medium. The composition of the layer is as follows: 49.25 wt% of pulverised encrustation from real excavation objects and 49.25 wt% of hydrated calcium sulphate ($CaSO_4$ $2H_2O$). To enhance the colour of the mixture and imitate the real case, ferrous oxide (Fe_2O_3) and carbon (C) were added in very small quantities (0.50 and 1.00 wt%, resp.). XRD analysis on the pulverised encrustation indicated the following components: sodium sulphate (Na_2SO_4), magnesium sulphate hydrate ($MgSO_4$ $6(H_2O)$), picromerite ($K_2Mg(SO_4)_2$ $6H_2O$), syngenite ($K_2Ca(SO_4)_2$ H_2O), gypsum ($CaSO_4$, $2H_2O$) and calcium carbonate ($CaCO_3$). The above mixture was applied wet by brushing in several layers on the freshly cut marble tablets in order to obtain a maximum thickness of about 1.5 mm.

For the characterization study, some fragments coming from a *tortile* column from Florence's cathedral (samples R) were selected. The composition and morphology of the black encrustation accumulated on the surface as well as the stratigraphy of the various layers and the decision of the cleaning limit on these fragments are discussed in previous studies [6, 12].

The ablation trials were performed both in dry and wet (water-assisted) conditions. The laser spot was maintained constant throughout the tests, while the fluence variation was achieved using the appropriate optical attenuators. Etch depth measurements, performed after laser ablation, were carried out using a mechanical stylus profilometer (Perthometer S5P, Mahr). Scanning electron microscopy (SEM) observations were performed with a Quanta FEI 200 instrument.

4. RESULTS AND DISCUSSION

4.1. Ablation rates

Figure 1 displays the ablation rate curves attained for the artificial samples. The measurements were performed both in dry and wet conditions. The behavior of the ablation rates is similar to the typical one of thermal ablation, which is characterized by a threshold fluence F_{th}, a linear regime and, in some cases, a saturation fluence F_s.

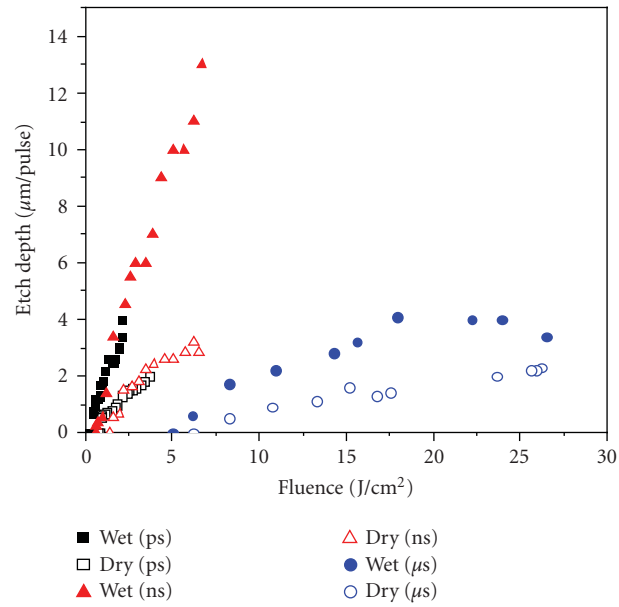

FIGURE 1: Ablation rate curves obtained for the artificial sample using Nd:YAG laser pulses at 1064 nm at three different pulse duration regimes.

From the observation of the different curves, it is noticed that, regardless the pulse duration, the ablation in wet conditions is more efficient than in the dry ones. Water penetrates into the black crust's pores and the fast heating of the liquid film, due to the absorption of energy from the laser pulse, leads to an explosive vaporisation of the water molecules. This explosion generates additional forces within the encrustation which make the ejection of the dirt particles more effective [13].

From the graph it can be also derived that the etching process is more efficient, at equal fluences, for shorter pulse lengths. The shorter the pulse duration, t_L, the shorter the thermal diffusion length $2\sqrt{Dt_L}$ in the substrate, where D is the material diffusivity. This means that with shorter pulses less energy is needed to reach the explosive vaporisation. On the other side, the slope of ablation curves associated to shorter pulses is steeper and this behavior leads to a less controllable cleaning process because a small increasing of fluence values results in a higher difference in material removal.

Another important result deals with the ablation threshold, which plays a fundamental role in the optimisation of the cleaning process. From Figure 1 and from the detail of Figure 2, it can be noticed that the ablation threshold increases with increasing pulse duration and thus higher fluence values are required when cleaning with longer pulsewidths.

The experimental threshold values are shown in Table 1.

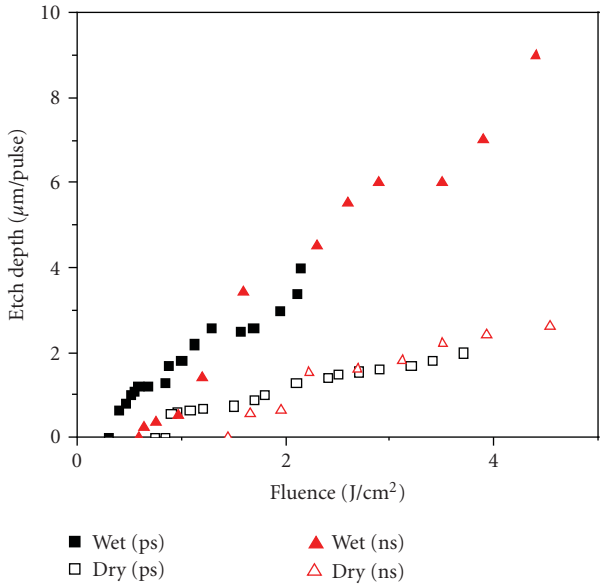

Figure 2: Detail of the ablation curves for the ns and ps regimes for Sample S.

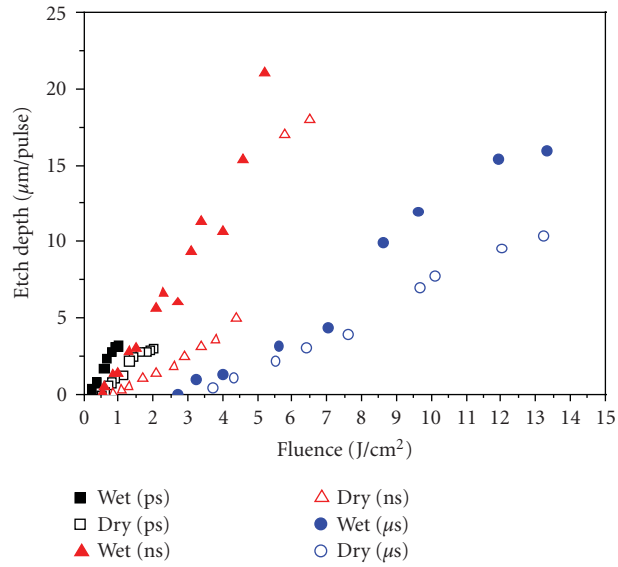

Figure 3: Ablation rate curves obtained for the real black crust (Sample R) using Nd:YAG laser pulses at 1064 nm at three different pulse duration regimes.

Table 1: Experimental threshold fluence values as derived from the measurements on the artificial sample.

Pulse duration	Conditions	F_{th} (J/cm^2)
90 μs	Wet	5.0
90 μs	Dry	6.2
15 ns	Wet	0.6
15 ns	Dry	1.4
150 ps	Wet	0.3
150 ps	Dry	0.8

Table 2: Experimental threshold fluence values as derived from the measurements on the real crust.

Pulse duration	Conditions	F_{th} (J/cm^2)
90 μs	Wet	2.70
90 μs	dry	3.50
15 ns	Wet	0.56
15 ns	dry	0.86
150 ps	Wet	0.20
150 ps	Dry	0.50

In Figure 2, a detail of the curves for the picosecond and nanosecond regimes is displayed. For low fluences, close to the ablation threshold, it seems that the ps pulses remove more material than the ns ones (especially in wet conditions) but, after a critical point (~1.6 J/cm^2 for both wet and dry irradiation), where the two curves are crossing, the removal rate is more or less the same.

Figure 3 displays the ablation rate curves obtained for the real black crust (Sample R). The measurements have been performed both in dry and wet conditions. The behavior of the curves is similar to that attained for the simulation samples.

From the observation of the different curves, it is noticed that, for the real crust too, the ablation in wet conditions is more efficient than in the dry ones. The increasing of the ablation threshold with the pulse duration is still present and the cleaning efficiency is higher for shorter pulse durations. The experimental threshold values are reported in Table 2.

A close inspection of the ps and ns ablation curves is displayed in Figure 4.

From Figure 4, it is clear that for low fluence values, close to the ablation threshold, ps pulses are, as expected, more efficient to remove the crust material both in wet and dry conditions. Unfortunately for this specific sample, composition and morphology of encrustation etch depth studies in the ps regime were stopped at 2 J/cm^2 (dry condition) and 1.5 J/cm^2 (wet condition) because, above these values, the underlying sample surface was starting to get visibly damaged. As a result, it is not possible to compare the ablation efficiency of ps and ns regimes for higher fluence values.

Comparing the etch depth attained for the artificial sample and for the real crust it is shown that, at the same fluence and for the same pulse duration and irradiation conditions, a larger amount of material is removed in the real black crust. The corresponding etch depths obtained for fluence values of about 1 J/cm^2 for ps and ns pulses both in wet and dry conditions are presented in Table 3. It should be taken into account that the real black crust is quite heterogeneous, both in thickness and in consistency and appears "softer" than the artificial crust.

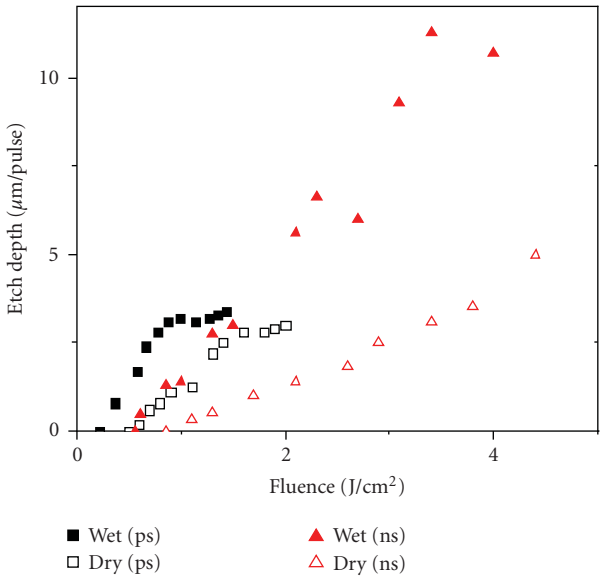

Figure 4: Detail of the ablation curves for the ns and ps regimes for Sample R.

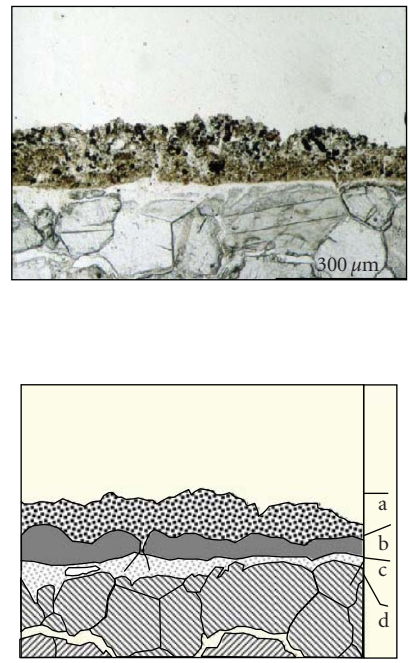

Figure 5: Stratigraphy of the tortile column. (a) Black crust, (b) Ca-oxalate film, (c) surface pseudomorphic sulphation, (d) substrate. The scale bar is 300 μm.

Table 3: Comparative etch depth values for the simulation (S) and the real (R) encrustation for fluence values of about 1 J/cm^2, in ps and ns cleaning regime for wet and dry irradiation conditions.

Pulse duration	Conditions	Sample	Etch depth (μm/pulse)
150 ps	Wet	S	1.8
150 ps	Wet	R	3.2
15 ns	Wet	S	0.5
15 ns	Wet	R	1.4
150 ps	Dry	S	0.6
150 ps	Dry	R	1.25
15 ns	Dry	S	No ablation (F_{th} = 1.4 J/cm^2)
15 ns	Dry	R	0.3

The cleaning problem

The stratigraphy of the *tortile* column is shown in Figure 5 [6]. From the outer to the inner layers, black crust, sulphated Ca-oxalate film, and surface pseudomorphic sulphation can be observed. The Ca-oxalate film includes a pigment load formed by ochres and black carbon. Cleaning trials were performed on the column using the three different laser systems in wet conditions. The fluence values used were as follow:

(i) 3.9 J/cm^2 and 9 J/cm^2 at 90 μs,
(ii) 0.85 J/cm^2 and 1.4 J/cm^2 at 15 ns, and
(iii) 0.55 J/cm^2 at 150 ps,

corresponding to values just above and well above the threshold values for each laser as measured through this study.

In Figure 6, three SEM images of the surface after cleaning with the three lasers are displayed.

In every case, the surface appears quite smooth and there is no evidence of mechanical damages. To the naked eye, very small colour differences were observed in the three different treated parts. The cleaning result is satisfactory in all conditions, taking into account the deteriorated state of the original surface of the column, which was most probably weathered before the black crust was deposited.

4.2. Degree of cleaning

In Figure 7, the stratigraphies of the treated parts are displayed, showing the final cleaning level achieved on the column using the three different laser systems.

The black crust was completely removed in all cases. The main differences among the three stratigraphies lay in the degree of removal of the Ca-oxalate layer and in the roughness of the cleaned surface. The surfaces treated with the different lasers appear smooth and the cleaning results effective but careful (Figures 7(a)–7(c)). In the area cleaned with the SFR-μs laser, the Ca-oxalate layer is clearly preserved (see, Figure 7(a)). The final surface is smooth and very homogeneous.

On the other hand, throughout this study, shorter pulsewidths did not result in similar cleaning effect as regards the Ca-oxalate layer. This result is under further investigation as it has often been reported in the literature that Ca-oxalate layers have been successfully preserved using Q-switched

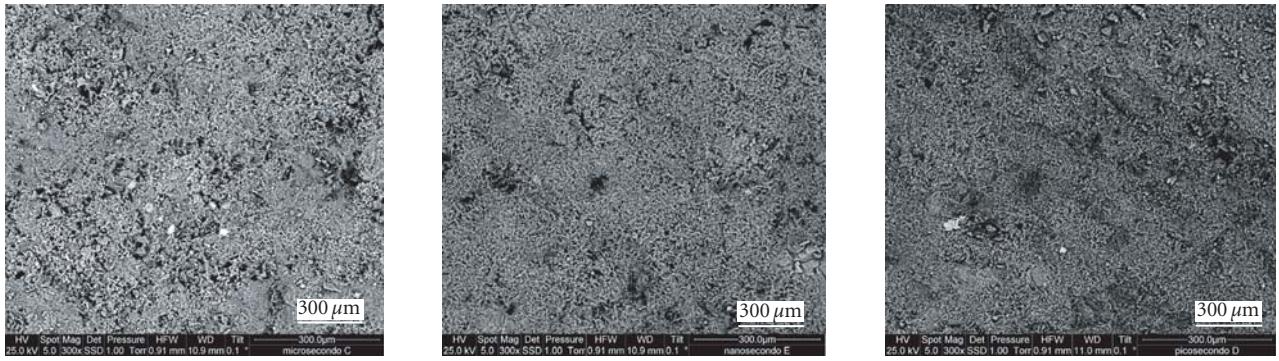

(a) (b) (c)

FIGURE 6: SEM pictures of the treated surface. (a) 90 μs ($F_L = 3.9\,\text{J/cm}^2$), (b) 15 ns ($F_L = 1.4\,\text{J/cm}^2$), and (c) 150 ps ($F_L = 0.54\,\text{J/cm}^2$).

(a) (b) (c)

FIGURE 7: Stratigraphies of the treated parts on sample R. (a) 90 μs ($F_L = 3.9\,\text{J/cm}^2$), (b) 15 ns ($F_L = 0.85\,\text{J/cm}^2$), (c) 150 ps ($F_L = 0.54\,\text{J/cm}^2$) (10× magnification).

Nd:YAG lasers in the ns regime, including the laser cleaning of the Parthenon West Frieze. The "ancient monochromatic surface layers," rich in Ca-oxalates, which uniquely characterize the sculpted surface of the Frieze were perfectly preserved during laser cleaning, using QS-ns pulses at 1064 nm in the range of 0.5–0.8 J/cm^2 [14]. This may be explained by the fact that the original surface of the column was deteriorated and in several areas the black crust was formed on already weathered surface. As it is very difficult to discern the existence of the Ca-oxalate layers beneath the thick black crust prior to cleaning, it may be possible that the comparative studies were performed on areas where Ca-oxalate layers were not uniformly preserved. Therefore, further studies must be undertaken to prove the initial experiments.

It is worth noticing that in the case of ns cleaning the fluence window to eliminate this kind of encrustation is very small: the use of a slightly higher fluence ($F_L = 1.4\,\text{J/cm}^2$) caused, indeed, an unacceptable etching of the marble substrate (Figure 8(a)). In contrast, laser cleaning trials in the μs regime at fluence values significantly higher than the threshold (9.0 J/cm^2, about three times the threshold value) did not cause any damage to the substrate, including the Ca-oxalate layers (Figure 8(b)). Therefore, it can be said that the "safe" fluence window for longer pulse durations is significantly bigger, allowing more flexibility to the operator and less possibilities to cause side effects on the original stone surface.

5. CONCLUSIONS

This work provides a characterization of the effects involved in laser cleaning of stonework under different operative conditions. Three Nd:YAG laser systems have been used having various pulse durations: 150 ps, 15 ns, 90 μs. The differences among ablation rates in dry and wet conditions, the degree of cleaning, and the appearance of the treated surface were characterized by using simulation samples and a stone artefact exposed outdoors. It was shown that, regardless the pulse duration, the cleaning in wet condition is more efficient than the dry one. In addition, the etching is more efficient, at equal fluences, for shorter pulse lengths. The ps laser, which was used here for the first time in cleaning of pollution crusts from stonework, did not cause any mechanical damage to the treated surface, but the fluence has to be kept quite low. The QS-ns laser was very effective in the removal of the black crust but the operative fluence window is very small: it is necessary to use a low fluence, very close to the threshold one, to avoid mechanical damages to the substrate. The SFR-μs laser, which was specifically designed for the cleaning of stonework, did not cause any thermal or mechanical damage to the surface even at high fluences. Throughout this study, the Ca-oxalate layer was better preserved with the SFR-μs laser and further studies are underway to confirm this

(a) (b)

FIGURE 8: Stratigraphies of the treated parts on sample R. (a) 15 ns ($F_L = 1.4\,\text{J/cm}^2$), (b) 90 μs ($F_L = 9.0\,\text{J/cm}^2$) (20× magnification).

result and explain the mechanisms that may influence such behavior.

ACKNOWLEDGMENTS

The first author acknowledges support from the "ATHENA" EST Marie Curie project (MEST-CT-2004-504067) at IESL-FORTH. The authors would also like to thank G. Doganis and A. Galanos (Lithou Sintirissis Inc. Conservation Associates, Athens, Greece) for fruitful discussions on the morphology and simulation of stonework encrustations and for the preparation of the reference samples with simulated crust.

REFERENCES

[1] M. S. D'Urbano, C. Giovannone, P. Governale, A. Pandolfi, and U. Santamaria, "A standardized methodology to check the effects of laser cleaning of stone surfaces," in *Proceedings of the 3rd International Symposium on the Conservation of Monuments in the Mediterranean Basin*, V. Fassina, H. Ott, and F. Zezza, Eds., pp. 955–962, Venice, Italy, 1994.

[2] S. Siano, F. Margheri, P. Mazzinghi, et al., "Laser ablation in the artworks restoration: benefits and problems," in *Proceedings of International Conference on Lasers*, vol. 18, pp. 441–444, Charleston, SC, USA, December 1995.

[3] P. Bromblet, M. Labouré, and G. Orial, "Diversity of the cleaning procedures including laser for the restoration of carved portals in France over the last 10 years," *Journal of Cultural Heritage*, vol. 4, supplement 1, pp. 17–26, 2003.

[4] V. Vergès-Belmin and C. Dignard, "Laser yellowing: myth or reality?" *Journal of Cultural Heritage*, vol. 4, supplement 1, pp. 238–244, 2003.

[5] G. Marakis, P. Pouli, V. Zafiropulos, and P. Maravelaki-Kalaitzaki, "Comparative study on the application of the 1st and the 3rd harmonic of a Q-switched Nd:YAG laser system to clean black encrustation on marble," *Journal of Cultural Heritage*, vol. 4, supplement 1, pp. 83–91, 2003.

[6] S. Siano, R. Salimbeni, A. Mencaglia, et al., "Phenomenological characterisation of stone cleaning by different laser pulse duration and wavelength," in *Proceedings of the 6th International Congress on Lasers in the Conservation of Artworks (LACONA VI '05)*, Vienna, Austria, September 2005.

[7] D. Bäuerle, *Laser Processing and Chemistry*, Springer, Berlin, Germany, 2000.

[8] S. Küper and M. Stuke, "Ablation of polytetrafluoroethylene (Teflon) with femtosecond UV excimer laser pulses," *Applied Physics Letters*, vol. 54, no. 1, pp. 4–6, 1988.

[9] J. K. Frisoli, Y. Hefetz, and T. F. Deutsch, "Time-resolved UV absorption of polyimide. Implications for laser ablation," *Applied Physics B*, vol. 52, no. 3, pp. 168–172, 1991.

[10] S. Küper and M. Stuke, "Femtosecond UV excimer laser ablation," *Applied Physics B*, vol. 44, no. 4, pp. 199–204, 1987.

[11] P. Pouli, G. Bounos, S. Georgiou, and C. Fotakis, "Femtosecond laser cleaning of painted artefacts; is this the way forward?" in *Proceedings of the 6th International Congress on Lasers in the Conservation of Artworks (LACONA VI '05)*, Vienna, Austria, September 2005.

[12] R. Salimbeni, R. Pini, and S. Siano, "Achievement of optimum laser cleaning in the restoration of artworks: expected improvements by on-line optical diagnostics," *Spectrochimica Acta—Part B: Atomic Spectroscopy*, vol. 56, no. 6, pp. 877–885, 2001.

[13] M. Cooper, *Laser Cleaning in Conservation: An Introduction*, Butterworth Heinemann, Oxford, UK, 1998.

[14] P. Pouli, K. Frantzikinaki, E. Papakonstantinou, V. Zafiropulos, and C. Fotakis, "Pollution encrustation removal by means of combined ultraviolet and infrared laser radiation: the application of this innovative methodology on the surface of the Parthenon West Frieze," in *Proceedings of the 5th International Congress on Lasers in the Conservation of Artworks (LACONA V '03)*, K. Dickmann, C. Fotakis, and J. F. Asmus, Eds., vol. 100 of *Springer Proceedings in Physics*, pp. 333–340, Osnabrueck, Germany, September 2003.

Hindawi Publishing Corporation
Laser Chemistry
Volume 2006, Article ID 75831, 7 pages
doi:10.1155/2006/75831

Research Article

Laser Cleaning Tests on Archaeological Copper Alloys Using an ND:YAG Laser

Capucine Korenberg and Alexandra Baldwin

Department of Conservation, Documentation and Science, The British Museum, Great Russell Street, London WC1B 3DG, UK

Received 14 September 2006; Revised 3 November 2006; Accepted 6 November 2006

Recommended by Costas Fotakis

Laser cleaning tests were performed on five archaeological copper alloy objects using a Q-switched Nd:YAG laser at 1064 nm. As a comparison, a section of each object was cleaned mechanically. Prior to cleaning, cross-sections were prepared to characterise the corrosion crust and help to locate the position of the original surface. Laser cleaning was not successful at removing burial deposits on two of the objects. For the other three objects, the laser removed most of the corrosion crust. This was not always satisfactory, as cleaning was sometimes accompanied by the loss of the original surface. In addition, laser-cleaned surfaces were matt compared to mechanically cleaned surfaces. In some instances, the former had a disfiguring purple hue which was attributed to the formation of particles that could be seen when examining the surface using scanning electron microscopy. For all the objects examined here, superior results were obtained by mechanical cleaning.

1. INTRODUCTION

The British Museum holds many archaeological metal artefacts within its collections. Most metal finds are covered by corrosion crusts that may have to be removed and the present study is focused on the cleaning of archaeological copper alloys. The formation of corrosion products on archaeological copper alloys can be complex and differ according to the burial environment and composition of the metal [1–4]. For example, in the case of bronzes, a selective copper dissolution often takes place leaving the outer corrosion layers of archaeological bronzes enriched in tin [5, 6] and brasses with substantial amounts of zinc are known to lose zinc through dezincification [2]. A detailed review of the corrosion process in copper alloys is beyond the scope of the present paper and only a schematic description of the process for pure copper is presented here. Throughout the lifetime of an object, the surface oxidises producing a very thin compact corrosion layer. During burial, the copper under the surface is further attacked and intergranular corrosion occurs. A compact layer of cuprite, Cu_2O, forms along the grain boundaries, filling the voids. This layer is called the "primary" cuprite layer. As corrosion progresses, the metal core reduces in size becoming pitted and formless. This is accompanied by the migration of copper ions through the primary cuprite layer and the formation of secondary corrosion products such as cuprite, malachite, and basic copper chlorides [1, 2]. The outer-most layers of corrosion often incorporate minerals and quartz grains from burial deposits [2]. Variation in burial environments will produce additional areas of different compounds, including sulphides and chlorides.

In this context, cleaning is defined as the beneficial removal of altered material originating from the object or externally deposited material. Archaeological metals are usually not cleaned back to the metal surface as, in the majority of cases, the metal core will be shapeless. Instead, the "original surface" is sought. In conservation, the term original surface denotes a layer within the corrosion products where decoration, tool marks, or evidence of wear can be found. The position of the original surface in copper alloy corrosion crusts varies depending on the condition and state of mineralisation of the object and can be anywhere in the corrosion crust. Detection of the original surface in the layers of corrosion can be difficult, but it is often a more or less continuous compact layer, which differentiates it from the less dense secondary corrosion products. The original surface retained in the mineralised deposits often has a smooth, even, and lustrous surface from original finishing of the object or due to

polishing throughout its useful life. Conservation cleaning does not aim to remove every trace of corrosion overlying the surface, but to reveal and preserve the original surface. Overcleaning can lead to removal of intergranular corrosion or disruption of the original surface creating a matt appearance. The choice of cleaning method for a particular object has to be assessed by conservators in terms of risk and benefit to the object, as no method currently in use is 100% successful. Chemical cleaning methods are not easily controlled and can be unpredictable, usually resulting in the loss of the original surface. Air abrasive, whilst useful, is often difficult to control and can produce a matt surface. The most accurate and adaptable method for archaeological copper alloys is mechanical cleaning using a scalpel. However, mechanical cleaning can take a long time and damage can occur either through breakage due to pressure applied to the object or scratching of the surface.

2. EXPERIMENT

Laser cleaning has gained considerable success as a valuable method of conservation since the 1970s and often has the advantage of being faster than conventional techniques, while producing equal or superior results on certain materials (e.g., [7]). Recently investigations of the use of the Nd:YAG laser to remove corrosion crusts on archaeological copper alloy artefacts have taken place. The results of these investigations have been varied. Pini et al. [8] laser-cleaned 16 bronze objects covered by green calcareous accretions and silicates, preserving the oxidation layer beneath. The Nd:YAG lasers used in their study had a pulse duration of either 20 μs or 2–10 ns, and Pini et al. report that long pulses were more efficient at removing thick encrustations than short pulses. They sometimes observed discolourations on the surface of calcareous encrustations, which changed from green to grey or red. This was not considered a problem since all the objects were cleaned down to the cuprite layer, where no colour change ever took place. A comparison was done with mechanical cleaning on one of the objects and the authors report that manual cleaning was more time-consuming and did not produce the same homogeneity of cleanliness as laser cleaning. In another study, Batishche et al. [9] have performed successful removal of corrosion layers from a bronze fastener to reveal surface detail and decoration using a combination of ND:YAG lasers with pulse durations of either 100–120 μs or 15 ns. They did not report any side effects from laser cleaning. Drakaki et al. [10] have laser-cleaned two Roman coins using a Q-switched Nd:YAG laser operating at 532 nm and 0.4 J/cm^2. On the first coin, the surface obtained was rather smooth with a bright colour and, from the photograph published, surface detail was lost. For the other coin, the laser-cleaned surface was smooth but had a dark colour, which was deemed less satisfactory. Although these three studies indicate that laser cleaning is successful at removing corrosion layers, none of them clearly assessed where the original surface of the objects lay and whether it was preserved by laser cleaning. The original surface does not always lie at the primary cuprite layer and it has not been demonstrated that laser cleaning is successful at retaining surfaces above this.

Figure 1: Objects after cleaning: the left side of each object has been laser-cleaned and the top right has been mechanically cleaned. The bottom right side was left uncleaned.

Descriptions of success or failure can be subjective depending on expectation and cleaning requirement. Systematic comparison with mechanical methods is also required so that the results can be objectively assessed before application.

The British Museum has recently acquired an Nd:YAG laser and the present study forms part of ongoing research into its use in cleaning metal artefacts in the Museum's collection. In particular, the aims of the current work were to look in more detail at the effects of laser on archaeological copper alloy in relation to its practical use in conservation, and add to the body of work in this field. The use of the laser has interesting possibilities as an alternative low contact cleaning method and the parameters of the laser require assessment before application on registered museum objects. Laser cleaning tests were performed on several archaeological copper alloy objects using an Nd:YAG laser and whether the laser treatment preserved the original surface was carefully assessed. In addition, mechanical cleaning was conducted as a comparison.

3. MATERIALS AND METHODS

3.1. Samples

As it is not possible to produce in the laboratory corrosion crusts similar to those present on archaeological objects, tests were performed on five unregistered archaeological copper alloy objects of unknown provenance (see Figure 1). Except for Object 1, the corrosion crust on each object was relatively thin and appeared homogeneous across the surface of the object. All the objects were covered by silicaceous burial deposits.

Prior to cleaning, analyses were performed to determine the composition of the alloys and the corrosion layers. Sections of each object were removed using an Isomet

saw, embedded in an epoxy resin, ground on carborundum paper and polished with diamond pastes of 6 μm and 1 μm. X-ray fluorescence (XRF) analyses were carried out on the uncorroded metal core of the objects using an ArtTAX spectrometer (voltage 50 kV and current 0.80 mA) and the results are shown in Table 1. The corrosion layers were examined in cross-section using polarised light microscopy, Raman spectroscopy, scanning electron microscopy (SEM), and energy dispersive X-ray analysis (EDX) to help in locating the position of the original surface. It should be noted that oxygen is easily detected using EDX and all the corrosion crusts were found to contain significant amounts of oxygen. However, the amount of oxygen calculated from the EDX analysis cannot be considered reliable due to inherent difficulties in calculating the background correction. Therefore, oxygen was not included in the calculations of the relative amounts of present elements. Also, it was not always possible to obtain Raman spectra of the compounds present in the corrosion crusts although most corrosion products are Raman active. This could be because corrosion products on archaeological metals are often poorly crystallised [6]. The results of the analyses are reviewed for each object in turn.

Table 1: Composition of uncorroded metal core determined using XRF. (The results should have an accuracy of c. ± 1-2% for copper and c. ± 5–10% (relative) for tin, zinc, and lead when present above 10% in a copper alloy, deteriorating to c. ± 20–30% (relative) when present above 1% but below 10%.)

Object	Composition (% wt)
1	86% Cu, 13% Sn, 1% Pb
2	77% Cu, 20% Zn, 3% Pb
3	87% Cu, 5% Pb, 5% Sn, 2% Zn, traces
4	73% Cu, 20% Zn, 7% Pb
5	78% Cu, 21% Zn, 1% Sn

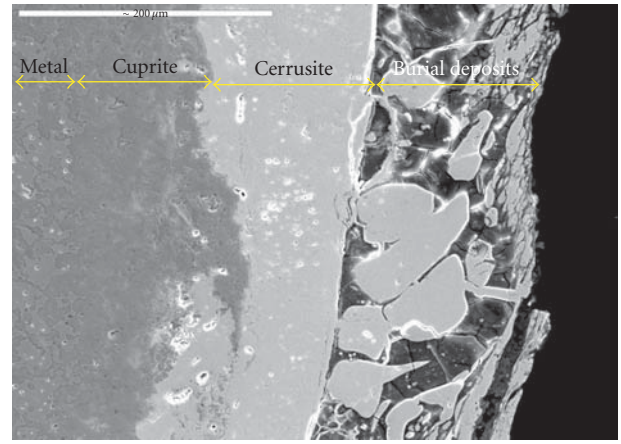

Figure 2: SEM picture of the cross-section of Object 3, showing the corrosion layers before cleaning. The core metal and the primary cuprite layer are located on the left of the picture. The light grey layer in the middle of the section is cerrusite and to its right is a corrosion layer containing particles of cerrusite and burial deposits. The original surface is at the top of the cerrusite layer. (Length of scale marker is 200 μm.)

Object 1

Analysis of Object 1 indicated that this is a leaded tin bronze. The corrosion crust on this object was uneven, with areas covered by either a thin corrosion crust or warts. The section was taken on an area covered by a thin corrosion crust. Next to the metal core was a very thin layer of oxidised metal and, beyond this, a thick corrosion layer containing mostly copper and silicon with small amounts of iron and aluminium. The Raman spectrum obtained for this layer suggested the presence of chrysocolla, $(Cu, Al)_2H_2Si_2O_5(OH)_4 \cdot xH_2O$. The original surface appeared to be just above the metal oxide layer.

Object 2

Object 2 is a leaded brass. There was a layer of cuprite next to the metal core, followed by three homogeneous layers. The layer immediately above the cuprite contained mostly copper, but also silicon and traces of zinc. The second layer had a similar composition as the first layer, but contained slightly less silicon and also small amounts of tin and iron. The outer layer contained mostly copper and silicon, with small amounts of iron and zinc. Chrysocolla was possibly present in this layer. The original surface appeared to lie just above the cuprite layer.

Object 3

Object 3 is a bronze containing copper, lead, tin, and zinc. Adjacent to the metal core is a layer of cuprite and possibly cassiterite. As distinct from the other objects, Object 3 has a compact layer of cerrusite which is not homogeneous across the surface of the object but interrupted by discrete areas of cuprite and malachite. The presence of cerrusite has been reported on archaeological bronze artefacts rich in lead (e.g., [11]). The outermost layer of corrosion was complex containing large amounts of lead, oxygen, and copper, as well as particles of cerrusite and burial deposits. The original surface lies at the top of the compact cerrusite layer, see Figure 2.

Object 4

The metal core of Object 4 is leaded brass. The corrosion layer next to the core contained cuprite. Above the cuprite was a layer containing copper, silicon, phosphorous, and lead. Raman spectroscopy showed the presence of malachite and possibly chrysocolla. The outermost layer contained inclusions of silica, copper, iron, lead, and phosphorous and is probably corrosion mixed with deposits from burial. The original surface of the object was at the top of the malachite rich layer.

Table 2: Parameters used for the laser cleaning.

Object	Fluence	Condition
1	400 mJ/cm^2	No water
2	400 mJ/cm^2	Immersed in water prior to cleaning
3	240 mJ/cm^2	Immersed in 50/50 water/IMS* prior to cleaning
4	900 mJ/cm^2	No water
5	600 mJ/cm^2	Water applied on surface

*IMS= industrial methylated spirits.

Object 5

Object 5 is a brass containing copper, zinc, and tin. Next to the core lies a very thin layer of cuprite with traces of zinc and tin. The adjacent corrosion layer contained a large amount of copper, silicon, tin, and phosphorous. It was found to contain malachite and possibly chrysocolla. The original surface of the object appears to be contained in this layer.

3.2. Methods

For the cleaning tests, the top surface of each object was divided into three areas: half of the surface was treated by laser, a quarter was left untreated, and the remaining quarter was cleaned mechanically. The laser used was a Lynton Phoenix Athena laser (wavelengths: 532 and 1064 nm, pulse duration: 5–10 ns). Only the 1064 nm wavelength was used in the present work as preliminary tests at 532 nm indicated that the cleaning process was extremely slow, making the use of laser at this wavelength impractical. The fluence used varies considerably, as each laser cleaning test was performed at the minimum fluence at which the overlying soil deposits could be removed on each sample object. Once the working energy levels had been established, the laser spot area was estimated by taking a burn pattern on a photographic paper and the average fluence was calculated by dividing the energy per pulse by the laser spot area. To achieve an even clean, the pulses were overlapped slightly, therefore only a few pulses per area were applied to the surface. A liquid was applied to the surface of some of the objects while using the laser, as this has been reported to improve the laser cleaning of metals (see, e.g., [10, 12–14]). Some objects were immersed in a liquid prior to testing to increase penetration into the corrosion crust. The parameters used for the laser cleaning of each object are summarised in Table 2. Mechanical cleaning was performed with a scalpel fitted with a Swann-Morton No.15 stainless-steel blade under ×40 magnification. All the objects were more time consuming to clean mechanically compared to the laser treatment.

After the cleaning tests, the treated surfaces were examined using an optical microscope (up to ×60 magnification). The corrosion crusts and the cleaned surfaces were examined using SEM-EDX and Raman spectroscopy. EDX spectra were measured using a JEOL JSM840 scanning electron microscope with an Oxford Instruments ISIS EDX analyser. Raman spectroscopy was carried out using a Jobin Yvon LabRam Infinity spectrometer with a green laser with a wavelength of 532 nm. Spectra were measured in the 100–1600 cm^{-1} region with a resolution of 2 cm^{-1}. Each spectrum was collected for between 10 and 60 seconds and at least five repetitions were used to produce a spectrum.

4. RESULTS AND DISCUSSION

4.1. Results of cleaning tests

Where the laser cleaning had been successful at removing burial deposits, the laser-cleaned surface was analysed using SEM-EDX and Raman spectroscopy (see Table 3 for the results of the SEM-EDX analyses). The results are reviewed for each object in turn.

Object 1

It could be observed with the naked eye that, unlike mechanical cleaning, the laser treatment had not removed the burial deposits from Object 1 completely. Due to the uneven thickness of the corrosion crust on this object, it was not possible to remove the warts during the laser cleaning tests without exposing the core metal in adjacent areas covered by thinner corrosion layers. The dendrite structure of the metal was also exposed as the laser had removed the intergranular corrosion. Slight discolouration to the cuprite layer was also noted under high magnification. As no liquid was used during laser cleaning on Object 1, it was investigated whether using a liquid would improve the cleaning process. Laser cleaning tests were done on the back of the object using water, but it was still not possible to remove the burial deposits. This is in agreement with the work of Degrigny et al. [15] who reported that using a liquid did not have any effect when laser cleaning tarnished silver threads.

Object 2

When the cross-section of Object 2 was examined using SEM-EDX prior to cleaning, it was found that the metal core was covered by several layers of corrosion, with the outermost layers containing small amounts of iron. It appeared that the original surface lies just above the primary cuprite layer. The laser treatment removed the burial deposits from Object 2, but the laser-cleaned surface had a matt appearance, which was very different from the lustrous surface obtained by mechanical cleaning, suggesting that the original surface had been removed. This can be seen in Figure 3 where original tool marks on the surface are less visible in the laser-cleaned areas. In addition, it was observed using an optical microscope that the laser had uncovered the core metal in a few very small areas (approximately 1 mm in size). This could be due to the hot spots in the laser beam or heterogeneities in the corrosion products. When analysing the laser-cleaned surface using SEM-EDX, the copper content was high and no iron was detected (see Table 3). In contrast, the presence of iron on the mechanically cleaned surface and relatively low copper content suggest that not all the outer-most corrosion

Table 3: SEM-EDX analyses for the mechanically cleaned surface and laser-cleaned surface for the objects, on which laser cleaning was successful at removing burial deposits.

Object	Mechanical cleaning (% wt)	Laser cleaning (% wt)
2	53% Cu, 19% Si, 16% Zn, 5% Pb, 3% Fe	88% Cu, 3% Si, 4% Zn, 5% Pb
3	7% Cu, 93% Pb	52% Cu, 38% Pb, 10% Sn
5	64% Cu, 28% Si, 3% Ca, 3% Fe, 2% P	92% Cu, 2% Si, 6% Zn

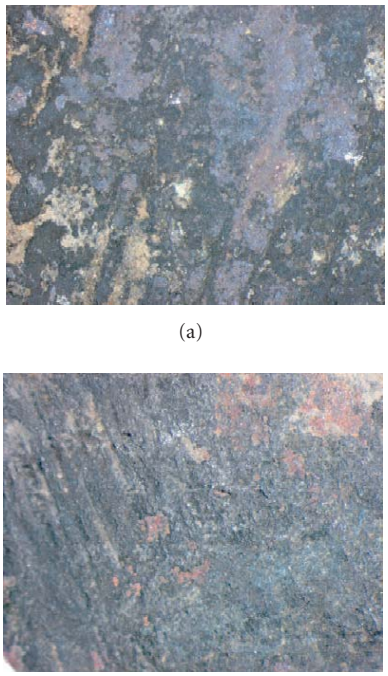

(a)

(b)

Figure 3: Cleaning results for Object 2: (a) laser-cleaned surface, (b) mechanically cleaned surface. (Horizontal field of view is 9 mm.)

layers have been removed. This indicates that, unlike mechanical cleaning, the laser has removed the outer-most corrosion layers and possibly some of the original surface. Some areas cleaned by the laser had become very dark compared to the mechanically cleaned surface, while others had a slightly purple hue. This is illustrated in Figure 3. Purple/blue tinges on oxidised copper plates irradiated by a Q-switched Nd:YAG laser have been reported by Kearns et al. [16]. Peaks at 301 and 624 cm^{-1} in the Raman spectrum on some areas of the laser-cleaned surface suggest the presence of tenorite, CuO. Tenorite forms at temperatures between 400 and 600°C and laser irradiation has been reported to cause the oxidation of cuprite to tenorite [16].

Object 3

The corrosion crust on Object 3 was different from that on the other objects as it contained cerrusite. When analysing the cleaned surfaces, the amount of lead was much lower on the laser-cleaned surface than on the mechanically cleaned surface (see Table 3). In addition, cuprite and cerrusite were detected by Raman spectroscopy on most of the laser-cleaned surface, whereas only cerrusite was detected on the mechanically cleaned surface. This indicates that, although a thin layer of cerrusite has been left by the laser treatment, most of the compact cerrusite layer, and therefore the original surface, have been removed. Also, the laser-cleaned surface was matt compared to the lustrous surface uncovered by mechanical cleaning further suggesting overcleaning and damage to the surface.

Object 4

The malachite rich layer on this object should be retained during cleaning as it is where the original surface lies. During mechanical cleaning, it was observed that the fragile original surface had been destroyed in many places by the corrosion process, but it was still possible to uncover the green corrosion layer on most of the surface. In contrast, the laser-cleaning tests were not successful as the burial deposits could not be removed completely. In the areas where the burial deposits had been removed, most of the green corrosion layer was removed by the laser and the original surface was lost in some areas down to the metal core. Cottam et al. [17] who laser cleaned a Roman bronze coin with a transverse excited atmospheric CO_2 laser emitting at 10.6 μm also reported the removal of a green corrosion layer and loss of surface details. The laser-cleaned surface of Object 4 was matt and had a distinct purple hue. The difference between the surfaces uncovered by mechanical cleaning and laser treatment is illustrated in Figure 4. As no liquid had been used while laser cleaning, a test was made on the back of the object using water. As with Object 1, the results were not significantly different from those obtained when no liquid was used.

Object 5

The green corrosion layer, which contained the original surface of Object 5, was retained during mechanical cleaning. In comparison, it was not possible to remove the burial deposits using the laser without removing the green corrosion layer, and therefore the original surface was lost. The laser-cleaned surface was mostly covered by cuprite, as identified using Raman spectroscopy and SEM-EDX. The laser-cleaned surface had a matt and slightly purple appearance.

(a)

(b)

Figure 4: Cleaning results for Object 4: (a) laser-cleaned surface, (b) mechanically cleaned surface. (Horizontal field of view is 5 mm.) Note that the purple hue of the laser-cleaned surface on Object 4 is not apparent using the microscope.

5. DISCOLOURATION

As reported earlier, there was a slightly purple discolouration to the laser-cleaned surfaces of Objects 1, 2, 4, and 5. For Objects 1 and 2, this was only on some areas, whereas on Objects 4 and 5, this was all over the laser-cleaned surface. When the green corrosion layer on the mechanically cleaned surface of Object 5 was lifted using a scalpel, it was noticed that the layer underneath the green corrosion layer had a brown colour. This shows that the unusual colour of the laser-cleaned surface has been caused by laser irradiation and was a surface effect. The discoloured areas on Objects 2, 4, and 5 were examined using SEM at a high magnification and it was observed that the purple hue was associated with the presence of particles, many of which were spherical. These are shown in Figures 5 and 6. Three spherical particles on Object 4 were analysed using SEM-EDX and found to contain copper and oxygen. The formation of particles on metals has been reported in the literature when laser cleaning tarnished copper coins [13], tarnished silver threads [15] and archaeological iron [14]. It has been suggested that this is due to the metal vaporising and being redeposited. The absence of dicolouration on Object 3 is possibly due to it being the only object with a cerrusite corrosion layer, or due to the significantly lower fluence at which it was laser cleaned (240 mJ/cm^2 compared to 400–900 mJ/cm^2 of the other objects). Pini et al. [8] and Batishche et al. [9] did not report any surface alterations at a microscopic level when cleaning archaeological copper alloys using an Nd:YAG laser at 1064 nm

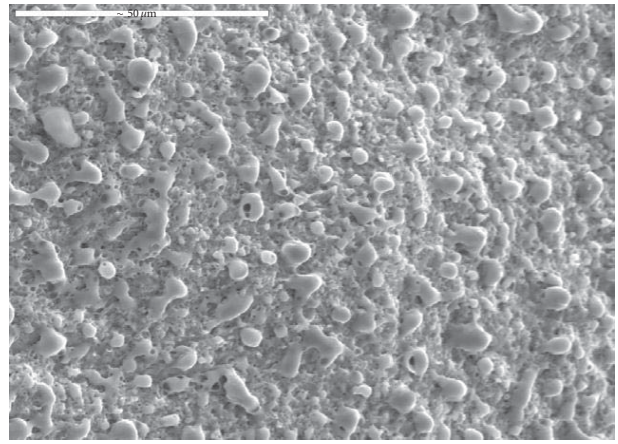

Figure 5: SEM photograph showing the presence of particles on the laser-cleaned surface of Object 5. (Length of scale marker is 50 μm.)

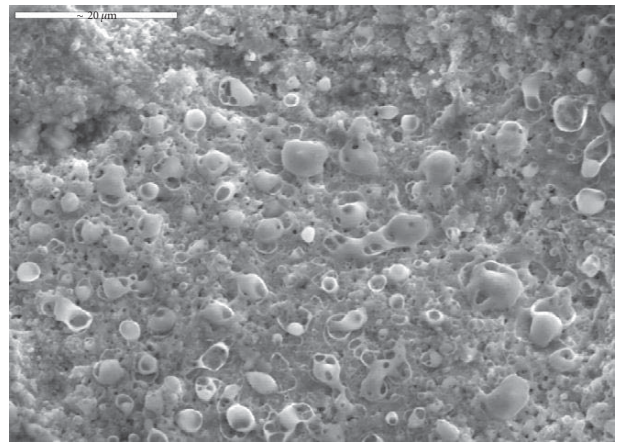

Figure 6: SEM photograph showing the laser-cleaned surface of Object 2. (Length of scale marker is 20 μm.)

and μs pulses. The use of longer pulse durations is expected to increase heat conduction to the bulk material compared to ns pulses and, as the laser-cleaned surfaces were not examined at high magnification in these studies, surface alterations may not have been detected. Alternatively, it is possible that the burial deposits on the objects cleaned in [8, 9] were very different from those examined here and could be removed at fluences that did not affect the oxidation layer.

6. CONCLUSIONS

From the results of the tests conducted, it can be concluded that the use of a Q-switched Nd:YAG laser at 1064 nm is not a suitable method of cleaning archaeological copper alloy objects. The burial deposits were hard to remove from the surface of the objects and the fluences used were different for each object probably because of the difference in

composition of burial deposits. On two of the five samples, laser cleaning was not successful at removing these incrustations. With a single laser pulse, it was not possible to control which corrosion layers were removed and which retained. The green corrosion layers containing malachite on Objects 4 and 5 were easily removed at the fluences required to clean off the burial deposits, exposing the cuprite layer, and on several objects the metal core was revealed in small areas. This resulted in uneven cleaning and loss of detail with the total removal of the original surface on those objects where it was contained within the carbonate corrosion layer. Some of the laser-cleaned sections had a disfiguring purple hue attributed to the formation of particles that could be seen when examining the surface using SEM. In all examples, the section of each object cleaned mechanically using a scalpel-produced superior cleaning results and greater retention of surface detail. Further work will be conducted to explore whether better results can be obtained using lasers with different wavelengths and pulse durations, as these parameters have been shown to affect the laser cleaning of metals (e.g., [10, 18]).

ACKNOWLEDGMENTS

The authors would like to acknowledge their colleague Quanyu Wang for useful discussions and her help with polarised light microscopy. Thanks must also be given to Leslie Webster and Barry Ager from the Department of Prehistory and Europe at the British Museum for donating the archaeological objects for the laser cleaning tests. Capucine Korenberg thanks the British Academy for awarding her an Overseas Conference Grant to attend the XI Conference on Laser Optics in St. Petersburg and present the work described in this paper.

REFERENCES

[1] J. M. Cronyn, *The Elements of Archaeological Conservation*, Routledge, London, UK, 1990.

[2] D. A. Scott, *Copper and Bronze in Art—Corrosion, Colorants, Conservation*, Getty, Los Angeles, Calif, USA, 2002.

[3] L. Selwyn, *Metals and Corrosion—A Handbook for the Conservation Professional*, Canadian Conservation Institute, Ottawa, Ontario, Canada, 2004.

[4] W. T. Chase, "Chinese bronzes: casting, finishing, patination and corrosion," in *Ancient and Historic Metals. Conservation and Scientific Research*, D. A. Scott, J. Podany, and B. B. Considine, Eds., pp. 85–117, The Getty Conservation Institute, Singapore, 1994.

[5] L. Robbiola, N. Pereira, K. Thaury, C. Fiaud, and J.-P. Labbé, "Decuprification phenomenon of Cu-Sn alloys in aqueous solution in nearly neutral pH conditions," in *Proceedings of the International Conference on Metals Conservation (Metal '98)*, W. Mourey and L. Robbiola, Eds., pp. 136–144, Draguignan-Figanières, France, May 1998.

[6] L. Robbiola, J.-M. Blengino, and C. Fiaud, "Morphology and mechanisms of formation of natural patinas on archaeological Cu-Sn alloys," *Corrosion Science*, vol. 40, no. 12, pp. 2083–2111, 1998.

[7] M. Cooper, *Laser Cleaning in Conservation: An Introduction*, Butterworth-Heinemann, Oxford, UK, 1988.

[8] R. Pini, S. Siano, R. Salimbeni, M. Pasquinucci, and M. Miccio, "Tests of laser cleaning on archeological metal artefacts," *Journal of Cultural Heritage*, vol. 1, supplement 1, pp. S129–S137, 2000.

[9] S. Batishche, A. Kouzmouk, H. Tatur, T. Gorovets, U. Pilipenka, and V. Ukhau, "Laser cleaning of metal surface—laboratory investigations," in *Proceedings of the International Conference LACONA V Lasers in the Conservation of Artworks*, K. Dickmann, C. Fotakis, and J. F. Asmus, Eds., pp. 87–93, Osnabrueck, Germany, September 2005.

[10] E. Drakaki, A. G. Karydas, B. Klinkenberg, et al., "Laser cleaning on Roman coins," *Applied Physics A: Materials Science and Processing*, vol. 79, no. 4–6, pp. 1111–1115, 2004.

[11] A. G. Nord, E. Mattsson, and K. Tronner, "Mineral phases on corroded archaeological bronze artefacts excavated in Sweden," *Neues Jahrbuch für Mineralogie Monatshefte*, vol. 6, pp. 265–277, 1998.

[12] Y. S. Koh and I. Sárady, "Cleaning of corroded iron artefacts using pulsed TEA CO_2- and Nd:YAG-lasers," *Journal of Cultural Heritage*, vol. 4, supplement 1, pp. 129–133, 2003.

[13] Y. S. Koh, "Laser cleaning as a conservation technique for corroded metal artefacts," Doctoral thesis, Lulea University of Technology, Lulea, Sweden, 2006.

[14] K. Dickmann, J. Hildenhagen, J. Studer, and E. Musch, "Archaeological ironwork: removal of corrosion layers by Nd:YAG laser," in *Proceedings of the International Conference LACONA V Lasers in the Conservation of Artworks*, K. Dickmann, C. Fotakis, and J. F. Asmus, Eds., pp. 71–77, Osnabrueck, Germany, September 2005.

[15] C. Degrigny, E. Tanguy, R. Le Gall, V. Zafiropulos, and G. Marakis, "Laser cleaning of tarnished silver and copper threads in museum textiles," *Journal of Cultural Heritage*, vol. 4, supplement 1, pp. 152–156, 2003.

[16] A. Kearns, C. Fischer, K. G. Watkins, et al., "Laser removal of oxides from a copper substrate using Q-switched Nd:YAG radiation at 1064 nm, 532 nm and 266 nm," *Applied Surface Science*, vol. 127–129, pp. 773–780, 1998.

[17] C. A. Cottam, D. C. Emmony, J. Larson, and S. Newman, "Laser cleaning of metals at infra-red wavelengths," in *Restauratrenblätter, Proceedings of the Conference LACONA I, Lasers in the Conservation of Artworks*, W. Kautek and E. König, Eds., pp. 95–98, Heraklion, Crete, Greece, October 1995.

[18] P. Mottner, G. Wiedemann, G. Haber, W. Conrad, and A. Gervais, "Laser cleaning of metal surface—laboratory investigations," in *Proceedings of the International Conference LACONA V Lasers in the Conservation of Artworks*, K. Dickmann, C. Fotakis, and J. F. Asmus, Eds., pp. 71–77, Osnabrueck, Germany, September 2005.

Hindawi Publishing Corporation
Laser Chemistry
Volume 2006, Article ID 64690, 5 pages
doi:10.1155/2006/64690

Research Article

Preliminary Laser Cleaning Studies of a Consolidated Prehistoric Basketry Coming from the Pile Building of Fiavè-Carera in the North-East of Italy

Romina Belli,[1] Antonio Miotello,[1] Paolo Mosaner,[1] Laura Toniutti,[1] and Marta Bazzanella[2]

[1] *Department of Physics, University of Trento, 38050 Povo, Trento, Italy*
[2] *Museum of Usi e Costumi della Gente Trentina, 38010 San Michele all'Adige, Trento, Italy*

Received 20 July 2006; Revised 6 November 2006; Accepted 30 November 2006

Recommended by Marta Castillejo

In the archaeological field, some specific advantages are recognized to laser cleaning, like, for example, the absence of mechanical contacts with the sample. The cleaning procedures generally involve a multilayer structure (dust, dirty, organic deposits, and, in some cases, consolidant substances). In this work, prehistoric wood samples (found and consolidated in 1970s) have been laser irradiated (KrF excimer laser) in order to restore their original surface aspect. A certain amount of burned matter was also present. Samples came from a fragment of a prehistoric basketry found in the lake dwelling site of Fiavè-Carera, Trento, Italy (1500–1400 BC). It was observed that the laser cleaning effects are strictly dependent on the irradiation parameters (power density and number of pulses). Efficient material removal was possible by using appropriate energy density. Moreover, for lower laser energy density, special structures appeared on the surface of the consolidating substance that we attributed to heating-induced stresses on the consolidant surface.

1. INTRODUCTION

The present research activity belongs to a cooperation project between the Department of Physics of Trento University and the Museum "degli Usi e Costumi della Gente Trentina" of San Michele all'Adige (North-East Italy); new techniques are tested in preservation of cultural heritage.

A fragment of basketry (Figure 1), recovered from the prehistoric lake dwelling site of Fiavè-Carera (the site was excavated just in those years by archaeologist Renato Perini of Museo Tridentino of Scienze Naturali, (Trento, Italy)), entered the Museum's collections in 1970 (it was a gift from the Museo Tridentino di Scienze Naturali). Giuseppe Šebesta, founder of the institution, strongly wanted this particular find to be kept in this otherwise ethnographic museum, since he maintained that the presence of some archaeological materials in the exhibition could bring one back to the pre- and protohistoric origins of the material culture of local rural communities (at the beginning the Museum ground was organized in the so-called "closed channels," that is, separate technoeconomical contexts, each defined as "the way": the way of wood, the way of copper, the way of iron, the way of wool, the way of the mill, etc.). In the early 1990s, in the course of a full revision of the permanent exhibition, the specimen was moved to the museum stores.

We do not have any information regarding the specimen, as far as the excavations records are concerned (stratigraphy, laying, etc.), nor about the subsequent cleaning and consolidation processes. However, a simple visual analysis allows us to state that the specimen underwent a partial carbonisation, which has changed its original colour. The specimen was also apparently cleaned rather hastily, so that the lake silt deposit has not been completely removed. Afterwards, to avoid collapsing of its texture, the fragment of basketry was treated with an unknown consolidant resin which induced a gleaming aspect and an unnatural stiffness to the fragment.

The fragment is a specimen of stake-and-strand basketry (manufact measure: length 267 mm; width 100 mm; thickness 18.1–28.2 mm) [1]. When compared to other basketry finds from same site of Fiavè-Carera [2], it could be located between the end of the Early Bronze Age and the end of the Middle Bronze Age (XVI-XIV C. BC).

The fragment was found in the peat bog of Fiavè just outside of Giudicaria valleys, in the South-west of Trentino. It is

Figure 1: Image of the fragment of stake-and-strand basketry recovered from the prehistoric lake dwelling site of Fiavè-Carera (Trento, Italy).

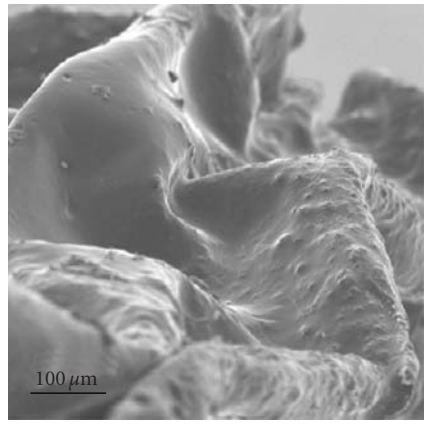

Figure 2: Particular of the sample. It is possible to see the complex morphology of the investigated surface.

a wide marshy area situated south of the modern village of Fiavè at 645 m a.s.l. which has occupied the basin of an ancient barrage lake of post-glacial origin, disappeared because of the progressive growth of peat-moss.

The first archaeological findings in the marsh of Fiavè took place in the context of to peat digging in the second half of the XIX C. Systematic excavations were carried out between 1969 and 1979 [3]; later, since 1981, there followed successive interdisciplinary surveys [4]. The good state of preservation of the settlement structures and material culture, with perishable materials like textiles and basketry artefacts, as well as the overall available stratigraphic series of the Bronze Age in the Southern Alps, support the point that Fiavè is one of the most important peat-bog sites of the whole of Italy.

The research activity reported in this paper is devoted to the use of laser cleaning to remove, after 40 years, the consolidant resin without damaging the original artefact. In addition, we will try to determine the raw material of the object in hand.

2. EXPERIMENTAL METHODS

Several pieces of the artefact previously described have been investigated. These pieces have been extracted from the archaeological find by cutting. The samples have a cylindrical geometry, with a 3-4 mm diameter.

Before starting the cleaning process with laser pulses (UV laser), a few preliminary investigations with Infrared Spectroscopy, Scanning Electron Microscopy, and Energy Dispersive Spectroscopy (FTIR, SEM, and EDS[1]) were made on the surface of basketry in order to obtain some information on composition and atomic bondings of the unknown resin. The irradiation source was a KrF excimer laser with a wavelength of 248 nm and a pulse duration of 20 nanoseconds. The repetition rate of the pulses was kept constant at 10 Hz to avoid excessive heating of the samples. All samples have been irradiated by using a special mask, with a circular hole (8 mm diameter), and by selecting a uniform beam profile. The beam and the sample were always at rest during the irradiation process.

By looking at our previous results obtained on vegetable samples [5], the first guess energy densities have been fixed at 600, 1000, and 1400 mJ/cm^2. The number of pulses is strictly dependent on the thickness of the material to be removed: the organic substances deposited on the surface of the present wood samples are characterized by drastically variable thickness. Therefore, the laser irradiation sessions have been interrupted several times and SEM analyses were made in order to test the conditions of the irradiated area. Laser parameters are then chosen to completely remove the consolidant without damaging the wood surface. The number of pulses was in the range between some tens and some thousands, depending on the energy density and on the layer thickness to be removed. In order to extend the cleaning effects to larger area and better match both the cylindrical geometry of the sample and the irregular surface morphology (Figure 2), the samples have been rotated around their main axis. The total angle rotation was 120°, subdivided in five steps of 30°.

3. RESULTS AND DISCUSSION

FTIR, EDS, and SEM analyses have been performed in order to establish the kind of resin that covers the manufact surface. The surface of the manufact and the fibres, which have been used by prehistoric craftsman to prepare the object, appeared rounded, shiny, and covered by a sort of translucent substance (Figure 3). With EDS analysis, we determined that carbon and oxygen are the main components of this substance. Small amounts of aluminium, silicon, sulphur, chlorine, and calcium have been detected.

The most common substances used in current consolidation of prehistoric basketry are reported in the literature. However, in our case, we did not have records to identify the utilized consolidants. FTIR analyses have been performed on some of the most probable consolidant resins used in

[1] FTIR (Bruker Equinox 55); SEM (conventional SEM, JEOL JSM 6300. Samples were covered with a 20 nm carbon film); EDS (Noran Instruments, Voyager).

Figure 3: Particular of the manufact surface. The presence of consolidant, round off the surface, makes it shiny.

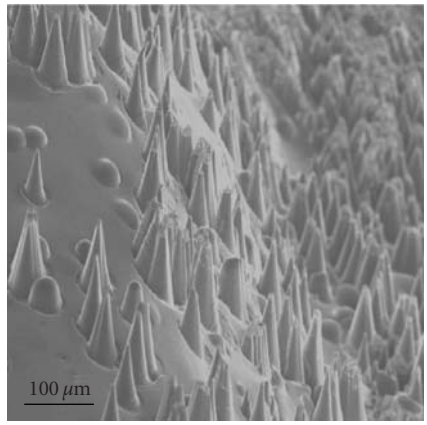

Figure 4: Cones formed on the consolidant surface at low laser energy density (600 mJ/cm^2, 500 pulses).

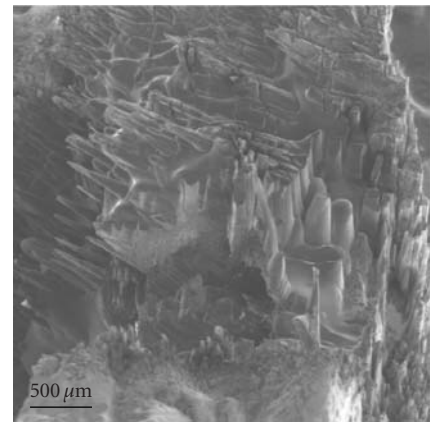

Figure 5: Different cone orientation because of sample tilting (1000 mJ/cm^2, 2000 pulses perpendicular to the surface and 500 pulses each at three different tilt angle, see experimental methods).

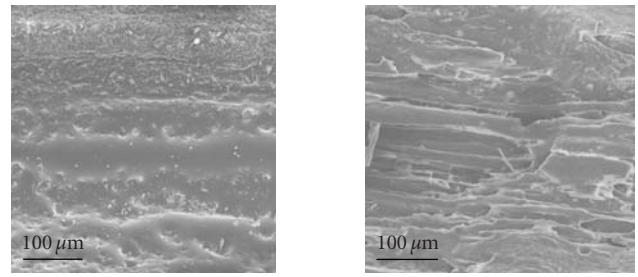

(a) (b)

Figure 6: Consolidated surface (a) before and (b) after high energy density laser irradiation (1200 mJ/cm^2, 50 pulses at different tilt angles).

the museum by restorer in 1970s (organic resin: Turpentine; synthetic resins: Paraloid B72, Primal, and *Araldite*): no one matched reasonably with FTIR data acquired from the unknown consolidant under investigation. We may only conclude that there is an overall similarity with resin spectra.

To investigate the interaction effects between laser and consolidant [6, 7], three small pieces have been detached from the manufact. These samples have been irradiated with laser pulses at different energy densities and the resulting effects have been analysed by SEM.

For low energy density (600 mJ/cm^2), the main result is the change in the surface morphology, which means the formation of a large number of cones (Figure 4). The size of these cones increases with the number of pulses; the same also occurs for their number until it reaches a saturation value after which only cones ablation is appreciable. The appearance of the cones on the surface is probably due to a well known thermal mechanism induced by laser irradiation on polymer surface [8]. The strong absorption of the laser pulse, below the energy threshold for macroscopic ablation, leads to a very fast heating of the surface coating followed by its thermal expansion; heating rates are estimated on the order of 10^{11} K/s. In such a condition, a portion of polymer, because of the induced thermal stresses, blows out: the final results are therefore structures (cones) expanding in the normal direction to the target surface. Removal of the previous cones has been observed, along with formation of new reoriented cones (Figure 5), by irradiating the tilted sample.

For high energy density (1200 mJ/cm^2), a very efficient consolidant removal has been observed (Figure 6). The number of irradiation pulses should be dependent on the consolidant thickness that unfortunately is scarcely uniform; therefore, a number of pulses can impinge on the wood itself, causing some alteration.

Moreover, it was established that an energy density of about 1000 mJ/cm^2 marks the threshold between cone formation and consolidant removal.

In a second step, we tried to identify the wood used to prepare the manufact. In the current literature, few species of wood are reported, used by prehistoric craftsmen to prepare basketry: *Cornus mas, Corylus avellenana, Salix alba*, and *Viburnum lantana* [2].

Despite of the degradation conditions, due to the age of the find and of its environmental lying condition, it was

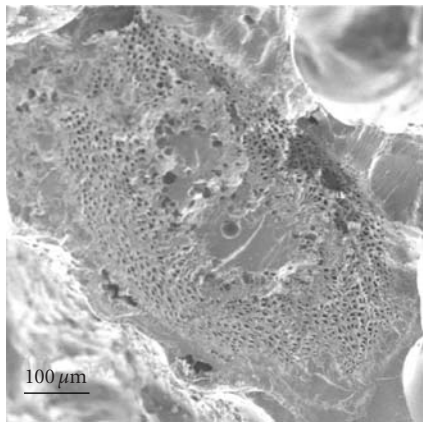

Figure 7: Cross-section of the sample.

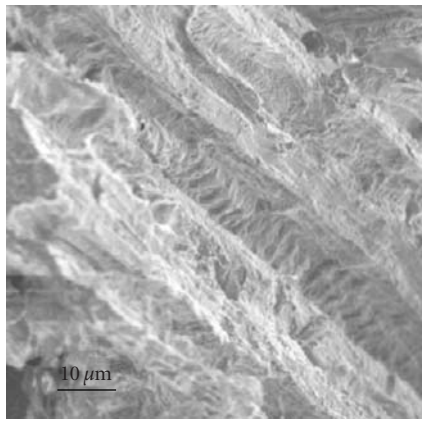

Figure 8: Longitudinal-section of the sample.

still possible to identify specific features that help in qualifying the wood. Indeed, as it can be seen in the cross-section (Figure 7), the sample has a diffuse-porosity with average size of pores of about 30 μm and pores uniformly distributed into the annual growth ring. It was also possible to exclude the presence of multilayered pith rays [9]. Concerning the longitudinal section (Figure 8), we recognized some traces of scaliform perforations.

By combining all these findings, we conclude that the most probable wood, used to make the archaeological basketry, could be *Viburnum lantana*. This is also compatible with literature data.

4. CONCLUSIONS

The present study on laser cleaning of a prehistoric manufact provides some preliminary interesting results that certainly deserve further investigation.

The analyses have not been able to identify the consolidant materials used to cover the archaeological find.

Laser irradiation seems to be a promising way to clean organic finds, but some points should be further investigated, as below specified.

(i) Irregular surface morphology: the beam energy density impinging on the sample surface depends on the morphology of the surface: the presence of peaks and valleys could screen some areas to laser beam.

(ii) Nonuniformity of the consolidant thickness: this makes difficult to have a uniform cleaning of the sample because it would require different number of pulses in the surface area interested by a single spot. Too many pulses might damage the substrate where the consolidant thickness is smaller.

The first problem could be partially solved by systematically changing the sample orientation. Furthermore, the tilting has a relevant effect on final cones configuration. Indeed cones are ablated, reoriented, and reduced in their number.

To solve the second problem, a small interaction area should be interested along with a feedback system. This system could analyse in real time the irradiated area and stop the irradiation when cleaning is attained in the selected area.

ACKNOWLEDGMENTS

The authors wish to thank D. Avi (University of Trento) for FTIR analysis and discussion and G. Kezich (Director of the Museum of San Michele all'Adige) for supporting the research activity.

REFERENCES

[1] W. Wendrich, *Who is Afraid of Basketry: A Guide to Recording Basketry and Cordage for Archaeologists and Ethnographers*, CNWS, Leiden University, Leiden, The Netherlands, 1991.

[2] R. Perini, "Scavi archeologici nella zona palafitticola di Fiavè-Carera. Parte II: campagne 1969-1976, resti della cultura materiale: metallo, osso, litica, legno," 1987, PSAT 9.

[3] R. Perini, "Scavi archeologici nella zona palafitticola di Fiavè-Carera. Parte I: campagne 1969-1976, situazione dei depositi e dei resti strutturali," 1984, PSAT 8.

[4] J. L. Brochier, P. Corboud, F. Marzatico, R. Perini, C. Pugin, and A. M. Rachoud-Schneider, "Gli insediamenti preistorici dell'antico lago di Fiavè nelle Giudicarie, strategia di studio globale di un sito in ambiente chiuso," *Archeoalp: Archeologia delle Alpi*, vol. 1, pp. 127–144, 1993.

[5] R. Belli, A. Miotello, P. Mosaner, and L. Toniutti, "Laser cleaning of artificially aged textiles," *Applied Physics A: Materials Science and Processing*, vol. 83, no. 4, pp. 651–655, 2006.

[6] L. D. Laude, D. Martinez, Cl. Dicara, Fr. Hanus, and K. Kolev, "The ablation of polymers under excimer laser irradiation: the physics of the process and the polymer structure," *Nuclear Instruments and Methods in Physics Research, Section B: Beam Interactions with Materials and Atoms*, vol. 185, no. 1–4, pp. 147–155, 2001.

[7] H. Horn, S. Beil, D. A. Wesner, R. Weichenhain, and E. W. Kreutz, "Excimer laser pretreatment and metallization of polymers," *Nuclear Instruments and Methods in Physics Research, Section B: Beam Interactions with Materials and Atoms*, vol. 151, no. 1–4, pp. 279–284, 1999.

[8] R. Kelly, A. Miotello, B. Braren, A. Gupta, and K. Casey, "Primary and secondary mechanisms in laser-pulse sputtering," *Nuclear Instruments and Methods in Physics Research Section B: Beam Interactions with Materials and Atoms*, vol. 65, no. 1–4, pp. 187–199, 1992.

[9] F. H. Schweingruber, *Anatomy of European Woods: An Atlas Fort He Identification of European Trees, Shrubs and Dwarf Shrubs* [*Anatomie Europäischer Hölzer: Ein Atlas zur Bestimmung Europäischer Baum-, Strauch- und Zwergstrauchhölzer*], Haupt, Bern, Germany, 1990.

Hindawi Publishing Corporation
Laser Chemistry
Volume 2006, Article ID 84781, 6 pages
doi:10.1155/2006/84781

Research Article

Observation of the Laser Cleaning Effect on the Gotland Sandstone Elemental Composition

Marta Jasińska,[1] Jørn Bredal-Jørgensen,[2] and Gerard Śliwiński[1]

[1] *Photophysics and Laser Technique Department, The Szewalski Institute of Fluid-Flow Machinery, Polish Academy of Sciences, Fiszera 14, 80-952 Gdansk, Poland*
[2] *School of Conservation, Esplanaden 34, 1263 Copenhagen K, Denmark*

Received 31 August 2006; Revised 23 November 2006; Accepted 24 November 2006

Recommended by Costas Fotakis

Changes of the elemental composition due to laser surface cleaning of a naturally crusted historical sandstone were investigated by means of the SEM/EDX technique. Data obtained for stone samples prior to and after laser irradiation were compared with those for noncrusted, reference ones. It has been observed that the crust removal resulting from ablative cleaning was accompanied by a decrease of the partial content of elements Al, S, K, Ca, and Mg in the range of 60–80% of their initial value recorded for the noncleaned, crust-covered stone surface. In the stone layer just under the crust coverage, a structure characterized by intergranular spaces between the SiO_2 grains being the main sandstone component filled with degraded binder was observed. From the coincidence of the binder destruction and chemical composition of the crust, the stone surface destruction due to the long-term interaction of environmental pollution was deduced. The spatial distributions of individual elements obtained by mapping after laser irradiation indicated that besides SiO_2 the content of elemental components in the sandstone surface layer decreased by 50%, whereas for Fe with the initial content of 4% and other surface remnants: P, Ti, Zn, and Cl—all below 1%, insignificant changes were only revealed. It was concluded in agreement with the literature that surface cleaning by means of the 1064 nm laser does not cause removal of iron from the sandstone surface.

1. INTRODUCTION

The laser cleaning is presently a well-established technique in conservation of artworks. It assures a localized, well-controlled removal of undesirable layers from the surfaces of historical objects made of various materials such as stone, glass, paper, wood, metal, and so forth by means of laser ablation [1, 2]. This rapid, noncontact process results from conversion of an initial photoexcitation into kinetic energy of particle motion, leading to ejection of atoms, ions, molecules, clusters, and aggregates from the irradiated surface [1–3]. Since 1972 successful applications of laser cleaning to various historical objects such as wall, oil and tempera paintings [4, 5], documents made on paper or parchment [6], photographs, sculptures and architectural details [7, 8], and stained-glass windows [9] have been reported. Most of the experimental data collected so far indicate that laser cleaning represent a useful and efficient technique allowing one to execute difficult, often unique restoration tasks.

One of the main advantages of laser cleaning consists in its usefulness in cases of objects which are fragile or sensitive to chemical solvents used in conventional cleaning methods. Here, the Gotland sandstone represents a good example. It is a soft, quite porous material frequently used in the past for construction and monuments in numerous locations of the Pomeranian Region [10]. Despite the stone composition, structure, and reaction with most common atmospheric pollution which were extensively investigated, the restoration of objects made of this material still represents a difficult task [10–13]. Most of the problems are related to the stone softness, porosity, and composition and occur mainly during cleaning and consolidation of historical objects. In particular, for the case of laser cleaning the problem of changes in the chemical composition has been extensively discussed in relation to the post processing surface discoloration [14–16].

In this work the SEM technique together with elemental analysis and mapping of the distribution of individual elements by means of the Energy Dispersive X-ray Spectroscopy is applied for investigation of the laser cleaning effect on

the historical sandstone material. The experimental data obtained for the laser cleaned samples and reference ones at various stages of the cleaning process are analysed and discussed.

2. EXPERIMENTAL

Samples of sandstone used for measurements were extracted from historical monuments in Gdansk. For ablative removal of the naturally developed black crust, the pulsed Nd:YAG laser (6 nanoseconds FWHM) operating at wavelength of 1064 nm, and constant fluence of 1 Jcm^{-2} was applied. Parameters of interaction were selected in accordance with results of earlier studies [17]. For each sample the irradiated spot was completely cleaned after application of up to 30 laser pulses and the cleaned area had a nearly circular shape of 1 cm in diameter. The SEM + EDX analysis was performed at locations selected so in the central parts as well as in the border regions of the laser processed areas.

The laser-cleaned and reference samples were analysed under conditions of the low vacuum mode provided by a JEOL scanning electron microscope 5310 LV equipped with a LINK Pentafet 6587 energy dispersive X-ray spectrometer (EDS) operated by an Oxford LINK ISIS system. For optical inspection magnifications of 50×, 150×, and 750× were applied. The data on elemental composition of selected sample's fragments were collected by means of EDS and mapped in the form of coloured images using the CAMEO numerical procedure.

The data processing by means of CAMEO allowed to perform an elemental analysis based on SEM photographs of the studied area. In this way not only elements present in the sample surface layer were detected but also their spatial distribution was obtained. The data have been presented in the form of coloured areas characterized by the hue and saturation. The hue was assigned to a defined excitation range of the recorded spectrum and expressed quantitatively in keV. The colour saturation gave information on the quantity of a given element and the various picture colours related to detected elements allowed to conclude on their elemental distribution.

3. CHANGES IN ELEMENTAL DISTRIBUTION DUE TO LASER CLEANING

Among various chemical, physical, mechanical, and biological causes of stone degradation the most typical damages of historical substance can be observed in urban areas, especially in industrial regions. Particularly active in attacking stone are the atmospheric pollutions. Oxygen, carbon dioxide, sulphur and nitrogen oxides, sulphuretted hydrogen, solid particles originating from fuels and floating dust—all are continuously present in air and cause changes in the rock minerals. The water usually intensifies action of these species by penetrating the rock and introducing the pollutant solutions or dispersions deep into the material. As a result, the binder components react with water solutions of air pollutants, producing salts which migrate through grain interspaces and are deposited on the stone surface [12, 13]. In this way the black encrustation is formed: a tight, rough layer accumulating dirt and dust particles, consisting of binder elements and air pollutants.

Black encrustation is the only layer of historical stony objects that should be treated during laser cleaning. Despite the fact that laser cleaning is a self-limiting process because of different absorbance of the black layer and the underlying substrate, it has to be performed with proper caution. The object should be thoroughly examined before cleaning, and a continuous process monitoring during the ablative crust removal is highly advisable. The sample examination before and after laser cleaning delivers useful data, too. In the case considered here, the combined SEM + EDS technique was applied for a detailed surface inspection and also in order to observe changes of the elemental composition at selected locations of the sample studied. Results of the EDS study performed for the crusted and noncrusted samples of the Gotland sandstone before and after laser application are presented in Table 1.

The data indicate a large oxygen content detected for excitation in the range of 0.1–1 keV. The CAMEO mapping in this excitation range reveals nearly exclusively this element represented by numerous, garish-green coloured pixels. This is caused by the fact that oxygen is present in all the minerals in sandstone and in the encrustation, too. Apart from oxygen the remnants of other elements: carbon and zinc are revealed. The value of carbon concentration was excluded from validation due to the data processing applied. The presence of Zn in the top layer of crusted stone results from capturing of this element from the polluted atmosphere. The EDS data indicate that Zn is not removed during the laser cleaning process.

In the excitation range of 1–2 keV the differences in CAMEO prints obtained for the laser cleaned and noncleaned samples become quite distinct—see Figure 1. The largest changes due to the laser surface cleaning are observed in concentrations of aluminum and silicon. The pictures of noncrusted grains show that most of them are composed of silicon grains exclusively which is represented by the blue colour on the CAMEO print. In case of the noncleaned reference sample—the left-hand side of Figure 1, the prevailing part of the surface picture corresponds to silicon. For the intergranular spaces filled with crust the presence of aluminum, being component of glauconite, micas, feldspars and maybe clays formed by weathering, is also detected and shown by a green coloured areas. It can be clearly observed in the mapping, that due to laser cleaning most of the aluminum present on the sample surface is removed. This is confirmed by the numerical data of Table 1, which indicate that the Al concentration decreases four times due to the cleaning but it is still twice as large as that measured for the noncrusted substrate.

Also in the range of 2–4 keV the differences between the reference and laser-cleaned samples are clearly visible. On the CAMEO images, see Figure 2, show the interface between the cleaned and noncleaned parts of the stone surface and thus the two different areas can be distinguished. The first one corresponding to locations covered with crust is blue and navy-blue, and the green area with numerous red, yellow, and navy-blue spots corresponds to the laser cleaned areas.

Table 1: Elements detected before and after laser cleaning by means of the EDX technique: concentrations are given in (%) and the corresponding excitation energy values in keV; data obtained for sandstone samples covered and not covered with encrustation.

Range of excitation energy	Element	Spectral line	Energy value (keV)	Mapping colour ascribed	Average concentration (%)		
					Before cleaning	After cleaning	Stone without crust
0.1–1 keV	Carbon	$K\alpha$	0.28	Yellow	—	—	—
	Oxygen	$K\alpha$	0.52	Green	52.99	52.99	61.25
	Zinc	$L\alpha$	1.01	Navy-blue	0.99	0.99	0
	Sodium	$K\alpha$	1.04	Navy-blue	0	0	0
1–2 keV	Zinc	$L\alpha$	1.01	Red	0.99	0.99	0
	Sodium	$K\alpha$	1.04	Red	0	0	0
	Magnesium	$K\alpha$	1.25	Yellow	0.40	0.12	0.10
	Aluminum	$K\alpha$	1.49	Green	2.90	0.75	0.36
	Silicon	$K\alpha$	1.74	Blue	31.22	39.01	36.55
	Silicon	$K\beta$	1.84				
	Phosphorus	$K\alpha$	2.01	Navy-blue	0.59	0.66	0
2–4 keV	Phosphorus	$K\alpha$	2.01	Red			
	Sulphur	$K\alpha$	2.31	Red	1.05	0.26	0
	Sulphur	$K\beta$	2.46	Yellow			
	Chlorine	$K\alpha$	2.62	Green	0.14	0	0.12
	Chlorine	$K\beta$	2.82				
	Potassium	$K\alpha$	3.31	Green	1.1	0.22	0.11
	Potassium	$K\beta$	3.59	Blue			
	Calcium	$K\alpha$	3.69	Blue	4.36	0.88	0.09
	Calcium	$K\beta$	4.01	Navy-blue			
4–10 keV	Calcium	$K\beta$	4.01	Red			
	Titanium	$K\alpha$	4.51	Red	0.26	0.34	0.39
	Titanium	$K\beta$	4.93				
	Iron	$K\alpha$	6.40	Green	3.96	3.47	1.57
	Iron	$K\beta$	7.06				
	Zinc	$K\alpha$	8.64	Blue	0.99	0.99	0
	Zinc	$K\beta$	9.57	Navy-blue			

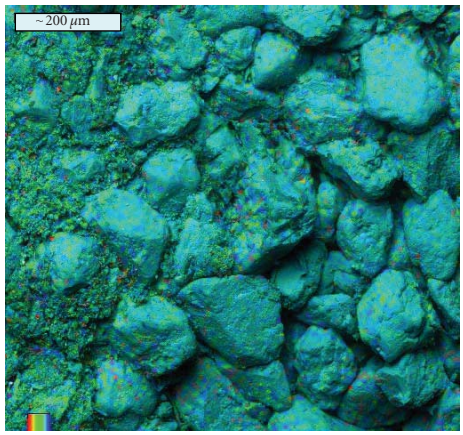

Figure 1: CAMEO print of the interface between the laser cleaned (right) and noncleaned (left) areas of the stone surface; excitation range 1–2 keV.

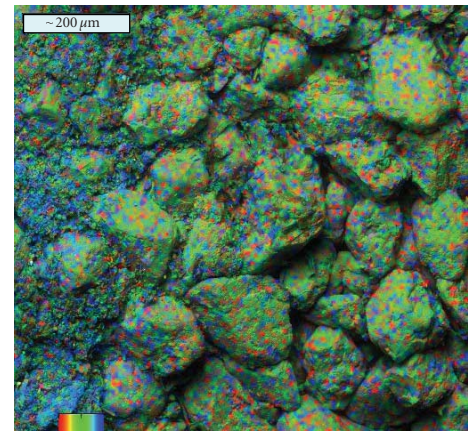

Figure 2: CAMEO print of the interface between the laser cleaned (right) and noncleaned (left) areas of the stone surface; excitation range 2–4 keV.

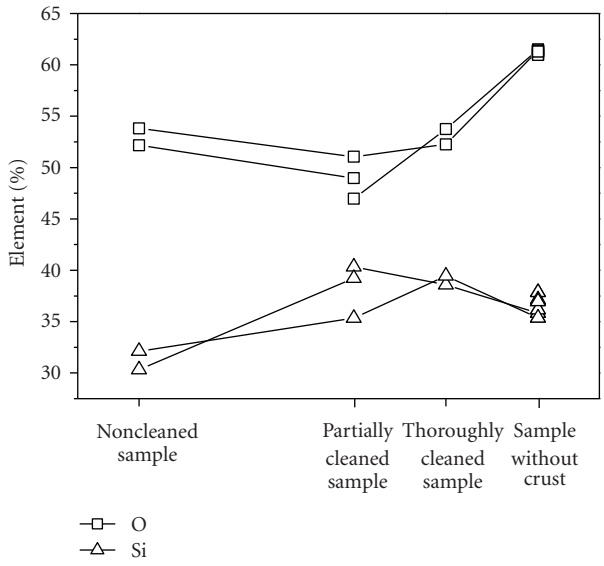

Figure 3: Change in concentration of Si and O measured for successive stages of lasercleaning; data for the noncrusted, reference sample are given for comparison.

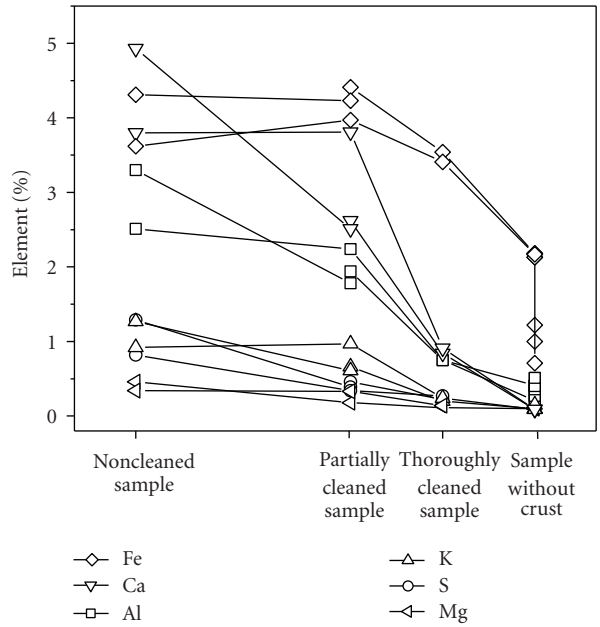

Figure 4: Concentration of aluminum, sulfur, potassium, calcium, magnesium, and iron in samples measured at successive stages of laser cleaning; data for the noncrusted, reference sample are given for comparison.

According to data in Table 1, the blue colour corresponds to calcium ascribed to the binder compounds: calcite, glauconite, and feldspars. Other elements in this part of spectrum are chlorine, potassium, and also phosphorus and sulphate represented by the green, red, and yellow colours, respectively. From this element collection only the presence of potassium and calcium can be clarified by their migration from the inner layers of sandstone. The elements Cl, P, and S can originate from the exterior and, as it will be discussed further in the text, they are residual components of minor contribution to the layer composition.

The highest spectral range does not show up any marked changes in the superficial stone layer due to laser cleaning. The presence of the $K\beta$ line of calcium and also $K\alpha$ and $K\beta$ lines of more massive elements: titanium, iron, and zinc is revealed. In the corresponding CAMEO prints it can be observed, that in the entire map the green colour corresponding to Cl, and K prevails but there are numerous spots of other colours, from amongst which the yellow one corresponding to iron, a component of glauconite, occurs most frequently. In this case and form data in Table 1 it can be concluded that the Fe concentration does not practically change due to the laser cleaning, though, it is twice as large as for the noncrusted substrate.

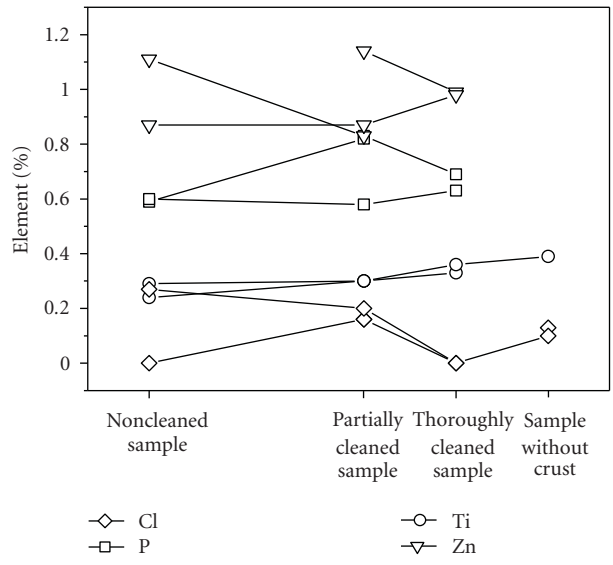

Figure 5: Concentration of phosphorus, titanium, zinc, and chlorine in samples measured at successive stages of laser cleaning; data for the noncrusted, reference sample are given for comparison.

4. RESULTS OF THE EDS ANALYSIS

From EDS measurements the semiquantitative data characterizing the chemical composition of the crusted and lasercleaned Gotland sandstone were obtained and the results are shown on Figures 3–5. The data were collected for four different samples: (1) crusted one before cleaning, (2) crusted partially cleaned, (3) crusted thoroughly cleaned and (4) a clean sandstone without crust. Three series of measurements were performed for each element and the results are averaged percentage values related to the summary content of 100% of the all elements detected in a given sample. The list of elements does not contain carbon in agreement with discussion of the EDS study summarized in [18].

The change of percentage contents of silicon and oxygen observed for consecutive stages of the laser cleaning process

Table 2: The average concentration change of selected elements in samples due to the laser cleaning.

Element	Al	S	K	Ca	Mg	Fe
Concentration before cleaning (%)	3	1	1	4.5	0.4	4
Concentration after cleaning (%)	0.75	0.2	0.2	0.9	0.12	3.5
Relative decrease (%)	75	80	80	80	60	12.5

is presented in Figure 3. These two elements make together 80–90% of the total mass of the sample material and their concentration increases with the surface cleaning progress and removal of the crust. The initial quantity characterizing the silicon and oxygen content of 84% before cleaning grows up to 87% for the partially cleaned sample and reaches the value of 92% after completion of the process. This in agreement with the elemental mapping already discussed reveals the presence of Si and O due to quartz grains, and agrees also with the result of contaminants removal due to laser ablation. It is worth noting that as the relative concentration of silicon grows, the oxygen level remains stable around 53% during the laser cleaning process. It is caused by the fact that Si as a component of quartz is gradually exposed by the cleaning process while the oxygen level remains unaffected as it is present in almost every chemical compound in the sandstone as well as in the crust.

A strong decrease in concentration due to laser cleaning is observed for the elements: aluminum, sulfur, potassium, calcium, magnesium, and iron—Figure 4. The corresponding average concentration of selected elements before and after cleaning and also the relative concentration changes are summarized in Table 2. Almost all the elements listed decrease several times their share in the top material layer. Iron is the only exception—its concentration after cleaning is almost the same as before laser application. This coincides with conclusions from the CAMEO elemental mapping, and is also in agreement with results of EDS studies on marble performed by other authors [14], which demonstrated that after the laser cleaning of stone under similar conditions, for example, by means of the 1064 nm, Q-switched Nd:YAG laser, iron remains on the sample surface. Moreover, it is worth noticing that concentrations of other elements shown in Figure 4 lie below 1% for the case of thoroughly cleaned substrate.

Almost all the elements listed in Table 2 originate from sandstone. The only exception is sulphur which comes from atmospheric pollutants. In the presence of water the sulphur oxides migrate in the form of water solution into the sandstone bulk, where they react with minerals, creating new compounds. Most likely these compounds move to the top layers of the stone and are deposited on its surface in the encrustation after evaporation of water [13].

The range and changes of concentration of the other elements: Cl, P, Ti, and Zn are relatively small—from 0 up to 1.2%, see Figure 5. The low content and weak concentration dependence on the cleaning stage both indicate that these elements belong to residual components of the studied sample layers.

The results show that the surface layer of the noncrusted, historical Gotland sandstone contains mainly the following elements: silicon, oxygen, calcium, potassium, aluminum, iron, magnesium, chlorine, and titanium. For the case of crust-covered sandstone two groups of elements are revealed. The one refers to the elements originally present in the nondestructed stone substrate: magnesium, aluminum, chlorine, potassium, calcium, and iron. The zinc, sulphur, and phosphorus belong to the second group of chemical components originating from the polluted environment and captured by the sandstone surface.

5. CONCLUSIONS

Samples of the naturally crusted historical sandstone were investigated by means of the SEM and EDX techniques in order to observe changes in the chemical composition due to the surface cleaning with laser. Based on the EDX data, also the elemental mapping at consecutive stages of the cleaning process was performed by means of the CAMEO image processing package. It was observed that besides SiO_2 the content of elements Al, S, K, Ca, and Mg in the sandstone surface layer decreased 3–5 times after the laser irradiation, whereas for Fe of an initial content of 4% and other surface remnants P, Ti, Zn, and Cl—all below 1%, only insignificant changes were revealed. In the cleaned region, silicon was predominantly observed while in the noncleaned region also aluminum and calcium were detected. The presence of these elements being natural components of Gotland sandstone was clarified by their migration in form of solutions and under the influence of polluted atmosphere into the top surface layer.

ACKNOWLEDGMENT

This work was supported by the Polish Ministry of Science and Higher Education via projects H-01/DWM-119 and COST/KN/DWM-102.

REFERENCES

[1] M. Cooper, *Laser Cleaning in Conservation*, Butterworth Heinemann, Oxford, UK, 1997.

[2] A. C. Tam, W. P. Leung, W. Zapka, and W. Ziemlich, "Laser-cleaning techniques for removal of surface particulates," *Journal of Applied Physics*, vol. 71, no. 7, pp. 3515–3523, 1992.

[3] J. C. Miller and R. F. Haglund, Eds., *Laser Ablation and Desorption*, Academic Press, London, UK, 1998.

[4] C. Fotakis, V. Zafiropulos, V. Tornari, et al., "Lasers in the conservation of painted artworks," in *Second GR-I International Conference on New Laser Technologies and Applications*, vol. 3423 of *Proceedings of SPIE*, pp. 292–296, Olympia, Greece, June 1998.

[5] M. C. Gaetani and U. Santamaria, "The laser cleaning of wall paintings," *Journal of Cultural Heritage*, vol. 1, supplement 1, pp. 199–207, 2000.

[6] K. Ochocińska, M. Sawczak, M. Martin, J. Bredal-Jørgensen, A. Kamińska, and G. Śliwiński, "LIPS spectroscopy for the contamination analysis and laser cleaning diagnostics of historical paper documents," *Radiation Physics and Chemistry*, vol. 68, no. 1-2, pp. 227–232, 2003.

[7] S. Siano, F. Margheri, R. Pini, P. Mazzinghi, and R. Salimbeni, "Cleaning processes of encrusted marbles by Nd:YAG lasers operating in free-running and Q-switching regimes," *Applied Optics*, vol. 36, no. 27, pp. 7073–7079, 1997.

[8] P. Pouli, K. Frantzikinaki, E. Papakonstantinou, V. Zafiropulos, and C. Fotakis, "Pollution encrustation removal by means of combined ultraviolet and infrared laser radiation: the application of this innovative methodology on the surface of the Parthenon West Frieze," in *Proceedings of the 5th International Conference on Lasers in the Conservation of Artworks (LACONA 'V)*, vol. 100 of *Springer Proceedings in Physics*, pp. 333–340, Osnabrück, Germany, September 2003.

[9] S. Klein, T. Stratoudaki, V. Zafiropulos, J. Hildenhagen, K. Dickmann, and Th. Lehmkuhl, "Laser-induced breakdown spectroscopy for on-line control of laser cleaning of sandstone and stained glass," *Applied Physics A*, vol. 69, no. 4, pp. 441–444, 1999.

[10] A. Jarmontowicz, R. Krzywoblocka-Laurow, and J. Lehmann, *Sandstone in Historical Architecture and Sculpture*, Towarzystwo Opieki nad Zabytkami, Warsaw, Poland, 1994.

[11] K. Malaga, M. Myrin, and J. E. Lindqvist, "Consolidation of Gotland sandstone," in *Proceedings of the 10th International Congress on the Deterioration and Conservation of Stone*, pp. 447–454, Stockholm, Sweeden, July 2004.

[12] A. Jarmontowicz, "Study of the sandstone durability of historical objects under atmospheric pollution conditions," *Ochrona Zabytków*, vol. 1, pp. 35–37, 1998 (Polish).

[13] W. Domaslowski, Ed., *Prophylactic Conservation of the Stone Historical Objects*, Wydawnictwo UMK, Toruń, Poland, 1993.

[14] S. Klein, F. Fekrsanati, J. Hildenhagen, et al., "Discoloration of marble during laser cleaning by Nd:YAG laser wavelengths," *Applied Surface Science*, vol. 171, no. 3-4, pp. 242–251, 2001.

[15] V. Vergès-Belmin and C. Dignard, "Laser yellowing: myth or reality?" *Journal of Cultural Heritage*, vol. 4, supplement 1, pp. 238–244, 2003.

[16] M. Jankowska and G. Śliwiński, "Laser cleaning of historical sandstone and the surface discoloration due to gas shielding," in *Lasers and Applications*, vol. 5958 of *Proceedings of SPIE*, pp. 3A1–3A8, Warsaw, Poland, August 2005.

[17] M. Jankowska and G. Śliwiński, "Acoustic monitoring for the laser cleaning of sandstone," *Journal of Cultural Heritage*, vol. 4, supplement 1, pp. 65–71, 2003.

[18] M. Jankowska and G. Śliwiński, "EDS analysis of the laser-cleaned Gotland sandstone and comparison with LIPS data," IF-FM Report 5601, Gdańsk, Poland, 2005.